MICROCOPY RESOLUTION TEST CHART

IREAU   STANDARDS 1963 A

ARO 21116.12-MS

②

AD-A194 337

MATERIALS SCIENCE AND ENGINEERING

University of Pittsburgh

Pittsburgh, Pennsylvania 15261
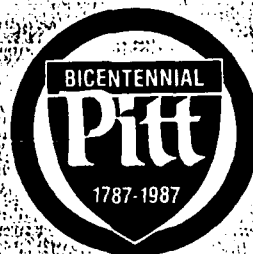
BICENTENNIAL
Pitt
1787-1987

DTIC
SELECTE
APR 1 1 1988
S ⚡ D
D

88   4   11   065

REPORT DOCUMENTATION PAGE

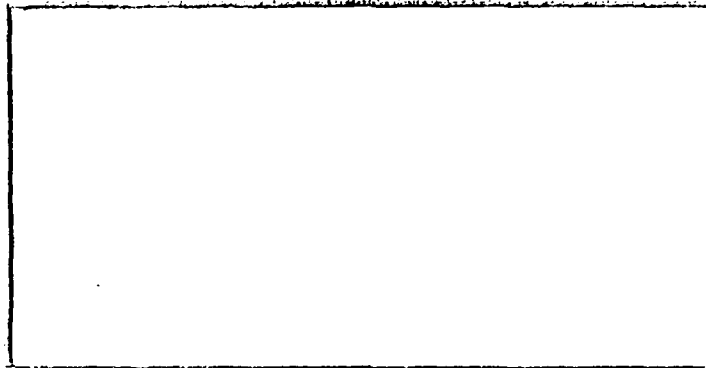| 1a. REPORT SECURITY CLASSIFICATION Unclassified		1b. RESTRICTIVE MARKINGS			
2a. SECURITY CLASSIFICATION AUTHORITY		3. DISTRIBUTION / AVAILABILITY OF REPORT			
2b. DECLASSIFICATION / DOWNGRADING SCHEDULE		Approved for public release; distribution unlimited.			
4. PERFORMING ORGANIZATION REPORT NUMBER(S)		5. MONITORING ORGANIZATION REPORT NUMBER(S) ARO 21116.12-MS			

6a. NAME OF PERFORMING ORGANIZATION University of Pittsburgh	6b. OFFICE SYMBOL *(If applicable)*	7a. NAME OF MONITORING ORGANIZATION U. S. Army Research Office
6c. ADDRESS *(City, State, and ZIP Code)* Pittsburgh, PA 15261		7b. ADDRESS *(City, State, and ZIP Code)* P. O. Box 12211 Research Triangle Park, NC 27709-2211

8a. NAME OF FUNDING/SPONSORING ORGANIZATION U. S. Army Research Office	8b. OFFICE SYMBOL *(If applicable)*	9. PROCUREMENT INSTRUMENT IDENTIFICATION NUMBER DAAG29-84-K-0074			
8c. ADDRESS *(City, State, and ZIP Code)* P. O. Box 12211 Research Triangle Park, NC 27709-2211		10. SOURCE OF FUNDING NUMBERS			
		PROGRAM ELEMENT NO.	PROJECT NO.	TASK NO.	WORK UNIT ACCESSION NO.

11. TITLE *(Include Security Classification)*
Study of the Erosion Corrosion of Alloys and Coatings

12. PERSONAL AUTHOR(S)
N. Birks and F. S. Pettit

13a. TYPE OF REPORT Final	13b. TIME COVERED FROM 5/7/84 TO 9/30/87	14. DATE OF REPORT *(Year, Month, Day)* December 1987	15. PAGE COUNT 29+

16. SUPPLEMENTARY NOTATION The view, opinions and/or findings contained in this report are those of the author(s) and should not be construed as an official Department of the Army position, policy, or decision, unless so designated by other documentation.

17.	COSATI CODES		18. SUBJECT TERMS *(Continue on reverse if necessary and identify by block number)*
FIELD	GROUP	SUB-GROUP	Oxidation, Scale Spallation
			Erosion Corrosion, Sulfur, Alloys, Coatings

19. ABSTRACT *(Continue on reverse if necessary and identify by block number)*

Apparatus has been developed that allows the erodent size, speed and impact angle on the target to be varied independently. The apparatus also allows temperature and atmosphere composition to be selected.

Reliable and reproducible kinetic data have been obtained for the exposure of samples of a range of metals and alloys in the apparatus.

When erosion and oxidation processes interact in the degradation of a specimen, an acceleration in the degradation is always observed.

20. DISTRIBUTION / AVAILABILITY OF ABSTRACT ☐ UNCLASSIFIED/UNLIMITED ☐ SAME AS RPT. ☐ DTIC USERS	21. ABSTRACT SECURITY CLASSIFICATION Unclassified	
22a. NAME OF RESPONSIBLE INDIVIDUAL	22b. TELEPHONE *(Include Area Code)*	22c. OFFICE SYMBOL

DD FORM 1473, 84 MAR   83 APR edition may be used until exhausted.
All other editions are obsolete.

Con't'd

The interaction between erosion and oxidation of metals can be divided into several distinct regimes which vary from pure erosion through erosion enhanced oxidation, in which the processes interact but are not modified, to oxidation affected erosion, where the interaction between the processes involves strong modification of the erosion and oxidation processes according to mechanism.

The regime of degradation mechanism in which a particular metal specimen finds itself depends upon the relative intensities of the erosive and oxidative processes.

Evidence has also been obtained for the coexistence of a further regime, based on scale spallation, at certain values of scale thickness.

The inclusion of sulfur in the atmosphere results in much more aggresssive attack of the specimen and the erosion component is suspected of modifying the scale in a physical manner such as to enhance the penetration by sulfur.

Both the metal and oxide phases studied so far appear to deform in a more or less ductile manner under the joint attack of erosion and oxidation over the temperature range 20-780°C.

STUDY OF THE EROSION CORROSION
OF ALLOYS AND COATINGS

FINAL REPORT

by

N. BIRKS AND F.S. PETTIT
Materials Science and Engineering Department
University of Pittsburgh

December 1987

U.S. ARMY RESEARCH OFFICE
DAAG 29-84-K-0074

APPROVED FOR PUBLIC RELEASE
DISTRIBUTION UNLIMITED

STUDY OF THE EROSION-CORROSION OF ALLOYS AND COATINGS

FINAL REPORT

TABLE OF CONTENTS

<u>APPENDICES</u>

Appendix 3   Mechanisms of Simultaneous
              Erosion-Oxidation Attack of
              Nickel and Cobalt at High Temperature
              by C. T. Kang, F. S. Pettit and N. Birks
              Met. Trans. 18A, 1785-1802 (1987).

Appendix 4   Papers to be Submitted for Publication

      A   Interaction between Erosion and High Temperature
              Corrosion of Metals: The Erosion Enhanced Oxidation
              Regime by S. L. Chang, F. S. Pettit and N. Birks

      B   Effect of Angle of Incidence on the Combined
              Erosion-Oxidation Attack of Nickel and Cobalt
              by S. L. Chang, F. S. Pettit and N. Birks

      C   Some Interactions in the Erosion Oxidation
              of Alloys by S. L. Chang, F. S. Pettit and N. Birks

      D   The Erosion-Corrosion Behavior of Nickel in Mixed
              Oxidant Atmospheres by D. Rishel, F. S. Pettit and N. Birks

STUDY OF THE EROSION-CORROSION OF ALLOYS AND COATINGS

STATEMENT OF THE PROBLEM STUDIED

Under an earlier contract DAAG 29-81-K-0027, several significant accomplishments were achieved. An apparatus was developed, constructed and used to study the erosion and corrosion of metals at high temperatures and high particle velocities. The erosion-oxidation of nickel in air was studied and the existance of several regimes of interaction between erosion and oxidation were proposed. The behaviour of cobalt was compared to that of nickel, allowing more detailed mechanisms for the interactions within the various regimes to be clarified. Some initial work was carried out on alumina and chromia forming alloys to allow the effect of a slow growing scale to be studied.

These results allowed a base to be established, from which the current program was planned to provide further insight into the erosion-corrosion degradation of pure metals, alloys and also to study the effects of introducing sulfurous gases into the airflow to provide information on some of the effects of complex atmospheres.

The specific objectives defined in the proposal for the present program were as follows:

1. To identify the regimes of degradation for nickel, cobalt, some Cr_2O_3 formers and some Al_2O_3 formers in erosion -oxidation and erosion-hot corrosion.

2. To describe the important mechanisms responsible for such degradation.

3. To describe the oxide scale properties important to resistance against erosion-oxidation and erosion-hot corrosion.

4. To describe the effects of the erosive component in terms of size, composition, impact angle and velocity.

1

5. To study the effect of temperature on the erosion -corrosion interaction.

6. To study and compare the erosion -corrosion characteristics of several state of the art systems.

7. To consider and develop or discard the concept of erosion -corrosion regimes of interaction

It will be seen in the following that these objectives have been met in the broad sense. In certain areas more intensive effort was applied than had been anticipated initially in order to confirm the interpretations presented . In other areas the emphasis was shifted somewhat in order to take advantage of the way the work developed, an example of this is the emphasis that was eventually placed on the effects of SO_2 and SO_3 in the gas stream whereas the influence of hot corrosion was not studied.

In order to address the above points it was necessary to develop the apparatus further. This is described in detail in Appendix 1.

SUMMARY OF THE MOST IMPORTANT RESULTS

Regimes of Degradation

Several regimes of interaction have been identified and described in detail in the papers published in Conference proceedings and in <u>Metallurgical Transactions</u> shown in Appendices 2 and 3. These regimes are described briefly as follows.

The PURE EROSION REGIME was observed when the oxidation component was small. This condition could be achieved by eroding the metal in atmospheres of low oxygen potential, such as pure nitrogen, or even in oxidising atmospheres at low temperature. For the oxide, pieces of pure oxide could be used however the technique adopted was to preoxidise a metal sample to a thickness such that the oxidation rate was so low as to be considered negligible.

2

During pure erosion of the oxides of both nickel and cobalt, material was removed by mainly ductile mechanisms and the surfaces showed cracks or tears, indentation marks from the particle impacts, cutting and plastic deformation -even at 25°C. Similar features were observed at 25, 600 and 800°C and the rate of material removal was higher at the higher temperatures. This behavior is interpreted on the basis that more energy is absorbed by the plastic deformation of the oxide at higher temperatures as the oxide becomes more ductile. A brittle mode of oxide removal has not been observed so far but it is quite possible that such might be observed at lower temperatures, or in the cases of other oxides such as Cr_2O_3 or Al_2O_3.

Pure erosion of the metals nickel and cobalt also results in extensive plastic flow, the metal is apparently extruded into platelets and gradually detached. It is significant that the rate of material removal by erosion in the absence of oxidation, at low or high temperature, is very much less than the degradation rates observed in the presence of both erosion and oxidation.

A regime of EROSION ENHANCED OXIDATION is observed when both erosion and oxidation processes proceed at similar rates. In this regime, the oxide scale that forms a barrier to further oxidation is, itself, continuously being removed by erosion. However the erosion process is not very severe and its mechanical influence on the metal substrate does not prevent the formation of a compact, uniform, scale. The removal of the surface of the scale by erosion, at a rate that is decided by the erosive conditions, means that the scale will thin down until it reaches a thickness at which its growth rate is the same as the erosion rate. At this stage a steady state should be reached in which the scale thickness remains constant and the metal degradation rate also remains constant. In this regime, although there is a significant interaction between the erosion and oxidation

3

processes that leads to an enhanced degradation rate, the interaction is not such as to cause the fundamental mechanisms, by which each process occurs, to be modified.

A detailed treatment of the erosion enhanced oxidation regime is given in Appendix 4A.

The OXIDATION AFFECTED EROSION regime is entered from the erosion enhanced oxidation regime simply by increasing the intensity of the erosion component to the point at which the formation of a uniform scale is no longer possible. Under such conditions, the surface of the metal consists of deformed metal, oxidation products and embedded erodent particles. It is considered that this is a composite surface layer whose properties control the rate of degradation of the metal. In this regime, the oxidation of the metal is greatly enhanced due to the fact that the erosive action is continually exposing a bare metal surface to the oxidizing atmosphere, whereupon it oxidizes at the maximum possible rate, furthermore the plastic deformation of the metal substrate causes small slivers or platelets of metal to be extruded out into the atmosphere. This greatly enlarges the area of metal exposed to the aggressive atmosphere and contributes further to the enhancement of the oxidation component. The erosion mechanism is also modified by the change in nature of the specimen surface and removes the oxide as rapidly as it can form. The surface is also quite probably subjected to a temperature increase due to the plastic working of the surface during which some of the incident energy is absorbed and converted into heat. This effect has not been measured in the current work, but the effect is in little doubt.

Effects of Particle Impact Angle

Much of the work carried out in identifying the various regimes of interaction between erosion and corrosion involved particle impact angles of 90 deg only. Of course impact angles are expected to vary greatly in operational situations and the

4

effect of impact angle was studied in this work for the cases of both nickel and cobalt. The two metals were found to differ in their response to erosion -corrosion attack using different impact angles. Nickel showed a maximum degradation rate at an angle of about 30 deg whereas cobalt showed a maximum at an angle of about 60 deg, both results referring to 800°C. The difference in behavior has been accounted for in the fact that cobalt oxidises much more rapidly than nickel and, at 800°C, the thick scale formed provides substantial protection to the underlying metal in that sufficient incident energy is absorbed to prevent excessive extrusion of metal at the wave crest. In the cases of both metals, wave patterns were developed on the specimen surfaces, the wavelength and amplitude varying with the angle. At 600°C the cobalt, having a much reduced oxidation rate at this temperature, behaved very similarly to nickel and showed maximum degradation at an angle of about 30 deg. The plastic deformation of the substrate in the case where the erosive beam is incident at 90 deg produces a pattern of hills and valleys, called 'moguls'. This gradually changes to give alignment of the hills and eventually a pattern of waves or ripples as the angle of incidence is reduced. The mechanisms proposed for the removal of material show that the deformation processes that occur on the top of a wave are very important in providing a means by which metal is exposed, oxidized and eventually removed from the specimen.

A detailed account of the studies of the effects of particle impact angle is given in the paper of Appendix 4B.

Erosion Oxidation of Alloys

The erosion-oxidation of alloys was studied for two reasons. First, it allows the behavior of scales of Cr_2O_3 and of Al_2O_3 to be studied by choosing the appropriate chromia and alumina forming alloys. Second, the consideration of the behavior of alloys introduces several extra parameters into the process that are

5

concerned with the selective oxidation of alloy components. For instance, the action of erosion may remove the thin scales before a protective scale of one oxide has been established, thus putting the alloy into a mode of extended transient oxidation during which the lack of the normal protective scale leads to rapid oxidation and correspondingly higher degradation rates are observed. This action at the surface of the alloy may also lead to the development of concentration gradients in the surface of the alloy, due to the selective oxidation of an alloy component and the removal of the oxide by erosion.

In the case of chromia forming alloys the effect of the high velocity air stream may also lead to enhanced evaporation of CrO3. This effect alone can lead to the breakdown of protective chromia scales developed in the early stages of exposure.

During the current work several alloys were used, including chromia and alumina formers, the results and their interpretation indicate that all of the above mentioned factors play significant roles in the degradation mechanisms.

A detailed account of these results and their interpretation is given in the paper of Appendix 4C.

Effects of Sulfurous Atmospheres

The use of air, to which SO2 and SO3 was added, as the atmosphere for testing resulted in immediate increases in reaction rates. This was due to the formation of a duplex scale composed of oxide with a continuous network of sulfide, through which the metal ions could migrate very rapidly. Furthermore, the action of erosion appeared to be to open up the scale to allow the formation of the sulfide to an extent that was much greater than expected to occur in the absence of erosion. In this case the interaction between erosion and oxidation is seen to lead to modification of the oxidation mechanism. The duplex scale formed also appears to be more easily deformed than the pure oxide scale conterpart as evidenced by flow of the scale over the specimen edges as observed in the presence of erosion.

6

A further phemonenon was the observation of scale spalling under certain conditions. This is found to arise under conditions of moderate erosion intensity that lead to the development of a scale of critical thickness. When the erosive intensity is low, the scale is apparantly too thick to spall away whereas, when the erosive intensity is high, the resulting thin scale is not susceptible to spalling.

These results are presented in detail in the paper of Appendix 4D.

The results that have been summarized very briefly above are being reported in the literature and , for this reason, the main body of results and discussion of the details of mechanisms is presented in the form of papers appended to the report. These papers are either in the form of preprints before submission for publication or reprints of published papers. Their relevence to the above overview of results has been indicated in the text.

CONCLUSIONS

1. Apparatus has been developed that allows the erodent size, speed and impact angle on the target to be varied independently. The apparatus also allows temperature and atmosphere composition to be selected.

2. Reliable and reproducible kinetic data have been obtained for the exposure of samples of a range of metals and alloys in the apparatus.

3. When erosion and oxidation processes interact in the degradation of a specimen, an acceleration in the degradation is always observed.

4. The interaction between erosion and oxidation of metals can be divided into several distinct regimes which vary from pure erosion through erosion enhanced oxidation, in which the processes interact but are not modified, to oxidation affected erosion, where the interaction between the processes involves strong modification of the erosion and oxidation processes according to mechanism.

5. The regime of degradation mechanism in which a particular metal specimen finds itself depends upon the relative intensities of the erosive and oxidative processes.

6. Evidence has also been obtained for the coexistence of a further regime, based on scale spallation, at certain values of scale thickness.

7. The inclusion of sulfur in the atmosphere results in much more aggresssive attack of the specimen and the erosion component is suspected of modifying the scale in a physical manner such as to enhance the penetration by sulfur.

8. Both the metal and oxide phases studied so far appear to deform in a more or less ductile manner under the joint attack of erosion and oxidation over the temperature range 20-780°C.

8

APPENDIX 1

DEVELOPMENT OF APPARATUS

INTRODUCTION

Originally designed under the previous research contract, the apparatus used under this contract, has undergone major modifications in order to perform erosion-corrosion experiments in mixed-gas environments and to improve data consistency. The apparatus, as shown in Figures 1 and 2, has the capability of delivering a high velocity (50-170 meter per second), high temperature (500-850°C) erodent laden gas flow for use in erosion-corrosion studies. The basic design criteria are presented below.

Original criteria

1.   In order to control accurately the composition of the impinging gas, the use of electric furnaces as a heat source as opposed to combustion gases, (with their inherent fluctuations in fuel composition and consumption rates), is made throughout.

2.   In order to avoid a wind chill effect, the temperature of the impinging gas must be kept higher than the sample temperature. This criterion was affected by the equipment modification however, in that the impinging gas is now the only source of heat for the sample, where as previously both the gas and an infrared lamp heated the specimen.

3.   In order to minimize the possibility of a steep velocity gradient at the discharge end of the nozzle and its effect in producing non-uniform erosion from

the center of the erosive stream towards its edge, a tube of a relatively large diameter (≈ 1 cm) is used to accelerate the erodent particles.

4.   The maintenance of a controlled and constant erodent particle delivery rate, ensures consistency in the comparison of kinetic data between different temperatures, velocities, gas compositions and angles of impingement.

Modifications for the current program

5.   A means was required of positioning the sample accurately, reproducibly and conveniently within the erodent laden gas stream at various impingement angles.

6.   A means was required of introducing highly corrosive gases, such as SO_2/SO_3 into the erodent laden gas stream in such a way as to minimize the component hardware actually exposed to the sulfurous gases.   This requirement was established to minimize replacement costs and the repair time required for replacement.

7.   A safe and reliable method of containing the SO_2/SO_3 and Al_2O_3 powder was required.

8.   A means was required of quickly removing exposed specimens from, and inserting new specimens into, the erosive gas stream without altering any variables (i.e. SO_2 flow, particle loading rate and temperature).

9.   Due to the high SO_2 levels used in some of this research, it would be unsafe to exhaust the spent erodent laden gas stream into the laboratory. A means had to be developed to remove all traces of sulfur but, at the same time,

be capable of handling large volumes of gas (up to 300 liters per minute).

Due to the large quantities of gas required, in house compressed air was chosen as the carrier gas. A series of filters and dryers are used to remove traces of oil, moisture and particulates. After purification, the carrier gas is passed through a flowmeter to an in-line fluid heater which preheats it to about 700°C. At this stage a SYLCO™ Mk-IX Powder Dispenser is used to deliver erosive particles for entrainment with the carrier gas at the entrance of a 1.5 meter long Inconel 601 acceleration tube. The acceleration tube conveying the carrier gas is further heated by a series of vertically mounted electric resistance furnaces. Sulfur dioxide is introduced into the erodent laden carrier gas at the end of the acceleration tube by means of an SO_2 injector.

Specimens are mounted in a specially designed holder. They may be held at any angle with respect to the gas flow and are heated by contact with the gas stream. A manipulator, which connects the sample holder, is used to provide remote placement of the sample within the flowing airstream.

The velocities of the alumina particles in the emerging erosive gas stream are measured by using a laser doppler velocimeter coupled to an Apple II+ computer. Excellent agreement has been obtained between measured particle velocities and calculated gas stream velocities, thus confirming that the erosive particles attain the gas velocity before exiting the acceleration tube and SO_2 injector.

The heart of this containment purification system is a blower which is designed to discharge large volumes of gas against high back pressures. This is necessary for two reasons. First, the blower must not only convey large volumes of carrier gas but also have the additional capacity to place a slight

vacuum on the containment, thus preventing the leakage of sulfurous gases into the laboratory. Secondly, the exhausted sulfur bearing carrier gas is discharged into a water filled, pH adjusted, 55 gallon barrel where complete removal of SO_2 and SO_3 is accomplished. Operational experience has shown that, for the flowrates and SO_2 concentrations typically employed ($\approx$100 lpm and 1500 ppm SO_2), the measured SO_2 concentration in the effluent of the barrel is below detectable limits (i.e. < 0.1 ppm SO_2). The various components of this apparatus are described in the following sections.

1 GAS SYSTEMS

1.1 Main Air System

The main air system's function is to deliver a clean, high temperature, pressure regulated and well defined flow of erodent laden, gas to the surface of a specimen. As shown in Figure 3 this system consists of various filters, oil and moisture removers, pressure regulators and gauges, flowmeters, fluid heaters, various electric resistance furnaces, assorted pipe fittings and the 1.5 meter long acceleration tube.

1.1.1 Gas Supply. The compressed air is delivered by a Gardner-Denver compressor whose capacity is well in excess of 300 liters per minute (LPM) against a back pressure of about 90 PSIG. For these experiments, both characteristics are adequate in maintaining the desired flow rates with a minimum of flow fluctuations.

1.1.2 Filters. The purpose of filter (a), as shown in Figure 3 is to remove solid

and liquid aerosols which may exist in the compressed gas. Filter (b) on the other hand exists primarily to remove any solid particles which may have become entrained in the carrier gas after its passage through the oil and moisture removers. The filters are manufactured by Wilkerson Corporation and are both Model No. M20-02-000. The filter elements used in Filter (b) are almost 100% efficient down to 0.01 microns.

<u>1.1.3 Flow Control Valve.</u> This valve (Wilkerson R20-04-000) controls the flowrate of the carrier gas through adjustment of the discharge pressure whenever a change in flowrate is required.

<u>1.1.4 Dryers.</u> After passage through the flow control valve, the main air stream enters a series of drying units where oil and water vapor are removed. The existing arrangement consists of one single and two pairs of series connected dryers supplied by Wilkerson Corporation. The first unit in line, is the single dryer unit, Model No. X03-02-000. This unit is filled with Type 13X Molecular Sieve and will reduce the oil content to 24 ppm/wt. The next two in line dryers, Model No. X04-02-000, are termed "dual-dryers", and when the desiccant is exhausted in one unit, the flow can be redirected, with only momentary flow interruption, to the parallel unit by switching a four way valve. The desiccant can then be changed without interrupting the air flow. The desiccant used in these units is silica gel, which will remove moisture down to 9.2×10^{-4} atm. of H_2O.

<u>1.1.5 Flowmeter.</u> The flowmeter originally installed in the apparatus was a Hastings mass flowmeter purchased from the Teledyne Corporation. Early in this stage of research however the flow cell failed and required replacement.

Due to its high cost and long delivery time, it was decided to purchase a less expensive, more reliable, readily available albeit less convenient and less accurate rotameter Model No. FL-1503A manufactured by Omega Engineering Inc. This has a range of 29.6-295.9 slpm, an accuracy of ±2% full scale and a repeatability of ±0.5% full scale. The major inconvenience of this flowmeter is that the flowrate read on the gauge plate must be corrected to standard pressure whereas the Hasting's mass flowmeter corrected the flowrate to standard pressure electronically.

1.1.6 Heating Arrangement. In designing the heating arrangement of this apparatus the following were considered to be of primary importance. 1) To heat a large amount of gas (50-300 lpm) in a very short time and 2) To protect the heating elements of the devices used from deterioration due to the erodent and the SO_2/SO_3 gases used in this research.

Through a series of connections and metal tubing, the main air passes from the flowmeter to the first stage of heating by means of two 4000 watt fluid heaters (GTE Sylvania, Inc., Model No. CGH-138823), which are used in parallel in order to balance the usage of each heater more evenly and provide a higher heat input per unit gas flow than proved to be possible with the earlier series connection. Depending on the required flowrate, the maximum temperature achieved under these conditions is 20-50°C higher than would be the case if the fluid heaters were series connected. About 95% of the gas impinging on the sample is actually heated by the fluid heaters. The remainder, used for particle or SO_2 injection, is heated by other means as discussed later.

The hot, main, air stream flowing from the fluid heaters is carried via various Inconel 600 1/2" NPT pipe fittings to a T-joint where the hot carrier gas

and the stream of air conveying the erosive particles are combined and mixed into a single gas stream which flows down the Inconel 601 acceleration tube. The flowing gas and particle mixture is heated further by a series of three vertically mounted electric resistance heaters. The first heater, or furnace, in line is termed the "upper heater" and was constructed in house. Designed for high heat transfer this furnace has a maximum power rating of about 400 watts. Its power supply is a 120V/10 Amp Variac. The second in line heat source is a large 3400 watt tube furnace, manufactured by Lindberg Furnace of Watertown, Wisc. Finally, the last furnace, termed the "lower heater", consists of two series connected 3"x5" cylindrical heaters (Model No. SK-244) supplied by Electro Heat Systems Inc., of Washington, Pa. This particular furnace has two functions. First, to prevent the length of acceleration tubing outside the Lindberg furnace from cooling off. Second, to ensure that the SO_2/Subair mixture is heated sufficiently prior to its injection into the erodent laden main air stream.

1.1.7 Acceleration Tube. The purpose of the acceleration tube is to allow the entrained erosive particles to reach the desired velocity and temperature. The tube must be long enough for the entrained erosive particles to reach the velocity of the gas stream. The inside diameter of this tube should also be large enough to prevent a steep velocity gradient from occurring at the discharge end of the tube. Furthermore, this tube must have good thermal shock resistance and mechanical strength at elevated temperatures, good oxidation resistance and high thermal conductivity. The tube which presently is installed and meets these requirements, is a 9.3 mm ID x 13.5 mm OD x 1.5 meter Inconel 601 tube. To improve the oxidation resistance and retard erosive wear, the inner wall of

this tube was coated with an aluminized layer by Turbine Components Corporation of Branford, Ct.

1.2 SO$_2$ /Subair System

The purpose of the SO$_2$/Subair system is to supply an SO$_2$ and air mixture to the SO$_2$ injector connected to the end of the acceleration tube. A diagram of this system is shown in Figure 4.

1.2.1 SO$_2$ Gas Supply. The sulfur dioxide gas used in this research is supplied as liquid in a 68.2 kg (150lb.) bottle by the Linde Division of Union Carbide, is anhydrous and has a minimum purity of 99.98% in its liquid phase which has a vapor pressure of 2.4 kg/cm^2 (34.4 psig) at 21°C (70°F). Liquid SO$_2$ was used because it provides greater flexibility in the selection of a gas mixture to which a sample is eventually exposed, than would be the case for a premixed bottle of SO$_2$ + Air (or O$_2$). Furthermore, since the main air flowrate will be different for each velocity and temperature condition, a means must be available to adjust the SO$_2$ flowrate from its source in order to maintain a constant SO$_2$ concentration in the gas flowing over the specimen.

1.2.2 Subair Supply. Air for the oxidation of SO$_2$ to SO$_3$ is supplied form either, bottled compressed air or the main air system as shown in Figure 4. In high velocity experiments, the pressure drop across the filters and moisture removers is so large that the main air system cannot provide adequate flow to the subair system. For circumstances such as these, the bottled compressed air is used. In experiments where it is desired that no SO$_3$ exist in the airstream, bottled nitrogen is used instead of compressed air in the subair system thus preventing

the oxidation of SO_2.

1.2.3 Flowmeters. The flowmeters used to measure both the SO_2 and subair flows, as shown in Figure 4, are Series 50 (FM 4350) stainless steel bodied flowmeters made by the Linde Division of Union Carbide Corporation which have an accuracy of ±10% full scale and a reproducibility of 0.5% of full scale.

1.2.4 SO_2 Regulator and Cross Purge Assembly. The sulfur dioxide gas is delivered to the SO_2 flowmeter at a constant pressure by means of a single-stage cylinder regulator designed to handle corrosive gases. This regulator, supplied by the Linde Division of Union Carbide is Model No. CRB-1-75-7-660, has a maximum inlet pressure of 21.1 kg/cm^2 (300 psig) and a delivery pressure range of 0-5.3 kg/cm^2 (0-75 psig). The cross purge assembly is connected between the SO_2 bottle and the SO_2 regulator, and allows all traces of SO_2 to be removed from the apparatus upon shutdown. This equipment is also supplied by the Linde Division of Union Carbide Corporation and is Model No. SG-4100-5La.

1.2.5 SO_2 Heater. The purpose of the SO_2 heater is to preheat the SO_2/Subair mixture to about 420°C prior to its entry into the SO_2 injector. This temperature was selected in order to limit corrosive degradation, of the tubing carrying this mixture. This heater was manufactured in house and consists of two series connected 1.25" x 18" long, 720 watt cylindrical heating elements supplied by Electro Heat Systems, Inc., Model No. SK-215. Power is supplied to this heater by a 120V/10A Variac.

1.2.6 Tubing. The tubing used to carry the SO_2/Subair consisted of either 3/8"

diameter Type 316 stainless steel seamless tubing or Inconel 600 seamless tubing, (both types having a 0.035" wall thickness). The tubing is stainless steel up to the SO_2 heater, the remainder of the tubing being Inconel 600 of higher corrosion resistance. Inconel tubing was not used throughout because of its relatively high cost. Both the stainless steel and Inconel tubing were supplied by Williams and Co., of Pittsburgh, Pa.

1.1.7 SO_2 Transition Piece. The purpose of this component is to provide a leak-tight means of passing the tubing conveying the SO_2/Subair mixture into the powder collection sump. Both on the exterior and interior sides of the powder collection sump, fittings are provided on the SO_2 transition piece, to connect the tubing from the SO_2 heater and Inconel flexible hose respectively. This component is made entirely of Inconel 600 fittings and plate and is of welded construction.

1.1.8 Inconel Flexible Hose. The purpose of this hose is to convey the SO_2/Subair mixture from the SO_2 transition piece to the SO_2 injector. A flexible hose allows for the vertical movement of the acceleration tube due to thermal expansion and contraction. The hose itself and its fittings are made of Inconel 600. This component was manufactured by Tofle America Inc., of Conshohocken, Pa.

1.1.9 SO_2 Injector. The last item in the SO_2/Subair system is the SO_2 injector. A schematic of this device is shown in Figure 5. The SO_2 injector serves as a catalyst chamber for the conversion of SO_2 to SO_3 which is injected into the main air stream. As for the acceleration tube, an aluminide coating was applied in order to improve its corrosion resistance.

Within the SO_2 injector, platinum foil and wire (with a total surface area of approximately 55 cm^2) was added to serve as a catalyst for the reaction.

$$SO_2 + 1/2O_2 = SO_3 \qquad (1)$$

It has been found however, that due to high flowrates, a higher actual temperature at the SO_2 injector or a poisoned catalyst, the actual conversion of SO_2 to SO_3 is only a small fraction of the equilibrium value.

2 SAMPLE HOLDER AND SAMPLE HOLDER MANIPULATOR

The function of the sample holder is to hold the sample securely in the flowing main air stream at the desired angle of incidence. The sample holder manipulator on the other hand positions the sample holder and hence the sample itself within the flowing airstream.

2.1 Sample Holder

As shown in Figure 6, the sample is supported vertically by the thermocouple probe and horizontally in compression by two spring loaded alumina rods. The ceramic block serves to minimize heat loss from the back sides of the specimen. The compression rod, compression rod holder and thermocouple holder are made of Type 316 stainless steel. The compression spring is made of Inconel X750 (with a spring constant of about 1 lbf/in). The sample holder frame is made from an aluminum alloy. The angle at which the main air flow impinges on the sample is adjusted by swiveling the sample holder with respect to the sample holder carriage.

2.2 Sample Holder Manipulator

The function of this device, as shown in Figure 7, is to provide movement in three directions. Remote placement of the sample while exposed to the main air stream, by the sample holder manipulator in 2 of 3 directions (X and Z) is possible by adjustment of the drive rod. Displacement of the sample in the Y direction however cannot be performed remotely. This movement is only possible by adjusting a drive screw when the sample holder is withdrawn into the specimen exchange chamber.

3 CONTAINMENT AND PURIFICATION SYSTEM

In order to conduct experiments safely , a containment and purification system was built. Since it would not be practical to construct a leak tight enclosure, a slight negative pressure was maintained in the containment. Thus, laboratory or atmospheric air may leak into the containment and ensure the safe confinement of the sulfurous gases.

The reaction chamber, tunnel, specimen exchange chamber and powder collection sump as shown in Figures 1 and 2 provide the containment for the SO_2/SO_3 gases and Al_2O_3 particles. The reaction chamber and tunnel are fabricated of 0.063 inch thick aluminum sheet and 1 x 1 inch aluminum angle. Joints and seams are made up predominantly by 0.125 x 0.5 inch rivets and 8/32 screw fasteners. Gas tight sealing is provided at these joints and seams by Dow Corning Silastic® 736 RTV, a silicon based adhesive/sealant formulated to perform continuously up to 260°C.

Quarter inch thick Pyrex® glass was selected for the reaction chamber viewing ports in order to withstand the high temperatures (100-175°C)

associated with the reaction chamber and to minimize any distortion of the laser beam used in conjunction with the particle velocity measurement device.

The function of the "bleeder valve" installed on the reaction chamber is to help control the pressure within the reaction chamber. This is important, for instance whenever the main air flowrate is much less than the capacity of the blower (to be described later). Under this condition, air may be bled into the reaction chamber. This is necessary in order to minimize the effect that a pressure substantially below atmospheric may have on the flow characteristics of the erodent laden main air stream as it emerges from the SO_2 injector. On the other hand, when the main air flowrate approaches the capacity of the blower, the bleeder valve is closed in order to maintain a slight negative pressure in the reaction chamber and thus prevent the leakage of SO_2/SO_3 into the laboratory. Although not shown in Figure 2, the bleeder valve is connected to a dryer unit of the type described in Section 1.1.4, to reduce the moisture content of the air which is sucked into the containment and thus minimize the formation of sulfuric acid within the containment/purification system.

The purpose of the SO_2/SO_3 sampling port is to allow the rapid insertion and removal of the Pyrex® sampling tube used in the gas sampling procedure.

The tunnel serves as the conduit connecting the reaction chamber to the specimen exchange chamber. The tunnel door serves to isolate the reaction chamber from the specimen exchange chamber whenever a specimen is inserted or removed from the sample holder. This permits safe specimen exchange without the necessity of terminating the SO_2 flow prior to specimen withdrawal.

The specimen exchange chamber is also, for the most part, fabricated of

0.063 inch aluminum sheet and 1 x 1 inch aluminum angle. Access to the specimen exchange chamber include a door to permit specimen exchange, a linear bushing to permit the inward and outward motion of the manipulator drive rod and electrical connections to permit thermocouple hookup. In addition, vacuum ports (connected to the suction side of the blower) and a bleeder valve permit the flushing of the specimen exchange chamber with atmospheric air.

The last component of the containment is the particle collection sump. Due to its relatively large volume and internal baffle arrangement, this component serves to provide a means of collecting the particles used in the erosion process.

A regenerative blower, as shown in Figure 8, is used to exhaust the gases from the containment system. This blower is manufactured by EG & G Rotron of Saugerties, N.Y., and is Model No. DR-313AK4HK. Of the variety of blowers on the market, i.e., rotary vane, rotary-lobe, turbine and centrifugal, the regenerative blower is of a relatively new design concept. The major advantage of a regenerative blower is that, as shown in Figure 9 it can operate over a wide range of pressures and flowrates. Another advantage that a regenerative blower has over a rotary vane, rotary-lobe or turbine blower is that it is not as susceptible to small amounts of dust and dirt because of the relatively large clearances which exist between the rotor vanes and housing. In addition, the blower actually installed has the following additional features. First, to prevent gas leakage, the blower assembly includes carbon double-face shaft seals, O-rings on all assembly bolts and RTV sealant on the gasket surfaces of the impeller housing. Second, to minimize corrosion, the impeller and impeller housing have an anodized aluminum coating.

The piping system as shown in Figure 3 connects the blower to the powder collection sump (where a suction is taken) to a 55 gallon drum (into which the blower discharges). The piping itself is carbon steel seamless tubing with a 1.5 inch OD and a 0.134 inch wall thickness. The joints in this piping arrangement are made up predominantly of 1.5 inch Swagelock tube fittings manufactured by Crawford Fitting Co. of Solon Ohio which permit relatively easy assembly and disassembly. The pipe OD was selected in order to minimize the head loss due to friction, while a 0.134 inch wall thickness was selected in order to ensure that the Swagelock fittings formed a leak-tight joint.

A filter, Model No. FA2-0B-000 supplied by Wilkerson Corporation, was installed on the suction side of the blower in order to protect the blower from any erosive particles not trapped in the powder collection sump. The filter element is designed to retain particles 5μm in size and larger.

In line, between the filter described above and the suction side of the blower, is a 12 inch long by 2.0 inch ID flexible radiator hose. This hose isolates the mechanical vibrations generated by the blower from the powder collection sump and thus the entire apparatus. This is important due to the sensitivity of the Laser Doppler Velocimetry equipment to vibration. In addition, the supports for the exhaust piping are mounted using "snubbers" to prevent vibration of the framing which supports both the furnaces and containment systems.

The piping arrangement at the blower was chosen to provide an additional means of controlling the pressure established in the containment volume. If, for instance, the capacity of the blower exceeds that of the main air system and the pressure in the containment is too high, the flow from the blower

can be reduced by slightly opening the bypass valve and throttling shut the discharge valve as necessary to establish the desired pressure. In this mode of operation, a portion of the exhaust gas is recirculated continuously through the blower.

The last component in the containment/purification system is a 55 gallon drum. When filled with water, gases are introduced into the bottom of the barrel by means of a "sparging" ring which serves to "agitate" or break up the gas flow into bubbles which will lead to improved SO_2/SO_3 absorption. Typically the barrel is filled with approximately 40 gallons of water and 2 lbs. of sodium bicarbonate. Water is found to be an extremely effective absorber of SO_2. This is reflected by the fact that the solubility of SO_2 in H_2O is 26 grams SO_2 to 100 grams of H_2O. The sodium bicarbonate is added to prevent the pH of the barrel water from becoming too low. As an added measure of precaution, the sulfur-free barrel effluent is exhausted to a fume hood via an elephant trunk.

The erosive particles used in this research are delivered to the acceleration tube by a Sylco Mark IX plasma spray powder feeder manufactured by Sylvester and Company of Cleveland, Ohio. Powder is delivered from a sealed powder cannister by means of a variable speed feed screw assembly. The sealed powder cannister and feed screw assembly are mounted on an electromagnetic vibrator to prevent lumping and clogging of the erosive particles. The output of the powder feeder is controlled by variation of the feed screw speed and the magnitude of vibration of the electromagnetic vibrator.

As presently configured, the amount of powder delivered from the powder feeder can be adjusted with the interval 0.25 to 5 gm/min. These

feedrates however are still too high for the experiments conducted. To remedy this situation a flow divider as shown in Figure 10 is used to lower the amount of powder actually injected into the main air stream. Measurements indicate that approximately 40% of the powder feeder output is actually injected into the acceleration tube.

Since an accurate determination of the particle loading rate is required, a means was developed to measure the amount of erosive powder actually injected into the acceleration tube. The procedure followed, involves a two step process to measure first the output of the powder feeder and then the powder "siphoned off" from the powder divider described earlier. The difference between the two measured values is the particle loading injected into the acceleration tube.

The device or trap used to capture the erosive particles works along the same lines as a gas washing bottle. However due to the pressures involved (generally 10-15 psig) the particle collector is made of metal. Whenever particle loading rates are measured, the particle collector is incorporated into the particle feed lines in such a manner as to minimize the perturbation of the air flow from the powder feeder to the powder divider, from the powder divider to the acceleration tube and the excess powder collector.

4 VELOCITY MEASUREMENT

In this research, the velocity of the erosive particles is measured by laser doppler velocimetry (LDV). The main advantage of this technique is that the erosive particle velocity can be measured directly without disturbing the main airstream flow. The components of the LDV system consists of a 15 mW He-Ne

laser, photodiode, electronic counter and an Apple II+ microcomputer. Velocity measurements over the exit cross-section of the SO_2 injector nozzle are accomplished by movement of the laser and with an X-Y table.
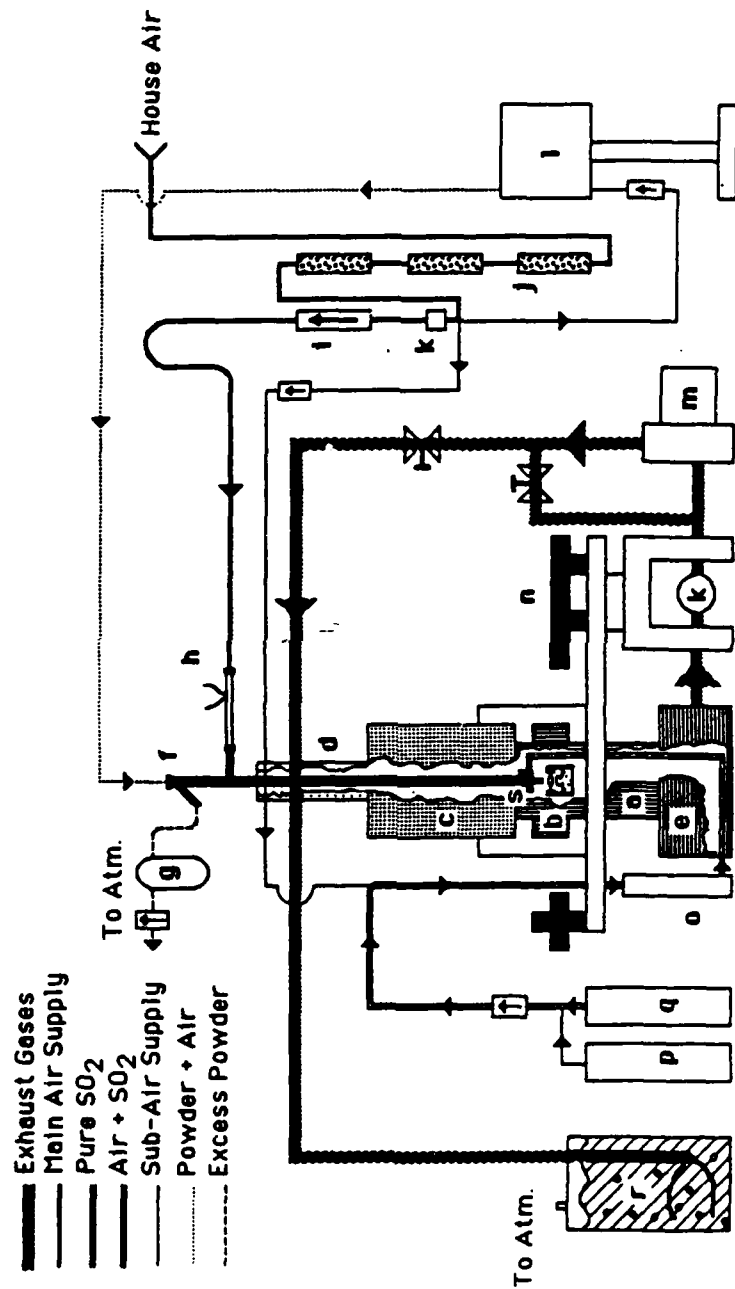
Figure 1: **Erosion Apparatus Schematic Cutaway with Sample in Position:** (a) reaction chamber; (b) sample holder; (c) Lindberg furnace; (d) upper heater; (e) powder collection sump; (f) powder injector/divider; (g) excess powder collector; (h) fluid heater; (i) flow meter; (j) oil/moisture separators; (k) filter; (l) powder feeder; (m) blower; (n) LDV equipment; (o) SO_2 heater; (p) nitrogen; (q) liquid SO_2; (r) 55 gallon drum; (s) SO_2 injector.

19
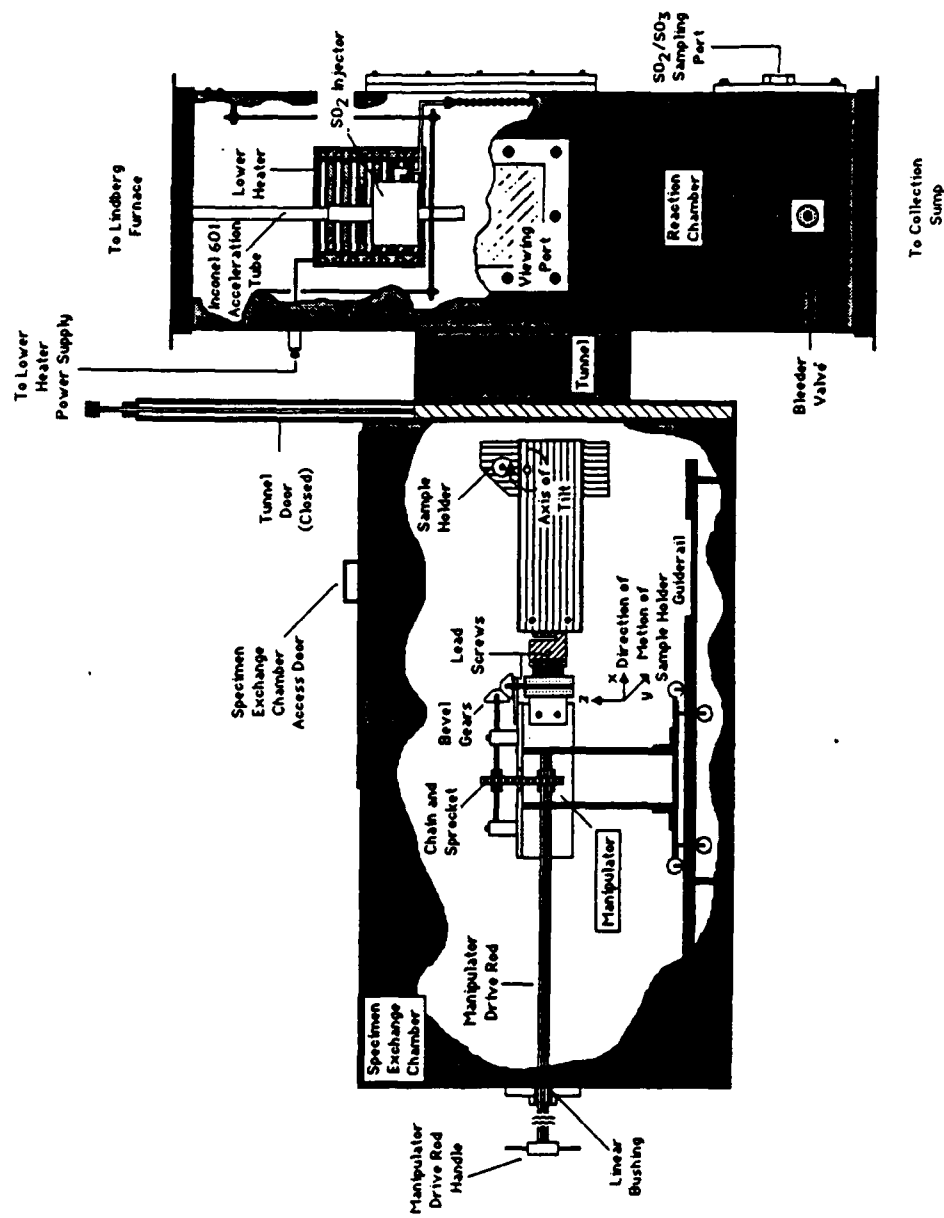
Figure 2a: Cutaway of Reaction and Specimen Exchange Chambers, (with Sample Holder withdrawn).

20
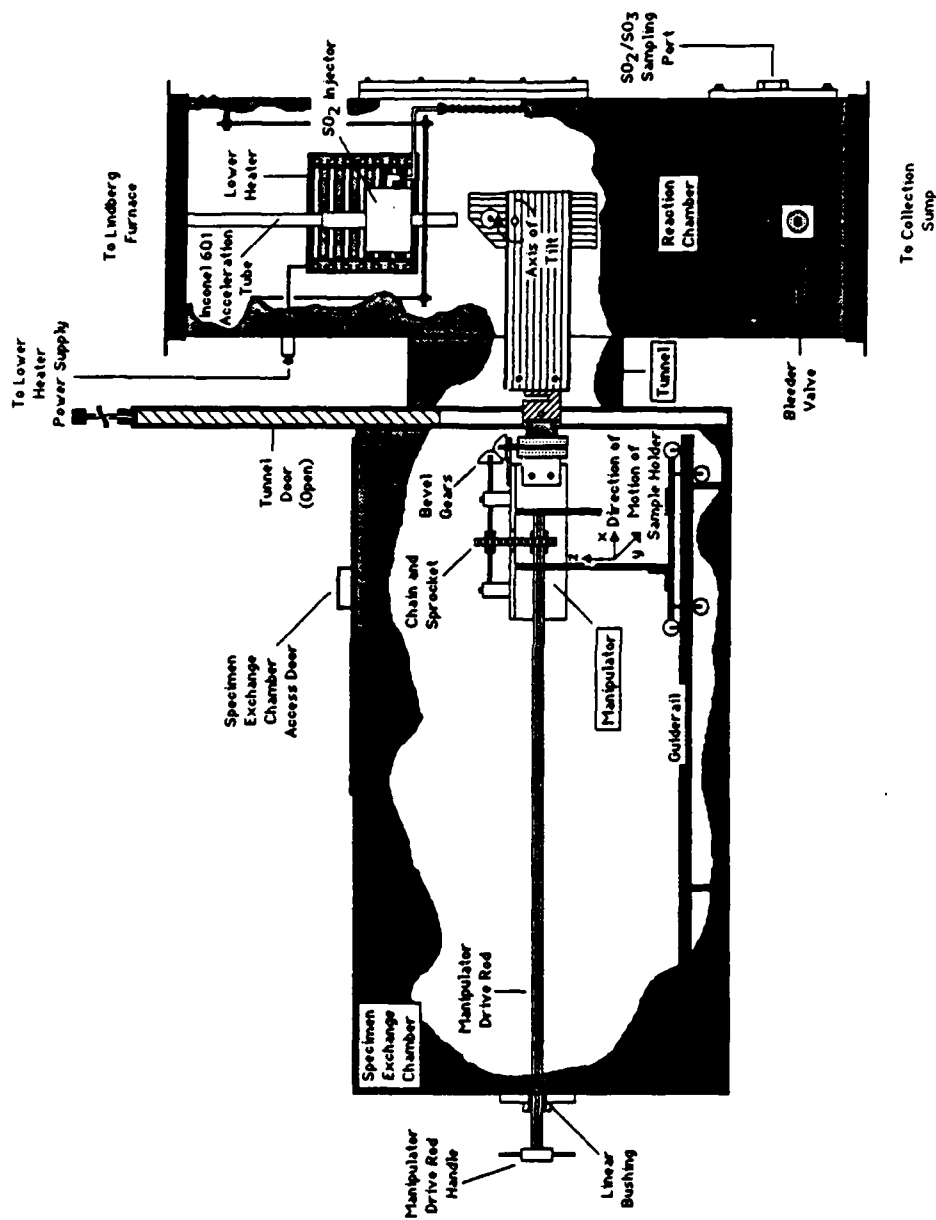
Figure 2b: Cutaway of Reaction and Specimen Exchange Chambers, (with Sample Holder inserted).
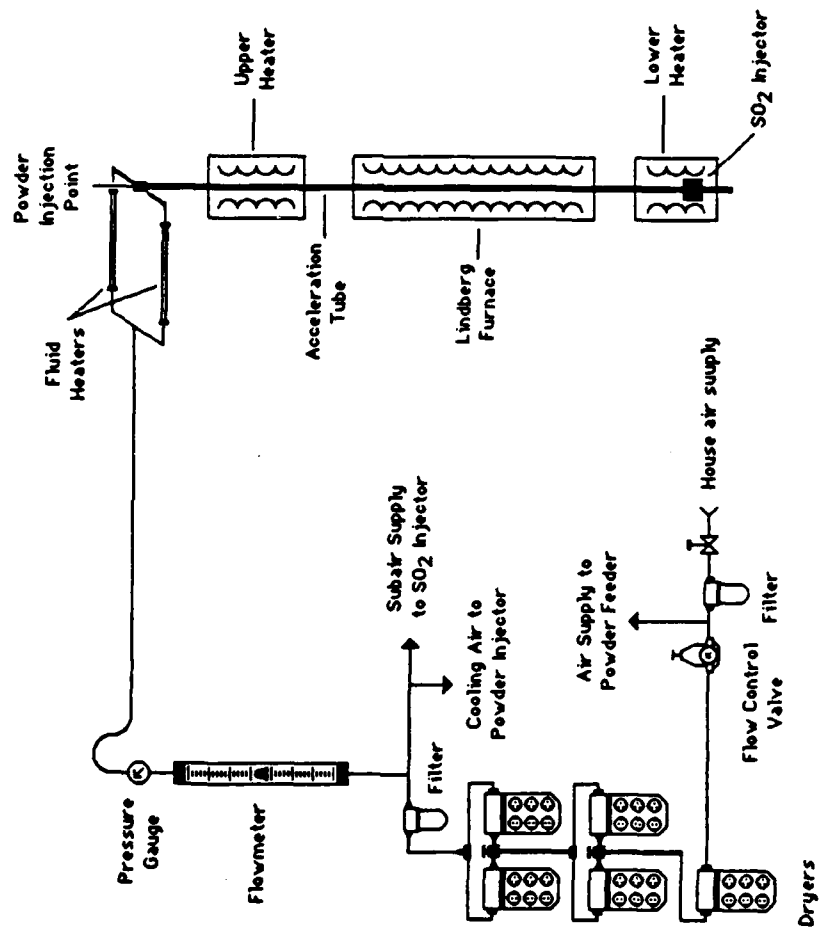
Figure 3: Schematic of Main Air System.
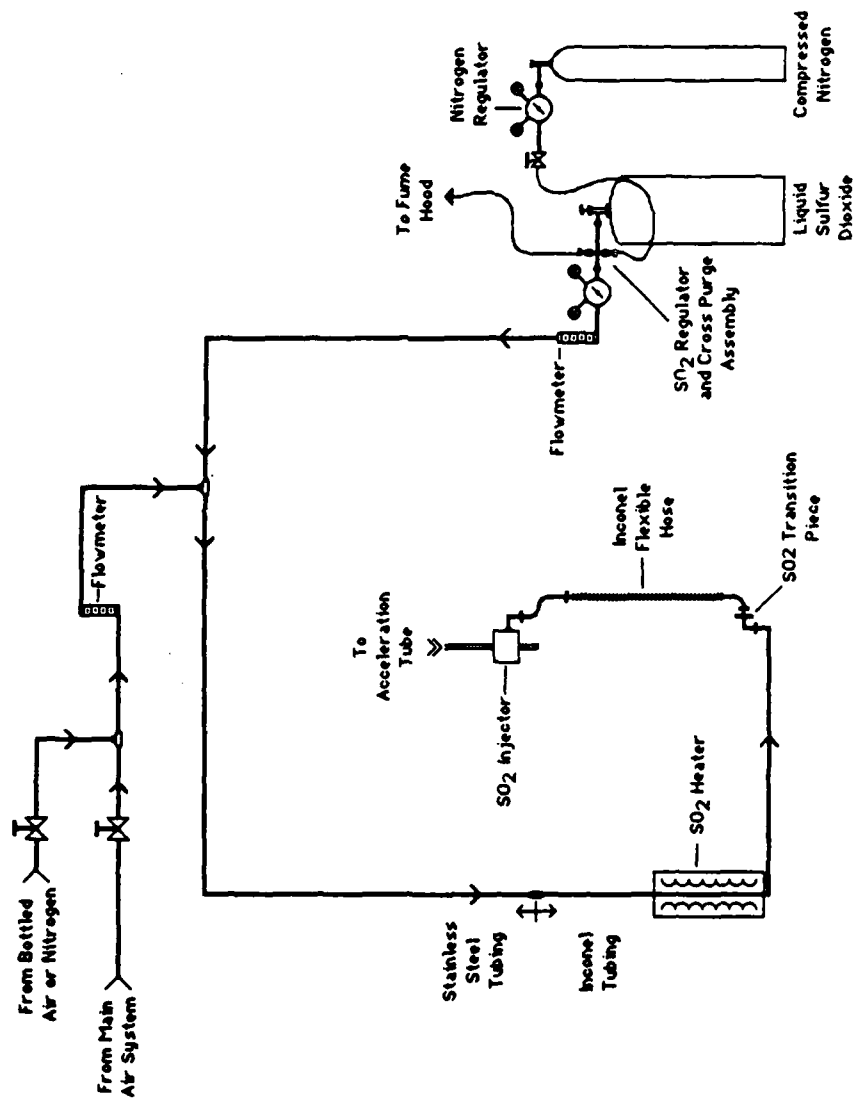
Figure 4: Schematic of SO₂/Subair System.
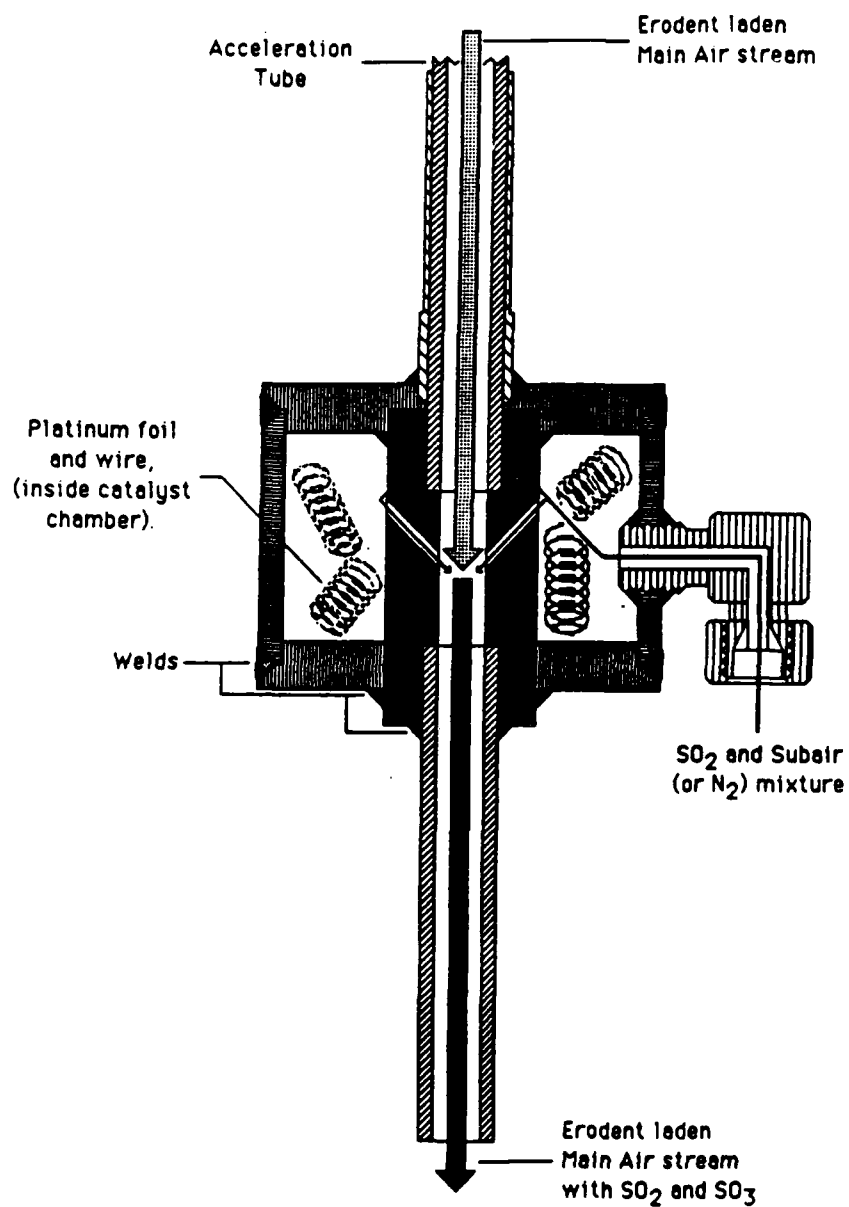
Figure 5: Cutaway of SO_2 Injector.
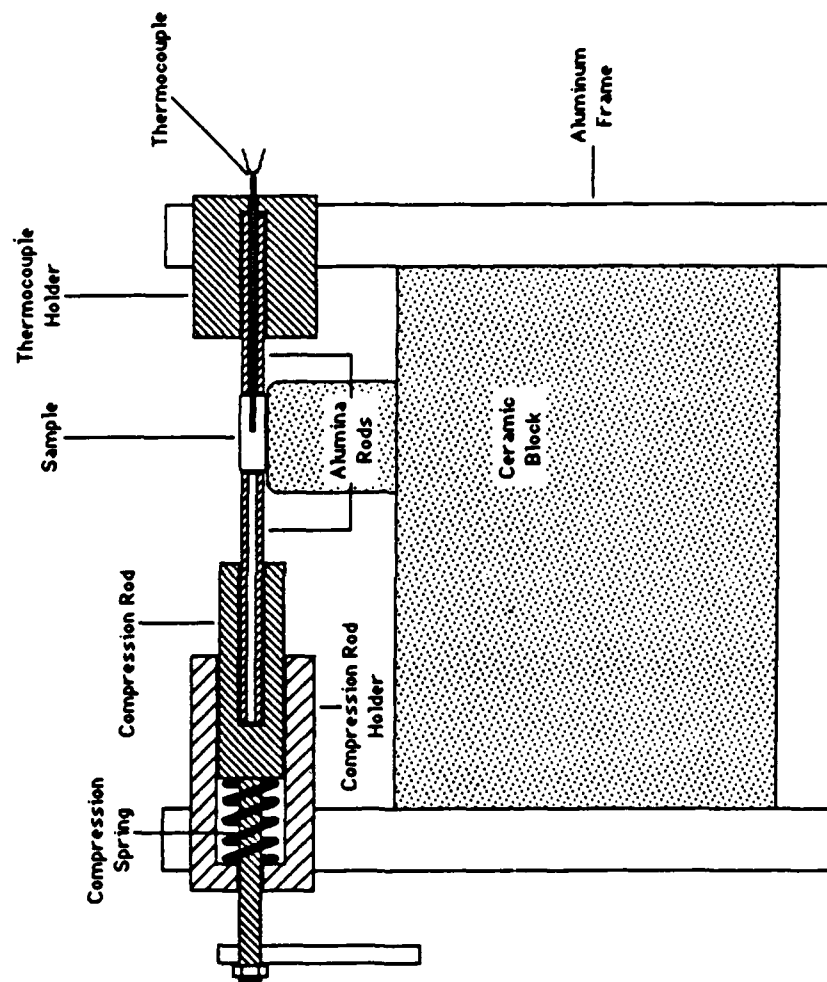
Figure 6: Cross-sectional view of Sample Holder.
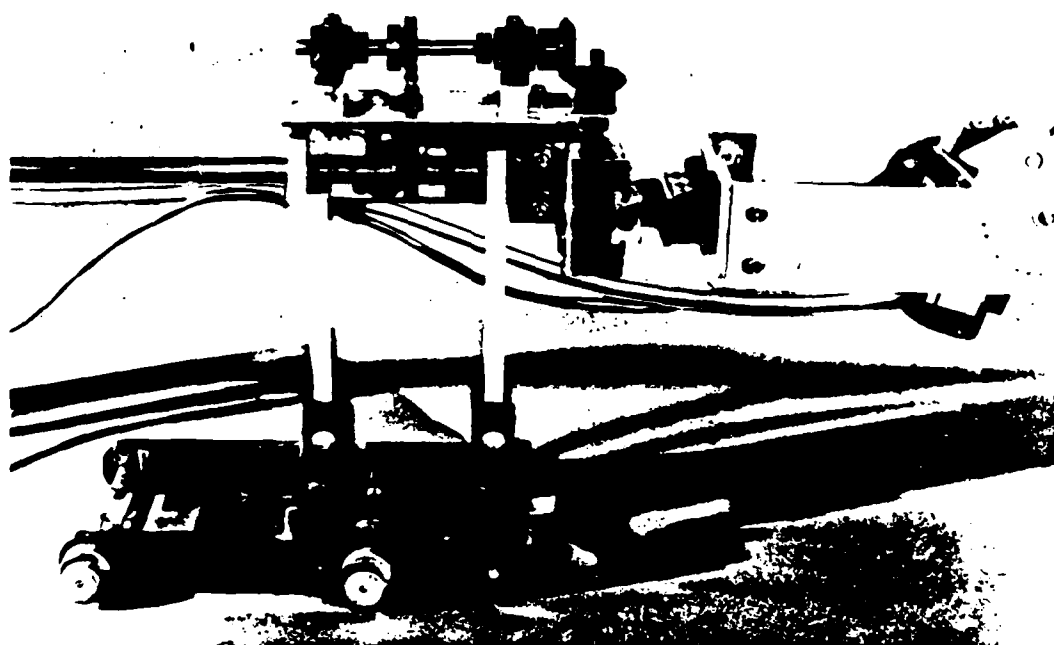
Figure 7: **Photograph of Sample Holder Manipulator.**

A. Rotary lobe
B. Rotary vane
C. Regenerative & rotary vane
D. Regenerative & rotary lobe

E   Turbine
F   Regenerative and turbine
G. Regenerative, centrifugal, & fan
H   Centrifugal & fan
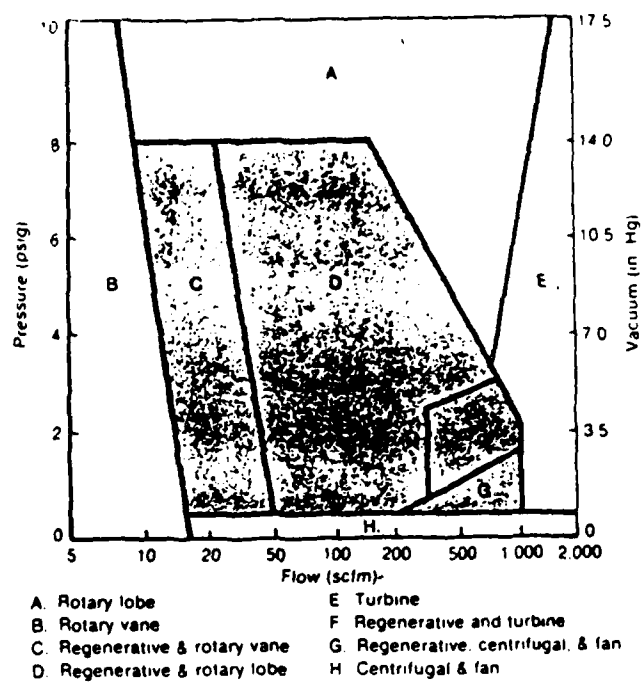
Figure 8:   Illustration of operating areas of various blowers.
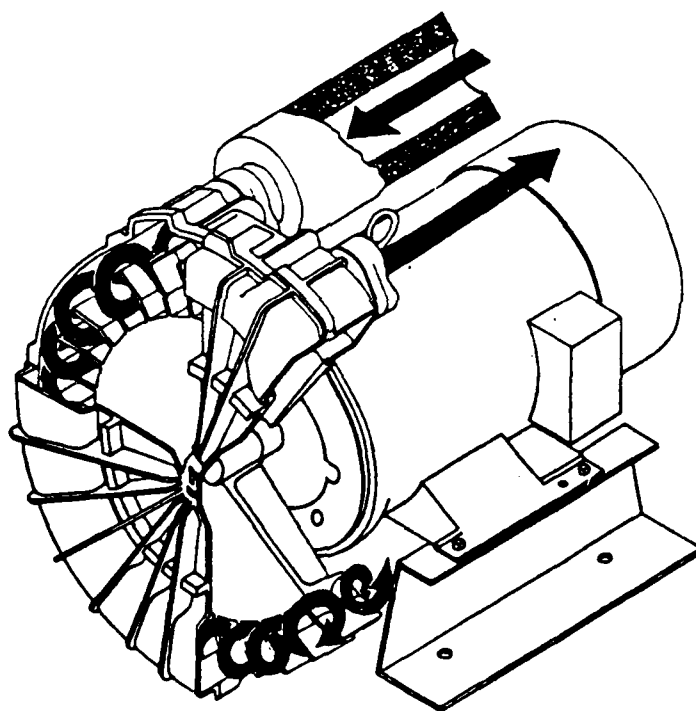
Figure 9: Cross-sectional view of regenerative blower.
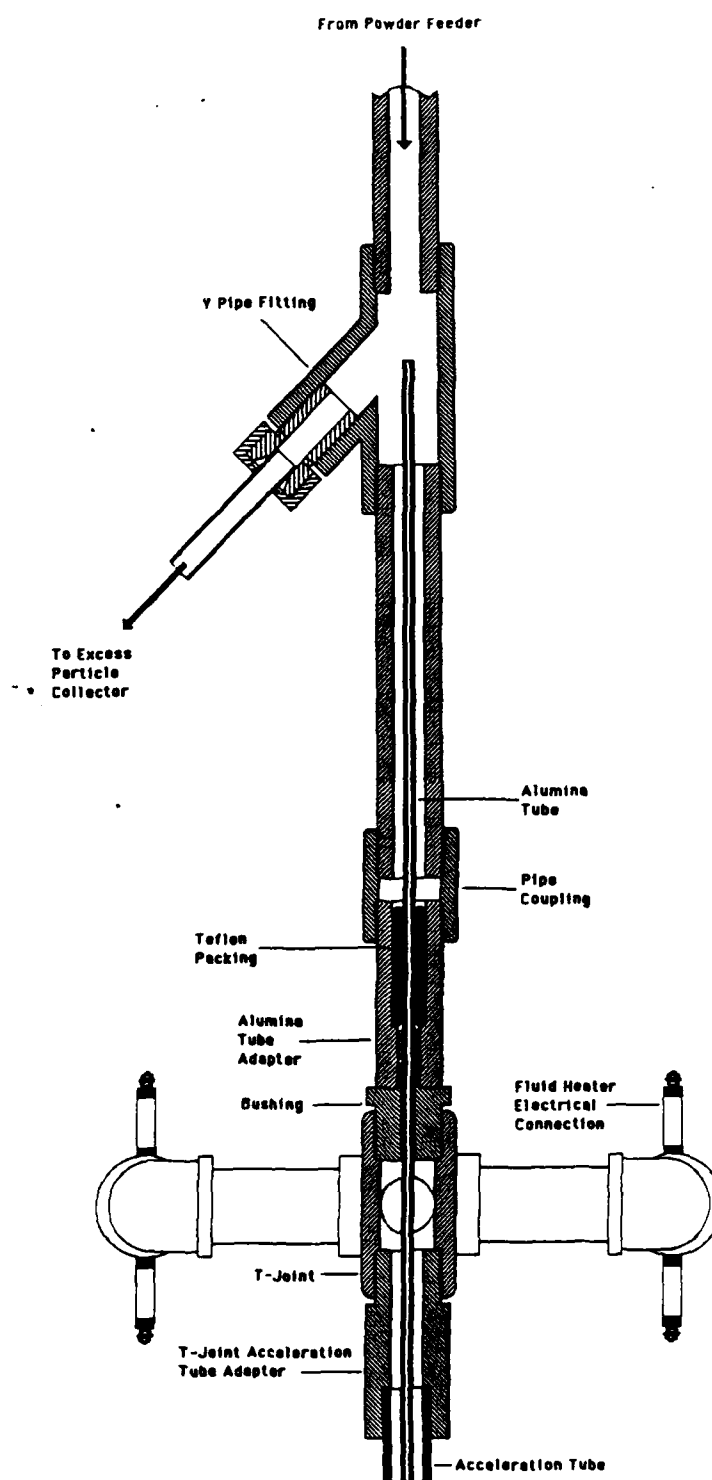
Figure 10: Cutaway of powder injector.

APPENDIX 2

Papers Published in Conference Proceedings

EROSION - CORROSION OF COATINGS AND SUPERALLOYS
IN HIGH VELOCITY HOT GASES

C. T. KANG, S. L. CHANG, N. BIRKS AND F. S. PETTIT
Metallurgical and Materials Engineering Department
University of Pittsburgh, Pittsburgh, PA U.S.A.

Particle induced erosion of alloys at low ($\sim$ ambient) temperatures and the corrosion of alloys at elevated temperatures in a wide variety of environments have been studied rather extensively. The effects of high velocity hot gases on corrosion of alloys have also been studied but to a more limited extent. On the other hand the degradation of alloys by combined erosion-corrosion in high velocity hot gases has not been studied in great detail. In this paper the erosion of alloys at ambient temperatures and the high temperature corrosion of alloys is briefly reviewed and then the combined erosion-corrosion of superalloys and coatings by hot gases is examined. It is shown that erosion-corrosion of alloys may occur by different mechanisms. When the particle energy is very large erosion can predominate to the extent that evidence of the corrosion process is extremely difficult to detect on the surfaces of alloys. Conversely, when the particle energy is low the effects of the erosion process can be neglected compared to the corrosion process. For some particle energies and corrosion rates interaction of the two processes can occur. Various types of interaction between erosion and corrosion processes are described.

INTRODUCTION

When structural alloys or coatings on such alloys are used at elevated temperatures in flowing gases conditions can be encountered where both corrosion processes (i.e. oxidation, mixed gas attack, hot corrosion) and erosion processes may take place concomitantly. It is therefore necessary to examine the mechanisms by which corrosion and erosion may take place concomitantly. In discussing combined corrosion-erosion a great range of conditions probably should be examined for a detailed understanding. At present the level of knowledge of corrosion-erosion processes is not sufficient to permit a totally general discussion. It therefore is appropriate to examine corrosion-erosion interactions under conditions similar to those which exist in some industrial applications. A reasonable choice is a gas turbine where materials can be exposed to elevated temperatures, high velocity gases containing particulate matter, and other environmental conditions that can cause oxidation, mixed gas attack and hot corrosion. While polymers as well as ceramics are used in gas turbines along with metallic alloys, this paper will consider only metallic systems. The two sections of a gas turbine in which conditions may be suitable for combined erosion-corrosion are the high pressure compressor and high pressure turbine. In the compressor the temperatures are often not high enough to cause substantial corrosion and alloys, especially coatings alloys, can be designed by considering only the erosion problem. In the high pressure turbine section very severe corrosion of alloys and coatings usually occurs, the presence of conditions producing erosion therefore represents a very

formidable problem. In practice when conditions causing combined corrosion-erosion are present in turbine sections a favored solution is to remove the particles from the gas stream through some sort of design change. Nevertheless, these conditions, when present, do represent conditions that can cause combined corrosion-erosion, and therefore they will be used in this paper as the basis for examining the interaction between corrosion and erosion.

In the following sections of this paper a very brief summary of metallic erosion will be presented followed by a concise description of the types of corrosion that can be observed in the high pressure turbine sections of gas trubines. Examples of combined corrosion-erosion will then be presented and discussed. These results will be used to begin to develop a map with which the different corrosion-erosion mechanisms can be compared and the factors important to transition from one mechanism to another can be identified.

EROSION OF METALLIC ALLOYS

The characteristic response of metals to erosive media as a function of time usually involves an incubation period during which very little erosion is evident, a period over which erosion is taking place at an increasing rate, and a period where the erosion rate is a maximum and approximately independent of time as indicated in Figure 1.
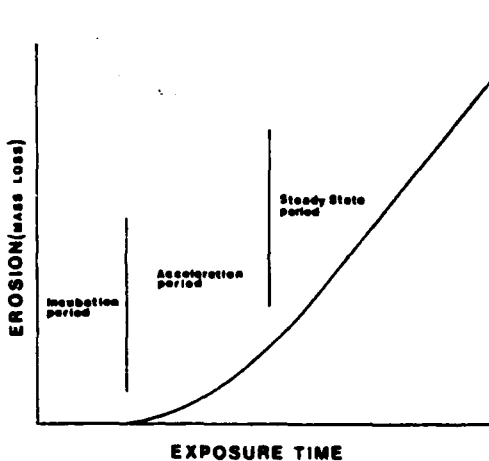
Figure 1. Erosion as a function of time of exposure.
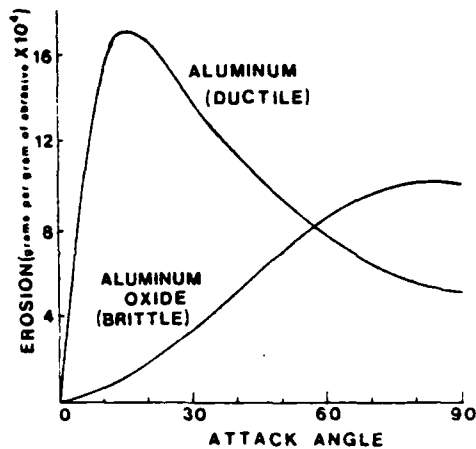
Figure 2. Erosion as a function of angle of impingement for aluminum and high-density aluminum oxide.

Most experimental erosion data are presented as the ratio of the mass of material removed to the mass of the impacting particles (gm/gm of abrasive) for a fixed exposure time increment where the exposure time corresponds to times at which the erosion rate is independent of time. Two types of response of materials to multiple solid impacts have been observed. One is a ductile response generally associated with metals and the other is a brittle response associated with

glasses or ceramics. The general form of the mass removal rate as a function of the angle of attack for each response is shown in Figure 2.

A number of theories have evolved to account for the erosion of materials. These models usually deal with ductile and brittle erosion separately. Rather complete descriptions of previous erosion research is available in review papers [1-3]. In this paper only the salient features of the current level of knowledge of erosion processes will be presented.

A common feature of many of the theories concerned with ductile materials is the application of a constant flow stress to represent material behavior. Finnie [4,5] treated the erosion of ductile materials as a gouging action similar to a tool cutting mechanism by using equations of motion for the abrasive particles. Bitter [6,7] divided the erosion process into a cutting wear mode (similar to Finnie's analysis) and a simultaneously occurring deformation wear mode. Bitter's model yields a relation between erosion rate and impingement angle which closely follows experimental data whereas the cutting wear model agrees with experimental data only at angles less than 45° unless empirical factors are used to account for roughening of the specimen surface. Bitter's model recognized that cutting wear does not occur at high impingement angles but it did not define the mechanisms by which material was removed by the deformation wear mode. Adjustable parameters with no assigned physical meaning were determined from measured data and used to account for the deformation wear mode. Hutchings and Winter [9-10] used optical microscopy and high speed photography to characterize the impact event. It was concluded that material removal can occur by plowing deformation or by two types of cutting deformation.

Mamoun [11] developed an expression for the erosion of a ductile target based on an erosion mechanism. He assumed that surface degradation could occur through a mechanism resembling fatigue as multiple particles impact the surface of a material. Particulate erosion in many ways is similar to wear and Jahanmir [12] has extended delamination theories developed to account for wear [13] to the case of particle erosion. The use of a delamination theory is similar to Mamoun's approach in that it does not presuppose that each instance of particle impact results in material loss, but postulates a mechanism for accumulating damage which eventually leads to material removal. Levy and Bellman [14] have observed that plastic deformation within the impacted surface leads to the formation of platelets similar to those documented for delamination wear [13]. They propose that such platelets, once formed, are quickly detached upon subsequent particulate impacts. Follansbee [15] has also observed platelet formation during erosion and has developed an erosion model based upon a fatigue fracture failure criterion.

In summary, the erosion of metals can consist of discrete, isolated impact craters, Figure 3a, or more uniformly eroded surfaces, Figure 3b. The uniformly eroded surfaces are common to erosion produced by multiple particle impacts and, as such, consist of materials removal processes involving accumulative deformation.

The mechanisms by which the accumulative deformation results in material removal are not well defined and probably are affected by numerous factors related to the elastic and plastic deformation of metals. It is also known that heat is generated in the specimen and the particle on impact but the effect of this on erosion mechanisms has not been established.
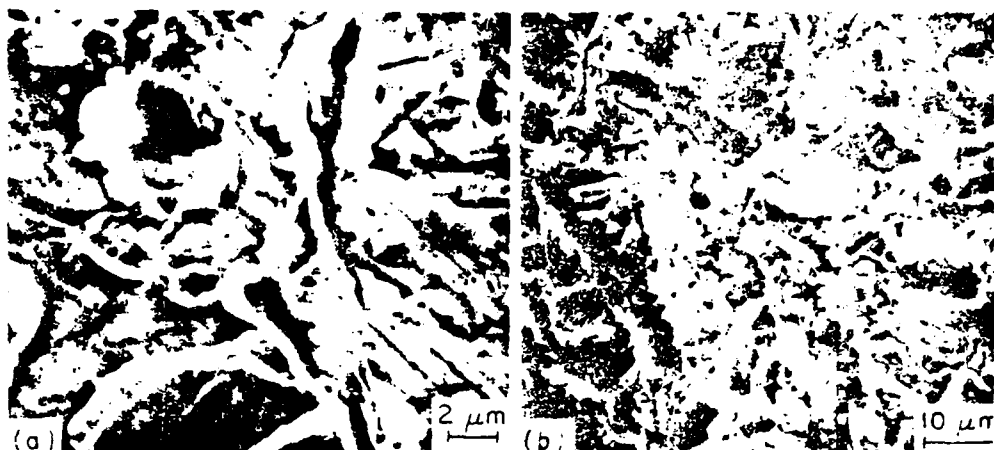
Figure 3. (a) Erosion impact craters on steel surface [16].
(b) AISI 310 steel surface after erosion at 25°C at 40 m/s [17].

In discussing the erosion-corrosion of metallic alloys it is also necessary to consider the erosion of ceramics since the corrosion products formed upon metallic alloys usually consist of some ceramics. Erosion of ceramics is usually viewed as a brittle process where material removal occurs mainly by chipping, Figure 4. A more modern view of ceramic erosion is based on the concept that the chipping process may consist of two regimes of cracking, namely, an elastic response regime and a plastic response regime [18]. Several types of fracture have been observed in the elastic regime, from single cone (Hertzian) cracks [19-21] to arrays of short circumferential surface cracks [18]. Material removal occurs by the interaction of these cracks, but the details of the process are complex and, as yet, poorly defined. It is evident that the fracture threshold will depend on specimen properties such as the surface flaw size distribution, the fracture toughness and the elastic wave speed. In the case of the plastic response both radial and lateral cracks are induced. The problem is an elastic-plastic one, and the hardness and the fracture toughness are the prime material parameters that control the extent of the fracture and consequently the erosion. The mechanism of material removal consists of chip formation which occurs due to the subsurface network of laterial cracks.

HIGH TEMPERATURE CORROSION OF METALLIC ALLOYS

A great number of high temperature corrosion processes could be considered when discussing corrosion in preparation for a discussion of combined erosion-corrosion. In practice, however, the systems of most interest are those which are relatively resistant to degradation, and consequently only corrosion resistant systems will be considered in this paper. In order for an alloy to be resistant to high temperature corrosion, the alloy must not react with the environment in which it is exposed (immunity) or, the product formed as a
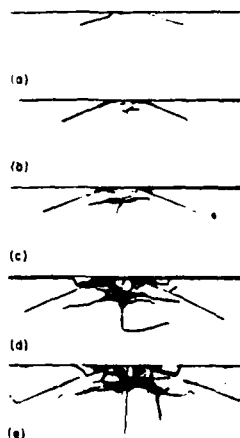
Figure 4. Photographs showing sequence of fracture damage when a sphere is pressed against a glass surface [18].
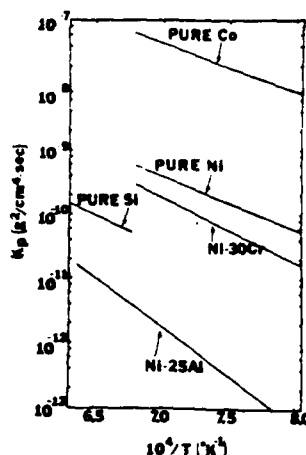
Figure 5. Temperature dependence of the parabolic rate constants for the growth various oxide barriers on metals and alloys (CoO on Co, NiO on Ni, SiO_2 on Si, Cr_2O_3 on Ni-30% Cr, $\alpha-Al_2O_3$ on Ni-25% Al). The oxidizing environments for the data presented were 0.1 atm. oxygen for Ni, Ni-30Cr and Ni -25 Al; 0.125 atm. oxygen for Co and 1 atm. oxygen for Si.

result of reaction must inhibit subsequent reaction between the environment and the alloy [22,23] (passivation). Very few practical alloys posses both immunity to corrosive environments and desirable physical properties, hence virtually all the alloys encountered in practice achieve resistance to corrosion by passivation.

In most of the environments in which engineering alloys are used oxygen is very often present. Oxidation of alloys is therefore a very important form of high temperature corrosion. Other reactants in addition to oxygen however can be present and corrosion of alloys concomitantly by a number of reactants (mixed gas attack) is an important form of high temperature degradation. While gaseous in-duced degradation of alloys is the principal means of high temperature corrosion, deposits can be formed on alloys during use which may significantly affect the gas-induced corrosion process. Deposit modified high temperature corrosion is called hot corrosion and is an important means of alloy degradation especially in the case of materials used in gas turbine engines. In summary, the important forms of high temperature degradation of corrosion resistant systems are oxidation, mixed gas attack and hot corrosion.

When an alloy is exposed to oxygen at elevated temperatures the type of oxide barrier which is formed upon the alloy surface is determined by the composition of the alloy. The most effective oxide barriers to inhibit attack are Al_2O_3, Cr_2O_3 and SiO_2 as can be seen by comparing rate constants for the growth of these oxides, Figure 5.

Alloys possessing resistance to high temperatue corrosion therefore usually contain sufficient concentrations of aluminum, chromium or silicon such that oxides of these elements can be formed as continuous layers over the alloys' surfaces via selective oxidation. Factors which affect the selective oxidation of such elements have been discussed in previous papers [22,23].

Even though continuous and protective barriers of oxides such as Al_2O_3, Cr_2O_3 or SiO_2 can be formed on alloys via selective oxidation, as the alloys are continually exposed to the oxidizing environment in service the barrier becomes damaged. A principal means of damage occurs through thermally induced stresses that cause cracking and spalling of the protective oxide barriers. Cracking and spalling of the oxide scale followed by development of new oxide barriers depletes the alloy of the elements which are to be selectively oxidized. Hence, eventually the alloy will become so severely depleted of the element relied upon for selective oxidation that it will not be possible for the desired oxide to be formed as a continuous layer over the surface of the alloy and a less protective scale will begin to be formed. The degradation sequence of alloys in oxygen therefore consists of the development of the most thermodynamically stable oxides and then less stable oxides as the alloy becomes degraded. In the case of corrosion resistant alloys the more stable oxides also provide the most protection, hence, as the less stable oxides begin to form, the oxidation resistance of the alloy begins to decrease as illustrated by the data presented in Figure 6.
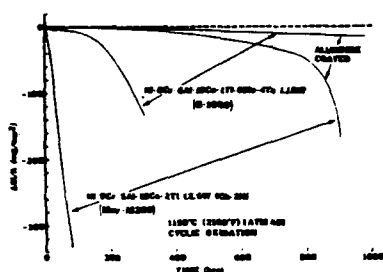
Figure 6. Weight change versus time data for the cyclic oxidation of two nickel-base superalloys and these two alloys coated using a diffusion aluminizing treatment. The degradation of these alloys consists of two stages. An initial stage of less severe attack (not evident on one of the uncoated alloys for the time scale used) and a subsequent stage of more rapid attack.
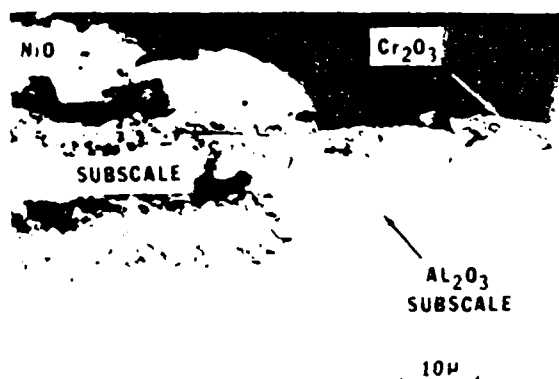
Figure 7. Nonuniform oxidation morphology developed on Ni-10Cr-1Al After 20 hr. of oxidation of 0.1 at: of oxygen at 1000°C. This type of oxide scale morphology frequently develops on alloys during cyclic oxidation testing as less protective oxides become stable.

This degradation sequence is followed for both structural alloys as well as coatings on such alloys. Since the coating alloys are designed for resistance to oxidation, it takes a longer time for the less protective oxides to be formed as can be seen upon comparing data for uncoated and coated alloys in Figure 6. In Figure 7 a photograph is presented which shows less protective nickel oxide being formed on an alloy which relies upon the development of a Cr_2O_3 scale for oxidation resistance.

In the case of mixed gas attack the most corrosion resistant systems are those upon which barriers of Al_2O_3, Cr_2O_3 or SiO_2 are formed. Many mixed gas environments contain sufficient oxygen for these oxide scales to be formed. When such alloys are used the degradation sequence described previously is followed but when the most protective oxide barrier can no longer be formed corrosion products involving the other reactants in the gas phase are formed as illustrated in Figure 8.

In the case of hot corrosion attack, the degradation sequence also involves formation of the most protective oxide barriers with the eventual formation of less protective corrosion product phases as indicated in Figure 9.

The hot corrosion process may involve a number of different mechanisms by which the protective oxide barrier is destroyed, depending upon the conditions causing the hot corrosion attack. It is sufficient in this paper to indicate that resistance to hot corrosion attack is obtained via selective oxide barrier formation and that the hot corrosion conditions usually decrease the time period over which the alloy is capable of resisting attack by repeatedly reforming the desired protective oxide barrier.

In this discussion on high temperature corrosion resistant systems, the importance of the degradation sequence has been emphasized. In particular, in the case of oxidation, mixed gas attack or hot corrosion the degradation sequence consists of an initial stage during which oxide reaction product barriers are formed via selective oxidation and protect the alloys from the environmentally induced attack. Eventually in this sequence lesser protective products begin to be formed and the alloys can be considered to be no longer resistant to the environment. It is worth emphasizing that the adherence of the oxide barrier is also another rather critical factor determining how long the alloy will be capable of sustaining the most protective oxide barrier on its surface. Oxygen active elements and/or inert oxide particles can be used to significantly improve the capability of oxide scales to resist cracking and spalling from the surfaces of alloys [24-26]. The mechanism by which such oxides or oxygen active elements improve the scale adherence is not known and a number of different mechanisms have been proposed.

EROSION - CORROSION OF ALLOYS

To illustrate some of the interactions that have been observed for combined erosion-corrosion, data obtained from specimens exposed at 870°C to α-Al_2O_3 particles (0.3, 2.5 and 20 μm average particle size) with velocities of about 190 m/s will be used [27]. The corrosion conditions consisted essentially of
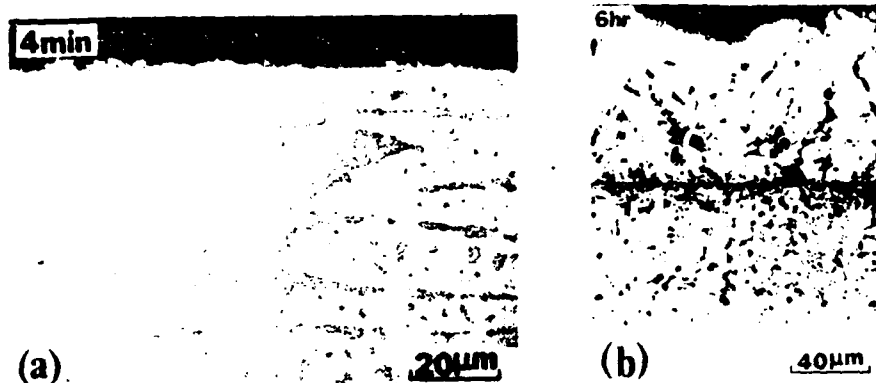
Figure 8. Photomicrographs showing the reaction products formed on Co-25Cr-6Al during exposure to a $H_2S/H_2/H_2O$ gas mixture with P_{S_2} = $10^{-5.35}$ at 900°C. (a) After 4 min. of exposure the reaction product is a very thin Al_2O_3 - rich scale which is not evident and the alloy substrate exhibits no features indicative of degradation. (b) After 6 hr. a substantial reaction product has been formed which is composed of sulfides above and below an oxide scale (arrows).

oxidation in air or hot corrosion in air induced by deposition of Na_2SO_4. Both superalloy specimens (i.e. X-40, IN738) and superalloy specimens with coatings (diffusion aluminide or MCrAlY) will be considered.

Exposure of specimens to oxidizing gases containing about 130 ppm of 20µm particles resulted in very severe degradation of all the alloys. For example, weight losses of about 200 mg/cm^2 were observed after about 30 hours of exposure. A significant difference between the α-Al_2O_3 formers (coated alloys) and Cr_2O_3 - formers (uncoated alloys) was not apparent. The surfaces of a typical specimen after preparation, after oxidation, and after oxidation-erosion are presented in Figure 10. Detailed examination of the surfaces of the specimens exposed to oxidation-erosion showed that as the angle of impingement was decreased the impact craters became more elongated, Figures 11a and 11b. These results are similar to those observed for erosion of metals at room temperature. The surfaces of all the specimens exposed to the oxidation-erosion conditions did not appear to contain any oxidation products. It was determined, however, that all of the surfaces were covered with very thin layers of oxide scales, Figure 11c. The results obtained with 20 µm particles show that the erosive component is very large compared to the oxidation component. Oxidation is occurring. The removal of metal due to cutting and deformation is so rapid, however, that the amount of oxidation on freshly exposed surfaces is negligible. For such conditions it appears that the oxidation process can be neglected and the metal loss can be assumed to be determined solely by the erosion process.

Oxidation tests performed under conditions similar to those described in the preceding paragraph but with 300 ppm of 2.5 µm α-Al_2O_3 particles rather than
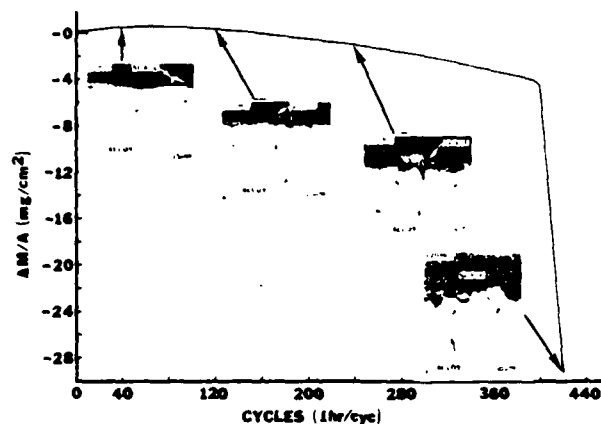
Figure 9. Weight change versus time data and corresponding microstructural features for the cyclic hot corrosion of Na_2SO_4-coated (5 mg/cm² applied every 20 hours.) Ni-30Cr-4Al in air at 900°C. The amount of sulfide particles (small black arrows) increases until the oxidation of the sulfide phases significantly affects the rate of attack.

20 μm particles caused a significant amount of alloy degradation. It was substantially less than that observed with 20 μm particles and it appeared to be influenced by the type of oxide scale which was formed on the surface of the alloys. For example after 30 hours of exposure, the Cr_2O_3 - formers lost about 60 mg/cm² compared to about 30 mg/cm² for the Al_2O_3 - formers. The surface of a typical specimen is shown in Figure 12. The surface features did not appear to be markedly dependent upon the angle of impingement. The features observed upon the surfaces of specimens appear to consist of platlets and may be similar to those observed on some metals during erosion at ambient temperatures [14]. The observation that the weight-losses of the Cr_2O_3 - formers were significantly larger than those of the Al_2O_3-formers indicates that the Al_2O_3 scales had some affect on the combined oxidation - erosion process. It has been determined that Cr_2O_3 scales do form volatile products (i.e. CrO_3) in gases at high velocities (e.g. ∿ 200 m/s) even at temperatures as low as 870°C [27]. It appears that in the case of the Al_2O_3 - formers the oxide scale was thick enough to affect the erosion process. Results obtained in other investigations [28,29] also suggest that oxidation products can inhibit erosion processes.

Oxidation-erosion experiments performed with 0.3 μm Al_2O_3 particles at 870°C did not produce any evidence of erosion on either the Al_2O_3-formers nor the Cr_2O_3 - formers. The results were similar to those obtained without any particles. These observations show that there are conditions where the erosion component is negligible compared to the corrosion component.

Specimens which were exposed to combined erosion-hot corrosion conditions using Na_2SO_4 to induce hot corrosion and 2 μm Al_2O_3 particles to cause erosion were very severly degraded. Results obtained for a coated cylindrical
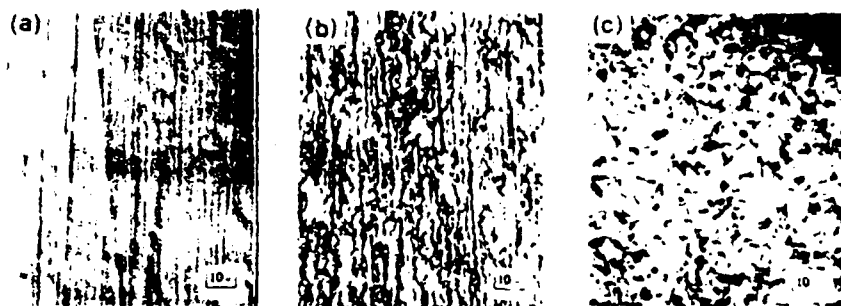
Figure 10. Scanning electron micrographs of replicas from X-40.
(a) pre-test condition (600 grit polish), (b) after 4.5 hours of
oxidation at 870°C, (c) after 4.5 hours of oxidation - erosion
at 870°C (130 ppm, 20 μm α-Al$_2$O$_3$ 90° impingement angle.)
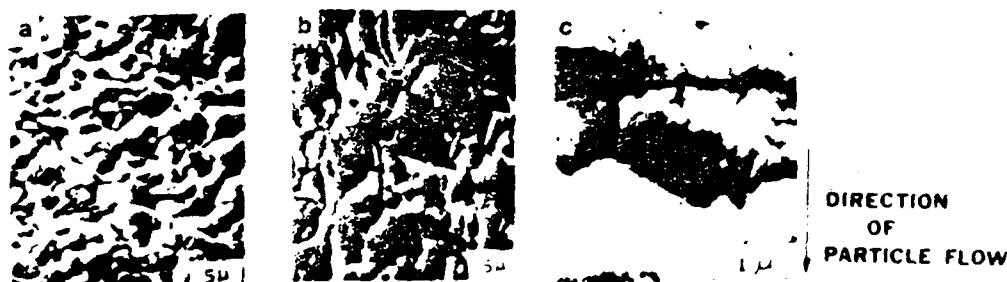

**DIRECTION
OF
PARTICLE FLOW**

Figure 11. Scanning micrographs illustrating surface features
developed on IN738 after 20 hrs. of oxidation-erosion testing
at 871°C using 20 μm α-Al$_2$O$_3$ at a loading of 130 ppm. At impact
angles of 90°, (a) craters having raised edges are ev lent. As
the angle of impact is decreased, the impact craters become
elongated and at 5°, (b) appear as micromachining markings.
Features were observed on the impact craters, arrows (c) that
indicated the surfaces of the specimens were covered with a
very thin layer of oxide.

specimen are presented in Figures 13. The leading edge of this specimen was
exposed to erosion-hot corrosion conditions whereas the trailing edge was
exposed to only the hot corrosion component. At some angles of particle im-
pingement the coating has been completely consumed, Figure 13d, whereas on the
trailing edge the coating has undergone very little degradation, Figure 13e.
The weight losses of the specimens exposed to the combined erosion-hot corrosion

conditions were substantially greater than the sum of the weight losses for hot corrosion with no erosion and erosion-oxidation. These results indicate that the erosion and hot corrosion processes are interacting such that their combined effect is greater than the sum of the two processes acting independently. In this paper it is not possible to discuss this observed interaction in great detail. As shown in Figure 14, it was observed that the specimens subjected to combined erosion-hot corrosion had less corrosion product on their surfaces than those exposed only to the hot corrosion conditons. It appears that the particles removed some of the porous oxide. This caused the hot corrosion component to be increased since the Na_2SO_4 was not retained in the porous scale and hence the Na_2SO_4 more effectively covered the alloy surface. As shown in Figure 15, the hot corrosion component caused portions of the alloys to be undercut. It is believed that such a condition permitted the particles to more efficiently remove metal from the surface of the alloy.
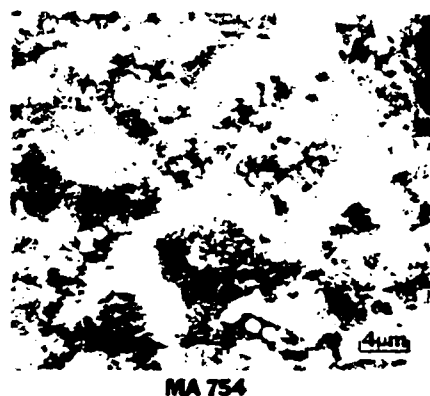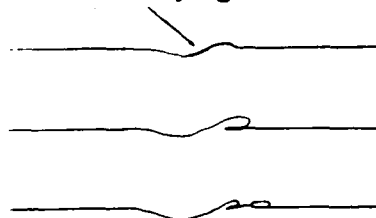
Figure 12. Surface features and schematic diagram of proposed mechanism of metal removal by 2 μm Al_2O_3 abrasive. Features are typical of high and intermediate impingement angles, the small particles on the surface possible becoming detached by a mechanism of the type illustrated in the sketch.

The results that have been presented on combined erosion-corrosion have not been very extensive. These results are sufficient however to illustrate some of the types of interactions which are believed to be important in regards to combined erosion-corrosion, in particular.

·When the relative magnitude of one of the erosive and corrosive components is very small compared to the other, the smaller of the two components does not exert a significant effect on the degradation process.

·When the magnitude of the components are comparible, interactions between erosion and corrosion can be expected, the following interactions have been observed.

- 97 -
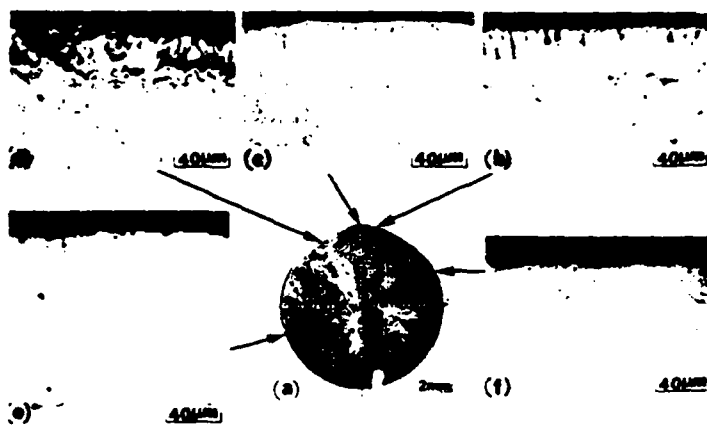
Figure 13. Typical microstructures that developed during exposure of a CoCrAlY coating on IN738 to 28 hours. of erosion-hot corrosion (2.5 μm Al$_2$O$_3$, 0.05 mg/cm^2 hr. of Na$_2$SO$_4$-22% K$_2$SO$_4$) at 871°C.
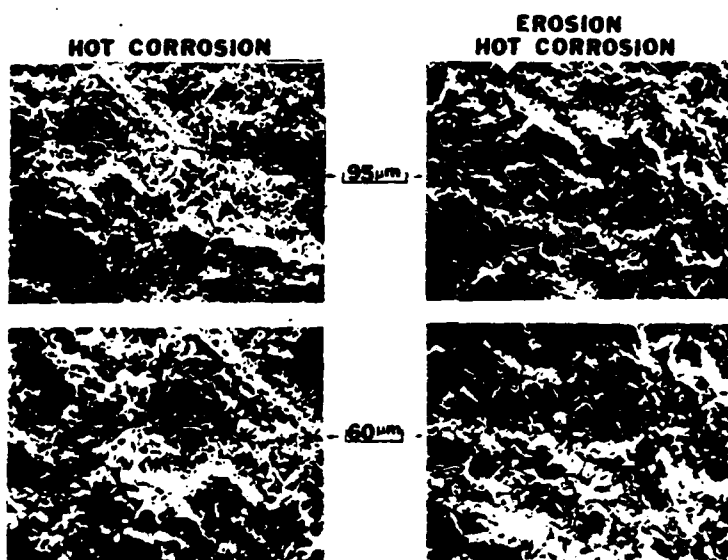

Figure 14. Scanning micrographs showing features of the oxide scales formed on IN738 after exposure to the hot corrosion test (0.05 mg/cm$_2$-hr. Na$_2$SO$_4$-22% K$_2$SO$_4$) and the erosion-hot corrosion test (0.05 gm/cm^2-hr Na$_2$SO$_4$ - 22% K$_2$SO$_4$ and 300 ppm 2.5 μm α-Al$_2$O$_3$ particles) at 871°C. The arrows identify the same areas at progressively higher magnifications. It is apparent that the erosive component has removed much of the porous oxide that is normally developed during hot corrosion attack.
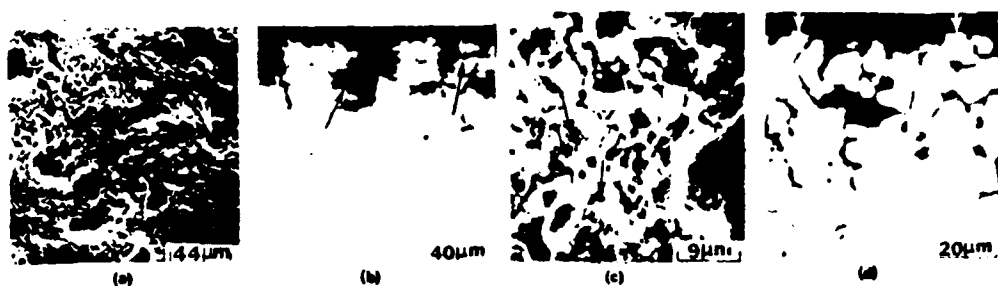
Figure 15. Photographs of IN738 after 28 hours exposure to erosion
hot corrosion conditions at 870°C to illustrate features of the
erosion-hot corrosion process; large craters on the surface, arrows
(a) are believed to occur because of dislodgement of oxide and alloy,
arrows (b) Numerous areas of the surface are covered with oxide,
black arrows (c) but exposed alloy or alloy covered with much
thinner oxide is also evident, white arrows (c) and (d).

- corrosion inhibited erosion
- corrosion enhanced erosion
- erosion enhanced corrosion

For instance relatively large particles (20 µm) impacting at high velocities
would be expected to cause vigorous erosion compared to which the oxidation
component is small, particularly if the oxide forms only slowly, e.g. Al_2O_3. If
the same conditions are maintained but the particle size is decreased to, say,
2 µm, the impact energy rate will be decreased and the oxide formed might begin
to inhibit the erosion process, possibly depending on the nature of the oxide
formed. Alternatively the impacts may crack the scale leading to enhanced
oxidation.

At extremely small particles sizes (0.3 µm) the erosion component may even
become negligible compared with oxidation degradation, in fact these particles
may deposit on the existing growing oxide scale.

The boundaries at which these changes in behavior occur will also depend
on the scale growth rate.

It may be possible to represent these complex interactions by using a
diagram, as sketched in Figure 16, using particle energy and scale growth rate
as coordinates. On Figure 16 are delineated areas of degradation by pure erosion,
oxidation inhibited erosion, erosion enhanced oxidation and pure oxidation.
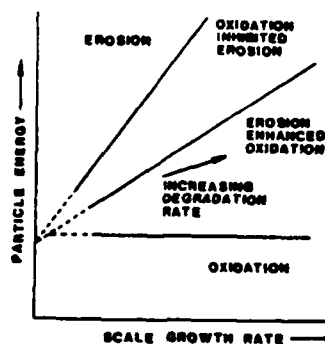
Figure 16. Schematic diagram to illustrate the possible relationship
between different regimes of materials degradation as a function of
particles energy and scale growth rate for a combined erosion-
oxidation process.

CONCLUDING REMARKS

The combined erosion-corrosion of alloys in high-velocity, hot, gases has
not been studied in great detail. In order to understand this type of alloy
degradation it is necessary to utilize the knowledge which is available on
ambient temperature erosion and high temperatue corrosion and apply it to
investigations of combined erosion-corrosion. The results which are available
indicate that, depending upon the magnitude of the erosive and corrosive com-
ponents, different types of degradation modes are important. It is necessary
to interrelate these degradation modes as a function of the intensity of the
erosive and corrosive components.

ACKNOWLEDGEMENT

REFERENCES

[1] Erosion Control In Energy Systems, National Materials Advisory Board,
     National Academy of Sciences, 1977, Report No. NMAB-334.

[2] W. F. Adler: Assessment of the State of Knowledge Pertaining to Solid
     Particle Erosion, Tech. Report, Effects Technology, Inc., 1979, NTIS,
     Report No. ETI-CR79-680.

[3] A. W. Ruff and S. M. Wiederhorn, Erosion by Solid Particle Impact; Treatise
     on Materials Science and Technology, Vol. 16, C. M. Preece, editor;
     Academic Press, New York, 1979.

[4] I. Finnie, Wear, 3(1960), 87.

[5] I. Finnie, A. Levy, D. H. McFadden, Fundamental Mechanisms of Erosive Wear
     of Ductile Materials by Solid Particles; Erosive: Prevention and Useful
     Applications, W. F. Adler, editor, ASTM STP 664, 1977.

[6] J. G. A. Bitter, Wear, 6(1963), 5.

[7] J. G. A. Bitter, Wear, 6(1963), 169.

[8] I. M. Hutchings, R. E. Winter and J. E. Field, Proc. Royal Society Landon, A 348 (1976), 379.

[9] R. E. Winter and I. M. Hutchings, Wear, 34 (1975), 141.

[10] R. E. Winter and I. M. Hutchings, Wear, 29 (1974), 181.

[11] M. M. Mamoun, Materials Science Division Coal Technology Third Quarterly Report, Tech. Report ANL-75-XX3, Argonne National Laboratory, 1975, Appendix: Analytical Models For the Erosive-Corrosive Wear Process.

[12] S. Jahanmir, Wear (1980), 309.

[13] N. P. Suh, Wear, 44 (1977), 1.

[14] R. Bellman, Jr. and A. Levy, Erosion Mechanism in Ductile Metals, Tech. Report, Lawrence Berkeley Laboratory, LBL-10289, 1980.

[15] P. S. Follansbee, Mechanisms of Erosive Wear of Ductile Metals Due to the Low Velocity, Normal Incidence, Impact of Spherical Particles, Ph.D. Thesis, Carnegie-Mellon University, 1981, Pittsburgh, PA.

[16] L. K. Ives, J. P. Young and A. W. Ruff, Nat. Bur. Stds., SP 468, (1977) 145.

[17] L. K. Ives, J. Eng. Mater. Tech. Trans. ASME 99(1977), 126.

[18] A. G. Evans and T. R. Wilshaw, J. Mater, Sci., 12(1977), 97.

[19] G. L. Sheldon and I. Finnie, Trans. ASME, 88B(1966) 393.

[20] W. F. Adler, Analysis of Multiple Particle Impacts on Brittle Materials, AFML-TR-74-210, (1974).

[21] W. F. Adler, Erosion of Fused Silica by Glass Beads, Erosion, Wear and Interfaces with Corrosion, American Society for Testing and Materials, STP 567 (1974).

[22] F. S. Pettit, C. S. Giggins, J. A. Goebel and E. J. Felten, Oxidation and Hot Corrosion Resistance, Alloy and Microstructural Design, J. K. Tien and G. S. Ansell, editors; Academic Press, New York, 1976.

[23] F. S. Pettit and G. W. Goward, High Temperature Corrosion and Use of Coatings for Protection, Metallurgical Treatises, J. K. Tien and J. F. Elliott, editors, The Metallurgical Society of AIME, Warrendale, PA., 1981.

[24] J. K. Tien and F. S. Pettit, Met. Trans. 3(1972) 1587.

[25] F. H. Stott, G. C. Wood and J. G. Fountain, Oxid, Metals, 14(1980) 135.

[26] D. P. Whittle and J. Stringer, Phil. Trans. Roy Soc. Lond. 295(1980) 309.

[27] R. H. Barkalow, J. A. Goebel and F. S. Pettit, Materials Problems in Fluidized - Bed Combustion Systems, High-Temperature Erosion-Corrosion by High-Velocity (200 m/s) Particles, CS-1448, Research Project 979-4, Electric Power Research Institute, Palo Alto, CA., 1980.

[28] J. P. Young and A. W. Ruff, J. Eng. Mater. Tech. Trans. ASME 99 (1977) 121.

[29] N. A. Mikhailova, Zashch. Metall. 11 (1975) 641.

SYNERGISM IN THE DEGRADATION OF METALS EXPOSED TO EROSIVE

HIGH TEMPERATURE OXIDIZING TEMPERATURES

by

C. T. Kang
Union Carbide
Coating Service
1500 Polco Street
Indianapolis, IN 46224

S. L. Chang, F.S. Pettit, N. Birks
Materials Science and Engineering Department
University of Pittsburgh
848 Benedum Hall
Pittsburgh, PA 15261

ABSTRACT

Degradation of metals in service, at high temperatures in oxidizing atmospheres, by the conjoint action of erosion and oxidation processes is observed in many situations which range from the low velocity, large particle impact, associated with fly ash in power producing coal fired boilers to high velocity, small particle impact associated with the stator and turbine stages of gas turbines. Whereas substantial progress has been made towards understanding the erosion processes at room temperature and oxidation processes at high temperature, progress in generating basic understanding of the conjoint action of these processes at high temperature has been slow. This has been due primarily to the difficulties of controlling all of the parameters involved in laboratory experiments. Previous work in this area is reviewed, an apparatus is described that allows the conjoint action to be studied under closely controlled conditions and initial results, carried out at 90° impact angle are described for the cases of nickel and cobalt metals. From the results obtained it is shown that several regimes of interaction exist and are observed depending on the relative severity or intensity of the erosion and oxidation components of the interaction.

INTRODUCTION

The degradation of materials due to the simultaneous action of erosion and high temperature corrosion is a serious form of degradation of alloys in service in energy producing systems. Although advances have been made in the understanding of room temperature erosion of materials and in our knowledge and in understanding of high temperature oxidation processes, very little is understood about the basic mechanisms by which the two processes, occurring simultaneously, interact to cause enhanced degadation of metals and alloys. There is very real need to identify and characterize the various modes, or regimes, of interaction of erosion and oxidation to the point that the behavior of specific materials can be predicted and suitable materials, or combinations of materials, can be designed to combat the synergistic degradation.

Erosion interacting simultaneously with high temperature corrosion or oxidation is observed in essential processes such as coal fired power producing boilers, fluidized bed combustors (both atmospheric and pressurized), incinerators, in the high pressure compressor and in the turbine sections of gas turbines, in fact the interaction is observed wherever metals are exposed to high temperature, high velocity gases. In all observed cases the degradation under conjoint action is seen to be more than the sum of the degradation expected under erosion or oxidation singly in the absence of the other component.

The single phenomena have been widely studied; erosion mainly at low temperatures and oxidation at high temperatures. The extent of current knowledge and understanding of both fields is well documented by the excellent review paper by Shewmon and Sundararajan (1) concerning the room temperature erosion of metals and by numerous papers and texts in the case of high temperature oxidation (2,3,4,5).

The mechanisms by which erosion is thought to occur were developed generally for low or room temperatures and can be divided into several groups according to the principle mechanism of removal proposed.

(a) Cutting:

It is proposed by Finnie, (6) that the erosive particles channel, or scoop, out a 'chip' of metal by a simple machining action. In effect this means that the volume displaced on impact is cut out and removed. In this case the particle was assumed to act in a manner very similar to the tip of a cutting tool. The analysis led to an interpretation of the variation of the extent of erosion damage with cutting angle rising to a maximum at about 20-30° incidence, but it is difficult to accept that an unsupported particle will maintain a constant alignment to the surface of the specimen.

(b) Ploughing:

It was later found (7) that very few of the incident particles, 10-12% of them, actually were involved in the process of removing metal. The majority of the impacts simply rearranged the surface by plastic deformation. In terms of a particle incident at an acute angle to the surface, this was called ploughing and the displaced material was piled up at the side of the trench formed during the raking impact.

(c) Delamination:

Other mechamisms involve work hardening which causes successive hardening of the surface by plastic shear and led to the nucleation of voids below the surface layer (8) which were thus caused to become unstable and eventually to detach.

(d) Low Cycle Fatigue

This was another mechanism that relied on the effect of repeated impacts in hardening the metal, promoting crack formation and encouraging detachment of lips of metal raised proud of the surface by the original impact (9).

(e) Platelet

The formation of platelets by the progressive deformation and extrusion of metal lips displaced proud of the surface by the initial impact. It is proposed (10) that, although local heating may restrict work hardening in the immediate surface

layers, below the surface a zone is hardened, or remains, hard and behaves as an anvil against which the surface is progressively displaced and extruded by the erosive impacts.

(f) Cracking

Cracking is a mechanism largely reserved for the explanation of erosive action on brittle materials (11). Cracks are held to form as a result of elastic deformation followed by brittle failure Alternatively, under the contact area between the particle and the substrate, plastic deformation may give rise to the elastic-plastic mechanism and lead to the formation of crack systems. The intersection of the crack systems loosens whole pieces of the brittle material which are then removed on subsequent impacts.

The work performed at room temperature and the mechanisms proposed to account for erosion form a useful starting point for the consideration of high temperature erosion. There is one important difference in that, at high temperature, work hardening does not occur, however the very high strain rates which have been estimated to be of the order of 10^5 -10^9 (12) almost ensure that strong local adiabatic plastic deformation will occur. This may give rise to strong heating and even to the formation of liquids. This concept has been addressed before (13) but the treatment of such high strain rates is lacking.

High temperature oxidation processes have been studied systematically and quite intensively for the last fifty years. Consequently it can be claimed that most of the mechanisms by which pure metals and simple alloys oxidize over a wide range of temperature and atmosphere compositions are well understood. The qualitative understanding is much better than our ability to predict quantitatively how a metal system will behave. Over the short term the oxidation behavior of a metal or alloy may be predicted, the real doubt arises when the long term is considered. An alloy derives its oxidation resistance from the formation of a surface layer of oxide which effectively separates the reactants and thereby passivates the metal. Further reaction proceeds only as

fast as metal ions, oxygen ions and electrons can migrate through the passivating oxide layer. Therefore an oxide layer which exhibits low ionic and electronic conductivities will oxidize only slowly. For this reason most practial heat resisting systems are based on alloys that form surface layers of Cr_2O_3, Al_2O_3 or SiO_2. Unfortunately this situation is not permanent and it is found, without exception, that these oxide layers lose their protection after long exposure. This can occur for many reasons as the scale begins to modify its protection in a process described as 'scale breakdown' and the process is completed when all substantial protection is lost and the system enters a behavior regime called 'breakaway'.

The processes of breakdown and breakaway can be intiated by several factors varying from the inward intrusion or migration of second oxidant species in the atmosphere to the outward migration and gradual continuation of the protective scale by cations such as Fe, Ni, Mn, mechanical deformation of the scale due to stresses induced during growth, thermal cycling, or any other source, must also be considered deleterious in this respect. Erosion is such a process that may cause mechanical deterioration and, by its severity, move forward the onset of breakdown and breakaway of a protective scale to shorter times.

The above example is a very simple view of how erosion can influence the degradation mechanism of an alloy in service at high temperature. Apart from any academic interest, the subject of conjoint erosion - oxidation attack of metals is important since it is almost certain that, until thermonuclear power becomes feasible, mid term power generation systems are likely to rely on coal combustion which inevitably will involve exposure of metallic components to rapidly moving, dust laden, erosive, oxidizing atmospheres.

Simultaneous erosion and oxidation of metals at high temperature has been studied by several groups of workers over about the last 10 years. The work carried out has involved different techniques of testing and wide ranges of velocity, impact angle and particle characteristics.

Ives (13) impacted 310 stainless steel using $150\mu m$ SiC particles travelling at 15 to 70 ms^{-1} to impinge at 90° in a combustion gas atmosphere at 975^oC. At the lower particle velocities, erosion damage was confined to the relatively thick oxide layer that formed in these atmospheres whereas, at high velocities, this scale was penetrated by the particles and the underlying metal was damaged. After exposure, the oxide surface had the appearance of having been deformed plastically during the impacts. The damage to 310 stainless steel by erosion at 975^oC in oxidizing atmospheres was found to be approximately an order of magnitude greater than that experienced at 25° by erosion alone.

Wright, Nagarajan and Herchoeder (14), Nagarajan, Wright, Merz and Stringer (15) and (16) have examined the erosion-corrosion attack of a large number of alloys including chromia-forming cobalt alloys, stainless steel, dispersion strengthened Ni-base alloys and Co alloys containing traces of Y, La and Ta. The work was principally directed towards the selection of alloys for fluid bed combustors and for gasifiers using corresponding, simulated, atmospheres at temperatures up to 871^oC. Alumina partcles $15\mu m$ in diameter were used as the erodent flowing at 19 and 53 ms^{-1} The results showed that, at $19ms^{-1}$ with the least erosion, the life was controlled by the oxidation processes whereas at $53ms^{-1}$ erosion became the dominant factor. It was also interesting to note that the softest alloys (AISI 446 and Inconel 671) deteriorated slowly and that the dispersion strengthened (MA 754 and Haynes 8077) also deteriorated slowly under erosion-oxidation conditions. The apparatus used was a rotating disc sample holder carrying 18 samples which rotated at 60 rpm, consequently the erosion-oxidation situation was experienced by the samples for a short fraction of the exposure time, the remainder of which was spent in oxidation only. The complexity of the alloys and the exposure system, while allowing comparisons in behavior to be drawn, make it difficult to obtain a description of the basic mechanisms by which erosion-oxidation conjoint action occurs.

Materials suitable for gas turbines, including MA754, IN738 and Si_3N_4, were also studied under combined erosion-oxidation situations by Barkalow, Goebel and Pettit (17). The cylindrical specimens were exposed continuously in a dynamic burner rig flowing at 275 ms^{-1} and 871^oC. The materials were examined closely after exposure and it was concluded that several regimes of interaction existed. The particle size of the powder was varied in this work rather than the velocity or temperature and the results were separated into regimes according to particle size. For particles greater than $15\mu m$ the degradation mechanism was dominated by erosion and involved direct metal removal, between $1-15\mu m$ diameter particles the degradation was of a mixed nature where the effect of erosion appeared to be modified by the oxidation processes. When very small particles less than $1\mu m$ were used, the particles tended to deposit on the specimens and thereby modify the oxidation behavior. Such a trend is clearly in line with the more vigorous erosion effect that is to be expected of larger particles at constant velocity. This was the first indication of the range of interactions that could be observed in erosion and oxidation interaction.

Levy and Zambelli (18) have eroded at 25^oC, nickel oxide scales that were formed at 1000^oC by oxidizing Ni200 coupons for 72 hours. Using quite large ($25\mu m$) erodent particles, flowing at 100 ms^{-1} at 20° and 90° incidence, they observed plastic deformation around the impact crater with a system of cracks below it. The large erodent particles may make it difficult to compare these results with those of investigators using smaller particles since Finnie (19) has shown that erosion mechanisms may change in character as the erodent size is changed.

Levy, Slamovich and Jee (20) compared several chromium steels under erosion and oxidation at $700 - 1000^oC$ using $5-100\mu m$ particles flowing at 5m sec^{-1}. They found that, at this low speed, the mechanism was dominated by corrosion processes which were found to be enhanced by the erosive component. The changes in scale structure were complex and were complicated by the fact that, at chromium

levels below 20% the steels have very long transient oxidation periods in the absence of erosion. This work was complemented by Levy, Yan and Patterson (20) studying ferritic and austenitic stainless steels between 25-900°C. Erosion was identified in these cases as occurring by the platelet mechanism, the austenitics eroding somewhat less than the ferritics.

Tabakoff (21) substantiated the higher erosion rate of Inco 600 at 577°C compared with 25°C using silica particles flowing at 200-300 ms^{-1} at impingement angles up to 70°. The results were not explained and metallographic examination was not carried out.

Nickel base superalloys were exposed to erosion in the effluent gases of a pressurized fluidized bed coal combuster which produced an oxidizing atmosphere that contained some SO_2. The effluent particles of SiO_2, Al_2O_3 and alumino silicate were between $10-15\mu m$ in size. The degradation of the specimens was enhanced by the presence of erosion and a thin porous oxide was found to form under high erosion rate conditions. Cracks were found to form in the metal parallel to the oxide metal interface when the scale was thin whereas, with thick scales, cracks radiating from the impact center were observed. The presence of SO_2 caused the formation of sulfides at the metal scale interface.

Wright, Nagarajan and Stringer (22) speculated about the mechanism of removal of Cr_2O_3 from the alloys tested suggesting that the Cr_2O_3 scale would undergo brittle damage, exposing the metal to more rapid oxide formation. Depending on the impact frequency, faster growing oxides could form and steady state, constant rate, kinetics result. If the particle were to penetrate the scale then cutting and ploughing of the alloy would occur resulting in the shattering of the oxide, formation of craters and lips with oxide and erodent embedment. It was suggested that a multiple impact sequence is required for material removal i.e. to set up lips and to cut them off. Clearly the amount of material lost as oxide may also be significant and it was found that the material loss at 43ms^{-1} using 12μm Al_2O_3 particles was significantly greater

in oxidizing atmospheres than in non oxidizing atmospheres.

It was found that, in inert atmospheres, the erosion rate was virtually independent of hardness and was greater at 30° incidence than at 90°. Under conditions of erosion under oxidizing conditions the effect of the angle of incidence was not so marked and may even have shown greater deterioration at 90° incidence.

From the literature it is apparent that the erosion-oxidation interaction is complex and leads always to enhanced degradation rates. The data that has been gathered so far has involved complex metal systems and conditions and has allowed some general conclusions to be drawn, however there is a real need for further investigation of this subject with the study of basic mechanisms of interaction as the prime objective.

The main conclusions drawn from the work carried out so far are,

- There are several regimes of interaction between erosion and oxidation operating simultaneously on metals.

- Material removal most probably involves a multi-impact mechanism such as ploughing and chipping.

- The conversion of metal to oxide is an important step in the interaction.

- Oxide may be easier to remove than metal.

The remainder of this paper will be concerned with an experimental study into the basic mechanisms of conjoint erosion and high temperature oxidation.

EXPERIMENTAL

An apparatus has been constructed, shown diagrammatically in Figure 1, for the investigation of these phenomena. Compressed air is cleaned and dried on filters to remove traces of oil, water and dust. The air stream is then passed through a pre-heater and heated to about

700°C. Particles are entrained from a Sylco particle dispenser using a second stream of air, about one tenth of this stream is added to the main air stream as it emerges from the preheater. The particle laden erosive stream is then passed down a vertical, heated, Inconel tube 1.5m long and 9.3mm internal diameter. The erosive stream is thereby heated and accelerated to operating temperature and velocity. Temperatures up to 900°C and velocities up to 300ms^{-1} can be achieved, the velocities measured using a laser doppler velocimeter have agreed closely with values calculated from simple gas laws. The velocimeter is used in situ without disturbing the apparatus.

Alumina particles of average dimension equal to 20μm are used as the erosive medium, they are sharp edged and angular rather than round or regular in shape. The size of 20μm was chosen since calculations showed that they would not be deflected by changes in gas streamlines as they neared the specimen surface.

The sample is heated by the preheated erosive gas stream with supplementary heating from the back using an infrared spot heater. It was found that the temperature variation through the specimen was about 5°C and the temperatures of individual specimens were measured using a thermocouple placed in a hole drilled to the center of the specimen.

Specimens of nickel and cobalt measured 12mm x 12mm x 2mm and 12.8mm diameter by 3mm thick respectively, were prepared by polishing through a 1μm alumina slurry. They were then cleaned ultrasonically in distilled water and rinsed in acetone.

During exposure only one side of the specimen was exposed to the erosive oxidizing environment. It was therefore necessary to ensure that the other surfaces underwent negligible weight changes during the exposure. This was accomplished with nickel specimens by preoxidizing for 72 hours in air at 1100°C to produce a layer of NiO about 120μm thick. The oxide was then removed from the surface to be exposed by grinding. In order to study the erosion of NiO similar specimens were prepared but the oxide was not removed.

Due to the high oxidation rate of cobalt this technique could not be used, instead cobalt specimens were aluminized and the coating was removed by grinding from the surface to be exposed.

In both cases of nickel and cobalt the weight changes referred to the exposed surface only since weight increases due to oxidation on the surfaces not exposed to the erosive stream were found to be negligible.

During an experiment, the particle laden gas stream was established at the required temperature and velocity and the specimen, with buried thermocouple, was swung into position for exposure. At the completion of the exposure the specimen was swung out of the heated gas stream and cooled in a stream of nitrogen to help preserve the surface features.

Specimens were examined using optical metallography, scanning electron microscopy and energy dispersive spectroscopic analysis. Cross sections were examined to observe the scale thickness and the nature of the interfaces.

RESULTS

Nickel and cobalt were chosen since both metals from rapidly growing, compact, adherent oxide layers under oxidizing conditions. This would allow the interaction between erosion and oxidation to be observed over a wide range of relative intensities of oxidation and erosion.

Erosion of Nickel Oxide

The erosion of nickel oxide was studied using 90° incidence of the erosion stream at 800°C, 650°C and 25°C. Figure 2 shows the measured erosion rates and it can be seen the highest rates are found at the lower temperatures and the higher velocities. This is in keeping with the morphology of the oxide surface shown in Figure 3 in which evidence of plastic deformation can be seen, thus the lower erosion rates measured at 800°C reflect the increased plasticity of the nickel oxide at the higher temperature when a larger fraction of the incident energy would be absorbed during plastic deformation. This trend is followed at 650°C and 25°C where

the most rapid erosion occurred, under all conditions the eroded oxide surface was found to remain flat and the nickel-nickel oxide interface was not affected by the erosion. Since the lines in Figure 2 all extrapolate through the origin, it is assumed that material removal begins immediately on expsoure of the specimen to the erosive stream.

Erosion of Nickel and Cobalt without Oxidation

By using nitrogen at elevated temperatures, or air at room temperature, oxidation of the metal could be avoided. Nickel was exposed at 800°C and 25°C to erosive flows of nitrogen and air respectively using velocities of 140ms^{-1} and 90ms^{-1} at 90° incidence. The experimental data are shown in Figure 4 and it is clear that, in the absence of oxidation, only slow degradation of the metal is achieved. The metal surface is however extensively deformed plastically with formation of the hill and valley surface macrostructure referred to as 'moguls' which consequently does not appear to require material removal or oxidation but to be due simply to material rearrangement by plastic deformation. At 25°C moguls did not form, indicating that, at this temperature, the ductility of the metal was not sufficiently high to undergo the necessary physical rearrangement with the incident erosive energy that was used. Alumina particles were also found to embed in the metal surface being transported down the mogul sides to accumulate in the valleys between the moguls as shown in Figure 5. The samples experienced a small weight gain initially which was taken to indicate the capture of alumina particles by the metal surface.

Cobalt metal, in the absence of oxidation, behaved almost identically showing low rates of erosion as shown in Figure 6. The plastically deformed cobalt surface was covered with a thin oxide layer thought to have formed on cooling after the nitrogen flow was terminated.

Erosion and Oxidation Combined

Experiments in which nickel and cobalt were exposed to conditions of erosion and oxidation simultaneously were carried out at 800°C and 650°C using velocities of 140ms^{-1} and 90ms^{-1} incidence. The results for the rate of deterioration of two metals are shown in Figures 4 and 6 respectively indicating that the degradation rate increased with temperature and with incident velocity.

Subsequent examination of the surfaces of specimens after exposure to simultaneous erosion and oxidation conditions showed that mogul development was slower at lower velocities and, at a given velocity, was slower in the case of cobalt than in the case of nickel. This is shown in Figure 7. The surface features once again were typical of plastic deformation and the metal scale interface had been subjected to strong plastic deformation with substantial particle capture. The mechanism by which mogul features are thought to be sustained, if not formed, is shown in Figure 8. The impacts on the mogul sides cause material flow down into the valleys. Impacts on the mogul tops and in the valley troughs cause plastic deformation resulting in the plastic flow indicated in Figure 8. That features similar to moguls can be formed, by reinforcement of plastic deformation alone in the absence of material removal, was demonstrated by using a computer simulation of many impacts each of which was represented by a depression with a rim of raised material of equal volume. The simulated surface after 10^6 impacts was rough and hilly rather than flat and smooth and confirmed that the formation of mogul-like features does not require material to be removed.

Using nickel, it was not possible to avoid the formation of moguls except at short times. This is because the rate of scale growth is slow compared with the rate of erosion and therefore the scale never manages to grow to a thickness that would protect the underlying metal from deformation by the impacts. Whenever a thick oxide layer, grown on nickel in the absence of erosion, was exposed to erosion in air, the oxide was removed until moguls formed. However using cobalt, which has a much higher oxidation rate constant, it was possible to balance the rate of oxidation with the rate of erosion and achieve a steady state scale thickness.

Under these conditions the rate of scale growth by oxidation is precisely equal to the rate of scale removal by erosion

$$\frac{dX}{dt} = \frac{k}{X} - k_e$$

Where

X = scale thickness
k = parabolic rate constant
k_e = erosion rate constant for the scale

Under steady state conditions the scale thickness does not change and

$$\frac{k}{X_+} = k_e$$

Thus the steady state thickness is given by

$$X^+ = \frac{k}{k_e}$$

This is held to be the simplest form of interaction between erosion and oxidation called "erosion enhanced oxidation" in which both processes are present but their basic mechanisms are not changed. The effect of erosion is to remove the oxide which, becoming thinner, causes the oxidation rate to be held at a value corresponding to that thickness. Thus a high rate of deterioration of the metal is observed which is higher than that in the presence of oxidation alone or that due to the action of erosion in the absence of oxidation.

The layer of scale formed on cobalt after 60 minutes in air at 800°C and 90ms⁻¹ is shown in Figure 9 together with the corresponding scale formed by oxidation only. One curious feature that has not yet been explained is why the Co_3O_4 surface layer is proportionally thicker in the case of erosion-oxidation than in the case of oxidation only. Increasing velocity of the erosive stream to 140ms⁻¹ at 800°C causes the formation of moguls as stated previously, a cross section of such a specimen in Figure 10 shows the oxide layer that forms under these conditions compared with the thicker scale formed under oxidation only. In this case the deformation has extended also to the metal to cause mogul formation.

When the erosion rate is increased with nickel specimens exposed under similar conditions, the metal is deformed and moguls form but, instead of an oxide surface scale, a composite layer is formed consisting of nickel oxide, captured alumina particles, which penetrate the composite layer and embed in the metal, and areas where plastically deformed metal has been extruded by the impacts back into the composite layer. Due to the lower value of the oxidation rate constant of nickel, this situation, shown in Figure 11, represents a step beyond that shown in Figure 10 for cobalt.

These results represent a regime of interaction referred to as "oxidation affected erosion" where the two processes not only proceed simultaneously but interact to the extent that the basic, individual, processes are modified.

Based on these results it is proposed that the interaction between erosion and oxidation can be discussed as follows in terms of regimes.

Oxide Erosion

In this regime the erosion component is extremely small compared with oxidation and the metal plays no role in the process. This is typical of the initial stages of the erosion of a thick oxide layer ·or scale.

Erosion Enhanced Oxidation

The erosion rate is comparable to the oxidation rate. The two processes of oxidation and erosion proceed simultaneously. Erosion acts on the oxide only, causing the oxide growth to be reduced, consequently the oxidation rate (which is diffusion controlled) is reduced less strongly than expected from the normal parabloic rate law. Eventually a situation is reached where the erosion rate of the oxide is equal to the oxidation rate of the metal and the scale thickness remains at a constant, steady state, value. At this state the deterioration rate of the metal becomes constant. This is a simple interaction where erosion acts on the oxide surface and the metal oxidizes, neither mechanism is modified by the presence of the other phenomenon but the degradation kinetics are modified substantially. All of the plastic deformation consequent upon erosion is confined to a narrow zone of

oxide at the scale-gas interface.

Oxidation Affected Erosion

In this regime the erosion rate of the oxide is high compared with the kinetics of oxidation of the metal. Consequently, only very thin oxide scales would be expected to form, such a simple case is not found however because, under these conditions, the zone of plastic deformation extends beyond the oxide layer and into the metal. This causes the interaction between erosion and oxidation in this regime to be much more complex, involving plastic deformation of both oxide and metal simultaneously. Under these conditions moguls are seen to form and substantial amounts of erodent are captured by the substrate. The surface or scale layer can no longer be regarded as a simple oxide layer but is a composite of oxide, embedded alumina erodent particles and extruded metal.

This interaction affects the erosion rate by extending the absorption of incident erosive energy to the more plastic metal substrate, it also affects oxidation by allowing metal to be extruded on impact *from the underlying situation to direct contact with the atmosphere.* Two mechanisms by which this interaction is thought to be likely are given in Figure 12. Figure 12(a) shows the situation when the impacting particle penetrates with the metal and establishes a seal at the particle-scale interface, the impact and material displacement results in a bulge being produced under the pressure and tears the oxide, exposing the metal to oxidizing gases.

In Figure 12(b) is shown the situation when the impacting particle does not seal well with the scale and the plastic deformation of the metal consequently occurs more locally causing metal to be extruded along the faulty seal. Such intense deformation would almost certainly be adiabatic and could cause the metal to melt and be sprayed into the atmosphere.

It can be appreciated that the interaction in this regime is exceedingly complex and many mechanisms are likely to be operating.

Metal Erosion in Absence of Oxidation

When oxygen is excluded, a low rate of material removal is observed. The energy of impact is absorbed almost entirely by plastic deformation of the metal substrate. Work hardening does not occur and it is likely that the surface temperature rises.

It appears from these results that the material removal is effected primarily by erosive removal of metal oxide and that the sequence of oxidation of the metal followed by erosive removal of the oxide is a necessary sequence. To this must be added what is probably a relatively small component due to direct ejection of liquidified metal as discussed earlier.

The possibilities of interaction between erosion and oxidation of a metal have been discussed in a systematic manner introducing regimes of interaction, moving from one regime to the next as the erosion component is considered to be increased in severity with respect to the oxidation component. This concept is shown in Figure 13 and it can be seen that for a given system in a given oxidizing environment it is possible to move from one regime to another simply by changing the erosive intensity of the air flow. This can be seen from the results with cobalt which, at 800°C, remains in the erosion enhanced oxidation regime when the erosive stream flows at 90ms^{-1} whereas increasing to 140ms^{-1} causes moguls to form and the system is then on the boundary of the oxidation affected erosion regime.

Similarly it is possible to use a constant intensity erosive stream and change regimes by changing the system where the systems have different oxidation characteristics. This is seen between cobalt and nickel where the much less intense oxidation characteristics of the nickel cause it to remain in the oxidation affected erosion regime whereas cobalt behaves mainly as if it were in the erosion enhanced oxidation regime under similar conditions.

CONCLUSIONS

Considerable and varied synergistic interaction between erosion and oxidation occurring simultaneously has been found at 90° incidence. The removal of oxide is accomplished quite readily. The oxide behaved in a predominantly ductile manner rather than in a brittle fashion.

The results obtained have been rationalized into a sequence of interactive regimes depending on the relative intensities of the erosion and oxidation components.

These conclusions refer to 90° incidence and ductile metal-oxide systems substantial extensions to the mechanisms may be found necessary to account for behavior at different angles or for brittle oxide systems.

REFERENCES

1. P. Shewmon and G. Sundararajan, Ann. Rev. Mater. Sci., 13, 301, (1983).

2. K. Hauffe, "Oxidation of Metals", Plenum Press, New York, 1986.

3. P. Kofstad, "High Temperature Oxidation of Metals", Wiley, New York, 1966.

4. S. Mrowec and T. Werber, "Gas Corrosion of Metals", NSB Trans., 1978, U.S. Dept. of Commerce NTIS, Springfield, VA 22161.

5. N. Birks and G. H. Meier, "Introduction to High Temperature Oxidation of Metals", Arnold, London, (1983).

6. I. Finnie, Wear, 3, 87, (1960),

7. R. I. Winter and I. M. Hutchings, Wear, 29, 181, (1974).

8. N. P. Suh, Wear, 25, 111, (1973).

9. P. S. Folansbee, G. B. Sinclair and J. C. Williams, Wear, 74, 107, (1981).

10. A. V. Levy and R. Bellman, Wear, 70, 1, (1981).

11. B. Lawn and R. Wilshaw, J. Mater. Sci., 10, 1049, (1975).

12. I. M. Hutchings, J. Phys. D. Appl. Phys., 10, L179, (1977).

13. L. K. Ives, Trans. ASME, 99, 126, (1977).

14. I. G. Wright, V. Nagarajan and R. B. Herchoeder, "Some Factors Affecting Solid Particle Erosion/Corrosion of Metals and Alloys", Corrosion-Erosion Behavior of Materials, ed. K. Natesan, TMS-AIME Mtg., St. Louis, MO, Oct. 16-17, 1978.

15. V. Nagarajan, I. G. Wright, W. E. Merz and J. Stringer, "Morphology of High Temperature Erosion-Corrosion of Oxidation Resistant Alloys", Int. Corros. Forum, NACE, April 6-10, Toronto, 1981.

16. I. G. Wright, V. Nagarajan, W. E. Merz and J. Stringer, "Kinetics of High Temperature Erosion-Corrosion of Oxidation Resistant Alloys", Ibid.

17. R. H. Barkalow, J. A. Goebel and F. S. Pettit, Materials Problems in Fluidized Bed Combustion Systems, Final Report EPRI Project 979-4, May 1980.

18. A. V. Levy, and G. Zambelli, Wear, 68, 305, (1981).

19. H. L. Oh, P. L. Oh, S. Vaidyanathan and I. Finnie, "Shaping of Brittle Solids by Erosion and Ultrasonic Cutting", NBS. Pub. p. 19.

20. A. V. Ley, J. Yan and J. Patterson, "Elevated Temperature Erosion of Steels", LBL Report 18256.

21. W. Tabakoff, Wear, 86, 65, (1983).

DISCUSSION

Question/J. H. Kosel

I believe you stated that the material removal rate for the oxidation-affected erosion regime, in which the oxide is very thin or discontinuous is very high. Is this due to a rapid oxidation rate due to exposure of bare metal, or is it due to easier removal of oxide once formed than metal?

Author's Reply

The rapid material removal rate in the oxidation affected erosion regime is believed to be due to the rapid removal of oxide which, as a consequence of the erosion, forms rapidly on the metal. Our results show that the metals involved are removed substantially as oxide whereas the erosive removal of metal has been found to be very slow at these temperatures. Consequently, under heavy erosion, the material removal rate may be limited by the rate at which oxide can form. Therefore both rapid oxide removal and rapid oxide formation are components of the deterioration mechanism, the more rapidly the oxide is removed the more rapidly it can form.

Question/J. Stringer

Several Points:

1. An observation: grinding, in which metal removal rates are very high, occurs much more readily in oxygen than in inert gas. Attribution of the differences in erosion rate under these two conditions to the presence of an oxide layer may not be correct.

2. You showed a picture of a specimen of cobalt oxidizing compared to one eroded under oxidizing conditions, showing a thinner layer of oxide on the surface in the latter case. This was claimed to be an example where the oxide was being eroded. However, the outer fine-grained layer of oxide was essentially the same thickness in both cases, so the outer layer/inner layer ratio is <u>higher</u> in the erosive case. This seems to be very difficult to understand, since I would expect the erosion to remove the outer layer fairly completely.

3. The situations you describe assume the particle is inert. Nicholls and Hancock have suggested that the situation where the particle may interact chemically with the surface is a quite different regime. Would you care to comment?

4. A more important philosophical point. You said that the condition of 90° impact was easiest. In fact, I believe it to be the most undesirable experimental condition, because, as Tabakoff has frequently pointed out, the particles tend to follow the gas streamlines and, for this arrangement, these are difficult to calculate and probably unstable. The real impact angles will thus be very different to 90°, and intrinsically incalculable.

It is my view that a concept of "moguls" introduced by Levy and used by you is misleading for this reason. If the specimen is tilted, the impact angle, while still different from the vertical value, is reasonably consistent and stable and, under these conditions one forms well-defined ripples, with straight fronts normal to the direction of impact in the surface. These waves move at well-defined velocities over the surface. It is well known that shapes similar to "moguls" are generated by interacting wave trains and I believe that this is indeed their origin in erosion situations. The fundamental process is thus the development of the ripples and, to the extent that your procedure generates 'moguls', it conceals the true physics of the surface deformation processes associated with erosion. Mathematical expressions exist to describe the development of moving wave trains in a medium with an excitation (fluid motion, shock wave etc.) moving parallel to the mean surface plane. More attention should be given to interpretation of surface morphologies in these terms.

Author's Reply

1. We have made the same observation concerning the relative thicknesses of the Co_3O_4 and CoO layers and do not understand why the thickness ratio

appears to change under erosion. There is no doubt that the scale thins under erosion as shown however the formation of Co_3O_4 on terminating erosion is ·not understood. This is only one result and more work is needed before generalizing.

2. .We have never found any evidence that our paticles are other than inert under the conditions used. In a situation where chemical reaction is possible then, with short residence times, I would speculate that solid reactions could be discounted but that the effect would be most pronounced where liquid phases could form. In this case strong adverse effects would be expected if the protective scale could dissolve in the liquid formed. In practice such conditions are likely to correspond to ash deposition, agglomeration and attack of the metal surface in energy production. Such behavior would naturally extend the interactive mechanisms further than those discussed in our paper.

3. We chose 90° incidence as a starting point because the oxide layers were expected to believe in a more brittle manner. This is not so in the systems with which we have so far conducted most of our work. We chose 20μm particles because we calculated that they would not be deflected by stream-lining and we believe that this is the case for particles above 5μm size under our conditions. However we are concerned about uncertainties in trajectory caused by interactions between incident and reflected particles. So far our work has been mainly qualitative and mechanistic and, so long as conditions have been held constant, this situation has not been a problem. It is doubtful whether any angle of incidence is completely free from interference from this cause especially when the erosive stream impacts over an extensive area.

4. We have in fact observed the formation of ripples when eroding at about 45° or less to the specimen surface, however we have not studied their formation or behavior so far.

Mogul is, as you say, a term taken over from Levy et. al and we have used this to describe a situation which we have not yet analyzed. At present we regard these features as arising simply from the plastic deformation of the substrate, whether they should be described in terms of interacting wave fronts or as individual disturbances of the surface has not been considered in any depth.
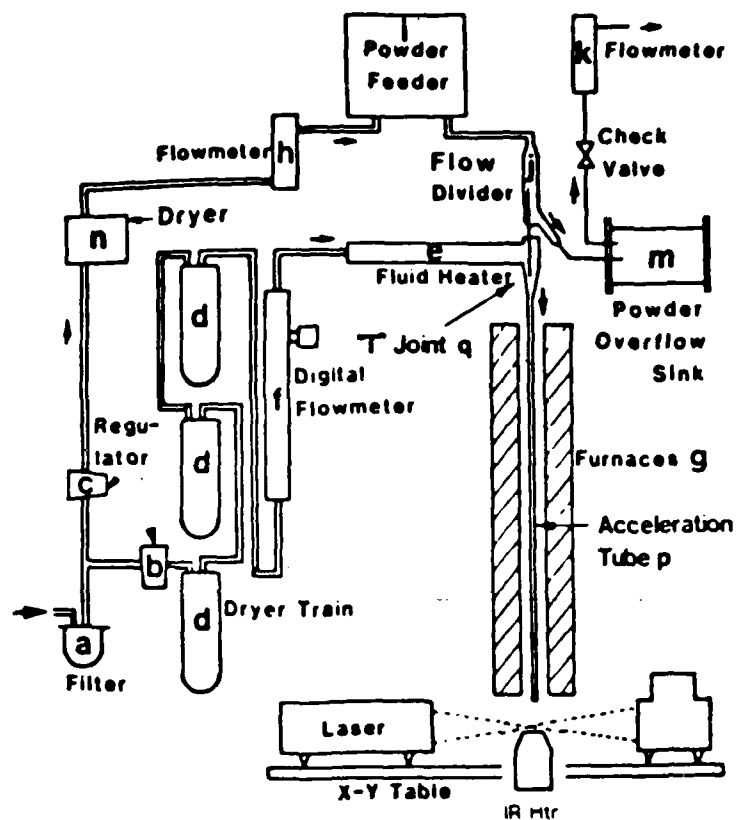
FIGURE 1: Schematic diagram of apparatus for the simultaneous erosion and oxidation of metals.
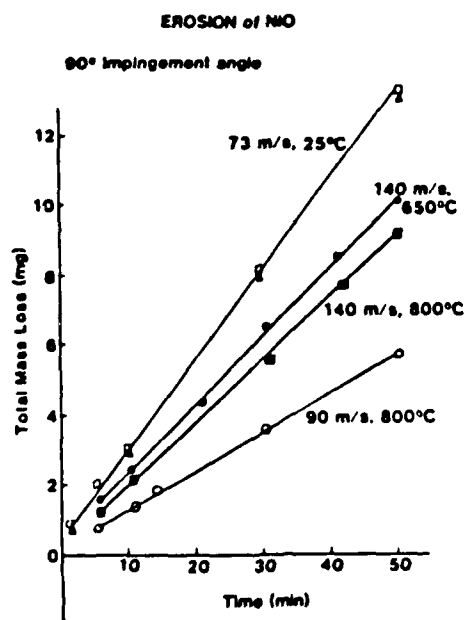
FIGURE 2: Mass loss vs. time for preoxidized nickel specimens exposed at 90° impact angel
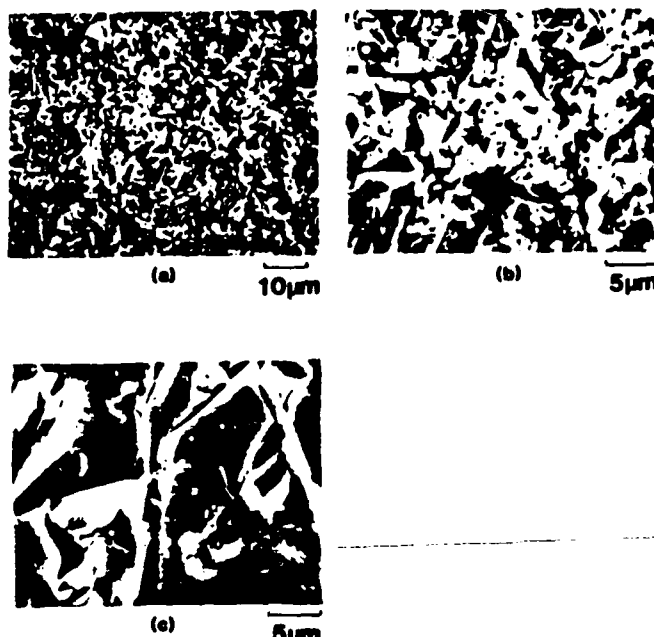
FIGURE 3:   NiO exposed at 800°C at 90°
             to 140 ms^{-1} erosive airflow;
             showing plastic deformation
             (a) and (b) and cracking or
             tearing (c).
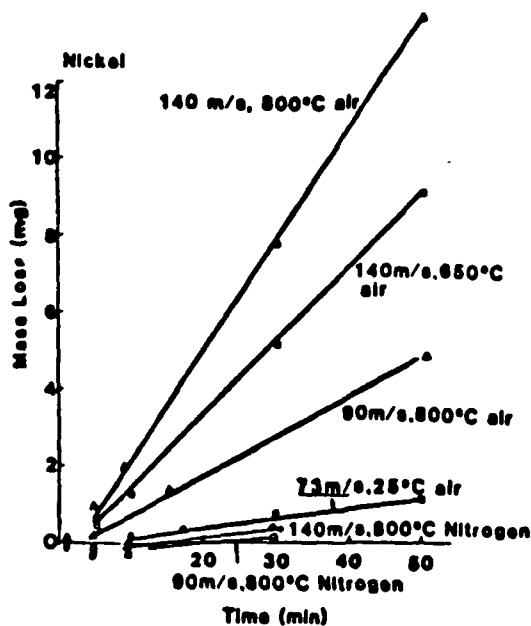
FIGURE 4:   Mass loss vs. time for nickel
             specimens exposed at 90°
             incidence to erosive stream.

Cross section of Ni exposed for 10 min at 800°C to 90 m/s nitrogen flow

30 min
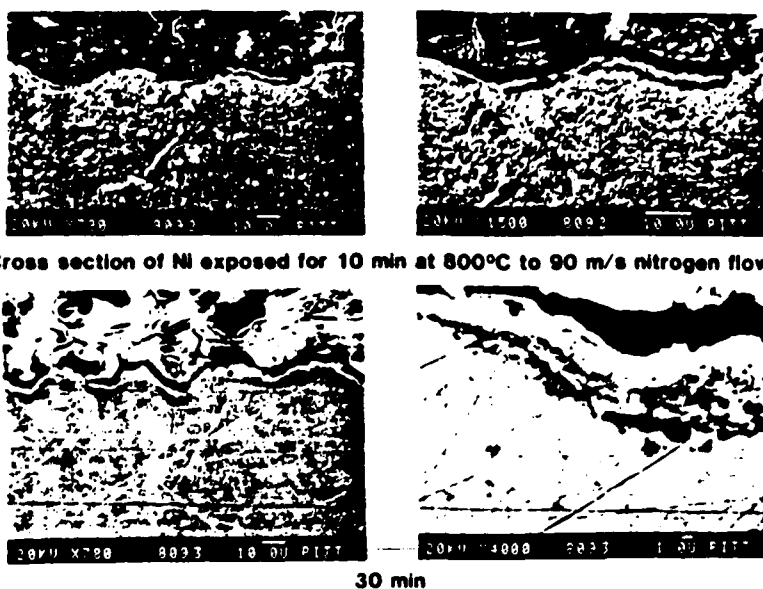
FIGURE 5:   Cross section of Ni exposed
at 800°C and 90 ms^{-1} erosive
flow of nitrogen showing
accumulation of alumina in
mogul valleys.
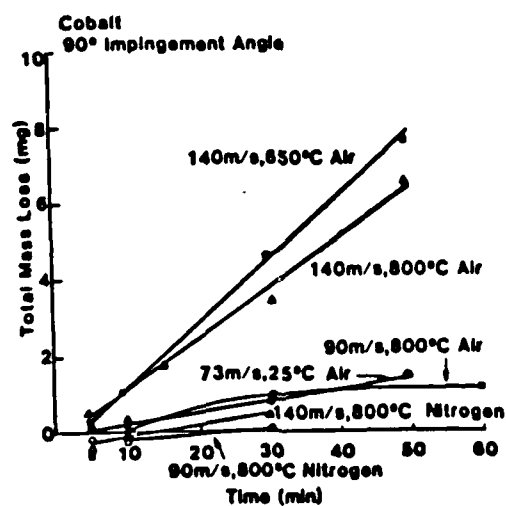
FIGURE 6:   Mass loss vs. time for cobalt
specimens exposed at 90°
incidence to erosive stream.

(a) 6 mins. 20µm (b) 10 mins. 20µm (a) 1 minute 20µm (b) 5 mins. 20µm

(c) 30 mins. 20µm (d) 50 mins. 20µm (c) 30 mins. 20µm (d) 50 mins. 20µm
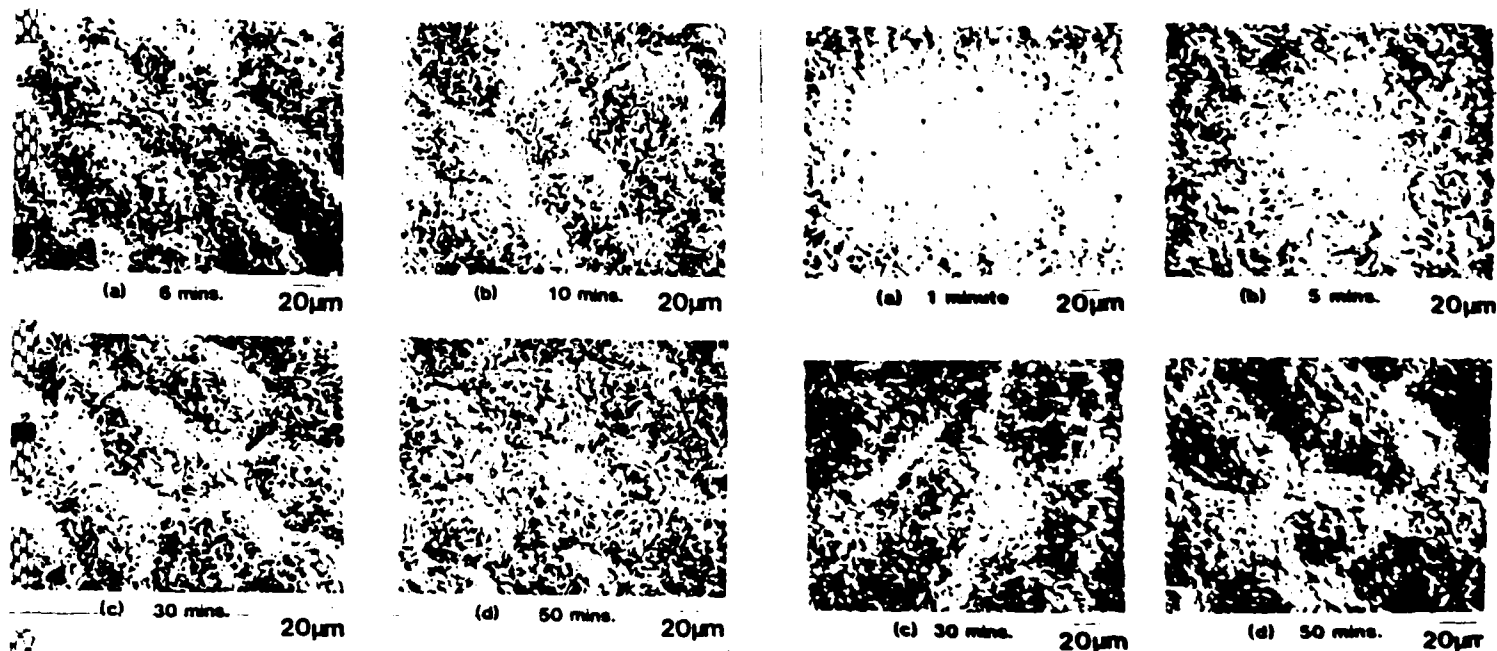
FIGURE 7: Development of moguls on nickel and cobalt samples exposed at 800°C to 140 ms^{-1} erosive airflow at 90° incidence.
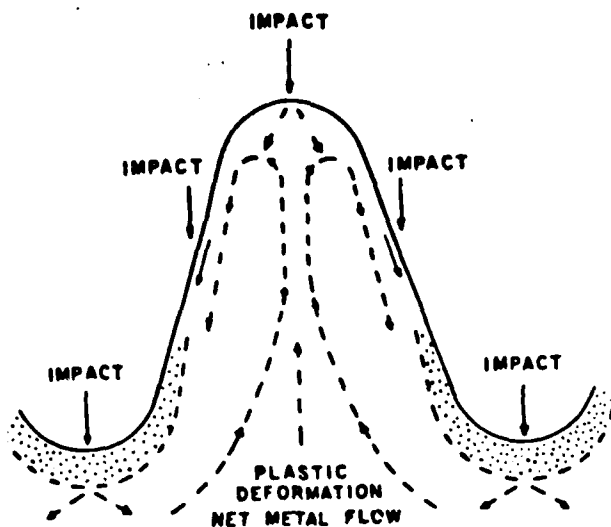
FIGURE 8: Mechanism of mogul formation. Impacts on sloping mogul trans-port material down to valleys in between moguls, impacts on horizontal surfaces cause metal flow as indicated to maintain mogul shape and size in a steady state situation.

Erosion and Oxidation   **Oxidation Only**
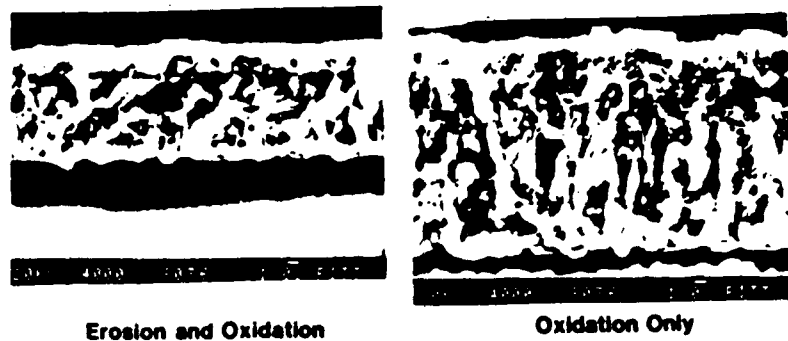
FIGURE 9: Cross section of Co eroded at 800°C for 60 min. in 90 ms^{-1} erosive flow at 90° incidence.
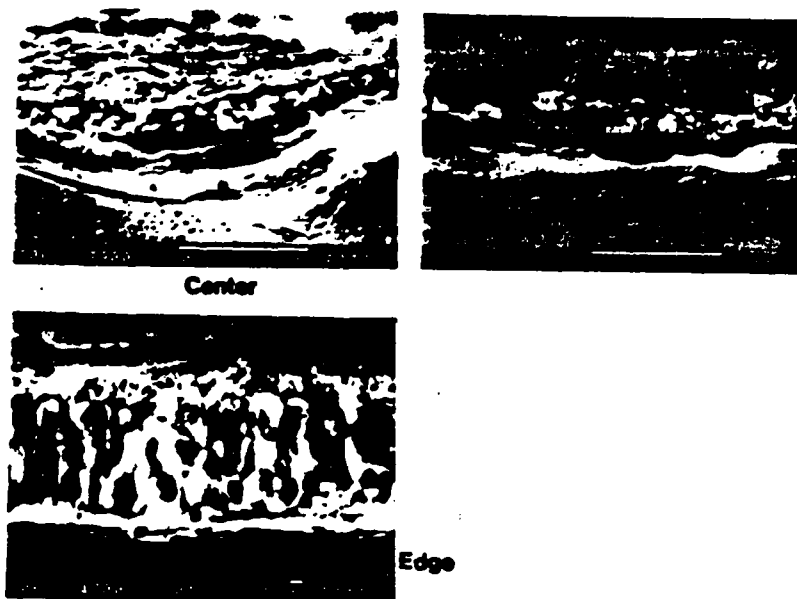
Center

Edge

FIGURE 10: Cross section of Co exposed at 90° incidence to 140 ms^{-1} airflow at 800°C shows thin oxide layer over center zone where moguls formed. Thick oxide layer at specimen edge free from erosion and at inter-mediate stage where erosion occurred but no mogul formed.

5μm   5μm
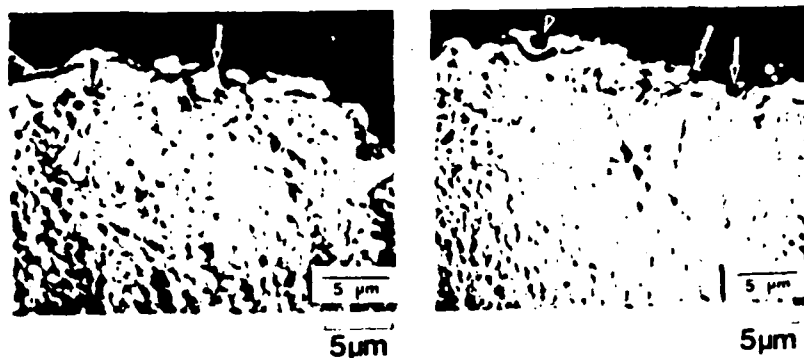
FIGURE 11: Composite layer formed on Ni exposed at 800°C to 140 ms⁻¹ erosive airflow at 90° incidence, showing embedded alumina and evidence of metal extrusion where indicated.
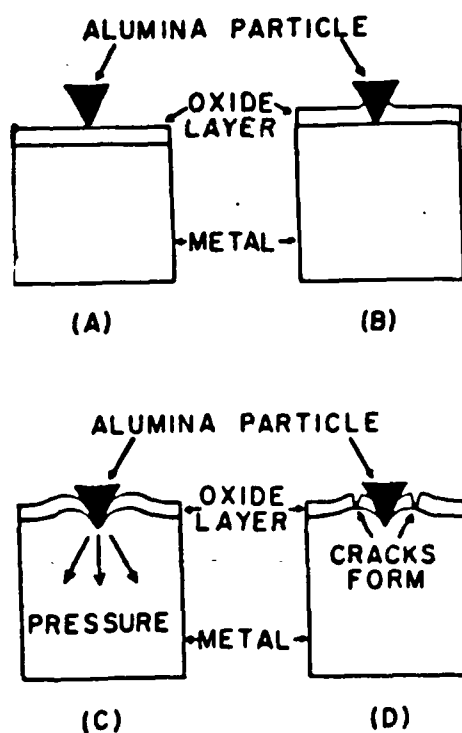
FIGURE 12a: Hypothetical sequence of events following particle impact leading to tear formation.
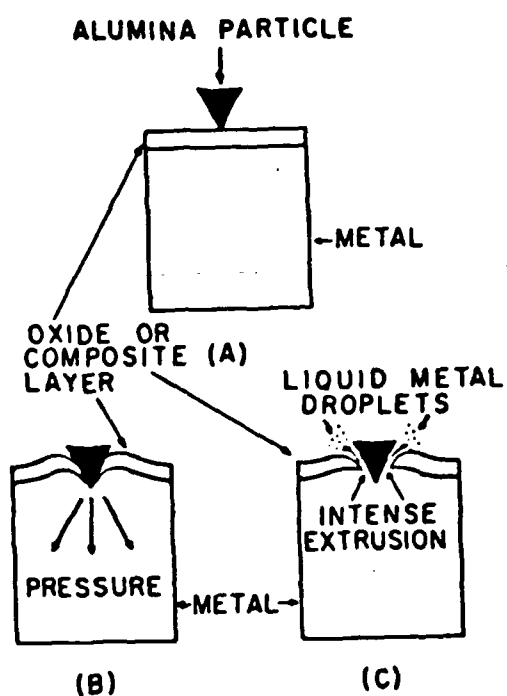
FIGURE 12b: Hypothetical sequence of events following particle impact leading to liquid formation by intense adiabatic extrusion of metal between oxide layer and alumina particle.
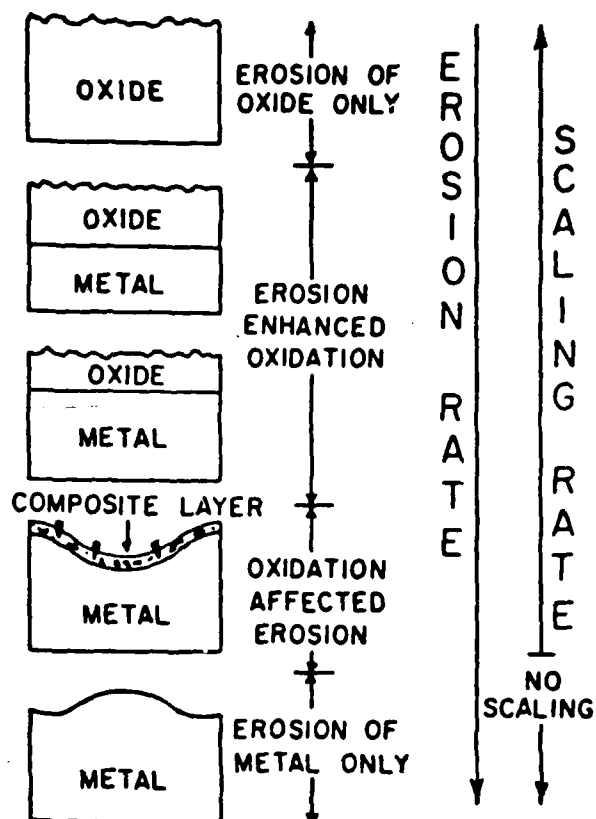
FIGURE 13: Relationship between type of degradation observed under conjoint erosion-oxidation conditions and the relative severity of the erosion and oxidation components.

HIGH TEMPERATURE COMBINED EROSION-OXIDATION
OF PURE METALS

C. T. Kang and N. Birks
MME Department University of Pittsburgh
Pittsburgh, PA 15261

INTRODUCTION

The high temperature oxidation of metals and alloys in both simple and multicomponent gases can be interpreted in detail on the basis of fundamental processes. The most important features are the processes that lead to (a) the formation of surface scales which, to varying degrees, passivate the metal and slow down the reactions, (b) the adherence of scale to metal and (c) the processes by which such protective scales degrade, especially in operational environments. Many of the aspects of complex gas and molten salt attack have been studied to the point of providing qualitative understanding with quantitative interpretation being possible in some cases.

Operational and laboratory conditions may differ by appparently small but, in practice, very significant detail. The presence of low concentrations of sulfurous or carbonacous gases or sodium salts can be extremely dangerous and effective in initiation of scale modification and eventual breakdown leading to very rapid deterioration of the metal. One further, important process that leads to rapid deterioration of a protective scale is erosion, which is particularly dangerous when it occurs in the presence of high temperature oxidation. Basically, once metals lose their protective scale the subsequent degradation of the metal is extremely rapid. Erosion readily removes oxide from the surface of a metal and thus exposes it to more severe oxidation, however the mechanisms by which erosion and oxidation interact when they occur simultaneously are not immediately clear.

Erosion alone has been studied for many years and various interpretations of erosive mechanisms have been proposed for both ductile and brittle materials. Reviews of these mechanisms have been published by Adler[1] and Shewmon and Sundarajan[2]. Although the mechanisms involve various modes of metal removal [3-10], it is extremely difficult to obtain direct evidence to substantiate any case. Consequently, much of the confirmation of a particular mechanism takes the form of comparisons between actual and predicted behavior and of making detailed examinations of the eroded surface to observe and interpret the features resulting from impact.

When a metal is exposed to an oxidizing environment in which hard, sharp, particles are moving very rapidly, there will be two competing processes. The metal will attempt to form a surface oxide and the erosive particles will attempt to remove both it and the metal. The possible interactions are not yet well understood; studies simulating conditions in gas turbines [11] and coal combustion [12] have allowed the behavior of various materials to be

compared but have not been sufficiently well controlled to allow the
fundamental mechanisms to be understood or even identified. However it is
clear from these results that significant interaction occurs and the object
of this present investigation is to study the interactions under well
defined and well controlled conditions.

Apparatus

The apparatus used has been described elsewhere (13), it supplies a
stream of gas and 20 µm alumina particles at up to 300ms^{-1} and 900°C. The
flow emerges from a 9mm diameter nozzle to impact upon a 15mm x 10mm x
2mm specimen which may be fixed at any angle to the airflow, most of the
studies being carried out at 90°. The specimen was heated by the incident
gas stream and also from behind by a focussed radiant heater. Temperatures
were taken using a thermocouple buried in the specimen. A laser doppler
velocimeter was used to measure the particle velocities directly. After
exposure, the specimens were examined using optical metallography and SEM-EDS.

The extent of degradation was measured by measuring the weight change
of the specimen. The specimen surfaces not exposed to erosion were shielded
from oxidation by either aluminizing or by causing a thick oxide to exist.
This was achieved by aluminizing or preoxidizing the sample and then polishing
away the protective layer from the surface of the metal to be exposed to
oxidation - erosion conditions.

RESULTS

Erosion of Nickel Oxide

Nickel oxide samples were prepared by preoxidizing a nickel metal sample
in air at 1100°C to produce an oxide scale about 100 µm thick. These oxide
surfaces were exposed to erosive streams at 90° to the specimen at 800, 650
and 25°C. The results of measured erosion rates, as seen in Figure 1, are
highest for the lowest temperature, 25°C, and the surface of the oxide shows
signs of plastic deformation, cracks and tears at all temperatures although
more tearing is evident at 25°C and more plastic deformation is evident at
higher temperatures. After erosion the surfaces remained flat or planar.

Erosion of Nickel and Cobalt

In order to be able to estimate the effect of the synergism between
erosion and corrosion, the erosion of nickel and cobalt was first studied in
the absence of any oxidizing processes. This was carried out by using oxygen-
free nitrogen as the erodent carrier at 800°C and air at 25°C. The results
for nickel and cobalt are shown in Figures 2 and 3 respectively and show that
the metal is removed only very slowly in the absence of oxide formation. On
examination the metal surfaces showed evidence of local plastic deformation
around the individual impacts and a system of mounds and valleys called moguls

was developed over a longer range as shown in Figure 4. The metal samples actually gained weight initially due to the embedding and capture of alumina particles.

Combined Erosion and Oxidation of Nickel and Cobalt

Samples of nickel and cobalt were exposed to erosive streams of air at 800°C and 650°C impacting at various velocities at 90° to the sample. The results are included in Figure 2 and 3 from which it can be seen that the rate of degradation increases markedly. Due to their different oxidation of characteristics, nickel and cobalt react differently to the same erosive stream. Nickel oxidizes very slowly and forms only a very thin scale that is identified as a composite scale of nickel oxide, nickel, and embedded alumnia. The sample also rapidly develops moguls on the surface which are covered with the composite layer as shown in Figure 5, together with the indentations and evidence of plastic deformation of both metal and oxide.

Cobalt, oxidizing very rapidly, can build up an oxide layer at 800°C and, under an erosive stream flowing at $90ms^{-1}$ mogus were not formed. The oxide layer that formed maintained constant thickness over the 60 minutes exposure, as determined by interrupted testing. A section of the oxide layer formed under these conditions was seen to be about half the thickness of one that formed after oxidation alone for the same time, this is shown in Figure 6. When the erosive velocity was increased to $180ms^{-1}$ at 800°C, the cobalt also showed the development of a mogul covered surface with a thin surface layer of CoO and a thinner layer of Co_3O_4 on top.

DISCUSSION

The results described above can be interpreted qualitatively in fundamental terms, the following discussion being restricted to erosive streams flowing normal to the specimen surface. The discussion is based on the classification of the interaction of erosion and oxidation into three main types; pure erosion, erosion enhanced oxidation and oxidation affected erosion.

Pure Erosion

The pure erosion of nickel oxide proceded at lower rates at higher temperatures, which is in keeping with the concept that the oxide is more plastic at higher temperatures and is thus able to absorb more of the incident energy by plastic deformation. The damage by erosion appeared to be confined to the immediate surface areas but the actual mode of material removal remains to be identified and may not be the same at all temperatures. There is evidence of oxide removal by adherence to the impinging particle but this is thought to be a minor mechanism and more emphasis is placed on extrusion or ploughing and cutting mechanisms as multistep processes as is suggested by the evidence of plastic deformation on the oxide surface. Brittle fracture of the oxide does not appear to be an important mechanism.

When pure nickel and cobalt are eroded in the absence of oxidation, very
low rates of erosion are observed but there is much evidence of plastic
deformation at all temperatures. This observation is in accord with the lower
erosion rates of oxide at higher temperatures where plasticity is higher. The
incident energy of the erosive stream on the metal therefore appears to be
absorbed in carrying out plastic deformation of the metal. This must, to
some extent at least, be an adiabatic process and lead to local heating of the
metal surface thus making fatigue and work hardening most unlikely mechanisms
of material removal. This is illustrated in Figure 7 where the alumina em-
bedded in cobalt, after erosion in nitrogen at 800°C for 30 minutes, is found
to accumulate in the valleys between the moguls. The alumina particles are
apparently transported down the sides of the moguls and Figure 8 gives a
schematic mechanism of metal plastic flow in the maintenance of the stable
mogul configuration that is observed.

Erosion Enhanced Oxidation

The above results, from pure erosion, suggest that the metal converted
to oxide could be removed from a specimen surface quite readily. Thus, if an
oxide layer is formed which is continuously removed the full protective
nature of the scale cannot be realized. This means that erosion could
maintain the scale at a smaller thickness at which the diffusion controlled
oxidation process will proceed at a higher rate. A situation should exist
where the scale thickness and the oxidation rate remain constant. The rate
of growth of a scale under such erosion-oxidation attack may be expressed as

$$\frac{dX}{dt} = \frac{k}{X} - k_e$$

where X is the scale thickness, k is the scaling rate constant and k_e is the
erosion rate. When a constant thickness is achieved at a critical thickness
X*

$$\frac{dX}{dt} = \frac{k}{X*} - k_e = 0$$

This phenomenon has been observed with cobalt as reported above and
shown in Figure 6, but not with nickel due to the much lower oxidation rates
experienced by nickel. Erosion and oxidation certainly interact in this case
and high sustained rates of damage to the metal result, however the interaction
is such that neither process modifies the fundamental mechanism of the other.

Oxidation Affected Erosion

In this regime of the interaction the basic processes are modified and
the behavior of nickel at 650°C and 800°C is a good example. In this case
the erosive stream has the capacity to remove the oxide just about as rapidly
as it can be formed. Some of the energy of the erosive stream is taken up in
the formation and maintenance of moguls by plastic deformation and this
regime is also characterized by the fact that the erodent particles can pierce

the surface layer, become embedded in the metal and thus be retained in the surface. The surface layer that forms is a composite layer of nickel oxide, nickel and embedded alumina particles. With such a layer it is not possible to predict the rate at which the metal will oxidize since the compact oxide scale to which current theories apply has ceased to exist. It is not known by what mechanisms metal removal occurs but it is thought that they include intense local adiabatic plastic deformation leading to exposure of the metal, by extrusion around impact sites, to the oxidizing atmosphere. Such oxide is then rapidly removed by the erosive stream.

A metal undergoing simultaneous erosion and oxidation may find itself in any of the above regimes depending on the relative oxidation rate and erosion rate. It is possible that different metals exposed to the same erosive situation may behave according to different regimes of the interaction of erosion and oxidation. This is most likely if the metals have very different oxidation rates as has been shown in this work for nickel and cobalt. A schematic of the interaction is shown in Figure 9.

CONCLUSIONS

The interaction between the erosion and oxidation processes applied to metals can vary from simple erosion which removes the oxide layer and imposes a high oxidation rate, to a complex interaction resulting in degradation rates that are very high compared with simple oxidation. The mechanisms are not fully understood but appear to involve severe plastic deformation of the surface layers of the metal. Under the same erosive conditions different metals will degrade according to different regimes of interaction depending on the relative severity of erosion rate of the metal oxide and the rate of formation of the oxide on the metal.

ACKNOWLEDGEMENTS

REFERENCES

1. W. F. Adler; Assessment of the State of Knowledge Pertaining to Solid Particle Erosion Tech. Report, Effects Technology Inc.; 1979. NTIS Report ETI-CR79-680.

2. P. G. Shewman and G. Sundarajan; Am. Rev. Mat. Sci., 13, 301, (1983).

3. I. Finnie; Wear, 3 87 (1960).

4. J. G. A. Bitter; Wear, 6 5, (1963) also 6, 169, (1963).

5. R. E. Winter and I. M. Hutchings; Wear, 29, 181, (1974) also 34, 141, (1975).

6. M. M. Mamoun; Mat. Sci. Div. Coal Tech. 3rd Quarterly Report, ANL-75-XX3 Argonne Nat. Lab. (1975), Appendix: Analytical Models for the Erosive Corrosive Wear Process.

7. P. S. Follansbee: Mechanisms of Erosive Wear of Ductile Materials Due to Low Velocity, Normal Incidence Impact of Spherical Particles, Ph.D. Thesis CMU Pittsburgh (1981).

8. R. Bellman Jr. and A. Levy; Erosion Mechanism on Ductile Metals. Tech. Rept. Lawrence Berkeley Laboratory L. B. L. 10289 (1980).

9. N. P. Suh; Wear, 44, 1, (1977).

10. S. Jahanmir; Wear, 309 (1980).

11. C. S. Giggins and F. S. Pettit; Effects of Erosion on Oxidation and Hot Corrosion of Coated and Uncoated Superalloys. Performed by Pratt and Whitney Aircraft, East Hartford for EPRI, Palo Alto, CA. Report 979-4 1975.

12. I. G. Wright; Effect of Alloy Variables on Resistance of a Material to Attack at High Temperatures where Erosion by Particulates and Corrosion can occur. Carried out by Battelle Columbus, OH, for EPRI, Palo Alto, CA. Report 589 1975.

13. N. Birks and F. S. Pettit; Interactions Between Erosion and Corrosion of Metals and Alloys at Elevated Temperatures. Final Report to U. S. Army Research Office on contract DAAG 29-81-K-0027 April 1984.

EROSION of NiO

90° impingement angle
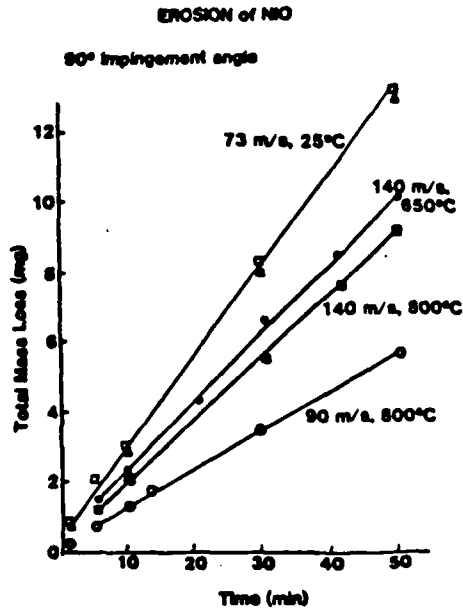
Figure 1. Erosion kinetics for nickel oxide exposed at 90° incidence.
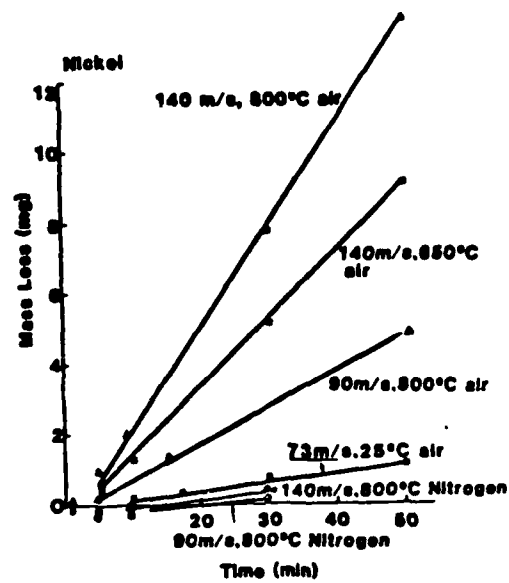
Figure 2. Erosion kinetics for nickel exposed at 90° incidence.
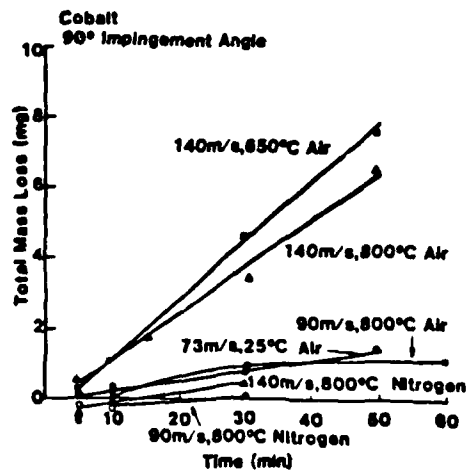
Figure 3. Erosion kinetics for cobalt exposed at 90° incidence
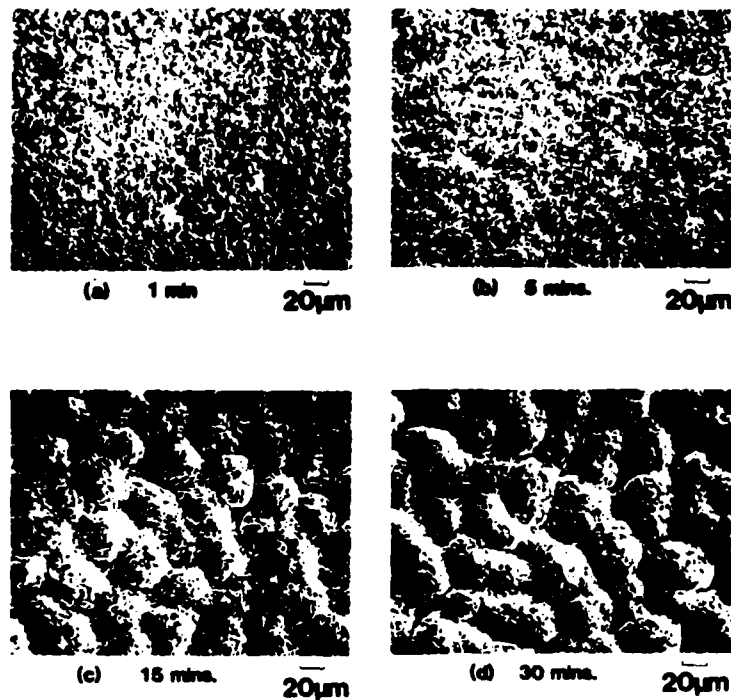
Figure 4. Development of moguls on nickel exposed at 800°C to an erosive stream flowing at 90ms⁻¹ at 90° incidence.
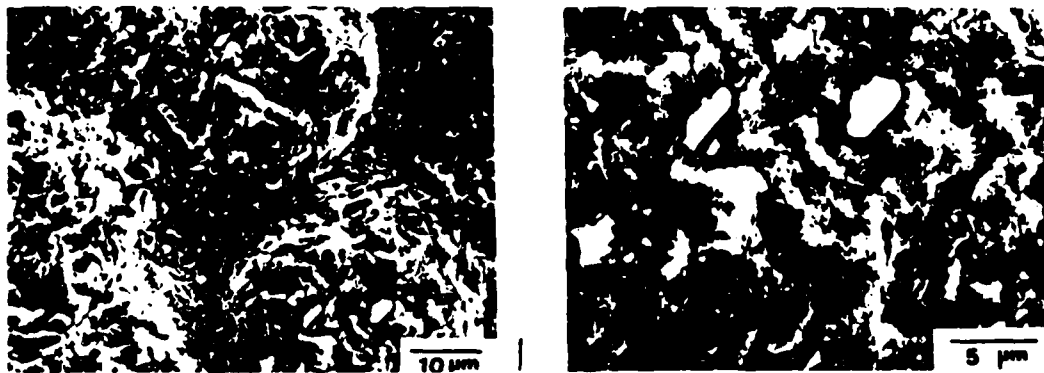
Figure 5. Outer surface of composite layer covering moguls formed on nickel after 10 min. exposure at 800°C to erosive stream flowing at 140ms⁻¹ at 90°C incidence.

Co₃O₄ and CoO labels shown on figure.
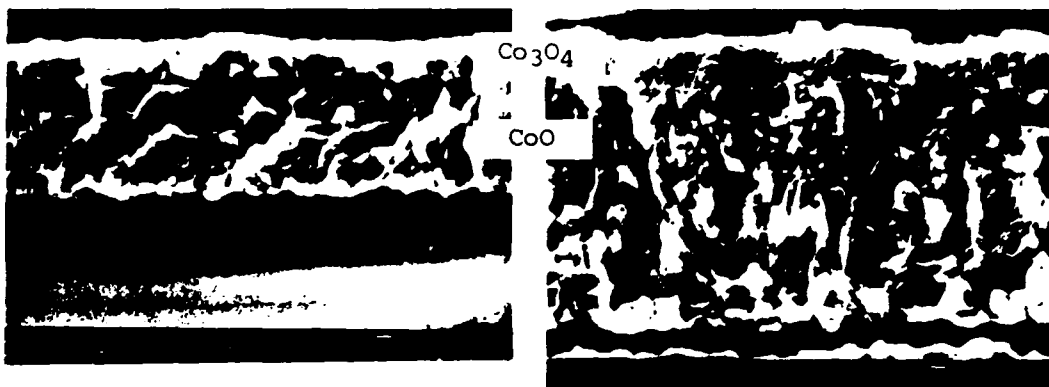
Figure 6. Cross section of scales formed on cobalt after 60 min. exposure at 800° C to (a) erosive stream of air at $90ms^{-1}$ and 90° incidence and (b) from the sample edge where no erosion occurs.
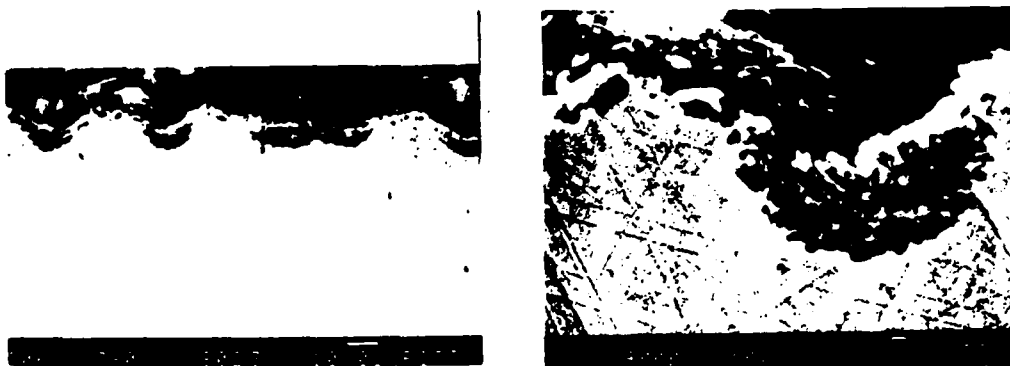
Figure 7. Cross section of cobalt eroded for 30 min. at 800°C in nitrogen flowing at $140ms^{-1}$ showing how erodent particles accumulate in the valleys between the moguls.
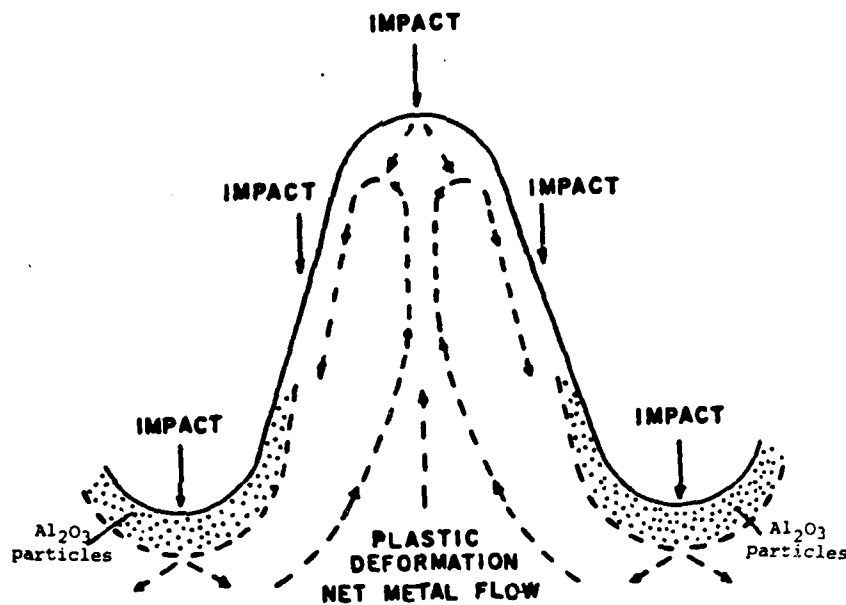
Figure 8. Mechanism of mogul formation. Impacts on sloping mogul face transport material (metal and embedded alumina) down to the valleys between the moguls. Impacts on horizontal surfaces cause plastic deformation resulting in metal flow as indicated, maintaining the mogul shape and size in a steady state condition.
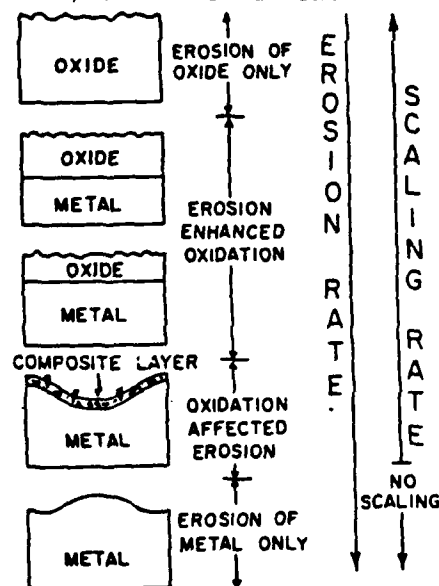
Figure 9. Summary of the modes of interaction of erosion and oxidation depending on the relative rates. The four regimes shown, with typical metal scale structures, are compared with scales for erosion rate and scaling rate. This applies only to systems with compact, adherent, plastic scales.

MECHANISMS OF SYNERGISTIC INTERACTION
BETWEEN EROSION AND CORROSION PROCESSES IN
METALS EXPOSED TO CONDITIONS RELEVENT TO GAS
GAS TURBINE EXPANDERS

by: C. T. Kang, S. L. Chang, F. S. Pettit and N. Birks
Materials Science and Engineering Department
University of Pittsburgh
Pittsburgh, PA 15261

INTRODUCTION

The mechanisms of the high temperature oxidation of metals are well understood, at least to the extent that the reactions between multicomponent alloys and complex gas systems can be explained qualitatively in terms of quite detailed mechanisms even in the presence of simultaneous salt deposition. The general feature of such reactions is that a product layer forms on the metal surface and causes the reaction to slow down, in such cases where diffusion through the scale is rate controlling the reaction rate should fall as the scale becomes thicker in accordance with the parabolic rate law.

Many components used in the hot sections of energy generating cycles rely on such scales for the protection to which they owe their economic working life. Of course, the ever present concern is that the protective nature of the scale layer may be lost. There are several mechanisms by which this might occur through sulfidation, hot corrosion, spalling and other mechanical forms of damage. Most of these mechanisms of deteriation of scales have been studied and are reasonably well understood.

A particular type of mechanical damage that is common to both oxide scales and metals is that of erosion. The erosion of materials has been studied quite extensively, generally at room temperature and in the absence of scale growth phenomena. Reviews of the mechanisms proposed by which material is removed have been published by Adler (1) and Shewman (2).

The mechanisms so far proposed include micromachining (3), plastic deformation (4), ploughing (5)(6), repeated impact fatigue (7), subcutaneous

cracking (8), delamination (9)(10). The predominant mechanism changes according to variables such as angle of impingement, size, shape, hardness, toughness and velocity of the particle; hardness and ductility of the target, the temperature and the composition of the gas.

When a metal is exposed to a rapidly flowing, particle laden, oxidizing atmosphere there is a tendency for a protective oxide layer to form on the surface and, simultaneously, for the erosive particles to remove the surface, be it oxide or metal.

The effects of erosion on high temperature oxidation of metals are not well understood, or even well characterized. Investigations that have been carried out have largely simulated conditions in gas turbines (11) or coal combustors (12). Although such studies allow the behavior of different materials to be compared under closely simulated commercial conditions, the experimental variables are not sufficently well controlled to allow the relevent interactions to be described or understood in terms fundamental mechanisms. Similarly, the problems and pratical difficulties involved in producing well defined and controlled conditions in the laboratory have retarded fundamental studies of these interactions. Consequently much of the data that is available pertains to the room temperature erosion of specimens that were previously oxidized at high temperature (8). Currently work is beginning to be done successfully to study the conjoint erosion and scaling of metals and alloys at high temperature.

The work carried out so far has indicated however that the interaction between erosion and oxidation at high temperature is significant and the present investigation had the objective of studying these interactions under well defined and well controlled conditions.

EXPERIMENTAL

The apparatus was designed to supply a stream of gas flowing at speeds up to $300ms^{-1}$ and at temperatures up to $900^{o}C$ carrying 20 µm alumina particles moving

2

at the same speed and temperature. This erosive flow was discharged through a 9mm diameter nozzel which allowed specimens 10mm x 15mm x 2mm to be used, this size being well suited for easy handling and examination.

As shown in Figure 1 the compressed air was cleaned of oil and particulates and dried to pass through a flowmeter and a fluid heater to be heated to 700°C. The alumina particles were fed into the air stream at this point by a secondary stream of air fed from a Sylco IX powder dispenser. Alumina particles 20 μm diameter were used since they were inert and calculation showed that they would not be deflected by the stream lines around the specimen. This particle laden gas stream was then passed down a 1.5m long Inconel tube, aluminized to prevent spallation of its surface oxide. The air stream emerged at the chosen temperature and velocity to impinge on the sample which could be held at any angle, although most of the work was carried out at 90° to the erosive flow.

The specimen was heated by the incident gas flow and also from behind by a focussed radient heater to ensure uniform temperature which was measured by a thermocouple buried in the specimen.

Particle speeds were measured using a laser doppler velocimeter coupled to an Apple II computer, excellent agreement being obtained between measured particle velocities and those calculated for the gas stream. The apparatus allows erosion-oxidation interactive attack to be studied over a wide range of parameters such as temperature, particle velocity, gas composition and incident angle, each of which can be controlled independently within wide limits. After exposure, the specimens were examined using optical metallography and SEM-EDS.

RESULTS

EROSION OF NICKEL OXIDE

Figure 2 shows the erosion kinetics for nickel oxide eroded at a 90° angle at various temperatures and particle velocities and shows that the erosion rate increases at lower temperatures and higher velocities. The initial oxide surface

3

of crystalline facets is completely modified to a more or less plane surface with frequent evidence of cutting and plastic deformation of the oxide after erosion at 800°C as seen in Figure 3. The surface after erosion at 25°C shows similar features but cracking or tearing is more frequently in evidence.

EROSION OF NICKEL AND COBALT

The erosion of these metals in the absence of oxidation was studied at 800°C in 99.999% pure nitrogen and at 25°C in air where oxidation may be neglected. In both cases, as shown in Figure 4, the metal surface shows evidence of cutting, indentation and plastic deformation, which led to the hill and valley topography referred to as moguls subsequently. The rapid oxidation characteristics of cobalt caused oxide nodules to form on these specimens during cooling. The rate of metal removed is very low as shown in Figure 5 where the rates of erosion of nickel and cobalt are given under a variety of conditions.

At 800°C, under an erosive stream of nitrogen laden with 20 μm alumina particles flowing at $140ms^{-1}$, moguls formed on both nickel and cobalt. A section through the mogul feature showed clearly that alumina particles had been captured and had been transported down the mogul sides to accumulated in the valleys between the moguls. This occurred with both nickel and cobalt and is shown in the case of cobalt in Figure 6. From these results it can be inferred that the extensive plastic deformation of the metal surface does not lead to rapid material removal but does lead to the formation of the hill and valley mogul surface feature referred to.

CONJOINT EROSION AND OXIDATION OF NICKEL AND COBALT

The rates at which the specimens were degraded can be seen in Figure 5 for both nickel and cobalt. It can also be seen that the erosion damage rate increases markedly when these metals are exposed to erosion in oxidizing atmospheres at high temperature.

Samples of nickel exposed at 650°C in air showed mogul development to be well established after 30 minutes exposure to a $140ms^{-1}$ eroding stream. Similar results

were obtained at 800°C in air exposed at a $140ms^{-1}$ erosion stream except that, at this temperature, the mogul development was achieved after only 6 minutes. The relationship between mogul development and the rate of energy input of the erosive stream is emphasised by the fact that at 800°C a nickel sample similarly exposed to a $90ms^{-1}$ erosive stream took 15 minutes to develop moguls as shown in Figure 7. The surface of this nickel specimen at high magnification as shown in Figure 8 shows clear evidence of cutting, plastic deformation, cracks or tears and alumina particle capture and embedment.

Although the runs were mainly carried out at an incidence of 90° to the erosive flow, several experiments were carried out at 45° to the flow, in these cases the surface was modified into ripples which showed the same microstructural features as with the 90° specimens, cutting, indentation and evidence of plastic deformation.

In section it was possible to examine the nature of the 'scale-metal interface' which is shown in Figure 9 and it is seen that there is no scale as such, instead a complex composite surface layer exists comprised of nickel oxide embedded alumina particles and nickel metal extruded into this layer by the individual erosive impacts.

Cobalt was exposed under similar conditions to nickel with broadly similar results. It also formed moguls but somewhat more slowly, in fact, after 30 minutes exposed to an erosive stream flowing at $90ms^{-1}$ at 800°C moguls had not formed, the specimen surface remained quite flat and an oxide layer had formed that was quite uniform but substantially thinner than the corresponding oxide layer grown in air at 800°C as shown in Figure 10 which compares 60 minutes exposure to erosion and oxidation with oxidation only. The eroded scale is seen to be about half as thick.

This is significant as it emphasises that an oxide scale formed under erosive conditions is similar to a normally formed oxide scale except that it is thinner due to erosive action at the scale gas interface. Figure 11 shows a section through moguls formed on cobalt at $140ms^{-1}$ at 800°C, the surface layer is a composite

layer comprised of cobalt oxide CoO with a thin surface layer of Co_3O_4 embedded alumina is also found in this surface.

In most cases when cobalt is exposed, a thin surface of Co_3O_4 forms, this is not thought to affect the overall process and it is not known whether it exists at temperature under conditions where moguls form.

DISCUSSION

The features to be explained are the removal of oxide from a simple oxide surface under erosive conditions, the very low rate of metal removal when oxide formation is precluded under identical erosive conditions and the interaction between erosion and oxidation that produces a surface composite layer and very rapid rates of material removal.

These phenomena can be addressed under the headings of what are regarded to be three distinct stages of erosion-corrosion interaction as follows.

PURE EROSION

Nickel Oxide

The kinetics of pure erosion of nickel oxide were measured on a weight loss basis, the loss in weight is a direct measure of the nickel oxide removed by the erosive processes and is expected to vary with particle loading, velocity, inclination and temperature. Somewhat surprisingly, the surface features of the nickel oxide show evidence of mainly plastic deformation with some tearing especially at the lower temperatures. It is clear from the kinetic data that the rate of erosion of nickel oxide increases at lower temperatures. The actual mode of material removal is not known however, in keeping with these results, it has been proposed that erosion of nominally brittle materials by small particles at high velocity can lead to ductile behavior in the vicinity of the impact site [13] Clearly, at high temperatures, where the oxide plasticity is greater the plastic mode of deformation would be expected to predominate.

NICKEL AND COBALT

When these pure metals are eroded in the absence of oxidation at both 800°C and 25°C the surfaces show signs of much plastic deformation, however the erosion rates are very low. Initially a weight gain is observed and is attributed to the accumulation of captured erodent particle fragments. Subsequently the corrosion rates settle down to a very low value. It appears that plastic deformation does not necessarily lead to removal of material and it is doubtful whether in these cases at 90° incidence, any mechanism involving fatigue or work hardening can be feasible. This doubt is justified in view of the very high strain rate of a small volume that is involved practically ensuring that the plastic deformation occurs adiabatically resulting in surface heating. The actual mechanism by which metal is removed is not known but, from the kinetics, both cobalt and nickel are sufficiently plastic over the temperature range 800°C-25°C for most of the incident energy to be absorbed. The formation of moguls is also observed to occur under these conditions and, consequently, it appears that mogul formation requires only plastic deformation and does not require material removal to occur.

EROSION ENHANCED OXIDATION

It was shown above that, while oxides can be eroded quite severely, metals which are ductile show only low rates under 90° incidence. Thus if a metal can be converted to oxide the erosion-oxidation synergistic attack should be enhanced. Erosion enhanced oxidation is the simplest form of coordinated attack by erosion and oxidation. Basically the erosion of the oxide maintains the oxide layer at a thickness which corresponds to a rate of growth of the scale that is equal to the rate of erosion. Under such conditions the scale remains at constant thickness. It should therefore be possible to calculate the rate of erosion by using the thickness of the limiting scale and the parabolic oxidation rate constant. However, a surface layer of damage in the oxide is thought to form as a result of the erosive impacts. The damaged layer being rich in dislocations and other defects will have a higher ionic

mobility than would be implied by from the normal value of the parabolic scaling constant whose use would thus lead to an under estimation of the erosion rate. This steady state phenomenon has been demonstrated in the case of cobalt but could not be achieved for nickel due to the latter's very low oxidation rates. The main point in this regime is that although erosion and oxidation interact they do so in a way that does not modify the fundamental behavior of each process.

OXIDATION AFFECTED EROSION

The oxidation rate of nickel is so low that only a very thin composite surface layer can be formed on the nickel surface. This surface is not a compact protective oxide layer but is the composite covering of a heavily plastically deformed metal surface with extensive mogul formation. The composite layer is about 1 μm thick and is composed of discontinuous nickel oxide with alumina particles embedded through it into the metal; the composite layer also includes nickel metal extrusion, thrown up by the plastic deformation of the impacts.

Under these conditions, the presence of the metal substrate, which can absorb some of the incident energy and cause particle capture, must modify the erosion behavior. Conversely the disruption of the surface layer by the impacts and the continued exposure of extruded nickel metal to the oxidizing atmosphere must impose oxidation rates that cannot be predicted by any data obtained in the absence of erosion. Consequently this regime produces removal of material and degradation at rates that cannot be predicted and represents a true complex interaction of the basic erosion and oxidation processes where each produces a fundamental modification to the mechanism of the other.

Although it is possible to hypothesise about material removal mechanisms there is very little direct evidence to use concerning the details of these mechanisms.

CONCLUSIONS

It has been demonstrated that considerable interaction exists between erosion and high temperature oxidation processes when both are present simultaneously.
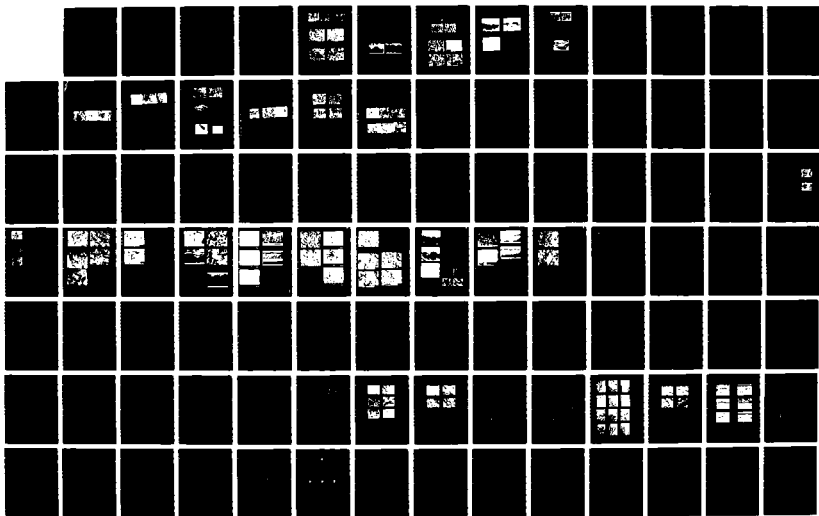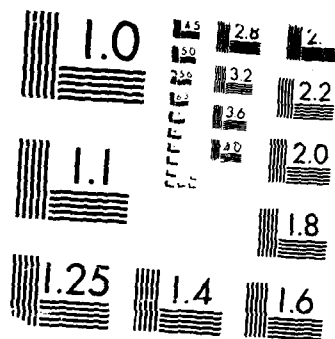
MICROCOPY RESOLUTION TEST CHART

The interactions vary from simple, partial removal of a growing oxide scale by erosion, resulting in less of protective behavior and the maintainance of high oxidation rates, to direct interaction between the processes in which the erosive impacts prevent the formation of a protective layer and, instead, a complex, unprotective, composite surface layer forms resulting in enhanced exposure of the metal to oxidation processes and its removal as oxide. Under the latter condition severe plastic deformation of the metal surface also occurs and local temperature increase is likely. The interaction that is observed depends upon the relative intensities of the erosion and oxidation rates and therefore varies strongly from one system to another under a given set of erosion and atmosphere conditions.

ACKNOWLEDGEMENT

REFERENCES

1. W. F. Adler; Assessment of the State of Knowledge Pertaining to Solid Particle Erosion Tech. Report, Effects Technology Inc.; 1979. NTIS Report ETI-CR79-680.

2. P. G. Shewman and G. Sundarajan; Am. Rev. Mat. Sci., 13, 301, (1983).

3. I. Finnie; Wear, 3 87 (1960).

4. J. G. A. Bitter; Wear, 6 5, (1963) also 6, 169, (1963).

5. R. E. Winter and I. M. Hutchings; Wear, 29, 181, (1974) also 34, 141, (1975).

6. M. M. Mamoun; Mat. Sci. Div. Coal Tech. 3rd Quarterly Report, ANL-75-XX3 Argonne Nat. Lab. (1975), Appendix: Analytical Models for the Erosive Corrosive Wear Process.

7. P. S. Follansbee: Mechanisms of Erosive Wear of Ductile Materials Due to Low Velocity, Normal Incidence Impact of Spherical Particles, Ph.D. Thesis CMU Pittsburgh (1981).

8. R. Bellman Jr. and A. Levy; Erosion Mechanism on Ductile Metals. Tech. Rept. Lawrence Berkeley Laboratory L. B. L. 10289 (1980).

9.   N. P. Suh; Wear, 44, 1, (1977).

10. S. Jahanmir; Wear, 309 (1980).

11. C. S. Giggins and F. S. Pettit; Effects of Erosion on Oxidation and Hot
     Corrosion of Coated and Uncoated Superalloys. Performed by Pratt and
     Whitney Aircraft, East Hartford for EPRI, Palo Alto, CA.   Report 979-4
     1975.

12. I. G. Wright; Effect of Alloy Variables on Resistance of a Material to
     Attack at High Temperatures where Erosion by Particulates and Corrosion
     can occur. Carried out by Battelle Columbus, OH, for EPRI, Palo Alto,
     CA. Report 589 1975.

13. I. Finnie and G. S. Sheldon; J. Eng. for Industry, Nov. 1966, p. 387.
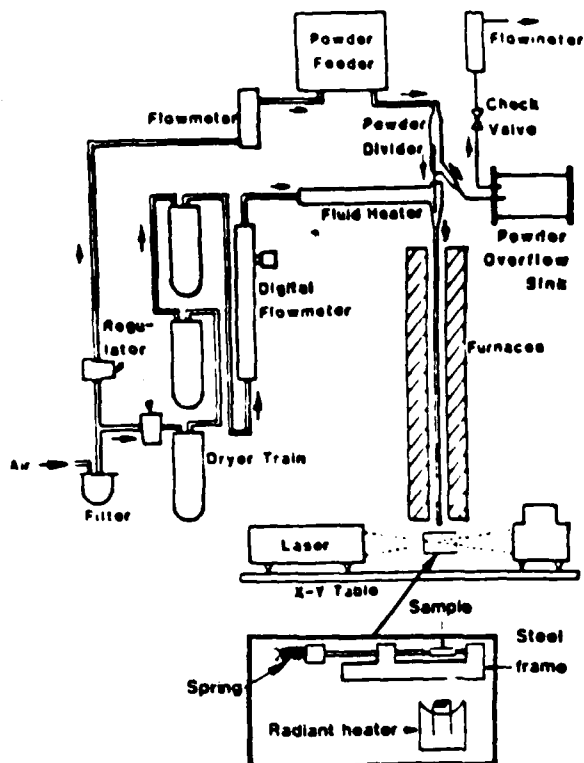
Figure 1
Diagram of appratus for simultaneous erosion and oxidation of metals.

EROSION of NiO

90° Impingement angle

73 m/s, 25°C

140 m/s, 650°C

140 m/s, 800°C

90 m/s. 800°C

Total Mass Loss (mg)

Time (min)
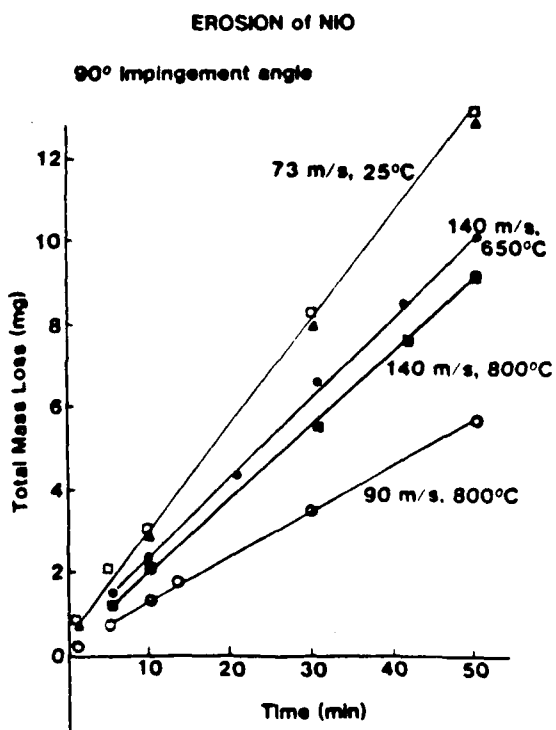
Figure 2
Erosion kinetics for NiO held at 90° to the erosive stream.
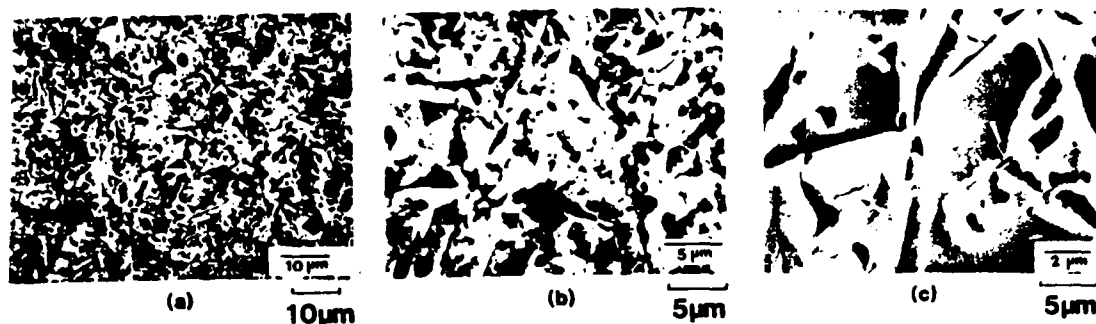
Figure 3 NiO eroded at 800°C and 140 ms^{-1} showing
plastic deformation and cracking or tearing.

(a)

(b)

(c)

(d)
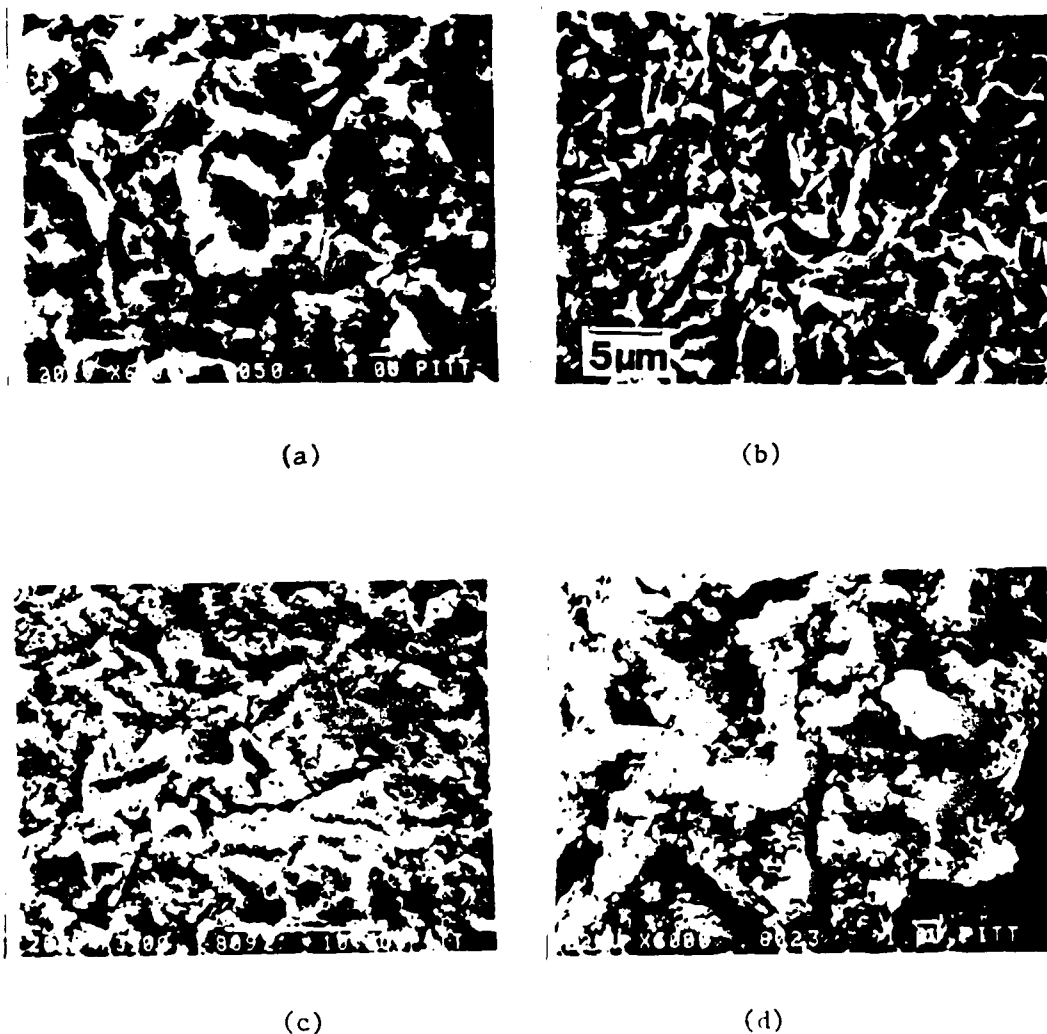
Figure 4 Surface of nickel and cobalt eroded at 800°C
and 25°C in the absence of oxidation.
(a) Ni, 25°C, air; (b) Co, 25°C, air;
(c) Ni, 800°C, nitrogen; (d) Co, 800°C, nitrogen.
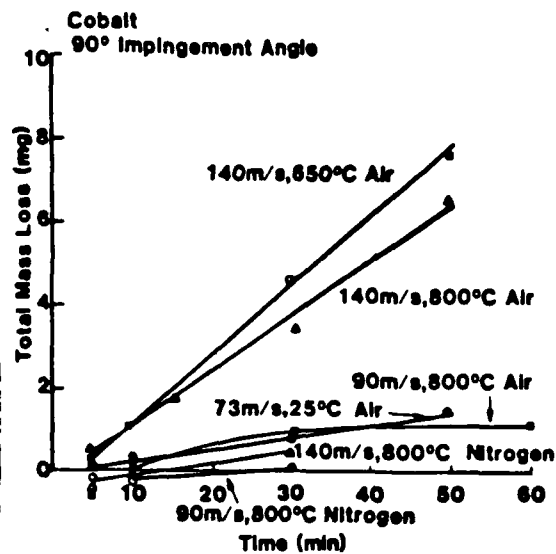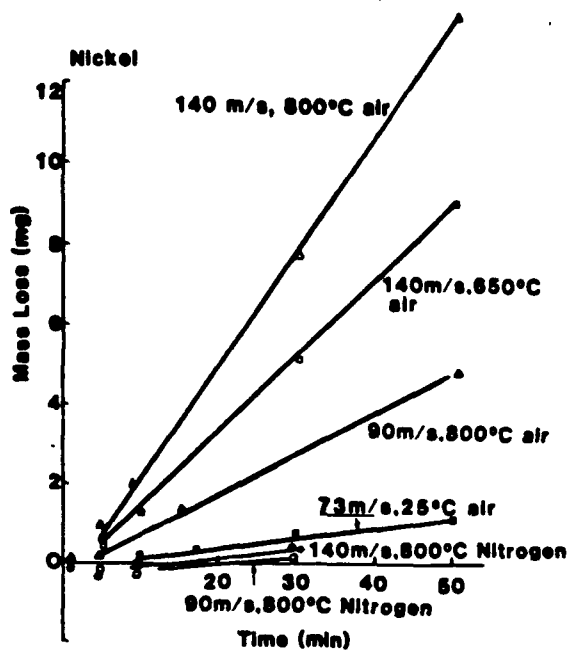
Figure 5   Erosion-oxidation kinetics for Ni and Co
            exposed at 90° to erosive stream under various
            conditions.
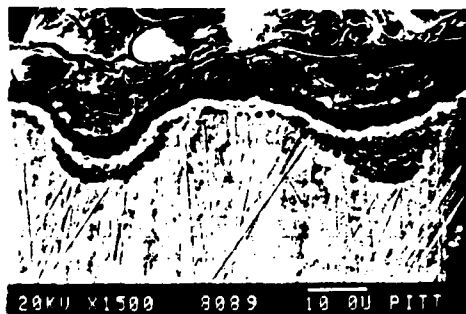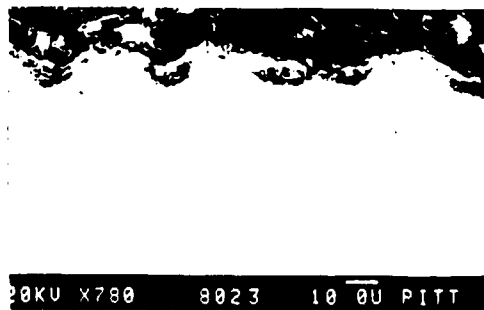
(a)   (b)

Figure 6   Sections through moguls formed during erosion
            in that oxidation at 800°C in nitrogen for
            (a) nickel and (b) cobalt after 30 minutes
            exposure. Alumina particles accumulate in the
            valley in each case.
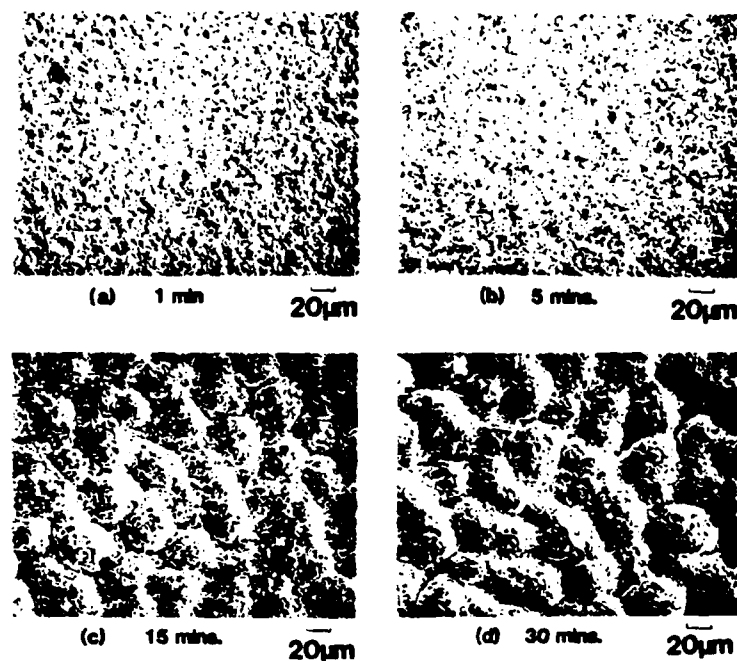
Figure 7 Development of moguls on Ni eroded at 800°C at 90° to erosive stream flowing at 90 ms^{-1}.

(a)

(b)

(c)

(d)
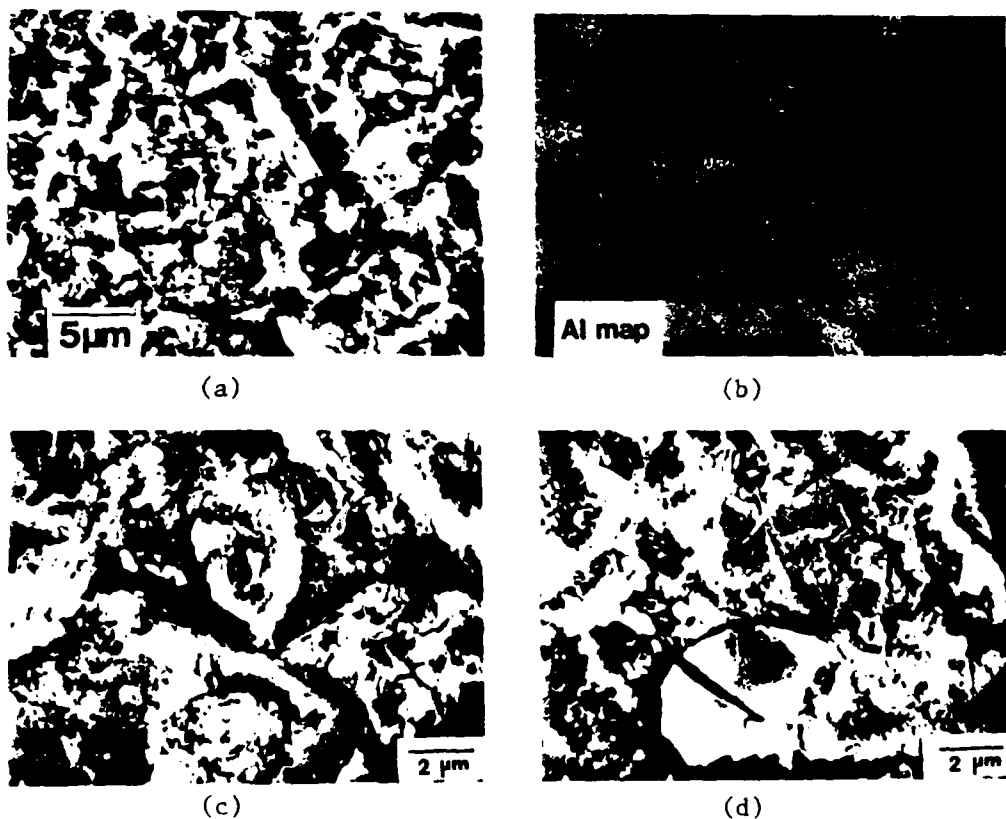
Figure 8 Surface of specimen of Figure 7(c) showing evidence of cutting, plastic deformation, and particle capture.

(a)

(b)

Scale

(c)   Al X-Ray map of 6(a)
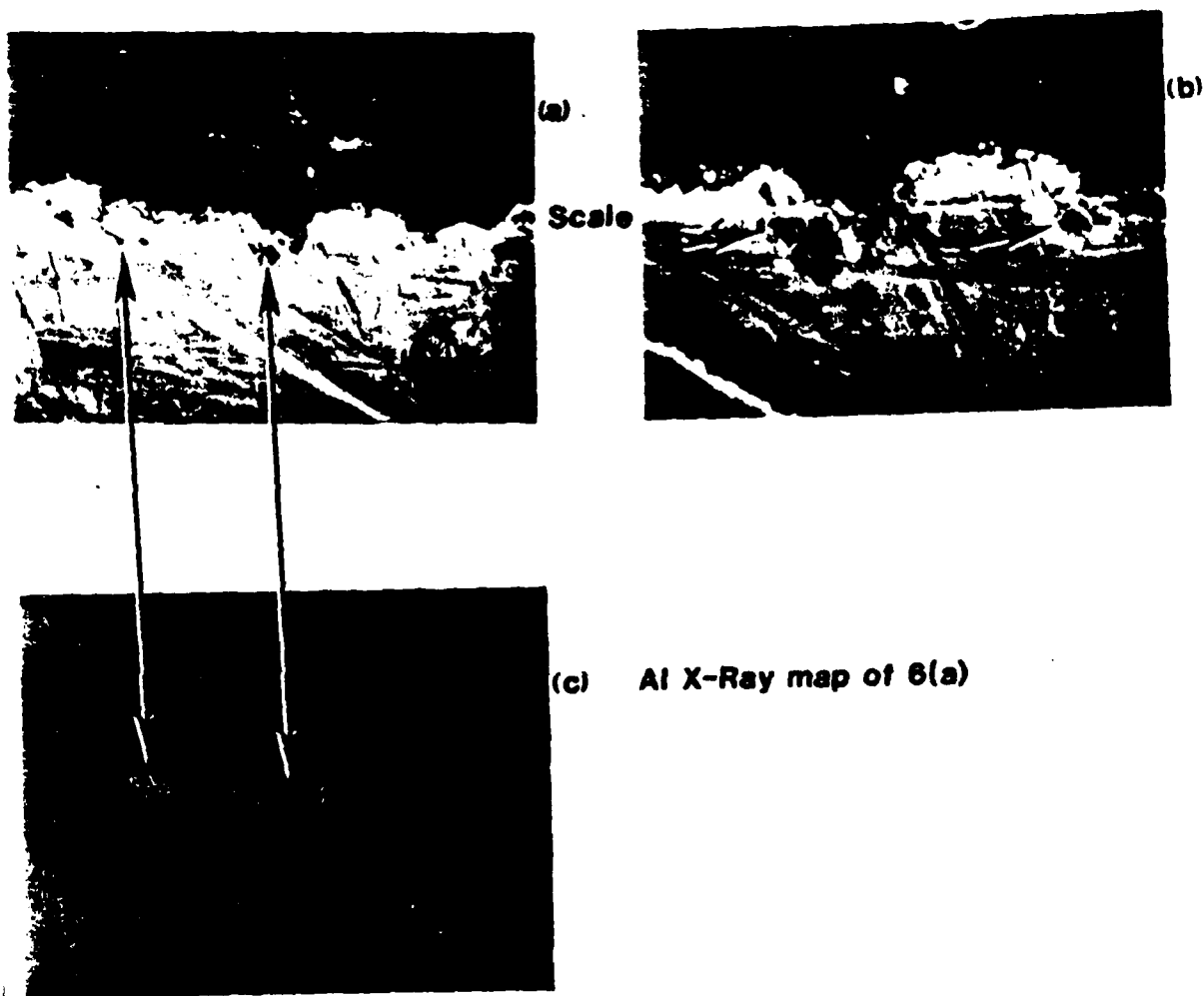
Figure 9   Section through composite layer formed on moguls
on Ni exposed to 190 ms^{-1} airflow at 810°C for
50 min.   Captured alumina particles are indicated.

(a)   (b)

Figure 10   Comparison of oxide layers formed on cobalt
             after (a) erosion-oxidation at 800°C in
             90 ms^{-1} airflow for 60 minutes and (b)
             oxidation only at 800°C in air for 60 minutes.

Figure 11   Section through mogul formed on cobalt showing
             Co_3O_4 cover as the surface layer.

SIMULTANEOUS EROSION AND OXIDATION OF NICKEL AT HIGH TEMPERATURES

C. T. Kang, F. S. Pettit and N. Birks

Metallurgical and Materials Engineering Department
University of Pittsburgh
Pittsburgh, PA 15261

ABSTRACT

Structural alloys and coating alloys have been developed that
successfully resist high temperature oxidation and, to a lesser
extent, hot corrosion—depending on conditions. Such protection
depends upon the maintenance of a surface layer of oxide that
effectively separates the metal from the reactive environment.

The oxide protective coatings may however be damaged by
erosion by solid particles in the gas flow, the effect being worse
when the velocity of the gas flow is high. Unfortunately the
detailed mechanisms by which the processes of erosion and oxidation
interact at high temperatures are not understood. Much of the
work carried out so far has involved studies of the erosion of
metals and oxidized metals at room temperature under controlled
conditions, or has involved tests at high temperature under con-
ditions designed to simulate those in gas turbines or coal com-
bustors. The data obtained from such tests are well suited to
producing reliable comparisons of the behavior of different materials
but do not readily lead to analysis of the mechanisms by which
erosion and corrosion interact at high temperature.

This paper is concerned with the erosion-oxidation of nickel.
An apparatus is described in which specimens can be exposed to
well defined and controlled conditions. Results are then pre-
sented on the erosion-oxidation of nickel and models are developed
to describe the observed interaction between these two processes.

INTRODUCTION

The high temperature corrosion, or oxidation, of metals and
alloys is quite well understood, at least to the extent that in-
teractions between multicomponent alloys and complex gas systems,
with and without salt deposition, can be explained in terms of
quite detailed mechanisms in a qualitative manner. A general
feature of this type of reaction is that the reaction product forms
on the surface of the metal and provides some degree of protection
from further attack. Thus, where the reaction rate is controlled
by the diffusion of species through the scale, the reaction rate is
expected to fall as the scale thickness increases, in accordance
with the well known parabolic rate law.

The erosion of materials has also been studied, mainly at
room temperature and usually in the absence of surface layers -
renewable or otherwise. From the work already carried out on
erosion, several mechanisms by which material is removed from the
surface have been proposed. These have been reviewed by Adler[1].
The mechanisms so far proposed include micromachining[2], plastic
deformation[3], ploughing[4], fatigue by repeated impact [5][6], sub-
cutaneous cracking[7] and delamination [8][9]. The predominant
mechanism changes according to the experimental parameters such as
angle of impingement, degree of ductility shown by the material, the
relative hardness of the eroding particle, etc.

When a metal is exposed to a rapidly flowing, particle laden,
oxidizing atmosphere, there is a tendency to form a protective
oxide layer and, simultaneously, for the incident erosive particles
to remove the oxide layer and, perhaps, begin to remove the metal
also. The effects of erosion on high temperature oxidation of alloys
are not well understood or even characterized. Investigations that
have been carried out have largely simulated conditions in gas
turbines[10] or coal combustors[11]. Such studies allow the re-
sponses of different materials to be compared, but the lack of
control and definition of the appropriate experimental variables
involved does not allow the observed interactions to be understood
in terms of fundamental mechanisms. Laboratory work into the
simultaneous erosion and oxidation of metals at high temperature
under well defined conditions has been held back by the associated
experimental problems. This has restricted the data obtained to a
limited range of variables or to that pertaining to the room
temperature erosion of specimens oxidized at high temperature.

Such work has, however, indicated that significant interaction
occurs between erosion and oxidation occuring simultaneously at
high temperature. The present work was undertaken to produce an
apparatus to study this interaction under well defined and con-
trolled conditions in order to improve our understanding of the
mechanisms by which the interactions occur.

EXPERIMENTAL

The design aims of the apparatus were to supply a stream of gas at speeds up to 300 ms^{-1} and temperatures up to 900°C. The gas stream was also to contain a controlled loading of alumina particles moving at the same speed and at the same temperature as the gas. A nozzel diameter of about 10mm was chosen in order to allow reasonably large specimens, 10mm X 15mm X 2mm, to be used in experiments. This size is well suited to subsequent handling and examination.

A diagram of the apparatus is shown in Figure 1. The gas used, compressed air, is cleaned and dried to remove traces of oil, water and dust. The air then flows through a flowmeter and fluid heater which preheats it to about 700°C. At this point the alumina particles are introduced to the gas stream. The particles used are 20µm alumina particles which were chosen since calculations showed that they would not be deflected by the gas streamlines around the specimen, also alumina is relatively inert and its properties are well characterized.

A second flow of compressed air is taken to a Sylco Mark IX dispenser to produce a particle laden air stream which is passed into a simple gas flow divider, one tenth being introduced to the heated air flow to form the erosive stream while the remaining nine tenths are collected in a filter bag.

The erosive gas stream, already at 700°C, is passed down a vertical, heated, Inconel tube, 1.5 meters long, to be accelerated and heated further. Gas and particles emerge at the 9.3mm diameter nozzel at speeds up to 300ms^{-1} and at temperatures up to 900°C. The Inconel tube is aluminized to avoid spallation of oxide from the inner tube surface into the erosive gas stream.

The specimens are held in a holder under spring compression to allow for differential changes in length due to thermal expansion on heating. The specimen may be held at any angle to the erosive flow and is heated by contact with this gas stream. In order to eliminate temperature gradients, the specimen is also heated by a focussed radiant heater from the back side. This is also shown schematically in Figure 1 together with the position of a laser doppler velocimeter used to measure the speed of the erosive particles.

The laser velocimeter is mounted on a table whose position may be adjusted accurately in both horizontal directions. This allows the velocity of erosive particles to be measured at positions over the entire cross section of the gas stream. An individual analysis measures the speeds of particles passing through a volume of 0.1mm^3 where the twin laser beams cross. The output of data from the
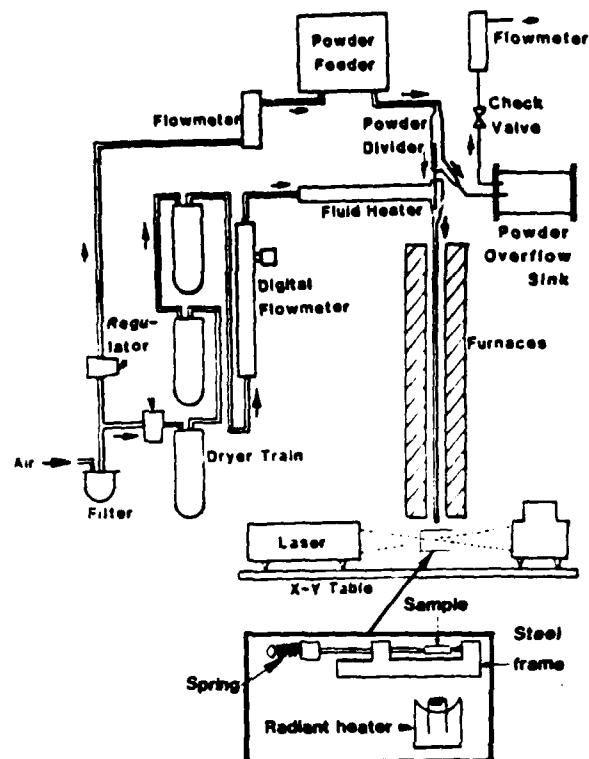
Figure 1. Schematic diagram of apparatus for the simultaneous erosion and oxidation of metals.

velocimeter is fed into an Apple II computer and, in Figure 2, the particle velocities are shown in the form of a frequency distribution whicn is not symmetrical about the mean velocity. For this gas velocity the peak velocity obtained from the distribution was 85m/s. Excellent agreement has been obtained between measured particle velocities and calculated gas stream velocities, which confirms both the accuracy of the velocimeter and also that most particles reach gas velocity before leaving the Inconel acceleration tube. The velocimeter integrates well with the apparatus and may be used in situ without disturbing the rest of the apparatus to measure velocities of both hot or cold gas streams; so far velocities up to 240 ms^{-1} have been used regularly.

Using this apparatus, specimens can be exposed to conjoint erosion-oxidation over a wide range of well controlled, well defined, particle velocities, temperatures and angles of incidence to the specimen. The gas composition can also be varied and deposits to simulate hot corrosion could be made to the specimen surface.

The specimens are examined after exposure using optical metallography and scanning electron microscopy with EDX analysis. Prior to exposure all specimens were polished through 1um Al_2O_3

MEAN = 81.2 m/s   T.I. = 0.065
% TOTAL = 97
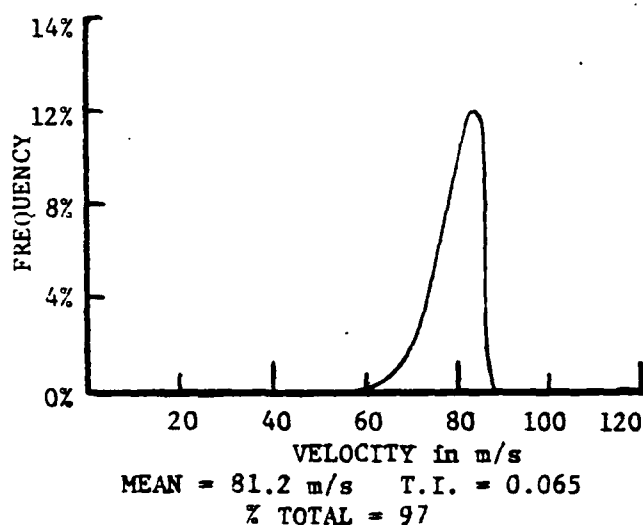
Figure 2. Frequency distribution of particle velocities in the
center of the erosive gas stream. The calculated gas
stream flow rate of 70 ms^{-1} is an average across the
nozzle aperture in the center of the gas stream, the
velocity is expected to be slightly higher in the center
than at the sides, thus the peak velocity here is
about 85 ms^{-1} which is taken to be good agreement between
measurement and calculation.

and cleaned by rinsing in acetone.

RESULTS AND DISCUSSION

Specimens of nickel, Ni-270, were exposed in air to different
conditions involving a variety of particle speeds, temperatures
and angles of particle impingement. After exposure, the specimens
were examined using the SEM and an electrolytic scale stripping
procedure to allow the metal and scale surfaces at the metal-scale
interface to be examined. In this paper results will be presented
for temperatures of 800°C, 650°C and 25°C and an impact angle of
90°.

Surface Morphological Features of Nickel

In the case of polished specimens, a thin (1μm) scale of NiO
was observed to form upon the specimens' surfaces under erosion-
oxidation conditions with 90° incidence of the erosion stream. In
addition, this oxide covered surface developed a surface topography
composed of hills and valleys, or moguls, Figure 3a. The moguls
became aligned into ripples at acute angles of incidence such as
45°, Figure 4a and 4b. The oxide scale was composed of nickel
oxide with embedded alumina particles, Figures 3b and 3c. There

was clear evidence of cutting and plastic deformation of the oxide, Figure 4c, and in many cases it appeared that plastic deformation of the metal had also taken place, Figure 5.

Plastic deformation of the metal below the scale is believed to be responsible for mogul formation since this was not evident on specimens with thick scales of NiO formed during preoxidation treatments. The particle impacts are also thought to cause extrusion of both metal and oxide when the oxide scale is thin, thus exposing a greater surface area of both to the gas atmosphere and consequently increasing the oxidation rate.

To attempt to account for mogul formation, via plastic deformation of the substrate, a model, using computer simulation, was constructed based on the formation of a well, or depression, having a raised rim with no material removal at each impact. The computer was used to sum the effects of many such impacts occurring at random over a surface. The resulting surface profile, shown in Figure 6, is very similar to the mogul pattern observed on nickel specimens having thin NiO scales, Figure 3a. Such results confirm the role of plastic deformation in mogul formation by causing

50μm	10μm	5μm
(a) Oxide Surface	(b) Oxide Surface with Embedded Particles	(c) as (b)
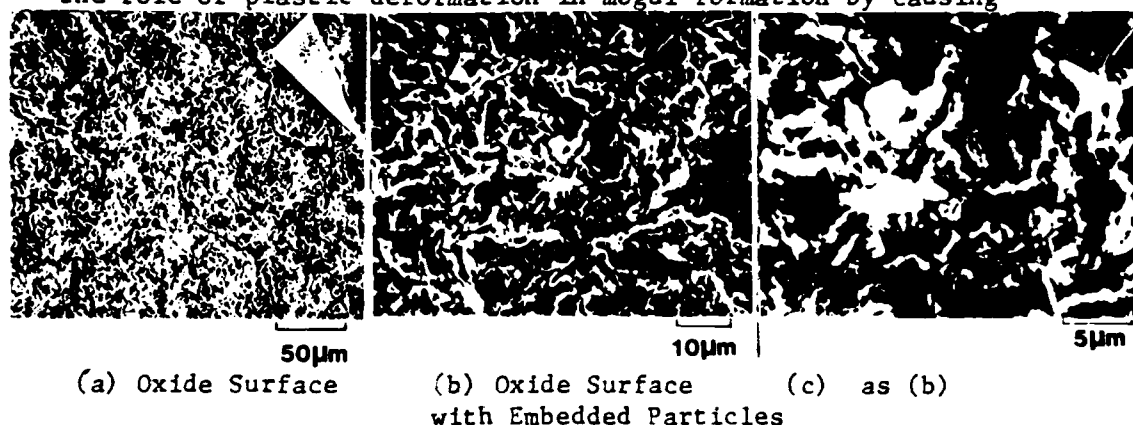
Figure 3. Nickel exposed for 8 min. at $810^{\circ}C$ at 90° impact angle to 190 ms^{-1} airflow containing 1500 ppm Al_2O_3.

surface rearrangement and also indicate that moguls may form in the absence of material removal. Nevertheless, removal of metal and oxide do occur in the erosion-oxidation process as will be shown subsequently.

The removal of material from specimens during erosion-oxidation is believed to occur by several different mechanisms. Material removal by adhesion to alumina erosion particles has been confirmed by examination of such particles after impact when NiO was seen adhering to the surfaces, Figure 7. Calculations show that about 10% of the material removal might occur by this mechanism. Another perhaps more important, process involves removal of material by

plastic deformation of the metal and the thin oxide scale. Typical features are shown in Figures 3c, 4c, and 5b. Repeated deformation of the composite surface (i.e. thin oxide on metal) results in the development of platelets and extrusions of oxide covered metal. Even when a given particle impact fractures the oxide, the exposed

(a) Oxide surface   (b) Oblique view of   (c) Surface showing
    showing ripples   surface in (a)   ripple, erosive
                                             cuts and embedded
                                             Al_2O_3.
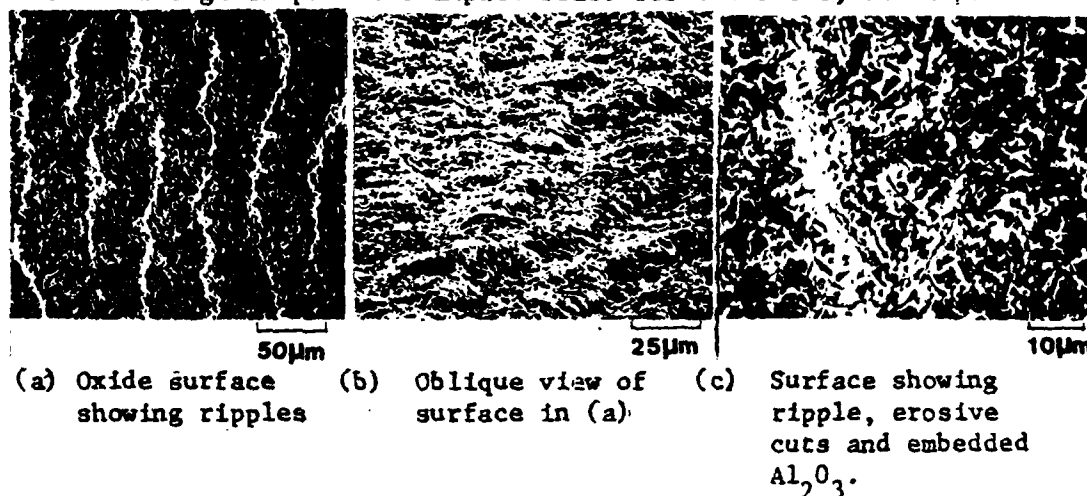
Figure 4. Nickel exposed for 30 min. at 730°C at 45° impact angle
           to 120 ms^{-1} airflow containing 2400 ppm Al_2O_3.

surface soon becomes oxide covered. Eventually small particles of metal, covered with thin oxide, become detached from the metal surface and excessive deformation results in fracture. It is important to emphasize the composite nature of the surface and that the response of the surface is dependent upon the thickness of the oxide scale present upon the metal.

A typical layer of oxide that formed upon a polished nickel specimen during erosion-oxidation is shown in Figure 8a. The scale was composed of nickel oxide, some extruded nickel, and some embedded alumina particles, Figure 8b. It is worth noting that in all of the experiments performed on the erosion-oxidation of nickel, the erosion rate appeared to be such that the scale approached some constant thickness. For example, when specimens were preoxidized and tested in erosion-oxidation, the scale thickness gradually decreased and approached values close to those observed on polished specimens subjected to no preoxidation treatment.

When experiments were performed at room temperatures or at elevated temperatures in nitrogen, no oxide scale was present except for a small amount of oxidation that occurred as the hot specimen was removed from the nitrogen gas stream. Typical surface morphological features are shown in Figures 9 and 10. Under both conditions substantial amounts of plastic deformation are evident. Most of these morphological features are similar to
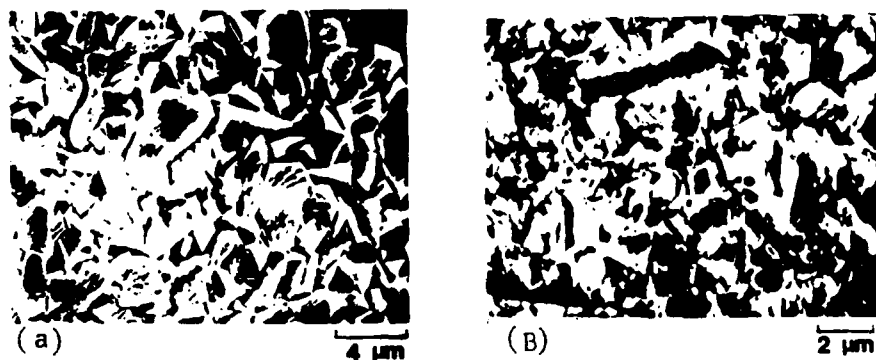
Figure 5. Appearance of scale before corrosion, (a), and (b) after to 74 ms^{-1} for 1 min. showing features consistent with plastic deformation of surface (at temperature of 20°C).

single impact plastic deformation profile
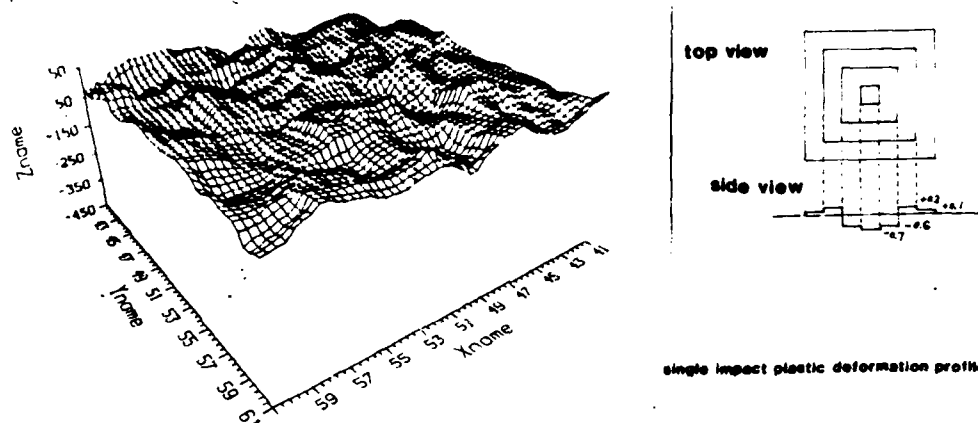
Figure 6. Computer simulation of surface morphology showing mogul formation after 10^6 random impacts each causing a plastic deformation profile as shown, assuming no material removal occurs.

Figure 7. Scanning electron micrograph showing attachment of nickel or nickel oxide to a bombarding Al_2O_3 particle.

those of the oxide covered surfaces except that more deformation
appears to have occurred on the specimens having neglible amounts
of oxidation.   It also was observed that more Al_2O_3 particles were
embedded in the sample eroded at $800°C$ in nitrogen, Figure 9.

Surface Morphological Features of Nickel Oxide

The erosion of nickel oxide was studied by using specimens of
nickel that were covered with thick (i.e. 120μm) layers of NiO
formed by oxidation at $1100°C$ in air for 72 hrs. Photographs show-
ing the surfaces of typical specimens eroded at $800°C$ and at room
temperature are presented in Figures 11 and 12 respectively. At
temperatures of about $800°C$, features indicative of a ductile re-
sponse are evident Figure 11b. Nevertheless, some cracking was de-
tected, Figure 11c. At room temperature some features indicating
ductile behavior are evident, Figures 12a and 12b, but cracking
and chipping have also occurred, Figure 12c, suggesting more brittle
behavior.

(a)   (b)   Al map of (b)

Figure 8.   Nickel exposed for 30 min. at $710°C$ at $18°$ impact angle
to 190 ms^{-1} airflow. (a) Removal of scale from metal
facilitated by electropolishing in H_2SO_4-H_2O bath at
1.5 volts for 20 minutes. (b) View of underside of
stripped scale showing embedded Al_2O_3 particles.

Weight Change Measurements of Specimens During Erosion-Oxidation

Weight-change data as a function of time for polished and for
preoxidized samples are presented in Figures 13 and 14, respectively.
These data conform to a linear rate law which is usually preceded
by a nonlinear period. These data are summarized in Table I in
terms of surface recession rates. The data presented in Table I
permits the following statements to be made about the erosion-
oxidation of nickel.

.At 800°C the surface recession rate decreases with particle
velocity.
.At a constant particle velocity the surface recession rate
decreases as temperature is decreased.*
.At 800°C the surface recession rate decreases dramatically
when oxygen is not present.

Figure 9.   Nickel metal eroded at room temperature using 20μm
              alumina at 73ms $^{-1}$ at 90° for 1 minute.
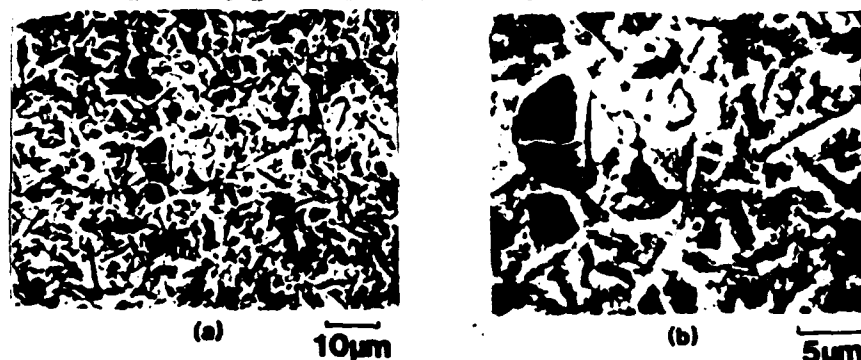
Figure 10.   Nickel eroded in pure nitrogen flowing at 140 ms $^{-1}$
              at 90° at 800° for 1 minute.

    The linear material removal rates observed for the specimens
undergoing combined oxidation and erosion along with the signifi-
cant dependence upon oxygen indicate that these two processes are
affecting each other. The generation of a thin scale on the nickel
specimens subjected to erosion-oxidation conditions is regarded as
reflecting the relative rates at which erosion of oxide by the
alumina particles and formation of the oxide can occur. It also
reflects the kinetic laws followed by the two processes. For in-
stance, if both oxidation and erosion occurred at constant rates,

---

*At a temperature of 850°C and a particle velocity of 125 ms $^{-1}$
the surface recession rate was less than that for 800°C. It is
believed at temperatures above 800°C more of the erosive particles
are retained in the metal-oxide zone which inhibits the material
removal process.

the rate of scale formation could be written, in terms of scale thickness X,

$$\frac{dX}{dt} = k_o - k_e \qquad (1)$$

where k_o and k_e are the rates at which oxidation of nickel and erosion of nickel oxide occur, respectively. Equation (1) would not result in an oxide of constant thickness but rather a scale of either increasing or decreasing thickness.

If the oxide scale is assumed to be protective, the scale thickness will change according to,

$$\frac{dX}{dt} = \frac{k}{X} - R_e \qquad (2)$$

where k is the parabolic rate constant for the oxidation of nickel defined by $X^2 = 2kt$
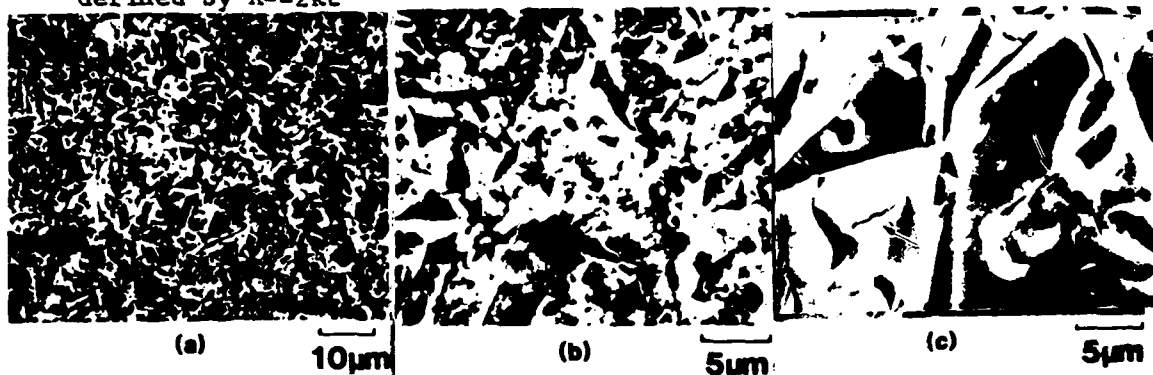
Figure 11. NiO exposed at 800° to 140 ms^{-1} in air at 90° showing plastic deformation in (a) and (b) and cracking or tearing in (c).
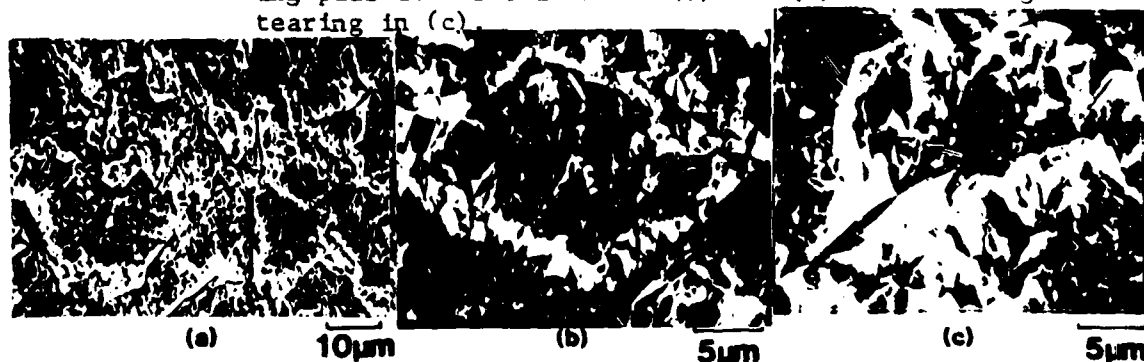
Figure 12. Appearance of NiO after erosion at room temperature in air to 73 ms^{-1} for 30 seconds at 90° showing evidence of plastic deformation in (a) and (b) and cracking or tearing (c).

The interplay between scale growth and erosion processes in this case would lead to the establishment of a steady state where the scale thickness approaches a constant value X* when dX/dt = 0 and hence,

$$X^* = k/k_e \qquad (3)$$

Although the scale thickness is constant, metal removal has not ceased, on the contrary it is being removed at a constant rate given by,

$$\frac{dx}{dt} = \frac{V_M}{V_{MO}} \frac{k}{X^*} = \frac{V_M}{V_{MO}} k_e \qquad (4)$$

where x is the metal surface recession and V_M and V_{MO} are molar volumes of metal and oxide, respectively. While in the case of nickel a constant oxide thickness appears to be formed, the assumption that the scale is continuous and protective does not seem to be justified since it is apparent that the scale is continually being penetrated and made nonprotective, at least in localized areas by the impacting alumina particles. It therefore seems reasonable to suppose that the nickel surface being eroded is a composite consisting of nickel oxide, nickel and embedded alumina particles. The rate of material removal can then be viewed as following the expression,

$$\frac{dx}{dt} = k_e' \qquad (5)$$

where the magnitude of k_e' is determined by the properties of the composite layer as influenced by the particle velocity, impact angle, particle loading, particle size and temperature.

The data presented in Figure 13 and Table I are consistent with such a proposal since,

$$k_e' = \frac{dx}{dt} = \frac{1}{\rho_{Ni}} \frac{d(\Delta M/A)Ni}{dt} \qquad (6)$$

where ρ_{Ni} is the density of nickel and $(\Delta M/A)Ni$ is the weight change per unit area of the nickel specimens. The observed decrease of k_e' with particle velocity at $800^{\circ}C$ is expected since the higher velocity should produce more damage to the oxide layer and also produce more deformation of the composite layer as observed with metals[1] at room temperature. In air at a fixed particle velocity k_e' decreases as temperature is decreased since the amount of oxidation decreases and, as will be discussed subsequently, oxidation is believed to affect the amount of deformation that the composite layer can withstand prior to fracture. The large reduction in erosion rate on going from air to nitrogen at $800^{\circ}C$ is also
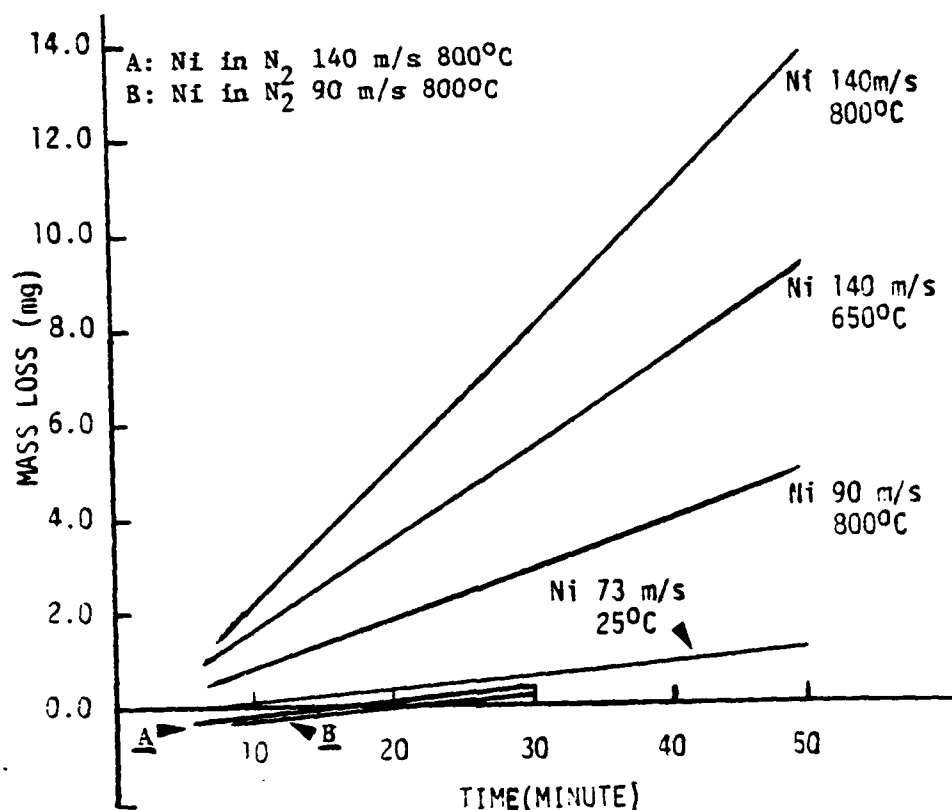
Figure 13. Mass loss versus time for polished nickel specimens exposed at 90° impact angle.

reasonable due to the absence of oxidation in nitrogen. Finally, the observed lower erosion rate at 800°C in nitrogen compared to 25°C in air may be due to work hardening becoming important at 25°C.

TABLE I

SURFACE RECESSION RATES FOR NICKEL AND NiO (cm/s)

EXPERIMENTAL CONDITIONS	NICKEL cm/s X 10[7]	NICKEL OXIDE cm/s X 10[7]
800°C, 140 m/s, air	6.91	8.4
800°C, 90 m/s, air	2.30	3.5
800°C, 140 m/s, N_2	0.71	
800°C, 90 m/s, N_2	0.35	
650°C, 140 m/s, air	4.50	6.2
25°C, 73 m/s, air	0.71	8.4
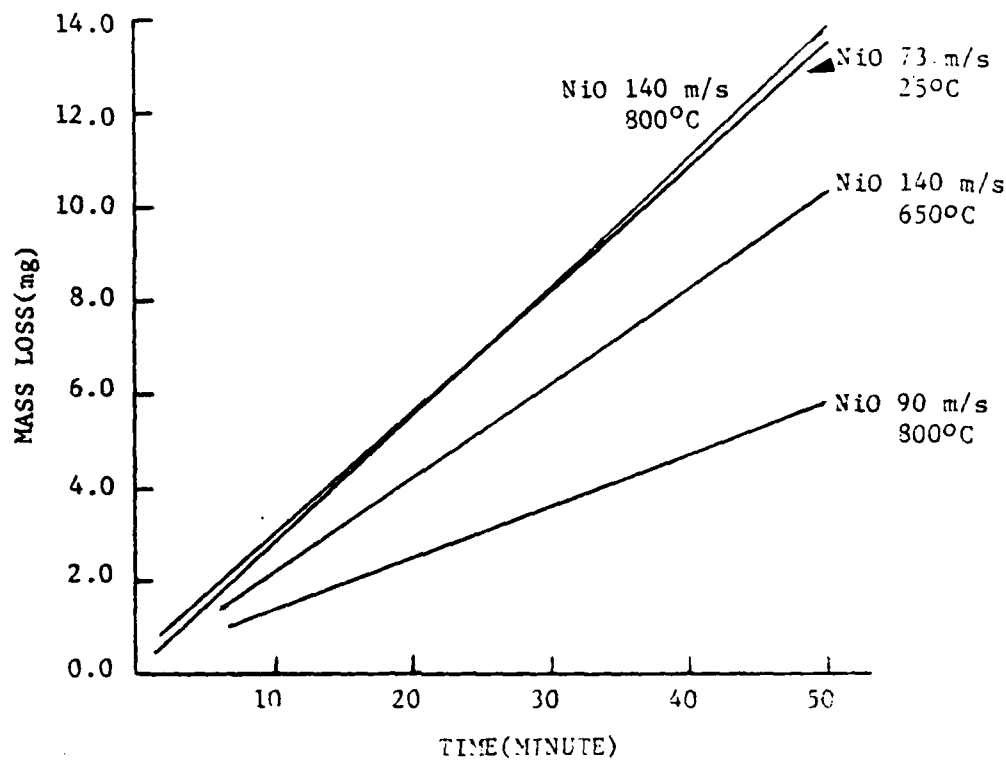
Figure 14. Mass loss versus time for preoxidized nickel specimens
exposed at 90° impact angle.

The data presented in Figure 14 and Table I show that the
erosion rate of nickel oxide decreases with particle velocity at
800°C. This is reasonable since the amount of deformation and
cracking can be expected to decrease with velocity. The dependence
of the erosion of nickel oxide on temperature is not at present un-
derstood. The surface recession rates at 800°C and 25°C are about
the same, however, the lower velocity used in the experiment at
25°C suggests a higher erosion rate at 25°C for the same velocity.
This difference could be accounted for by proposing that the erosion
of nickel oxide occurs by two modes, namely, by cracking (brittle
mode) and through repetitive deformation (ductile mode) with more of
the former at room temperature. More recent results obtained at
650°C, however, give an erosion rate that is lower than at 800° and
25°C. This puzzling result is currently being checked. If sub-
stantiated, it may be evidence for a change in fracture mechanism
of the oxide at a temperature below 650°C with the ductile mode
decreasing as temperature is decreased. Finally, it is worth noting
that the erosion of nickel oxide, in terms of surface recession, is
always greater than that for nickel for similar test conditions.
Such results are plausible, since regardless of the mode of erosion

that predominates in nickel oxide, the properties of nickel oxide compared to nickel can be such that higher recession rates occur. For example, erosion of nickel oxide by a ductile mode may lead to the formation of thin sections of displaced oxide that are readily cut and removed by subsequent impacts. In the case of nickel, the metal displaced by plastic deformation may not be removed so readily but rather welded back to the surface by subsequent impacts. This distinction is a direct result of the higher ductility of nickel and is supported by the increased removal rate of nickel at room temperature, compared to 800°C in nitrogen, where work hardening can occur and welding is less likely.

MOdel for Combined Erosion-Oxidation of Nickel

A schematic model for the combined erosion-oxidation of nickel is presented in Figure 15. When polished nickel is subjected to erosion-oxidation a thin oxide layer is formed, Figure 15a. As erosion occurs, the particles deform the surface and penetrate the oxide scale. For reasons discussed previously, the deformation caused moguls to be developed which results in the particle impact angle being altered. Material begins to be removed by adhering to the ejected alumina particles, Figure 15a. As erosion continues, the exposed metal is oxidized and platelets of metal and oxide begin to extrude out over the surface. Small portions of these platelets eventually become detached from the surface due to subsequent particle impacts cutting them off or by producing deformation to the extent that fracture occurs, Figure 15a. Continuation of this process thus results in the formation of a composite layer consisting of nickel oxide, nickel and parts of embedded particles.

Moreover, this composite layer is maintained at a relatively constant thickness independent of exposure time due to the simultaneous removal of material by excessive deformation and cutting in combination with oxidation of freshly exposed metal surfaces and embedding of additional alumina particles.

In the case of erosion of nickel oxide, and thick layers of nickel oxide on nickel, Figure 15b, the erosion process may involve material removal by both ductile and brittle modes with the ductile mode being more important at 800°C, and perhaps 650°C. In the case of the ductile mode, the mechanisms is similar to that described for nickel with deformation of nickel oxide resulting in very small platelets of oxide being removed. At lower temperatures the brittle mode may become more important with extensive cracking giving rise to the formation of chips of oxide.

For the conditions examined thus far, the erosion rate has always been sufficient to reduce the thicknesses of preformed layers of oxide on nickel to values similar to those developed on polished nickel samples. Hence, for sufficiently long times, preoxidized nickel develops a composite layer virtually identical to that formed on nickel specimens with no preformed nickel oxide.
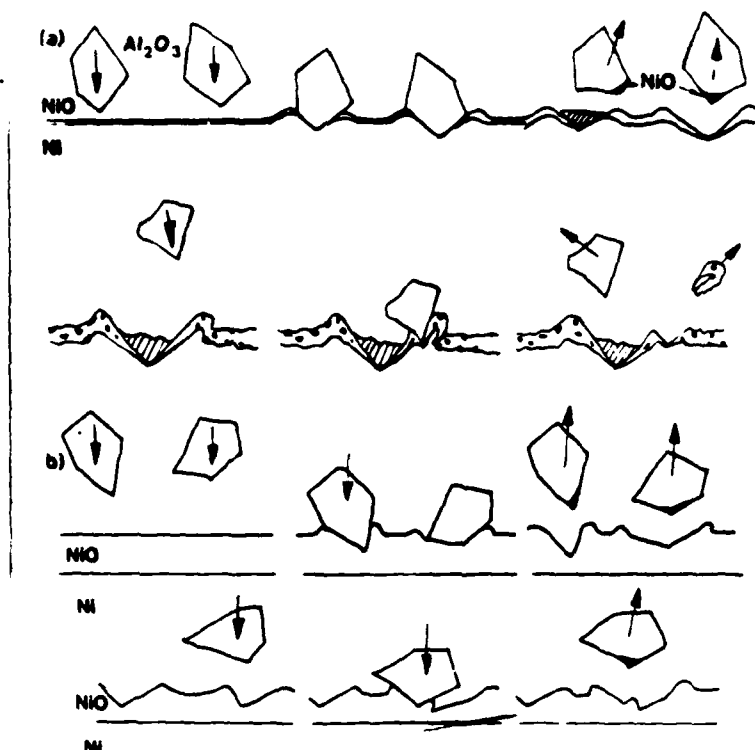
Figure 15. Steps in the erosion-oxidation mechanism of nickel.
(a) clean nickel surface, Al_2O_3 particles embed and
both metal and oxide deform plastically on impact
until fracture. (b) Nickel with thick preoxidized
scale, plastic deformation of oxide and cracking
reduce thickness until conditions of (a) develop.

CONCLUDING REMARKS

The combined erosion-oxidation of nickel has been investigated
at temperatures of 25°, 650° and $800^\circ C$ using alumina particles.
The oxidation process has been found to significantly increase the
erosion process due to the formation of a composite layer con-
sisting of nickel oxide, deformed nickel metal, and embedded
alumina particles. The observed erosion rates have been accounted
for by considering the characteristics of the composite layers
that are formed.

Work is now in progress to investigate the erosion-oxidation
of cobalt which has an oxidation rate substantially greater than
that of nickel.

ACKNOWLEDGEMENTS

REFERENCES

1. W. F. Adler; Assessment of the State of Knowledge Pertaining to Solid Particle Erosion. Tech. Report, Effects Technology, Inc. 1979, NTIS, Report No. ETI-CR79-680.

2. I. Finnie; Wear, 3, 87 (1960).

3. J. G. A. Bitter; Wear, 6 5, (1963) also 6, 169, (1963).

4. R. E. Winter and I. M. Hutchings; Wear, 29, 181, (1974).

5. M. M. Mamoun; Mat. Sci. Div. Coal Tech. Third Quarterly Report No. ANL-75-XX3. Argonne National Lab (1975). Appendix: Analytical Models for the Erosive-Corrosive Wear Process.

6. P. S. Follansbee, Mechanisms of Erosive Wear of Ductile Metals Due to Low Velocity, Normal Incidence, Impact of Spherical Particles. Ph.D. Thesis (1981), Carnegie Mellon University, Pittsburgh, PA.

7. R. Bellman Jr. and A. Levy; Erosion Mechanism in Ductile Metals. Tech. Report. Lawrence Berkeley Laboratory, LBL-10289 (1980).

8. N. P. Suh; Wear, 44, 1, (1977).

9. S. Jahanmir, Wear, 309, (1980).

10. Effect of Erosion on Oxidation and Hot Corrosion of Coated and Uncoated Superalloys. Performed by Pratt and Whitney Aircraft, East Hartford, CT. for EPRI, Palo Alto, California (R.P. 979-4, 1975).

11. Effect of Alloy Variables on Resistance of a Material to Attack at High Temperatures where both Erosion by Particulates and Corrosion can occur. Performed by Battelle - Columbus, Columbus, OH, for EPRI, Palo Alto, Ca. (RP 589, 1975).

FUNDAMENTAL ASPECTS OF THE MECHANISMS OF INTERACTION BETWEEN EROSION AND CORROSION OF METALS AND ALLOYS AT HIGH TEMPERATURES

by

S.L. Chang, D. Rishel, F.S. Pettit and N. Birks
Materials Science and Engineering Department
University of Pittsburgh
Pittsburgh, PA 15261

ABSTRACT

The characteristics of degradation of nickel and cobalt have been studied over a range of temperatures and other relevant parameters under conditions of simultaneous erosion and oxidation. The results showed that the interaction between the erosion and oxidation process is complex, however careful metallographic examination and kinetic studies have allowed the interaction to be resolved into a range of interactions depending on both the absolute and relative intensities of the two primary processes of erosion and oxidation. The introduction of sulfurous gases, SO_2 and SO_3, to the atmosphere used was found to have a profound effect leading to the formation of sulfides and thicker more easily deformed scales.

INTRODUCTION

Conditions under which materials are exposed to the simultaneous effects of erosion and corrosion are frequently encountered and this type of conjoint attack is being recognized as a major problem in the application of materials, particularly at high temperature. Examples of problem areas where erosion-corrosion is becoming critical are in gas turbines, coal gasification plant and fluid beds for coal combustion. These three examples represent a very wide range of conditions that cover oxidizing and reducing atmospheres, large and small particles, particles that are hard or soft and reactive or inert, as well as a wide range of velocities and temperatures.

The interactions between erosion and corrosion have, until quite recently, been only poorly understood and, as a result the action taken has been to attempt to avoid the problem by such techniques as filtration or limiting the temperature. Such steps are not always feasible or are not economically acceptable, consequently programs of investigation have been carried out to improve our understanding of the subject in order to be able to design materials that are capable of resisting the attack. The studies carried out on metals(1-8) emphasized the complex nature of the interaction especially when simulating actual conditions rather than studying model systems to develop basic understanding of the processes.

The studies of erosion of materials at room temperature(9-11) identified a variation of erosion rate with the angle of incidence. The maximum rate being observed at 30 deg. in the case of ductile materials and at 90 deg. in the case of brittle materials. This difference in behaviour was ascribed to the different mechanisms by which material is removed in the two cases. The erosion of ductile materials is thought to occur by a cutting mechanism (9) or by a ploughing mechanism (12), in both cases the material is removed by a process involving plastic deformation of the surface as is usually evident from the surface structure. The erosion of brittle materials on the other hand is considered to occur by the removal of fragments formed by the intersection of systems of hertzian cracks formed during the impact.

High temperature oxidation can be regarded as a process during which the metal is protected from further attack by the formation of a scale on the surface. The extent of the protection afforded increases with the thickness of the scale but also depends on factors such as defect structure, scale adherence and porosity.

The interaction between erosion and oxidation at elevated temperature is clearly going to depend on how the nature of the scale and the scale metal interface can be modified under the influence of erosion. The variables that will influence the interaction are the scaling rate, particle size, particle velocity and angle of incidence.

RESULTS

In this paper some of the conclusions of recent work will be discussed, some of which is published (5) and some of which is still being prepared (13,14). These studies used alumina particles of about 20 microns flowing at between 50 -150 meters per second, at temperatures up to 800°C to study the erosion corrosion interactions on nickel and cobalt. These metals were chosen because the oxidation characteristics of both are well documented and cobalt oxidizes about 200 times faster than nickel. The apparatus used has been described previously (5), and served to provide an accurate stream of particles in terms of temperature, velocity, loading and angle, to impact on a 9mm diameter specimen whose temperature could be monitored. Most of the initial work was carried out to an angle of incidence of 90 degrees i.e. normal to the surface.

Since the erosion stream was impacting on an oxide surface, the effect of erosion on oxide alone was studied initially. The weight lost after exposure was measured and plotted against exposure time for the various temperatures as shown in Figure 1. The surfaces of the samples were examined closely using SEM-EDS and it was found

that the oxides of both nickel and cobalt were deformed by the
erosive stream in a predominantly plastic or ductile manner even at
room temperature. The sufaces showed clear imprints of the impacts
with plastically displaced material on the sides ready to be removed
by a subsequent impact.

From Figure 1 it can be seen that the rate of material removal
increases as the velocity is increased and as the temperature is
reduced, such as would be expected if the oxide responded to erosive
impact in a ductile manner and if the ductility increased with
temperature. In this case more of the incident energy would be
absorbed in carrying out plastic deformation of the oxide at the
higher temperatures leaving less available for material removal.

Experiments were also carried out using metal samples at
various temperatures, in air and also in pure nitrogen to remove the
oxidation component. The results for nickel and cobalt are shown in
Figures 2 and 3 respectively from which it can be seen that, in the
absence of oxidation, the rate of metal removal is very low. This
is seen also from the results at room temperature when no oxide
forms. The implication is that the metal itself, due to its high
plasticity, can absorb much of the energy of the erosive beam by
plastic deformation. However, the less deformable oxide cannot
absorb energy to the same extent and, under oxidizing conditions the
metal is thought first to convert to oxide which is then removed by
the erosion process. The results in Figures 2 and 3 confirm this in
that, for a given erosion condition, higher degradation rates are
observed in air at higher temperatures, where oxidation rates are
higher. It can also be seen that higher degradation rates are
observed at higher erosive velocities for a given temperature in air
in the cases of both nickel and cobalt.

Metallographic observation of the specimen surfaces showed that
both nickel and cobalt carried typical erosive indentation
impressions but, whereas the nickel specimen surface was deformed
into a pattern of hills and valleys (called moguls), that of the
cobalt specimen had remained quite flat until erosive velocities of
above 120 meters per second were used when the surface was similar
to those of the nickel specimens. Clearly the mode of attack is
changing with velocity in the case of cobalt to resemble the
surface morphology that is typical of nickel specimens. This
phenomenon was studied by exposing samples of both metals to erosion
-oxidation under conditions where the velocity of the erosive stream
was increased regularly from 50 to 140 meters per second. The
specimen surfaces confirmed the above observations and, in section,
showed that the cobalt specimens were covered by a quite uniform
layer of oxide whose thickness decreased as the erosive velocity
increased. At velocities above about 120 meters per second, the

scale metal interface of the cobalt specimens was found to be
convoluted which indicated that the metal substrate had undergone
plastic deformation during the erosion process. In comparison,
although the nickel specimens in cross section showed a convoluted
interface, the surface layer was not a compact scale but rather a
mixture of nickel oxide, metal and embedded alumina particles, or in
otherwords a composite layer.

REGIMES OF INTERACTION

If the interaction between erosion and oxidation is regarded as
two competing processes, trying respectively to remove and to form a
scale, then so long as the scale is compact and uniform the rate at
which the scale thickens can be represented as

$$dX/dt = K/X - K(eo)$$

where K is the parabolic scaling rate constant, X is the scale
thickness and K(eo) is the erosion rate constant. There exists a
steady state situation where the rate of scale removal is equal to
the rate of scale formation when

$$dX/dt = 0$$

and consequently $K/X = K(eo)$

Since K and K(eo) are both constants it follows that the scale
thickness, X, must also be constant under these conditions

$$X+ = K/K(eo)$$

It should therefore be possible to measure X+ and relate it to the
rate constants for scaling and erosion.

Specimens of cobalt, having the highest reaction rate, were
eroded in air at 780°C for a series of increasing times and then
sectioned in order to measure the scale thickness. The results of
these experiments are shown in Figure 4 from which it is clear that
scales of constant thickness are indeed obtained and, furthermore,
the thickness is smaller under the more aggressive erosion
conditions. Knowing the values of K(eo) for cobalt oxide, obtained
by ɟirect measurement of the erosion of cobalt oxide or by
calculation from the rate of weight loss of specimens in the steady
state situation described above, it was possible to calculate the
values of the parabolic scaling constants for formation of CoO and
Co_3O_4. The calculated values of compared well with values from the
literature.

In this type of interaction the two processes of erosion and oxidation proceed together, the basic mechanisms of neither process are modified by the other. The interaction arises because the erosion results in the modification of the scale thickness which in turn controls the rate at which the metal is oxidized. Thus, since the scale is held at a small thickness by erosion, the oxidation rate does not reduce with time as it would in the absence of erosion. This regime of interaction has been called Erosion Enhanced Oxidation.

Because the erosion only acts on the oxide scale in this regime, the weight loss rate is the rate at which metal is being removed as oxide from the sample, if this is converted to the equivalent weight of oxide then the resulting oxide removal rates should be identical to the values obtained for the erosion of oxide only, under the same conditions. In Figure 5 appropriate data for cobalt are plotted against the erosive velocity and it can be seen that, up to about 100 meters per second, the agreement is good. Above about 100 meters per second the deterioration rate of cobalt increases rapidly, this departure corresponds to the development of a deformed specimen surface showing the 'mogul' features.

When the underlying metal substrate begins to be plastically deformed by the erosive impacts, the metal-scale interface begins to lose the features of a compact oxide scale and, instead, there develops a surface layer that consists of oxide and embedded erodent particles. It is suspected that, at temperature, this layer also contains slivers of metal that have been extruded from the substrate by the impact of the erodent when the surface layer is thin. Such slivers of metal would be oxidized rapidly and removed as a continuous process, no direct evidence is available to confirm this mechanism however.

Since the metal surface is so heavily deformed, and is brought into direct contact with the oxidizing atmosphere, it is to be expected that the rate of oxidation would increase to rates well in excess of those predicted for a compact adherent scale. This is, in fact, observed and this condition represents a new regime of interaction between erosion and oxidation that has been called Oxidation Affected Erosion due to the fact that in this regime the oxidation process has markedly enhanced the rate of metal degradation compared with the erosion of the metal in the absence of oxidation.

In the oxidation affected erosion regime there is considerable modification of the two basic processes when both are present, the erosion exposes the metal to the atmosphere thus enhancing the

oxidation process and the oxidation product modifies the surface to promote more effective erosion.

EFFECT OF ANGLE OF IMPACT

The effect of the value of the angle of incidence with which the particles impact the specimen surface has been studied for both brittle and ductile materials at room temperature (9). The results indicate that the erosion rate achieves a maximum value at an angle of about 30 deg for ductile materials and at 90 deg. for brittle materials. In the cases of cobalt and nickel at 780° the erosion oxidation rates vary as a function of angle of incidence as shown in Figure 6. As can be seen, the angle for maximum deterioration occurs at about 30 deg for nickel but at about 60 deg. for cobalt. This difference is explained by the action of the scale in the conjoint erosion-oxidation process. In the case of nickel, the scale is very thin, in fact it is more like a composite scale as described previously, whereas the scale that forms on the cobalt is a continuous oxide scale and is substantially thicker than the composite layer on nickel. During erosion the surface layer on nickel is too thin to absorb much of the energy of the impacts, consequently appreciable energy is available to deform the underlying metal which forms a series of ripples on the specimen surface. The metal at the crest of the ripple is forged into small platelets which are detached eventually, having rapidly converted to oxide. This mechanism is at maximum effectiveness at an angle of 30 deg. which provides both a normal component sufficient to cause the formation of well defined ripples and a parallel component strong enough to shear the metal of the wave crests into platelets.

In the case of cobalt, the oblique erosion also causes the development of a ripple system but the thicker surface oxide layer succeeds in absorbing the incident erosive energy such that the metal at the wave crest is not sheared into platelets. This mechanism is therefore absent in the case of cobalt at $780^\circ C$ and the angle of maximum deterioration is found to be at about 60 deg. the predominant mechanism by which material is removed being the ploughing and cutting mechanism referred to earlier.

It can be seen then that the removal of material under conditions of conjoint erosion and oxidation can be expressed in terms of several mechanisms, which may be acting concomitantly, depending strongly on the conditions of exposure. In the cases of nickel and cobalt, the angle dependence for nickel is similar to that of a ductile material whereas that of cobalt resembles a brittle material. This reflects the observations that nickel is in the oxidation affected erosion regime whereas cobalt is in the erosion enhanced oxidation regime during which removal of material occurs by the removal of the significantly less plastic oxide only.

EROSION- MIXED CORROSION

A limited program of work has been carried out into the erosion behavior of nickel in atmospheres containing partially equilibrated air, SO_2 and SO_3 at 600°C, 70 m/s, normal incidence angles with 20μm alumina under variable particle loading rates. Results indicate that, although the presence of SO_2 promotes the formation of a duplex scale consisting of oxide and sulfide, the effect is much more pronounced when SO_3 is also present in the air + SO_2 mixture. When erosion was present, the resulting scale formed in these conditions (i.e. air + SO_2/SO_3) flowed relatively easily as evidenced by the speed of the scale over the specimen edge.

A more significant effect was noted under conditions of lower particle loading rates in air + SO_2/SO_3 atmospheres. Under these situations, a higher scale growth was promoted, as evidenced by a thicker duplex scale (inspite of scale being removed by erosion), than would be the case in similar atmospheres without erosion present. The interpretation of this observation is that erosion damages the growing duplex scale in such a manner as to enhance the outward transport of nickel cations and/or the inward transport of gaseous SO_2 and SO_3.

It was also observed that, under high particle loading rates in air + SO_2/SO_3, spallation of the scale occurred. This observation extends the types of interaction of erosion to an area that has not been studied systematically although some spallation has been observed on cobalt during erosion-corrosion in air. In this case, the spallation appeared to be confined to regions that represented a narrow range of scale thicknesses. Clearly this aspect deserves more systematic study in order to develop understanding of the mechanisms which operate.

Acknowledgement

REFERENCES

1. I. Wright, V. Nagarajan and R. B. Herchenroeder, "Some Factors Affecting Solid Particle Erosion/Corrosion of Metals and Alloys", Corrosion Erosion Behavior of Materials, edited by K. Natesan, Proceedings of a Symposium at the Fall Meeting of the Metallurgical Society of AIME, Oct. 1978, Warrendale, PA.

2. R. H. Barkalow, J. A. Goebel and F. S. Pettit, "Materials Problems in Fluidized-Bed Combustion Systems", Tech. Report, EPRI, May 1980, CS-1488, Project 979-4 Final Report, Electric Power Research Institute, Palo Alto, CA.

3. L. K. Ives, "Erosion of 310 Stainless Steel at 975°C in Combustion Gas Atmospheres", J. Eng. Mater. Tech. Trans. ASME, 99, 126, (1977).

4. A. V. Levy and G. Zambelli, "Particulate Erosion of NiO Scales", Wear, 68, 305, (1981).

5. C. T. Kang, F. S. Pettit and N. Birks, "Mechanisms in the Simultaneous Erosion-Oxidation Attack of Nickel and Cobalt at High Temperatures"; Met. Trans. A., 18A, 1785, (1987).

6. D. J. Stephenson, J. R. Nicholls and P. Hancock; "The Erosion of Gas Turbine Blade Materials by Solid Sea Salt", Corrosion Science, 25, 1181, (1985).

7. D. J. Stephenson, J. R. Nicholls and P. Hancock; "Particle Surface Interactions During the Erosion of a Gas Turbine Material (Mar M002) by Pyrolytic Carbon Particles", Wear 111, 15, (1986).

8. D. J. Stephenson, J. R. Nicholls and P. Hancock; "The Interaction Between Corrosion and Erosion During Simulated Sea Salt Compressor Shedding in Marine Gas Turbines", Corrosion Science, 26, 757, (1986).

9. W. F. Adler, "Assessment of the State of Knowledge Pertaining to Solid Particle Erosion", Tech. Rept. U. S. Army Research Office, NTIS Report no. ETI-CR79-680, June 1979.

10. P. S. Follansbee, "Mechanisms of Erosive Wear of Ductile Metals Due to Low Velocity, Normal Impact, of Spherical Particles", Ph.D. Thesis, (1981), Carnegie-Mellon University, Pittsburgh, PA.

11. P. Shewmon and Sundararajan, "The Erosion of Metals", Ann. Rev. Mater. Sci., 13, 301, (1983).

12. I. M. Hutchings and R. E. Winter, Wear, 27, 121-128 (1974)

13. S. L. Chang, Ph.D. Thesis, University of Pittsburgh, 1987.

14. D. Rishel, Unpublished work.
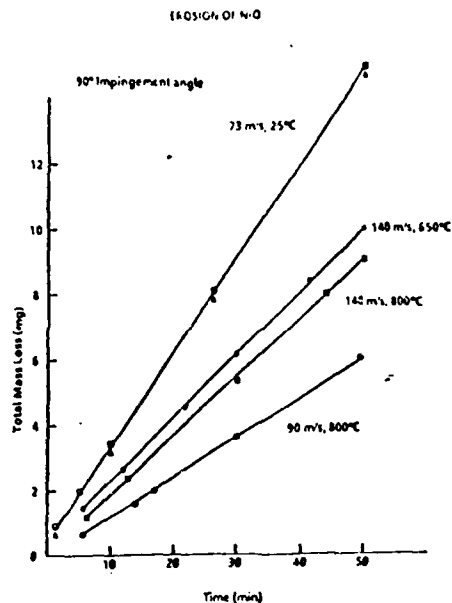
Figure 1. Mass loss vs. time for
preoxidized nickel specimens exposed
at 90° impact angle to airflow.
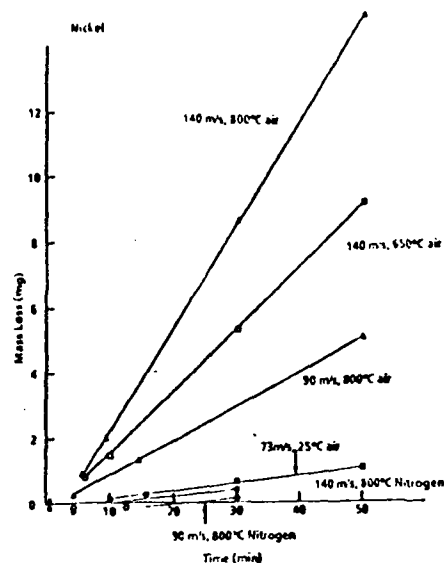
Figure 2. Mass loss vs. time
for nickel specimens exposed
at 90° incidence to erosive
stream.
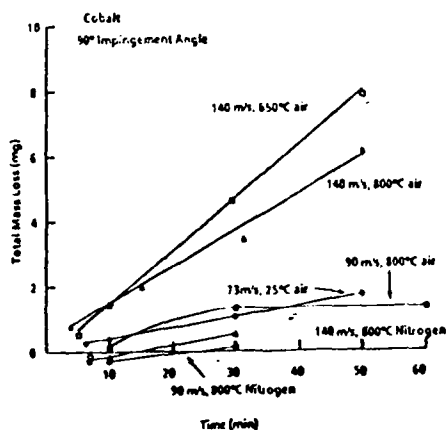
Figure 3. Mass loss vs. time for
cobalt specimens exposed at 90°
incidence to erosive stream.
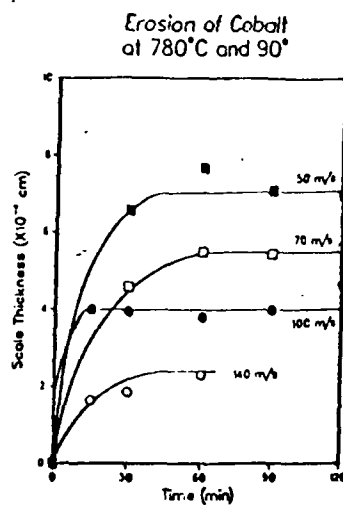
Figure 4. Reaction kinetics
of combined erosion and
oxidation of cobalt to show
the relationship of oxide
scale thickness with exposure
time.

Erosion at 780°C and 90°
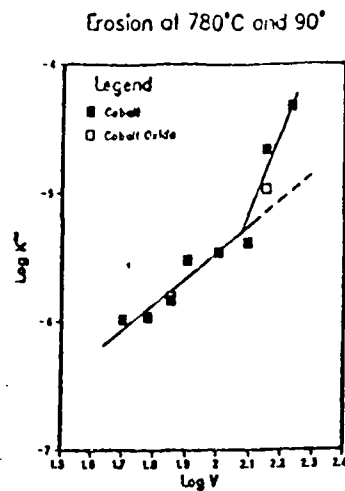
Figure 5. Summary of the relationship
between the erosion rate constant and
the particle velocity for the combined
erosion and oxdiation of cobalt and
cobalt oxide at 780°C and 90° incidence.
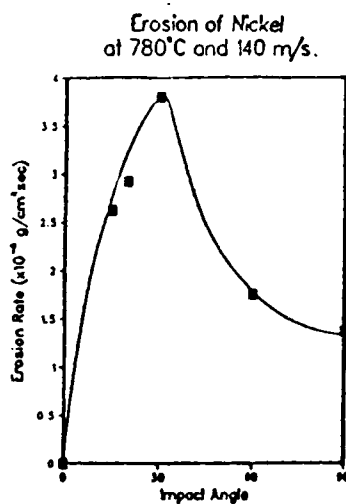
Figure 6a. Angular dependence of
the erosion rate for the combined
erosion and oxidation of nickel
at 780°C and 140 m/s.
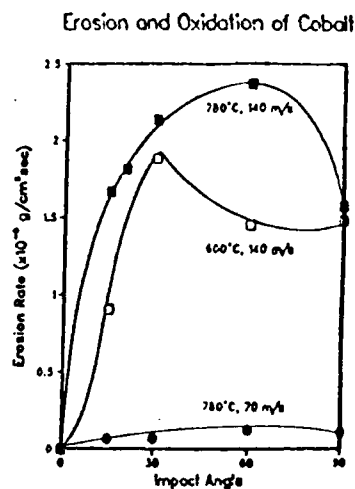
Figure 6b. Angular dependence of
the erosion rate for the combined
erosion and oxidation of cobalt
at 780° and 600°C.

APPENDIX 3

Papers Published in Metallurgical Transactions
<u>18A</u>, 1785–1802 (1987)

Mechanisms in the Simultaneous Erosion-Oxidation Attack of Nickel and Cobalt at High Temperature

C. T. KANG, F. S. PETTIT, and N. BIRKS

An apparatus is described by which a specimen may be exposed to a well-defined erosive gas stream containing 20 μm alumina particles. Samples of nickel and cobalt were exposed to conditions of erosion and high temperature oxidation simultaneously, using 90 deg impact angle, at velocities up to 140 m/s^{-1} and at temperatures up to 800 °C. From the results of erosion kinetics, surface morphologies, and cross section metallographic observations it is concluded that several definite regimes of interaction between erosion and oxidation exist. These regimes are described in qualitative terms, and it is shown how they arise as a result of the balance between the relative intensities of the erosion and oxidation processes.

I. INTRODUCTION

IN some equipment or machines such as gas turbines, pressurized fluidized bed combustors, and incinerators, materials can be subjected to both erosive and corrosive processes concomitantly. The erosion of metallic systems and ceramics at ambient temperatures has been studied extensively[1-4] and, while many questions concerning the correlation of erosion properties and physical parameters remain unanswered, a very substantial and meaningful body of knowledge is available.[5,6] An enormous amount of work has also been performed on the high temperature corrosion of metals and alloys[7,8,9] and a smaller, yet still significant, amount of research into the corrosion of ceramic materials has been performed.[10,11] A large amount of data and substantial understanding therefore exists for the high temperature corrosion of materials at elevated temperatures.

While significant research has been performed and understanding exists for room temperature erosion and high temperature corrosion processes, very little understanding is available for combined erosion-corrosion processes. Some studies have been performed[12-19] and, although not greatly concerned with mechanism development, the results do show that when erosion and corrosion processes occur together there is a strong interaction. Examples are available that show: (a) nonprotective scales replace protective scales when erosive particles are present in the gas stream; (b) an oxide scale formed at elevated temperatures can cause metallic surfaces to become more erosion resistant; and (c) combined hot corrosion-erosion can proceed at rates greater than the sum of the rates for these two processes acting independently. A need now exists to consider different erosion-corrosion processes and to begin to describe, in a systematic way, the various interactions that may occur.

The alloys or coating systems that are used in the erosive-corrosive environments that arise during operation of different machinery or equipment usually have rather complex compositions. It is therefore appropriate first to consider

pure metals and then to extend the investigation to related but more practical alloy compositions. This paper will present results obtained from experiments performed on nickel and cobalt as well as nickel oxide.

II. EXPERIMENTAL

A schematic of the apparatus that was used to study the combined erosion-corrosion of metals in the present investigation is shown in Figure 1. The gas is cleaned and dried to remove traces of oil, water, and dust. The gas then flows through a fluid heater which preheats it to about 700 °C and, at this point, particles are added to the gas stream. The gas for the particle laden stream is also cleaned, dried, and passed through a Sylco Mark IX powder dispenser whereby the gas entrains particles at a controlled rate.

A flow divider is used to direct only one-tenth of the particle laden gas into the main gas stream at 700 °C, the remaining nine-tenths being collected in a filter bag. The main gas stream, now ladened with particles and at 700 °C, is passed down a vertical, heated Inconel tube, 1.5 meters long, to be accelerated and heated further. Gas and particles emerge at the 9.3 mm diameter nozzle at speeds up to 300 m/s and at temperatures of up to 900 °C. The Inconel tube is aluminized to avoid spallation from the inner tube surface into the erosive gas stream.

The specimens are held about 0.8 cm from the end of the Inconel tube. Two different specimen holders were used. For 90 deg impingement the sample holder is a ceramic cone shape, Figure 1, which is also used as a cover to protect the infrared heater from erosion. The sample is placed in an indentation in the ceramic cone and is held in place by the flowing gas. A sample holder that is spring loaded, to allow for differential changes in length due to thermal expansion on heating, is used for impact angles other than 90 deg. In both types of specimen holder, in order to reduce temperature gradients, the specimens are also heated from the back side using a focused radiant heater.

During the design and construction of this apparatus, as well as during its initial use, it was necessary to analyze a number of factors concerning the definition of conditions and development of the desired range of test variables. These factors are discussed in the following.

C. T. KANG is Project Engineer, Union Carbide Coating Service, 1500 Polco Street, Box 24184, Indianapolis, IN 46224. F. S. PETTIT, Professor and Chairman, and N. BIRKS, Professor, are with the Department of Materials Science and Engineering, University of Pittsburgh, Pittsburgh, PA 15261.
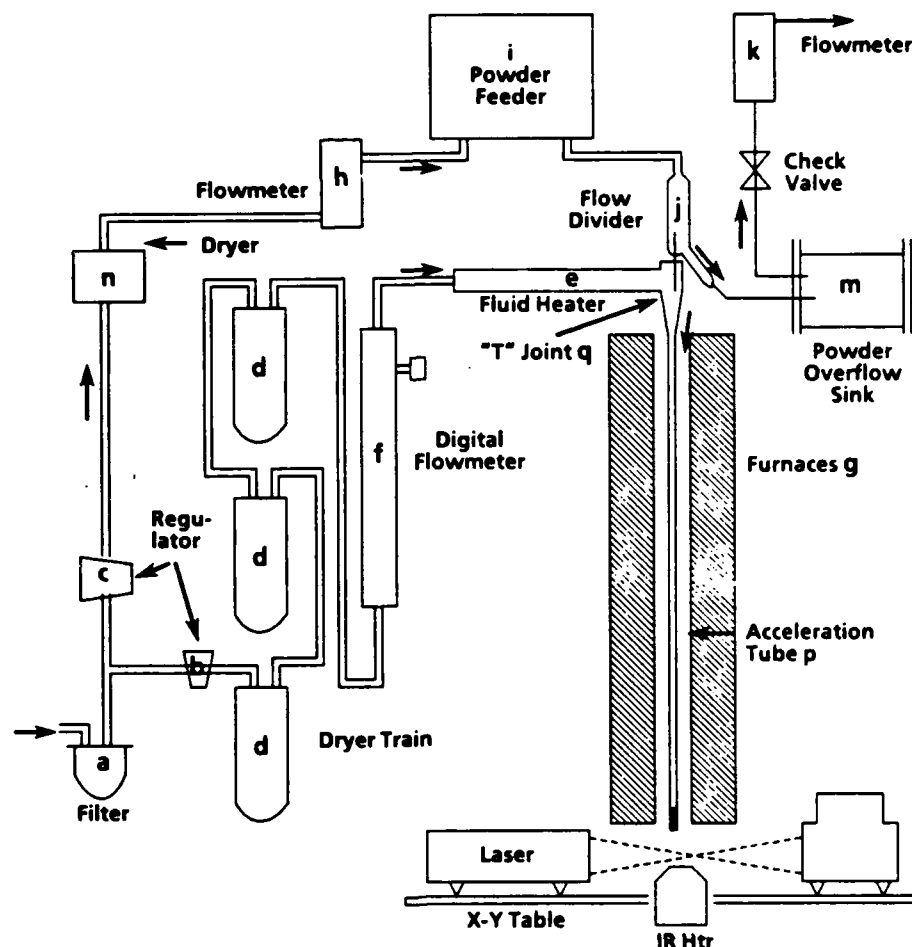
Fig. 1 — Schematic diagram of apparatus for the simultaneous erosion and oxidation of metals.

A. *The Gas Flow*

The functions of the gas flow are to accelerate the particles, heat the specimen, and to establish the oxidizing environment.

Although this apparatus has the capability of using a variety of gases (*e.g.*, SO_2-O_2, CO_2-O_2), the current investigation used air or nitrogen. The compressed air was delivered from a compressor with a flow rate well in excess of 300 liters per minute. The nitrogen was 99.995 pct pure with 1 ppm oxygen. Four nitrogen cylinders were connected together to obtain the necessary gas flow. The nitrogen or compressed air was passed through a filter to remove particles larger than 1 μm mechanically. These gases were then passed through three dryers containing silica gel and two types of molecular sieves to remove moisture and oil vapor.

The gas was heated further, to the temperature required for the experiment, and the particles were accelerated in a 1.5 m Inconel acceleration tube. Alumina was used as an erodent since it is both hard and thermodynamically stable. An average particle size of 20 μm was chosen since calculations showed that such particles would not be deflected by the modified gas flow close to the specimen and would impact on the specimen at angles determined primarily by the incidence of the specimen to the acceleration tube. Angular, crushed alumina was used. It was fed at a constant rate of 0.92 g/minute in all of the experiments. When the

entrained particles are accelerated in the tube, the ideal condition is to have the particle velocity reach the gas flow velocity at the end of the tube. Based upon this criterion, the length of the acceleration tube was made to be 1.5 m by using a formula developed by Klinzing.[20]

Particle velocities were measured over the entire cross section of the gas stream by using a laser velocimeter mounted on a table whose position may be adjusted accurately in both horizontal directions. The speeds of particles passing through a volume of 0.1 mm^3 are measured where the twin laser beams cross. The output of data from the velocimeter is fed into an Apple II computer where a large amount of data can be collected and treated sufficiently rapidly using a program to calculate the mean velocity, standard deviation, and velocity distribution. Excellent agreement has been obtained between measured particle velocities and calculated gas stream velocities. The velocimeter integrates well with the apparatus and may be used *in situ* without disturbing the rest of the apparatus to measure velocities of both hot or cold gas streams. The particle velocity profile across the acceleration tube was such that the velocities decreased as the walls of the tube were approached. A typical profile is presented in Figure 2.

In this apparatus the sample is heated by the preheated gas that impinges upon its surface and by an infrared spot heater focused on the back side of the specimen. Gas heated to 900 °C and flowing at a rate of 130 l/min contains enough thermal energy (~560 cal/s) to heat a nickel specimen to

Flow Rate: 142 l/min.

Gas Temperature: 1073 K

Average Velocity: 125.5 m/s

Maxl. Velocity: 156.8 m/s Calculated
147.7 m/s Measured
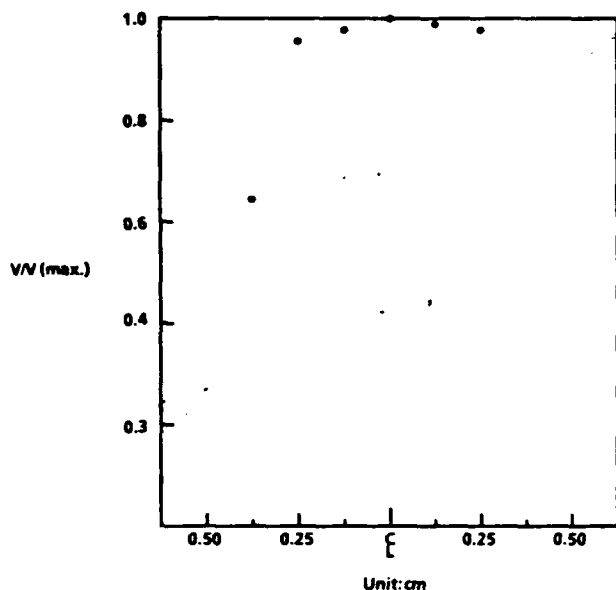
Fig. 2 — Measured particle velocity profile when particles were accelerated by air flowing at 142 l/min^{-1} at 1073 K.

800 °C (~370 cal/s is needed for a specimen of four grams). The heating of the specimens was verified by measuring the temperature of specimens using thermocouples placed at both top and bottom surfaces of the specimens and in a hole drilled into the center of the specimen. The desired test temperature was obtained throughout the specimen to within 5 °C.

B. Measuring Degradation of Specimens

The effects of combined erosion-corrosion attack were determined by measuring the weight change of the specimen as a function of time. Since only one surface of the sample is exposed to the erosive stream, it was necessary to ensure that weight changes over the remainder of the sample area were negligible. Two methods were used to obtain such a condition.

In the case of nickel, specimens were oxidized at 1100 °C for 72 hours in air to produce a layer of NiO about 120 μm thick over the entire specimen. The nickel oxide was then removed, by grinding, from the surface to be exposed to erosion-corrosion conditions. The weight increase of the remaining specimen surface still covered with a NiO scale was less than one microgram during the erosion-oxidation experiment and hence was negligible compared to the weight changes developed on the surface exposed to combined erosion-oxidation.

To study the erosion of nickel oxide, preoxidized specimens as described previously were also used but nickel oxide was not removed by grinding. Measurements of weight change as a function of time were used to determine the amount of erosion. In such experiments, under especially severe conditions, the nickel oxide scale was even-

tually reduced to thicknesses for which oxidation began to contribute to the results.

Since cobalt oxidizes several orders of magnitude faster than nickel, the reaction rate cannot be reduced to negligible levels by the preoxidizing technique used for nickel. Cobalt specimens were therefore pack aluminized at 780 °C in a mixture of 3 pct (by weight) NH$_4$Cl, 85 pct Al$_2$O$_3$ powder, and 12 pct Al powder. The aluminide coating was removed, by grinding, from the surface to be exposed to the erosion-corrosion conditions. During the experiments an alumina layer was formed on the aluminide coating, producing weight increases that were negligible compared to the weight changes caused by the erosion-oxidation of the uncoated surface.

C. Specimen Preparation

Pure nickel plate Ni-270 (99.98 pct Ni, 0.01 pct C, 0.003 pct Mn, remainder of impurities <0.001 pct) and electrolytic cobalt (99.9 pct Co, 0.07 pct Ni, 0.002 pct C, 0.001 pct Cu) were used for specimens. The nickel specimens had dimensions of 12 mm × 12 mm × 2 mm. The surfaces to be exposed to erosion-oxidation conditions were polished through a 1 micron alumina slurry. The cobalt specimens were circular in shape and had a diameter of 12.8 mm and a thickness of 3 mm. All specimens had a hole of 1 mm diameter drilled from one side to the center of the sample for temperature measurement during the experiment and were cleaned ultrasonically using distilled water and then rinsed in acetone.

D. Typical Test Procedure

In performing an experiment the gases were first heated, the flow rate was established, the erosive particles were added to the gas stream, and the temperature of the gas discharging from the acceleration tube was monitored using a thermocouple. After the desired gas temperature was obtained, the thermocouple was removed and a particle velocity profile across the gas stream was obtained by using the laser doppler velocimeter. A specimen was then placed in the erosion position, with a thermocouple inserted into its center. The specimen temperature was controlled by varying the input power to the infrared heater. At the end of an experiment, the specimen was removed from the erosion position and quenched in a stream of nitrogen to attempt to preserve the features developed at the test temperature. The specimen was weighed before and after the test to determine the weight change that occurred during the experiment.

E. Specimen Evaluation

After exposure to the erosion-oxidation test the surface morphology, cross section and subsurface regions were examined to evaluate the material removal process. The surface morphology was examined by using optical metallography, scanning electron microscopy, and energy dispersive spectroscopy (EDS). A low speed diamond saw was used to section the specimen, normal to the eroded surface. After mounting in an epoxy resin, the specimens were polished through 1 μm diamond paste and etched by immersion for 15 to 30 seconds in a mixture of 50 ml acetic acid and 50 ml nitric acid. Two electropolishing techniques were also used to help elucidate features on the surfaces of the speci-

mens. One technique, used to remove corrosion products from the specimens, involved dissolution of the metallic substrate by using an electrolyte of 400 ml distilled water and 600 ml concentrated sulfuric acid with the specimen connected to the positive terminal of a DC source at 1.5 volts. The metal along the oxide layer/metal interface was preferentially dissolved and the oxidation product could be separated from the metal sample. The surface morphologies of the oxidation products were examined before and after electropolishing, and it was concluded that this procedure did not affect the features of the oxidation products. A second electropolishing procedure was used to remove the oxidation products and reveal the morphology of the metal below. The specimen was made the anode in an electrolyte consisting of a mixture of 60 ml distilled water, 25 ml hydrofluoric acid, and 25 ml glacial acetic acid with a stainless steel beaker as the cathode, ten volts being applied across the cell for one and one-half minutes. After removal from the electrolyte, the oxidation products were separated from the metallic substrate by immersion in distilled water in an ultrasonic cleaner. A nickel specimen was exposed to this electropolishing procedure and examined with the SEM. Comparison of features before and after exposure showed that this technique had no effect on the nickel metal morphology.

III. RESULTS AND DISCUSSION

A. Introduction

The results obtained in this investigation can be classified into several groups, each of which represents a different regime of the interaction between erosion and oxidation at high temperature. The results will therefore be presented and discussed under the headings of these regimes, namely pure erosion, erosion-enhanced oxidation, and oxidation-affected erosion.

Apart from a few initial experiments, the erosion oxidation exposures were carried out using specimens held at 90 deg to the erosive stream. Specimens held in this way showed the development of a series of undulations referred to previously[15] as 'moguls' and shown in Figure 3. A specimen held at 45 deg to the erosive stream was found to develop a system of surface ripples shown in Figure 4. In both cases some of the incident, erosive, alumina particles were embedded in the specimen, as shown in Figures 3 and 4. Similar ripples also developed at the surface of a specimen held at 18 deg to the erosive stream. All subsequent experiments described below were carried out with the specimens held at 90 deg to the erosive stream.

B. Pure Erosion

This section concerns results that were obtained under conditions where high temperature erosion could be studied without interference from the oxidation reaction. In particular, the erosion of nickel oxide in air and of nickel in nitrogen was studied.

1. Nickel oxide

Nickel oxide specimens were obtained by preoxidizing nickel to provide a scale 100 μm thick. The erosion of nickel oxide was studied at 800 °C, 650 °C, and 25 °C at 90 deg incidence and at several velocities; the results are

(a) oxide surface

(b) oxide surface with embedded Al$_2$O$_3$ particles

(c) as (b)
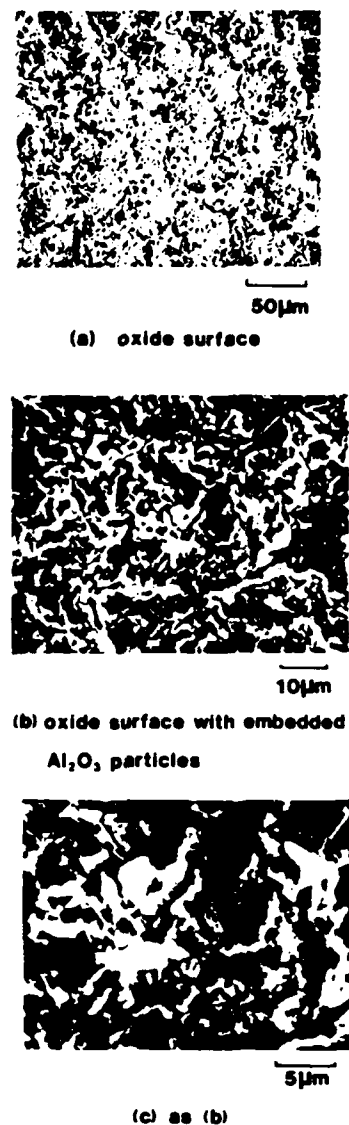
Fig. 3 — Nickel exposed for 8 min at 810 °C at 90 deg to 190 m/s^{-1} airflow containing 1500 ppm 20 μm Al$_2$O$_3$.

shown in Figure 5 where total mass loss is plotted as a function of time. Material removal apparently begins as soon as the specimen is exposed to the erosive stream since all of the data lines extrapolate through zero. The most rapid erosion of the oxide was observed at 25 °C using an erosive stream flowing at 73 m/s^{-1}. At this temperature the surface of the eroded oxide shows signs of cracks, indentations, cutting, and some plastic deformation which contrasts with the original, faceted, oxide surface as shown in Figure 6.

The erosion rates observed at 800 °C in erosion streams flowing at 140 m/s^{-1} and 90 m/s^{-1} were substantially below that for 25 °C (Figure 5). The surface morphology of a specimen exposed at 800 °C (Figure 7) shows cracks, fissures, plastic deformation, and some evidence of local melting that was not present, or not observed, on specimens exposed at 25 °C. The lower erosion rates at 800 °C are taken to reflect the greater plasticity of the nickel oxide at the higher temperature, and to indicate that more of the incident energy is absorbed by carrying out plastic deformation of the specimen.

(a) oxide surface showing development
of ripples

(b) oblique view of surface in (a)

(c) specimen surface showing ripple,

erosive cuts, and embedded Al_2O_3
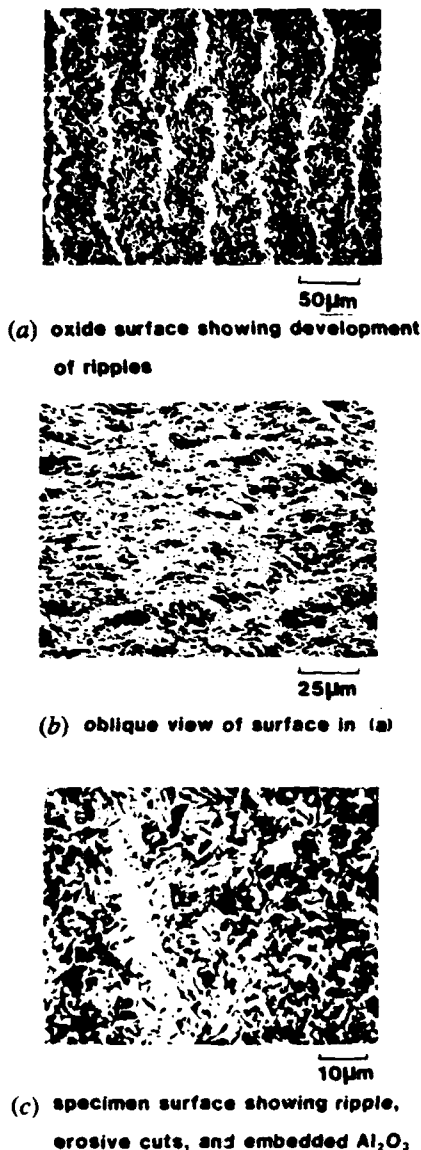
Fig. 4—Nickel exposed for 30 min at 730 °C at 45 deg to 120 m/s^{-1} airflow containing 2400 ppm 20 μm Al_2O_3.

Nickel oxide exposed at 650 °C to an erosion stream flowing at 140 m/s^{-1} erodes faster than at 800 °C but slower than at 25 °C (Figure 5). This confirms the trend of higher erosion rates with lower plasticity assuming that nickel oxide is less ductile at 650 °C than at 800 °C. After 50 minutes under these conditions at 650 °C the oxide scale thickness was reduced from the original 100 μm to about 45 μm (Figure 8). It should also be noted that the eroded oxide surface remains flat and that the nickel-nickel oxide interface is unaffected by the erosion under these conditions. The surface morphology was found to be very similar to that at 800 °C except that evidence of local melting was rarely seen. The deformation of the nickel oxide surface appears to be confined to the fairly shallow depths typical of the cutting action and plastic deformation on the surface.

2. Erosion of nickel in the absence of oxidation

The erosion of nickel metal in the absence of oxidation at high temperature was studied by using nitrogen as the carrier gas for the erosive particles; similarly, exposure at
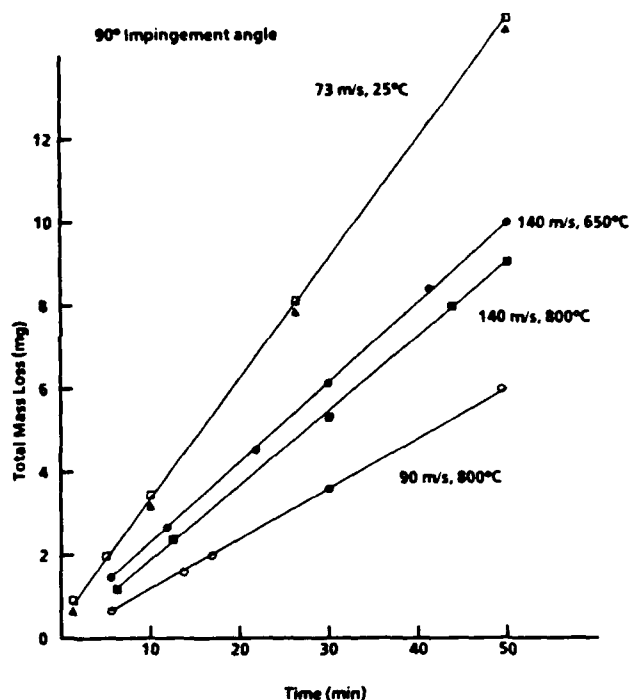
Fig. 5—Mass loss vs time for preoxidized nickel specimens exposed at 90 deg impact angle to airflow.

25 °C using air as the carrier did not involve oxidation phenomena.

Nickel samples were exposed at 800 °C to erosive nitrogen streams flowing at 140 m/s^{-1} and 90 m/s^{-1} using 90 deg incidence; since the oxygen content of the nitrogen was of the order of 1 to 10 ppm ($\sim 10^{-6}$ atm), oxide formation did not play a role under these conditions, the kinetic data for which are shown in Figure 9. In the absence of oxide formation the rate of degradation of the metal is very low and extensive plastic deformation of the surface occurs, resulting in the formation of moguls. Clearly, therefore, neither oxidation of the metal nor removal of material is an essential part of the mechanism of mogul formation.

Cross sections of the nickel eroded in this way show that alumina particles embed in the metal and are transported down the sides of the moguls to accumulate in the valleys of the structure. This is shown in Figure 10 and is clear evidence of the highly plastic nature of the metal under these conditions. The accumulation of embedded alumina is thought to account for the initial gain in weight by nickel samples eroded in the absence of oxidation.

Since 800 °C is well above the recrystallization temperature of nickel, work hardening is discounted as part of the mechanism of erosion at that temperature. Even at 25 °C the low degradation rates suggest the possibility of surface heating by the impacts of the erosive particles. The absence of mogul formation indicates that plastic deformation did not extend deep into the specimen.

3. Erosion of cobalt in the absence of oxidation

Cobalt metal samples were also eroded in pure nitrogen at 800 °C and in air at 25 °C under conditions identical to those employed for nickel. In this case also the rate of degradation by erosion alone was low (Figure 11). Moguls formed on

(a)

20μm
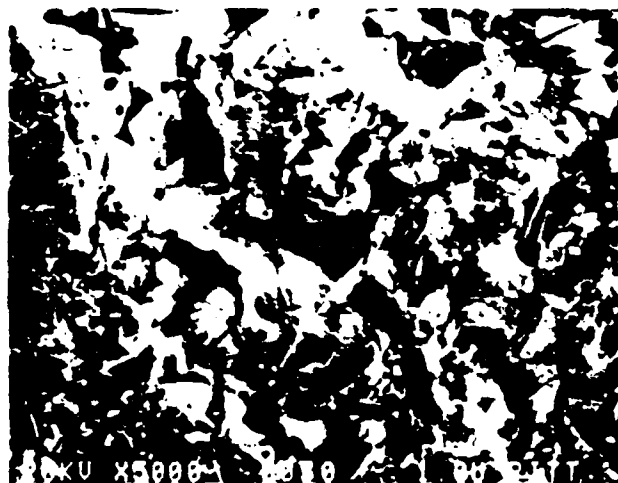
(b)

Fig. 6 — (a) Original nickel surface compared with (b) surface of NiO after exposure to erosive stream flowing at 73 m/s⁻¹ at 90 deg incidence for 30 min at 25 °C.
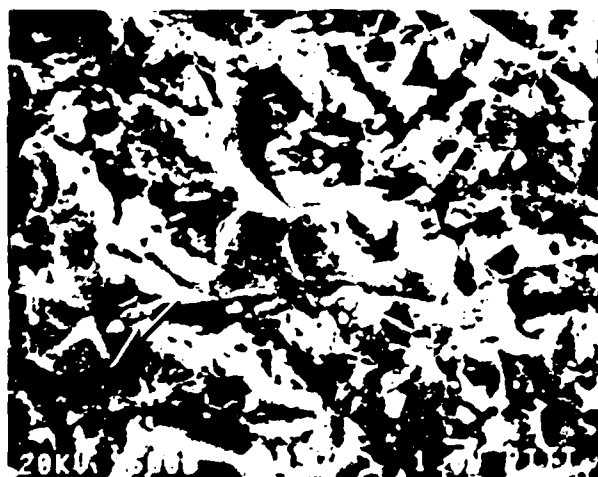
(a)

(b)

Fig. 7 — NiO surface after erosion at 800 °C under 140 m/s⁻¹ airflow at 90 deg incidence for 50 min, showing evidence of plastic deformation and local melting.

the cobalt surface and developed more rapidly under the higher velocity at 800 °C.

The surface morphology of the cobalt eroded at 800 °C in nitrogen shows a structure of deformed metal with alumina particles embedded in the surface covered with a very thin layer of oxide which is thought to form during cooling after the nitrogen flow is switched off. This was not seen on nickel which oxidizes much more slowly than cobalt. The morphological features on the cobalt surface are shown in Figure 12 and in section in Figure 13.

After erosion at 25 °C in air, cutting and deformation of the cobalt metal surface occurred. Moguls did not form and little or no alumina was embedded. The rate of erosion was very low.

C. *Erosion-Enhanced Oxidation*

In erosion-enhanced oxidation the erosion process does not alter the scale growth mechanism but simply modifies the way in which the scale thickness varies with time and, therefore, influences the variation of the oxidation rate with time.
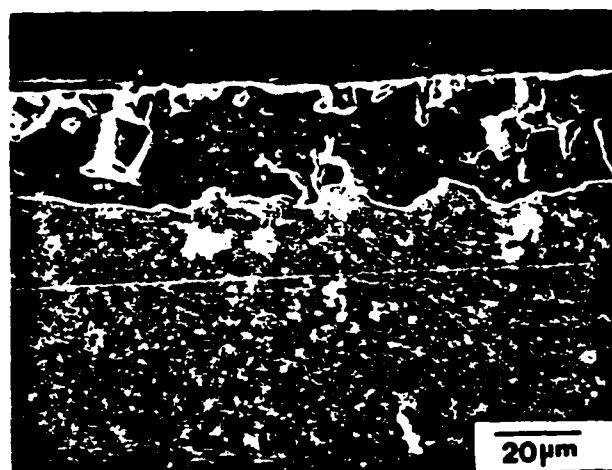
(a)

(b)

Fig. 8—Section of NiO scale 45 μm thick after erosion at 650 °C in 140 m/s⁻¹ airflow at 90 deg incidence for 50 min. Note planer oxide surface and absence of deformation at metal-scale interface.

1. Preoxidized nickel

A nickel specimen preoxidized in air at 1100 °C for 120 minutes formed an oxide layer 10 μm thick. When the oxide surface was exposed for 30 minutes at 800 °C at 90 deg to an erosion stream flowing at 135 m/s⁻¹, the oxide scale thinned down in a nonuniform manner, reflecting the variation in erosive severity across the erosive stream. In the center of the specimen, where erosion was most severe, the oxide thickness was greatly reduced and mogul formation had occurred. The oxide thickness increased toward the rim of the specimen where erosion was less intense. These peripheral regions, which were covered with a thick (10 μm) oxide, had undergone relatively mild erosion due to the lower particle density and velocity at the edge of the erosive stream. This situation corresponded to erosion-enhanced oxidation conditions whereas in the center, which was subjected to heavy erosion due to the higher particle density and velocity, the oxide scale had been very strongly eroded and drastically thinned to the point where the underlying metal was deformed. This latter condition has the characteristics of oxidation-affected erosion, which will be discussed in the next section.
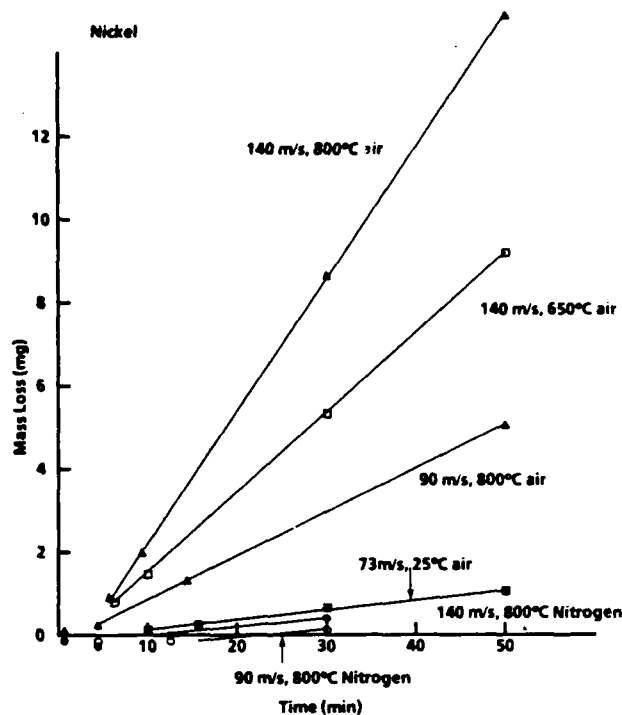
Fig. 9—Mass loss vs time for nickel specimens exposed at 90 deg incidence to erosive stream.

In the current apparatus, it was not possible to reduce the particle loading to observe erosion-enhanced oxidation over the whole specimen in the case of nickel. However, cobalt oxidizes much more rapidly than nickel and, consequently, the higher rate of scale formation allowed the erosion-enhanced oxidation region of behavior to be studied for the case of cobalt as described below.

2. Cobalt

The oxidation rate of cobalt was so rapid that, when exposed at 800 °C at 90 deg to an erosion stream of air and alumina particles flowing at 90 m/s⁻¹, the whole surface becomes covered with a thick oxide layer and no moguls are formed. The oxide layer consisted of an inner zone of CoO and an outer region of Co_3O_4. The surface of this oxide is shown in Figure 14 and the cross sections of the eroded sample are shown in Figure 15. The thickness of the oxide formed in the specimen center, i.e., in the center of the erosion stream, was measured to be the same after 60 minutes as it was after 10 minutes exposure. This points to the existence under these conditions of a balance between the rate of formation of the oxide by oxidation processes and the rate of oxide removal by the erosion process. This is an excellent example of erosion-enhanced oxidation in which the oxide scale growth by oxidation is precisely balanced by the erosion of its outer surface and is thus maintained at constant thickness. The outer, peripheral, regions of the specimen are subjected to less severe erosion and, consequently, the scale grew continuously since the oxidation kinetics there were more rapid than scale removal by erosion. Sections of the specimen taken from both central and peripheral areas, Figure 15, show that the oxide grains of the CoO layer in the center region, subjected to the most severe erosion, are equiaxed whereas they have the usual columnar shape in the outer regions where erosion was
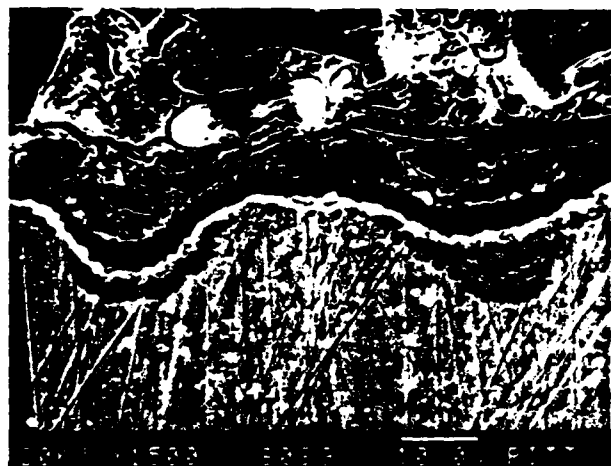
(a)
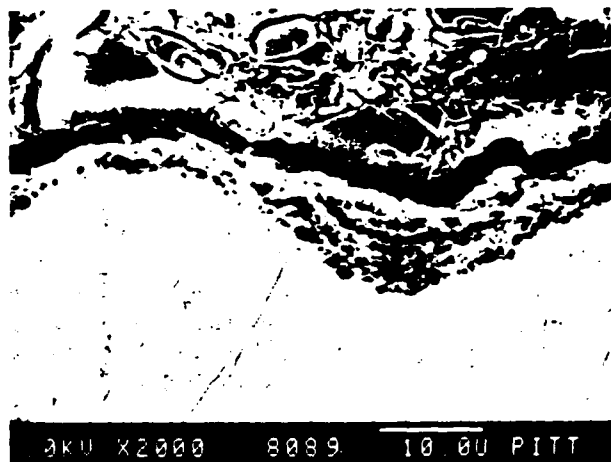
(b)

Fig. 10 — Section of nickel exposed for 30 min to 140 m/s⁻¹ nitrogen flow containing Al₂O₃ erosive particles which are seen to accumulate in the valleys.
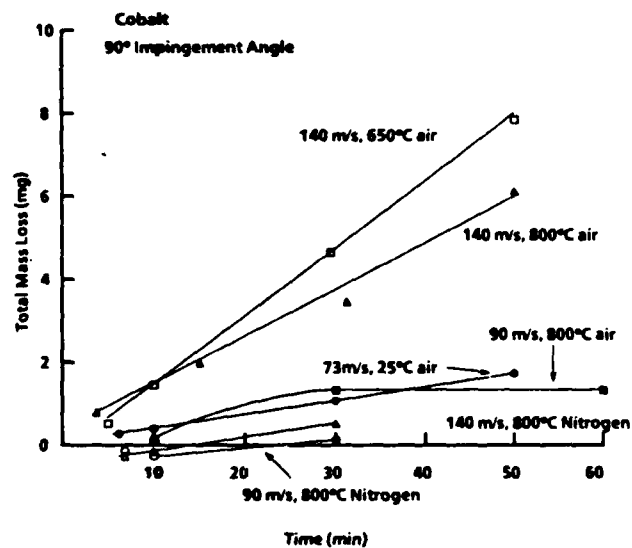
Fig. 11 — Mass loss vs time for cobalt specimens exposed at 90 deg incidence to erosive stream.

(a)
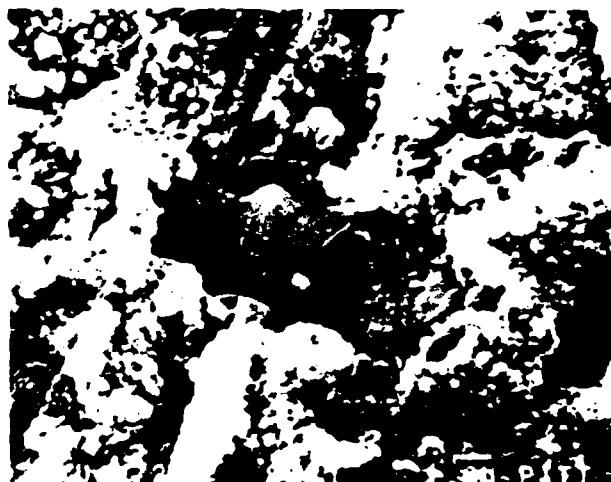
(b)

Fig. 12 — Surface of cobalt eroded at 800 °C in nitrogen showing (a) orange peel appearance and (b) ploughing marks and embedded alumina particles.
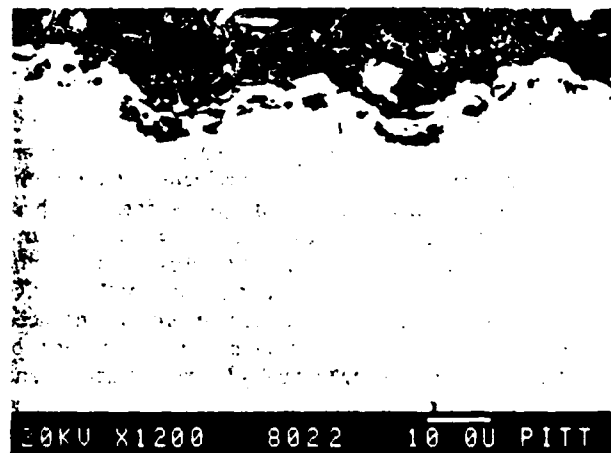
Fig. 13 — Section of cobalt eroded for 10 min in 140 m/s⁻¹ nitrogen flow containing alumina particles which are seen to accumulate in the valleys.
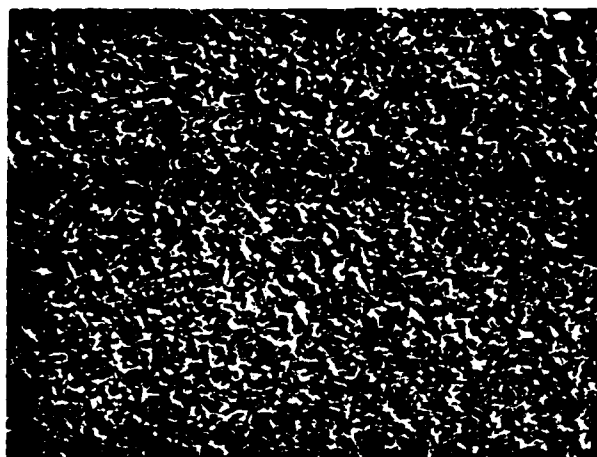
(a) 5 mins. 20μm
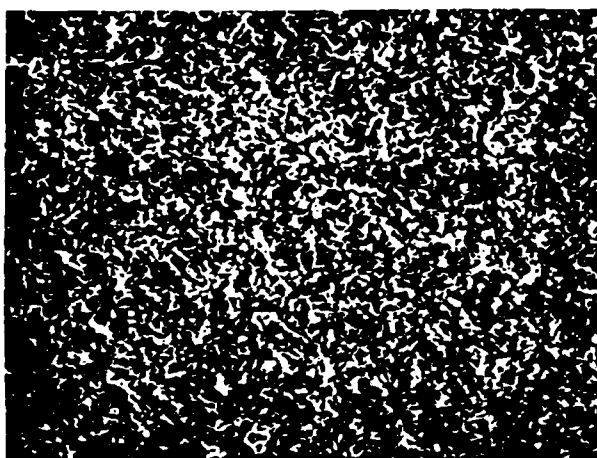
(b) 10 mins. 20μm
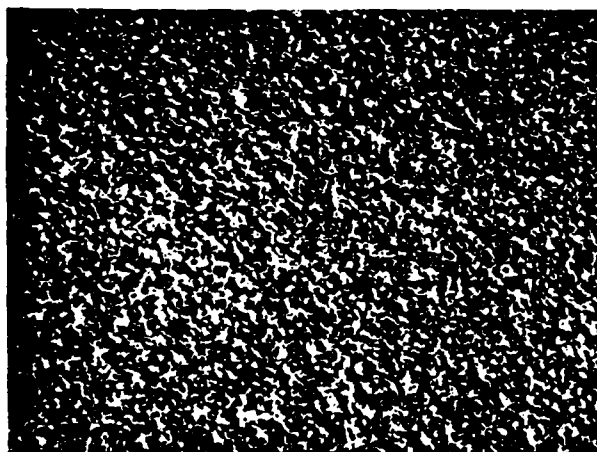
(c) 30 mins 20μm

Fig. 14 — Micrographs of surface of cobalt exposed to erosive airstream flowing at 90 m/s⁻¹ at 800 °C and 90 deg incidence for various times showing lack of mogul formation.

(a) **Erosion and Oxidation**
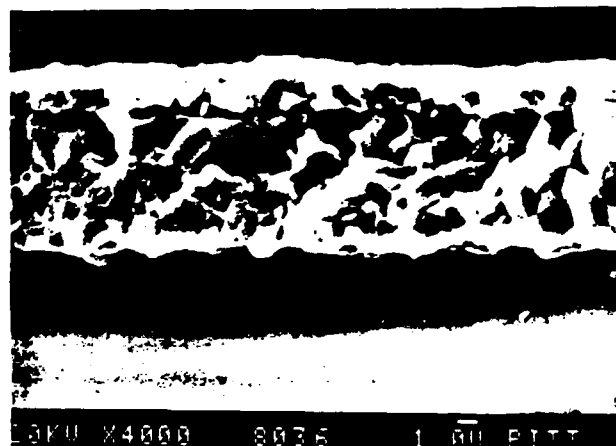
(b) **Oxidation Only**

Fig. 15 — Sections of cobalt specimens eroded at 800 °C in 90 m/s⁻¹ erosive airflow showing the duplex scale at (a) center of erosion and (b) edge of sample where no erosion occurred.

much less severe or absent. In both regions the rapid growth of the oxide layer ensured that erosion damage is confined to the scale-gas interface of the scale. Evidence of cutting, plowing, and plastic deformation is seen in Figure 16, but an absence of cracks indicates that cobalt oxides behave in a predominantly ductile manner at 800 °C. Few indications of melting were found and these were confined to the vicinity of the embedded alumina particles.

D. *Oxidation Affected Erosion*

From the foregoing discussion it is evident that the relative intensities of oxide erosion and oxide scale formation exert a strong influence in determining the behavior of a metal exposed to erosive and oxidizing atmospheres. For instance, for any given metal, with fixed scaling characteristics, a relatively low erosion rate will lead to the steady growth of an oxide scale with simple erosion of the outer scale surface. As the erosion rate is increased, the scale

(a)

(b)
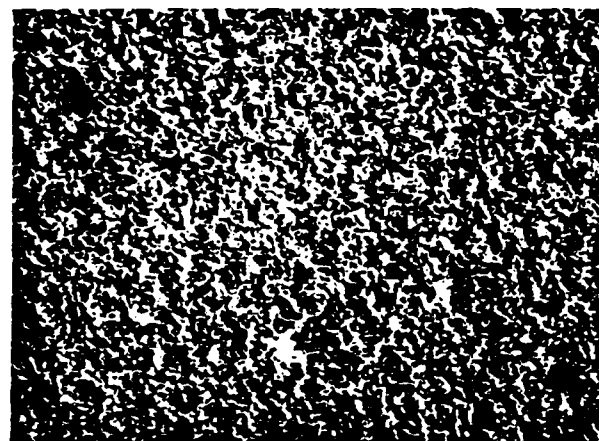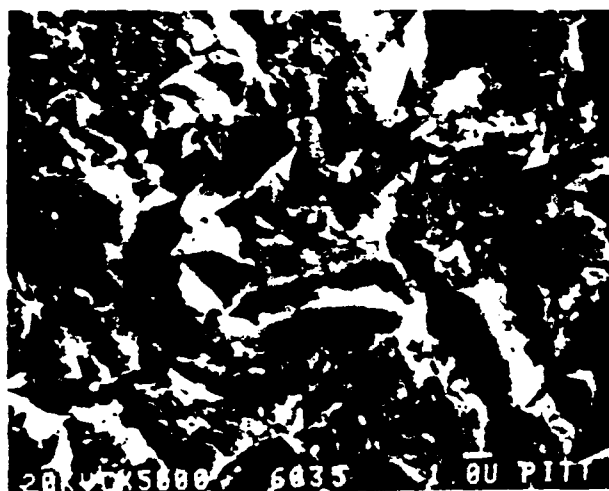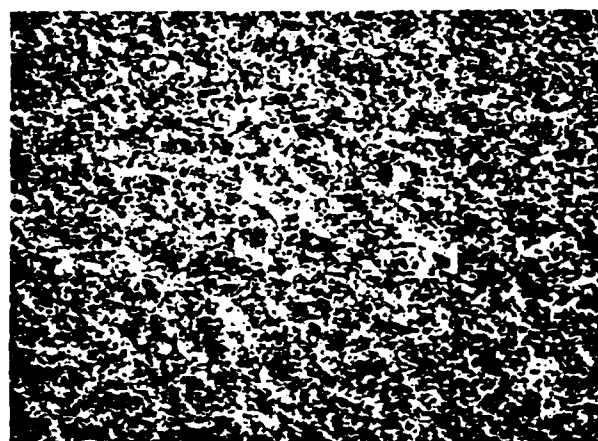
Fig. 16—Surface of cobalt oxide on cobalt specimen exposed to erosive airstream flowing at 90 m/s⁻¹ at 90 deg incidence showing evidence of cutting, ploughing, and plastic deformation but no cracking.

thickness that is eventually established will be reduced. However, if a vigorous action is applied, which removes the oxide very rapidly compared to the rate of oxide scale formation, then the erosive action is no longer confined to the oxide surface but, instead, involves the underlying metal, thus causing a very complex interaction between erosion and oxidation processes to arise. This is the "oxidation-affected erosion" regime which was studied using both nickel and cobalt specimens.

1. Nickel

The weight loss kinetics for nickel specimens, exposed at 800 °C inclined 90 deg to an erosion stream flowing at 140 m/s⁻¹ and 90 m/s⁻¹, are given in Figure 9. The eroded surfaces showed evidence of cutting and deformation, and a mogul morphology developed completely within 15 minutes under a 90 m/s⁻¹ erosion stream (Figure 17).

Under these conditions the sample was rapidly degraded and a very thin composite layer formed on the metal surface, composed of nickel oxide, alumina particles, and nickel

(a)   1 min   20μm
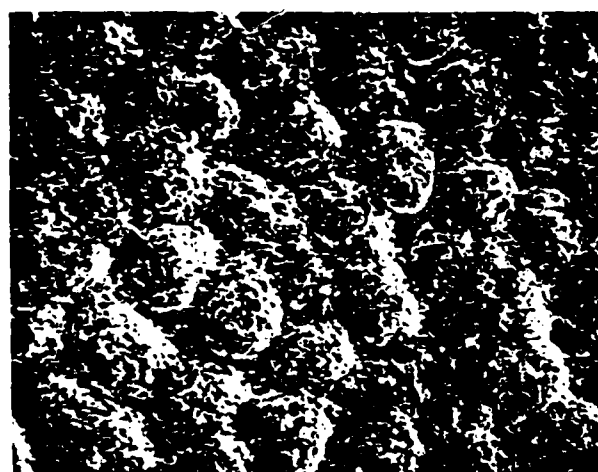
(b)   5 mins.   20μm

(c)   15 mins.   20μm

Fig. 17—Formation of moguls on nickel specimen exposed for increasing times to erosive airflow flowing at 90 m/s⁻¹ at 800 °C and 90 deg incidence.
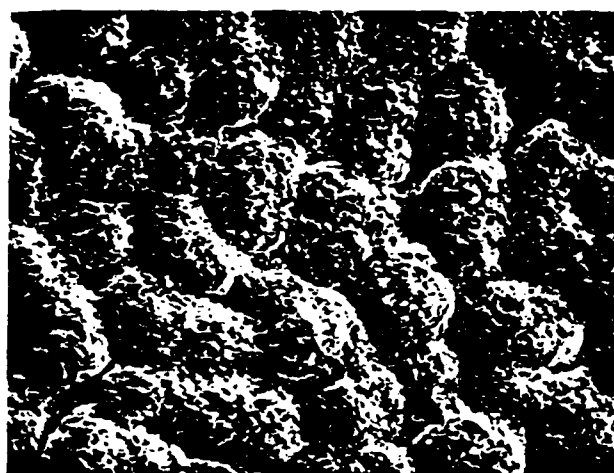
(d) 30 mins.   20μm

Fig. 17 Cont. — Formation of moguls on nickel specimen exposed for increasing times to erosive airflow flowing at 90 m/s⁻¹ at 800 °C and 90 deg incidence.

metal. This surface layer has numerous tears, especially adjacent to the impact craters (Figure 18). Such tearing is thought to be caused by tensile stresses induced in the surface scale by the plastic flow of the metal at an impact site. Embedded alumina particles are also evident, some of which are cracked, presumably by the direct impact of a subsequent alumina particle.

The underlying nickel surface was revealed by stripping away the composite layer using the electropolishing technique, and Figure 19 shows it to have a heavily-deformed surface with extensive evidence of plastic flow of the metal around the impact site. Alumina particles were found to have penetrated the thin composite layer to embed in the metal below.

Examination of the scale removed electrolytically and of cross sections of exposed nickel specimens confirmed that the scale formed under these conditions was not a simple oxide scale but a complex, composite scale consisting of nickel oxide, alumina particles, and nickel metal (Figure 20). Nickel metal was being thrust out from beneath the impact sites to form part of this composite layer which,

2 μm

(a)

2 μm

(b)

Fig. 18 — Surface of composite scale formed on nickel exposed to erosive airflow at 800 °C and 140 m/s⁻¹ showing indication of plastic deformation.

5 μm

(a)

5 μm
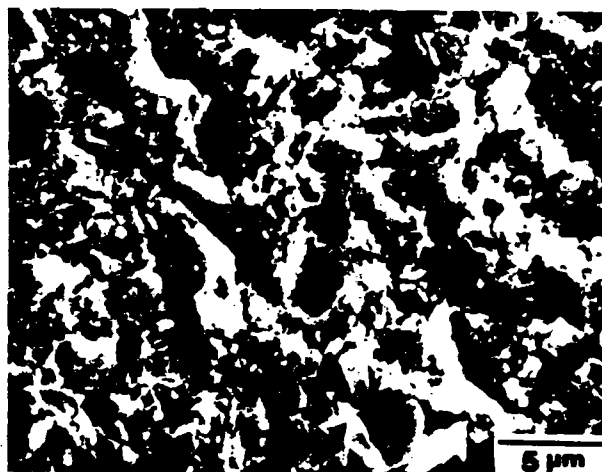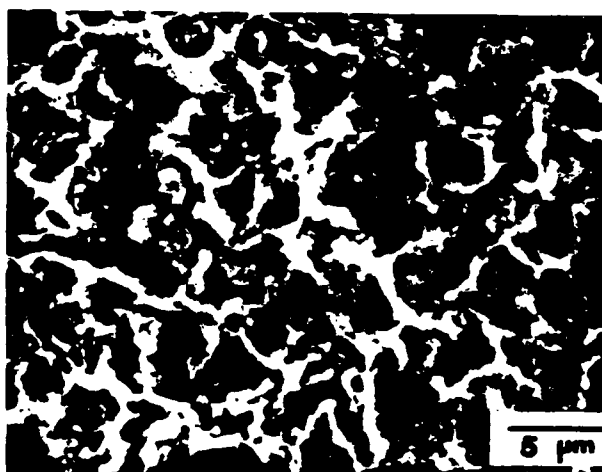
(b)

Fig. 19 — Surface of nickel exposed for 1 min to 140 m/s⁻¹ erosive airflow at 800 °C: (a) surface layer before stripping. (b) nickel surface after stripping showing extrusion of metal and embedded particles.
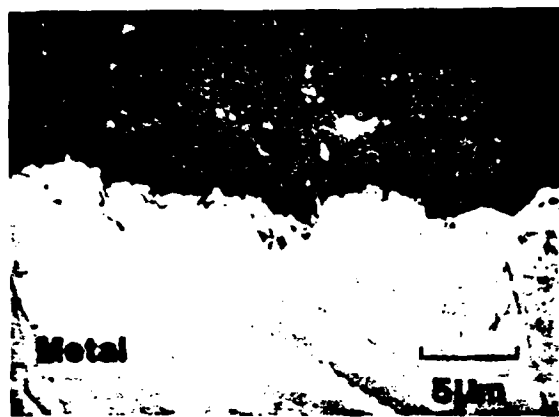
(a)

(b)

(c)
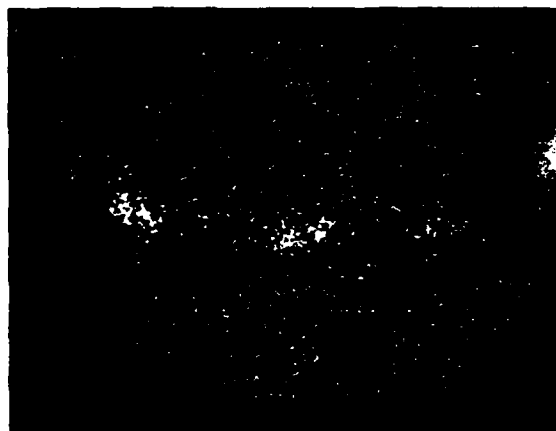
Al X-Ray map of 6(a)

Fig. 20 — Section of nickel exposed for 50 min at 810 °C to 190 m/s⁻¹ erosive airflow at 90 deg incidence showing complex nature of surface layer containing captured alumina particles.

when cooled to room temperature, appeared to be about 1 μm thick; furthermore, the thickness was found not to vary with time. Figure 20 also shows the continuous nature and uniform thickness of the composite scale on the surface of the moguls that also form under these conditions.

Close examination of the surfaces of the eroded specimens yields evidence that impacts of eroding particles have resulted in cutting and ploughing of the surface accompanied by extrusion of oxide, metal, or both around an impact site. Particle capture is observed most readily when the surface layer covering the specimen is so thin the impacting particle can penetrate to the underlying metal. Under erosion at 800 °C, nickel oxide appears to behave as a ductile but stiff material; there was no evidence to suggest that brittle fracture of the oxide occurred.

Nickel specimens exposed in a similar manner at 650 °C developed similar morphological features but were degraded at a somewhat lower rate than at 800 °C, as can be seen from Figure 9. Moguls were formed at 650 °C, and a thin composite surface layer was formed similar to that described for specimens exposed at 800 °C.

2. Cobalt

Cobalt oxidizes more rapidly than nickel and forms two oxides Co_3O_4 and CoO, at 800 °C. When cobalt specimens were exposed to 800 °C at 90 deg incidence to an erosive stream flowing at 140 m/s⁻¹, the higher rate of oxidation was immediately apparent in that moguls formed only in the center of the specimen where erosion is most intense and formed more slowly than in the case of nickel as shown in Figure 21. The extent of degradation of cobalt specimens under a variety of conditions is shown in Figure 11.

The surface layer over the moguls formed on cobalt was about 3 μm thick at the center, where erosion was most intense, increasing to 9 μm at the edge of the specimen where only oxidation was experienced. In both areas the scale consisted of CoO with a surface layer of Co_3O_4, the Co_3O_4 layer being relatively thicker at the center of the specimen where erosion was most severe. In Figure 22 the eroded surface shows the usual cutting and deformation features together with embedded alumina particles.

When the particle velocity was reduced to 90 m/s⁻¹ at 800 °C, a thick oxide scale was formed; these results have been discussed under erosion-enhanced oxidation.

(a) 1 minute   20µm   (b) 5 mins.   20µm

(c) 30 mins.   20µm   (d) 50 mins.   20µm
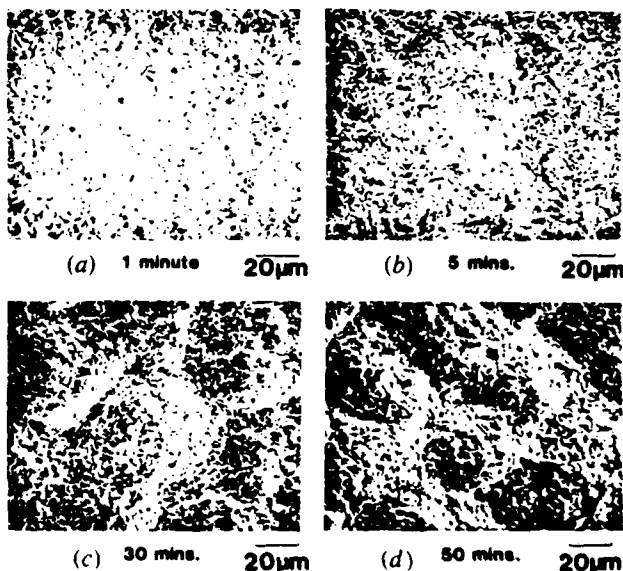
Fig. 21 — Formation of moguls on cobalt surface exposed for increasing times to erosive 140 m/s⁻¹ airflow at 800 °C and 90 deg incidence.

(a)

(b)

Fig. 22 — Eroded surface of cobalt oxide showing (a) cutting deformation and (b) embedded alumina after 50 min at 800 °C and 140 m/s⁻¹.


(a)

(b)

Fig. 23 — Section of cobalt exposed to erosive airflow of 140 m/s⁻¹ at 650 °C and 90 deg incidence for 50 min at (a) center of erosion and (b) toward specimen edge.

When cobalt was exposed at 650 °C to erosive streams of air flowing at 140 m/s⁻¹ incident at 90 deg, moguls formed on the eroded area similar to those formed at 800 °C, but the surface layer was substantially thinner, 1 to 3 μm, as shown in Figure 23. The extent of degradation appeared to be somewhat greater at 650 °C than at 800 °C, as seen in Figure 11. Circumferential tears are observed around an impacting particle, Figure 24, which are thought to be caused by the plastic deformation of the metal which, on impact, pushes back against the surface oxide, causing it to tear under the induced tensile stress.

E. *Discussion of Mechanisms*

The stages of the interaction between erosion and oxidation have been identified and referred to as (a) pure erosion, (b) erosion-enhanced oxidation, and (c) oxidation-affected erosion. The mechanisms by which these interactions arise will now be considered.

1. *Pure erosion of the oxide*

The appearance of the eroded oxide surface shown in Figures 6 and 7 indicates that the surface was deformed

plastically rather than by brittle fracture even at 25 °C; furthermore, the damage was confined to the surface layers of the oxide. From this evidence of cutting and plastic deformation shown in Figures 6 and 7 it is surmised that oxide removal occurs by production of a thin, extruded, oxide segment by initial impact which is then severed by a subsequent impact. It is expected that when the oxide is more ductile more of the incident energy is absorbed by plastic deformation, thus leaving less energy available to remove material from the surface. This agrees with the data of Figure 5 which shows that nickel oxide is eroded most rapidly at lower temperatures where the oxide is expected to be less ductile. The mechanism by which oxide is removed is not clear; however, there are three main possibilities: (a) initial impact may deform the surface and extrude thin oxide segments that are severed by a subsequent impact; (b) adiabatic melting at the impact site may eject liquid oxide particles; some evidence of this is shown in Figure 7; (c) examination of alumina particles after erosion showed that some of them had smears of nickel oxide adhering to the corners; the extent of oxide removal by this mechanism was judged to be of the order of 1 pct.

The response of oxides to erosion is usually elastic or elastic-plastic in nature at room temperature.[21,22] In the elastic response, which is more usually experienced with large blunt erodents, Hertzian cracks form around the point of impact and material is lost as chips when the cracks intersect. In the elastic-plastic regime a zone of plastic defor-
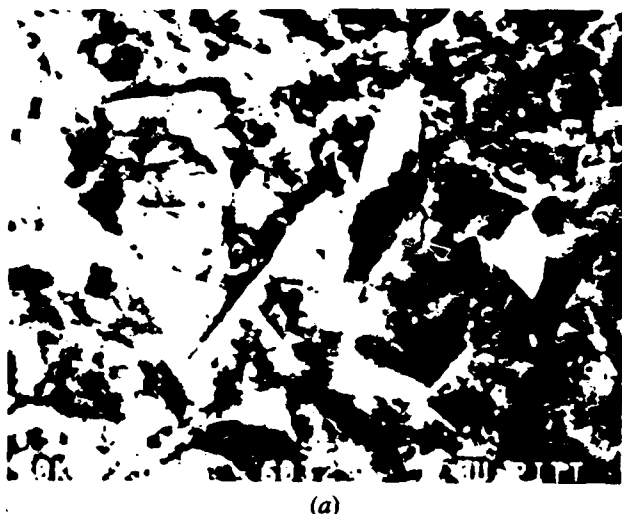
(a)
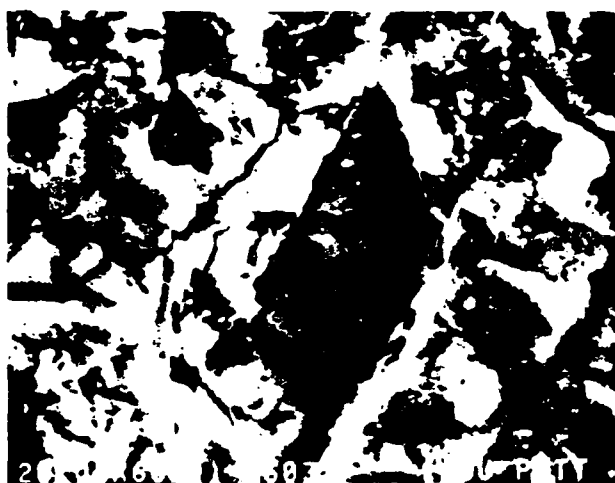
(b)

Fig. 24—Surface of cobalt exposed for 10 min at 650 °C and 90 deg incidence to 140 m/s⁻¹ airflow showing circumferential tears around particle impacts.

mation is formed immediately around and under the impact site. Below this zone a system of cracks forms which eventually intersects and aids material removal. Such plastic deformation has been seen together with localized melting.[23] Finnie has also proposed that brittle materials can behave in a ductile manner under erosion depending on the size and velocity of the particles.[23]

Although data on the erosion of nickel oxide at high temperature have not previously been obtained, it is worth noting that Levy and Zambelli[15] eroded, at room temperature, a nickel oxide layer 80 μm thick grown on nickel. They used 250 μm particles at velocities up to 100 m s⁻¹ at 20 deg and 90 deg incidence. They found that a zone of plastic deformation formed around the impact sites with cracking below the surface as described above. In the present case it is expected[24] that the smaller (20 μ) particles would result in less brittle fracture and more plastic deformation being observed, as was in fact observed in the present study at room temperature. At high temperatures it is expected that the plastic mode would predominate, as also observed.

2. Pure erosion of the metal

The specimens, which were exposed at 90 deg incidence, showed an initial weight gain probably due to particle capture,[25] but showed no sign of classical 'cutting' as suggested by Finnie[26] and Bitter.[3,27] In fact, Hutchings demonstrated that material removal by cutting is rare,[28,29] and the low rate of material removal indicates that neither fatigue[30,31,32] nor platelet[33] mechanisms were very successful in providing material separation. This indicates that, under the present conditions, work hardening mechanisms were not operating and the surface features of the nickel and cobalt samples certainly indicate that extensive local plastic deformation has occurred. It must be remembered in considering the effects of erosive impact that the strain rates are extremely high, of the order of 10^4 s⁻¹.[33] The contact time of an impact has been estimated[6] to be about 10^{-5} seconds. Thus it can be assumed that the plastic deformation occurs adiabatically and consequently significant local heating can be anticipated.

Shewmon and Sundararajan[6] have discussed this together with the mechanism of lip formation and have concluded that the repeated forming and flattening of lips will lead to a layered structure similar to that seen in the valleys between the moguls in the present work. It is more difficult to explain how a metal lip actually leads to material removal but, considering the high rate of transfer of kinetic energy to a substrate undergoing local plastic deformation, Shewmon and Sundararajan have suggested that material removal might occur by necking resulting from the inertia of the moving 'lips' or by the formation of adiabatic shear bands beneath the impact site, thus allowing pieces of material to be removed. Both Sundararajan[34] and Hutchings[29] have found that particles can be removed from specimens at speeds well in excess of that of the incident particle, confirming the violent nature of the interaction between erodent and the target surface.

Thus, the effect of erosion in the absence of oxidation reactions appears to be very strongly dependent upon the ductility of the specimen, the lower erosion rates being observed with the more ductile material. It should also be noted that the very ductile metals also showed mogul formation which apparently occurs as a result of plastic deformation and does not require the removal of material. In order to test this, a computer model was devised using a standard indentation, surrounded by a rim of raised material equal in volume to that of material displaced during indentation. Using random number selection to define the site of an impression on the surface, it was possible to add the results of a large number of randomly distributed impressions to produce a computer-simulated surface as shown in Figure 25 that is very similar to the moguls but was generated assuming no material removal. Mogul formation is therefore considered to be a consequence of the repeated plastic deformation of a ductile surface by the incident erosive particles. The lack of mogul formation on the eroded oxide surfaces reflects the lower ductility of the oxide compared with the metals.

3. Erosion-enhanced oxidation

Although highly ductile pure metal erodes only slowly at 90 deg incidence in the absence of oxidation, if the metal were first converted to oxide, that oxide could be removed rapidly by erosive processes. The interaction between the erosive processes and oxidation may be expressed as the
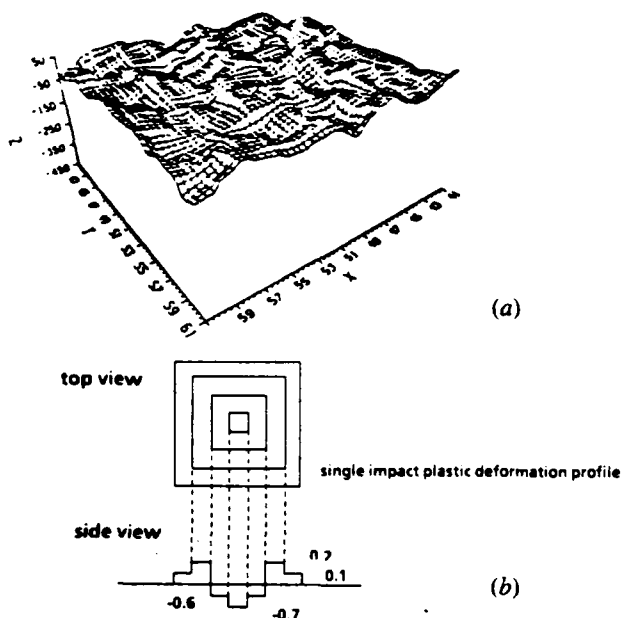
(a)

top view

single impact plastic deformation profile

side view

(b)

Fig. 25 — Computer simulation of surface morphology showing mogul formation after 10^6 random impacts assuming that no material removal occurs.

difference between the rate of formation of the scale by oxidation and the rate of removal by erosion:

$$\frac{dX}{dt} = \frac{k_p}{X} - k_{eo} \qquad [1]$$

Here X is the scale thickness, k_p is the parabolic rate constant defined as $X^2 = 2k_p t$, where t is the time of exposure for pure oxidation, and k_{eo} is the rate at which the oxide surface is removed by the erosive process.

Consider a metal sample on which an oxide scale is growing which is subjected simultaneously to erosion. The surface of the scale will be eroded but the scale will continue to grow. If the growth rate exceeds the erosion rate, the scale will thicken and this will continue until the thickness is such that the growth rate is equal to the erosion rate. Should such a situation be achieved, the value of the limiting thickness of the scale X^* will be given from the equation

$$dX/dt = k_p/X^* - k_{eo} = 0 \qquad [2]$$

from which

$$X^* = k_p/k_{eo} \qquad [3]$$

Similarly in the example above, if the scale erosion rate exceeds the growth rate the scale will thin down until the value X^* is reached. This range of situations is called erosion-enhanced oxidation of which the pure erosion regime for the oxide is a special limiting case where the oxide growth rate is virtually zero.

It should be noted that, although X^* is constant, the scale is not static but is being removed at the same rate as that at which it is being formed. The material removal process is the same as that for erosion of pure oxide, and this process is rate controlling. Consequently the sample still loses weight; however, the rate of weight loss under this condition corresponds to the rate of loss of the nickel contained in the oxide that is removed by erosion. In contrast, with a very thick oxide scale, where the term k_p/X is so small as to be

negligible, the weight loss rate corresponds to the rate of loss of nickel oxide. This must be considered very carefully when interpreting weight loss data from samples exposed to combined erosion oxidation conditions. This is illustrated in Figure 26 where the variation, with time, of oxide thickness, metal degradation rate, and total weight loss are compared for a specimen initially having a thick oxide layer.

The foregoing discussion has assumed that the oxidation process is unaffected by the erosive impacts. Although this is acceptable while considering a relatively thick oxide layer, it is to be expected that the continuous impact of the erosive stream will cause the structure of the oxide surface layers to be modified by the introduction and maintenance of a high dislocation density which would enhance the diffusion of ions through this layer. Thus, as the scale layer becomes thinner, the value of k_p for normal oxidation will no longer adequately represent the scaling process. The thickness of the surface oxide layer affected in this way will be greater as the energy of the individual impacts is increased. In principle, it should be possible to contol the value of X^*, the thickness of the steady state oxide formed, by controlling the erosive stream velocity. In the present work this has been achieved only in the case of cobalt, whose oxidation rate constant is several orders of magnitude greater than that of nickel. More detailed study of this regime of interactions is currently under way.
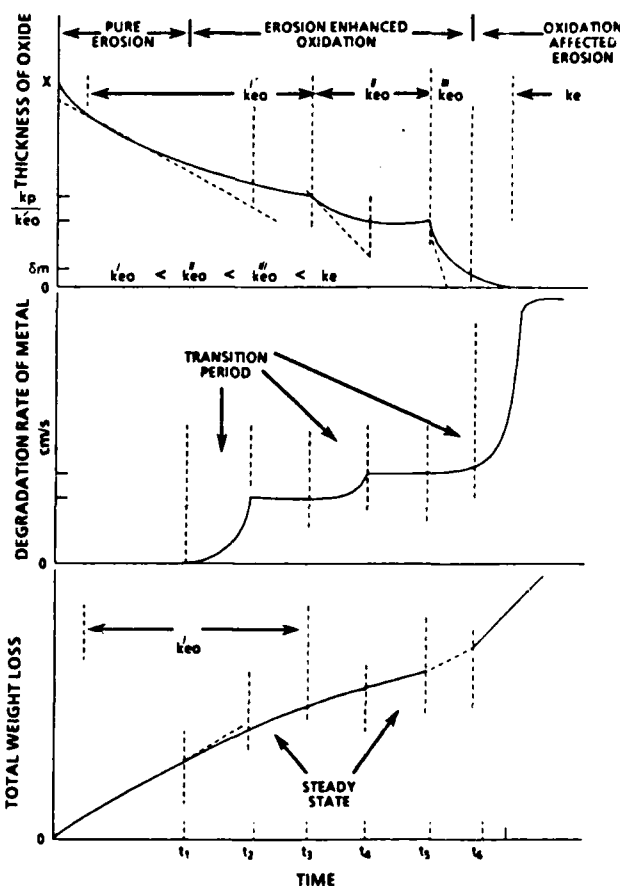
Fig. 26 — Variation with time of oxide thickness, metal degradation rate, and total weight loss for a preoxidized metal sample eroded in an oxidizing atmosphere.

4. Oxidation-affected erosion

The oxidation rate of nickel is so low that the erosive stream rapidly thins down an oxide layer to produce a situation where the impacting particles begin to deform the metal substrate; this marks the onset of complex interactions between the erosion and oxidation processes. Plastic deformation of the metal substrate is accompanied by the onset of mogul formation which, as shown by the computerized simulation, does not necessarily require removal of material. Furthermore, the individual erosive particles penetrate the thin oxide layer, impact into the ductile metal, and remain embedded in the specimen surface. Although the computer simulation explains the initial formation of moguls, it does not explain the steady state situation of mogul size and shape that was observed under conditions of severe erosion. From the results of both nickel and cobalt exposed to erosion under nitrogen atmospheres, shown in Figures 10 and 13, it is clear that some material is continuously displaced from the mogul sides to accumulate in the valleys.

A mechanism to account for the constant appearance of the moguls is shown in Figure 27. It is considered that impacts on the valleys and peaks of the moguls cause plastic deformation and material movement, as indicated, such that interaction with deformation following impacts on the mogul sides produces a circulation of material that explains both the transport down the sides and the stability of the size and shape of the moguls.

Apart from the formation of moguls, the oxidation-affected erosion regime is also marked by the formation of a complex, composite, thin surface layer composed of oxidized metal, embedded alumina particles, and extruded metal. Under such conditions the oxidation rate cannot be predicted from the thickness of the composite layer and the oxidation rate constant; the rate of removal of material by conjoint erosion-oxidation is therefore expressed by a relationship such as

$$\frac{dY}{dt} = k_e'$$
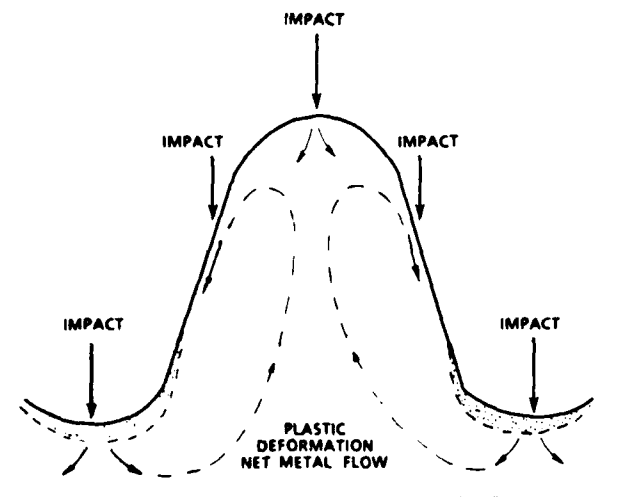
where Y is the position of the composite surface relative to the position of the surface of the specimen before test and k_e' is an erosion constant for the imposed conditions.

The formation of moguls with the simultaneous development of a composite surface layer under oxidation-affected erosion conditions is depicted schematically in Figure 28 while the cross section of the composite layer at 800 °C and 650 °C is shown in Figure 29. It is seen that the extruded metal is more likely to be observed at 650 °C since, at 800 °C, such features are likely to be oxidized very rapidly and consequently not be retained on cooling to room temperature.

The sequence of events thought to occur during an impact is shown schematically in Figure 30. On initial impact of the sharp edge of a particle the oxide layer is pierced and the underlying metal is put under pressure by the intrusion of the particle. The pressure causes the oxide layer to be distended around the particle, putting the surface of the oxide layer in tension and thus causing tears to develop.

The question of heating of the specimen surface is very important in view of the way in which the mechanical properties and oxidation behavior change with temperature. The kinetic energy of the particles incident upon the specimen surface is used to deform the surface both plastically and elastically. Plastic deformation is accompanied by generation of heat, whereas elastic deformation is stored momentarily and, on release, results in the rebound of the particle. Thus, depending upon the nature of the specimen, particularly at the point of impact, the energy of the particle will be used in these two ways. This explains why particles are observed to remain embedded in those specimens with very thin oxide layers, since the underlying metal is heavily deformed and little energy is stored elastically to ensure par-
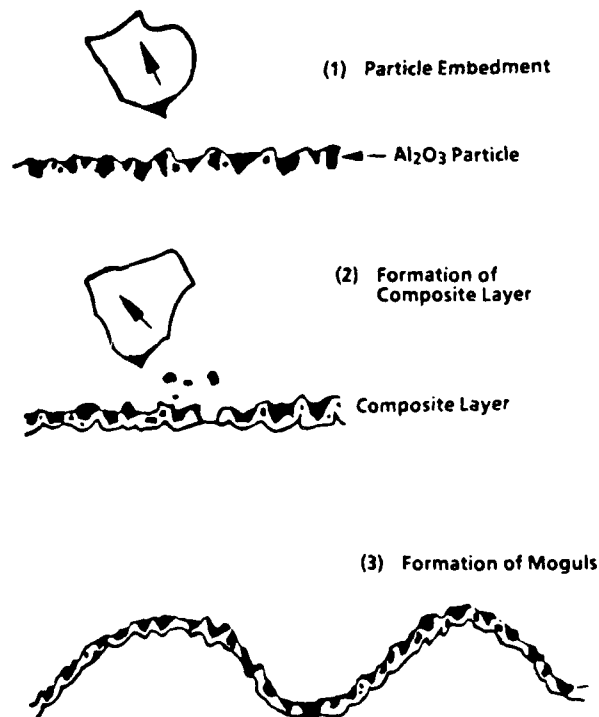
Fig. 27 — Mechanism of mogul formation. Impacts on sloping mogul face transport material down to valleys in between moguls. Impacts on horizontal surfaces cause metal flow as indicated to maintain mogul shape and size in a steady state condition.

Fig. 28 — Schematic diagram of the three stages of mogul formation found on nickel samples subjected to conjoint erosion and oxidation attack.

(1) Particle Embedment

Al₂O₃ Particle

(2) Formation of Composite Layer
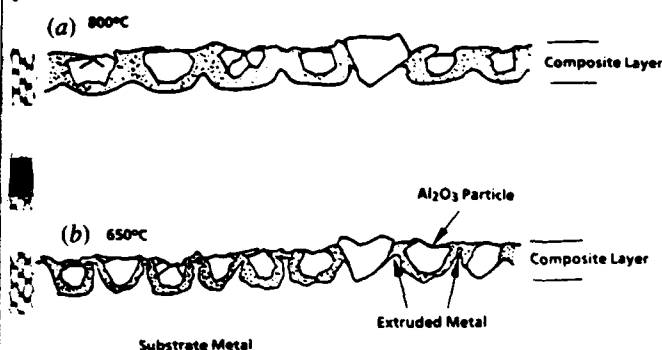
Composite Layer

(3) Formation of Moguls

Fig. 29—Schematic diagrams of section of composite layers formed on nickel samples eroded in air at (a) 800 °C and (b) 650 °C.
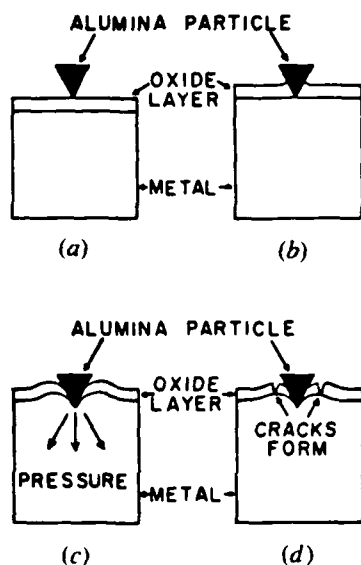

Fig. 30—Hypothetical sequence of events following particle impact leading to tear formation.

ticle rebound. Indeed, the elastic limits of nickel and cobalt are probably not observable so far above their recrystallization temperatures.

When the oxide layer is thicker, such that particle penetration to the metal does not occur, the oxide layer behaves as a solid, or rigid, shell covering a soft interior. On impact, a particle cuts and deforms the oxide locally at the immediate point of impact; it also causes deflection of the oxide layer against the metal which behaves as a hydrostatic spring. Thus this part of the energy is available to rebound the particle and explains why relatively few particles are observed embedded in thick oxide layers.

In certain cases, as shown in Figure 7, signs of melting have been observed which indicate clearly that high local temperatures have been achieved. In order for this to happen rapid, adiabatic local plastic deformation of either the metal or the oxide must have occurred. It is tempting to think of a particle impacting on its flat surface and causing local deformation of the oxide layer which then 'splashes' to either side of the impact. However, the eroded surfaces show very few, if any, signs of such impact; on the contrary, the indications are that the impacts occur on a tip or edge of an incident particle. One possible way in which liquid could be produced, when the particle penetrates the surface layer,

is by intense local extrusion of the metal between the particle and the oxide as shown in Figure 31. Such a mechanism also explains the loss of hydrostatic pressure on the soft metal which consequently cannot rebound the particle and, as observed, many particles remain embedded under this situation where the particle penetrates the surface layer.

The above discussion explains in broad mechanistic detail how the three regimes of erosion arise and how, together, they form a spectrum of behavior in which the regime boundaries are not clear but diffuse. This is illustrated in Figure 32 which shows not only the different regimes, but also that the type of regime observed depends upon the relative interactions of erosion and oxidation. Thus for a given erosion rate, a metal with a low oxidation rate such as nickel could be in the oxidation-affected erosion regime whereas cobalt, having a much higher oxidation rate, would be in the erosion-enhanced oxidation regime, as in fact was observed when these metals were exposed to 140 m/s^{-1} at 800 °C. It is expected that for a given erosion rate, the oxidation-affected erosion regime can be reached by reducing the oxidation rate or, for a given oxidation rate, by increasing the erosion rate.

In Figure 32 the temperature dependence is presented for degradation via pure erosion of NiO and the oxidation-affected erosion of nickel. The rate of degradation within the oxidation-affected erosion regime increases with temperature due to the importance of oxide formation in the mechanism of degradation of this regime. Conversely, the rate of degradation in the pure erosion regime decreases as temperature is increased, because the oxide becomes more plastic at the higher temperatures.

IV. CONCLUSIONS

1. An apparatus has been constructed that enables the conjoint effects of erosion and high temperature oxidation of metals to be studied quantitatively under a wide variety of conditions.
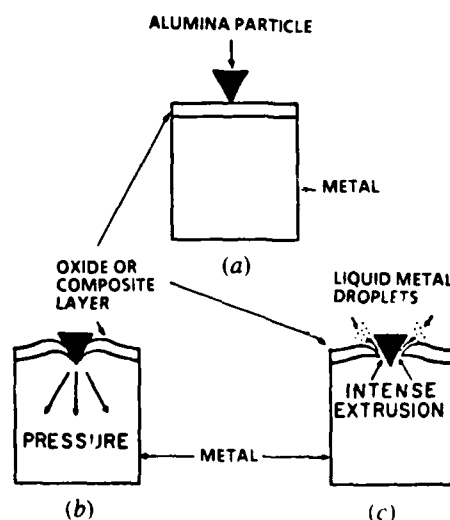
Fig. 31 — Hypothetical sequence of events following particle impact leading to liquid formation by intense adiabatic extrusion of metal between oxide layer and alumina particle.
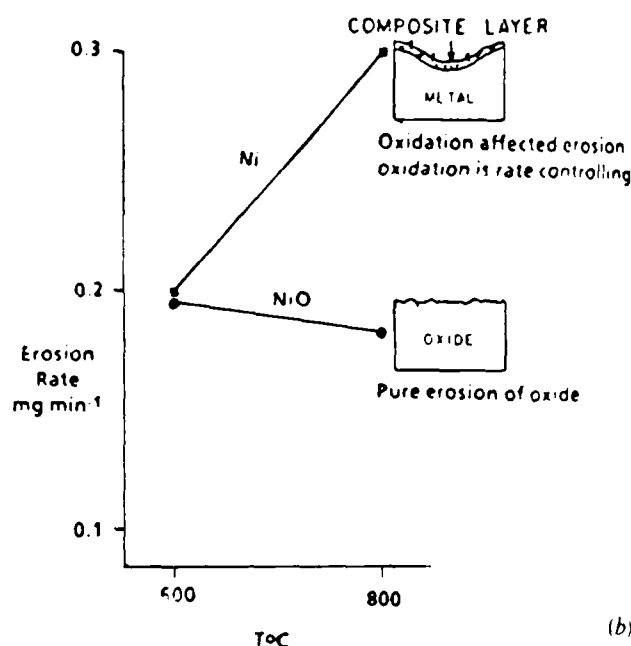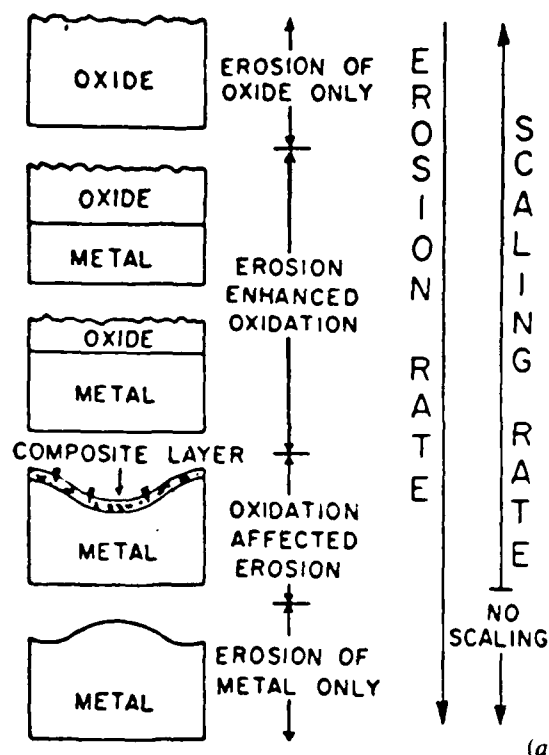
Fig. 32 — (a) Relationship between type of degradation observed under conjoint erosion-oxidation conditions and the relative severity of the erosion and oxidation components. (b) Dependence of degradation rate on temperature for different erosive-oxidation interaction regimes. Particle velocity 140 m/s⁻¹ in all cases.

2. It has been shown that there is considerable synergistic interaction between the two processes at high temperature.

3. An erosion beam incident at 90 deg to a specimen surface in the absence of oxidation causes erosive damage to a bare metal surface that is confined to plastic deformation with very little actual material removal compared to the oxidizing case. This is true for metals at temperature in nonoxidizing atmospheres or at room temperature where scaling is a very slow process.

4. Erosion of metal oxide occurs readily in erosive streams incident at 90 deg to the specimen. For a given incident velocity, the rate of oxide erosion is greater at lower temperatures, reflecting the greater proportional absorption of energy by plastic deformation of the oxide at higher temperatures.

5. A limiting oxide scale of constant thickness should be produced when the rate of scale formation by oxidation processes is equal to the rate of scale removal by erosion. This is called erosion-enhanced oxidation.

6. When the erosion rate is very high compared with the scaling rate a very thin, composite, surface layer is produced and extensive plastic deformation of the metal is seen. This situation leads to complex interactive mechanisms by which the metal deteriorates involving extensive plastic deformation, exposure of bare metal continuously to the erosive stream, embedding of erodent particles in the substrates, and continuous removal of the oxide formed by erosion. These mechanisms are not understood in detail, but the degradation rates of the metal under these conditions of oxidation-affected erosion are very high.

7. It has been possible to characterize the interaction of erosion and oxidation on metals at high temperature into pure erosion, erosion-enhanced oxidation, and oxidation-affected erosion regimes as described above.

8. In the systems studied the oxide behaved in a predominantly ductile manner at high temperature under erosion and did not show brittle crack formation.

ACKNOWLEDGMENTS

REFERENCES

1. I. Finnie: Wear, 1960, vol. 3, pp. 87-103.
2. I. M. Hutchings and R. E. Winter: Wear, 1974, vol. 27, pp. 121-28.
3. J. G. A. Bitter: Wear, 1963, vol. 6, pp. 169-90, Part II.
4. R. Winter and I. M. Hutchings: Wear, 1974, vol. 29, pp. 181-94.
5. W. F. Adler: Tech. Report, U.S. Army Research Office, June 1979. Contract No. DAAG 29-77C-0039
6. P. Shewmon and G. Sundararajan: Ann. Rev. Mater. Sci., 1983, vol. 13, pp. 301-18.
7. K. Hauffe: Oxidation of Metals, Plenum Press Publ., New York, NY. 1966.

8. P. Kofstad: *High Temperature Oxidation of Metals*, John Wiley, New York, NY, 1966.
9. N. Birks and G. H. Meier: *Introduction to High Temperature Oxidation of Metals*, E. Arnold Ltd., London, 1982.
10. A. R. Cooper: *Ceram. Eng. Sci. Proc.*, 1981, vol. 2, pp. 1963-89.
11. D. Cubicciotti and K. H. Lau: *J. Am. Ceram. Soc.*, 1978, vol. 61, pp. 512-17.
12. S. Bhattacharya, C. Hales, and V. Hill: Tech. Report "Corrosion-Erosion Behavior of Materials," K. Natesan, ed., Oct. 1978, Conference Proceedings of the Fall Meeting, St. Louis, MO, pp. 244-67.
13. R. H. Barkalow, J. A. Goebel, and F. S. Pettit: Tech. Report, EPRI, May 1980, CS-1448 Project 979-4, Final Report.
14. I. G. Wright, V. Nagarajan, and R. B. Herchoeder: *Corrosion-Erosion Behavior of Materials*, K. Natesan, ed., Proceedings of a symposium at the Fall Meeting of TMS-AIME, St. Louis, MO, Oct. 17-18, 1978.
15. A. V. Levy and G. Zambelli: *Wear*, 1981, vol. 68, pp. 305-31.
16. W. Tabakoff: *Wear*, 1983, vol. 86, pp. 65-99.
17. S. M. Benford, G. R. Zellars, and G. E. Lowell: NASA Technical Memorandum, No. 81715, 1980.
18. L. K. Ives: *Transactions of the ASME*, 1977, vol. April, p. 126.
19. V. Nagarajan, I. G. Wright, W. E. Merz, and J. Stringer: The International Corrosion Forum Sponsored by the National Association of Corrosion Engineers, April 6-10, 1981, Toronto, ON.
20. G. Klinzing: *Gas Solid Transport*, McGraw-Hill, New York, NY, 1981.
21. A. G. Evans, M. E. Gulden, and M. Rosenblatt: *Proc. R. Soc. Lond. A*, 1978, vol. 361, pp. 343-65.
22. D. B. Marshall, B. R. Lawn, and A. G. Evans: *Am. Cer. Soc. Journal*, 1982, vol. 65, no. 11, pp. 561-66.
23. I. Finnie and G. L. Sheldon: *Jour. of Engineering for Industry*, 1966, vol. Nov., pp. 387-92.
24. H. L. Oh, P. L. Oh, S. Vaidyanathan, and I. Finnie: "On the Shaping of Brittle Solids by Erosion and Ultrasonic Cutting," National Bureau of Standards, Special Pub., pp. 119-32.
25. J. H. Nielson and A. Gilchrist: *Wear*, 1968, vol. 11, p. 124.
26. I. Finnie and D. H. McFadden: *Wear*, 1978, vol. 48, pp. 181-90.
27. J. G. A. Bitter: *Wear*, 1963, vol. 6, pp. 5-21, Part I.
28. I. M. Hutchings: *Erosion: Prevention and Useful Application*, W. F. Adler, ed., ASTM STP 664, 1979, pp. 59-76.
29. I. M. Hutchings, R. E. Winter, and J. E. Field: *Proc. R. Soc. Lond. A*, 1976, vol. 348, pp. 379-92.
30. P. S. Follansbee: Ph.D. Thesis, Carnegie-Mellon University, Pittsburgh, PA, 1981.
31. I. M. Hutchings and T. J. O'Brien: *Int. Jour. Mech. Sci.*, 1981, vol. 23, pp. 255-61.
32. Argonne National Lab., Materials Science, Division Coal Technology, Second Quarterly Report Tech. Report ANL-75-XX-2, Appendix I, 1975.
33. A. V. Levy and R. Bellman: *Wear*, 1981, vol. 70, pp. 1-28.
34. G. Sundararajan: Ph.D. Thesis, The Ohio State University, Columbus, OH, 1982.

APPENDIX 4

Papers to be Submitted for Publication

INTERACTION BETWEEN EROSION AND HIGH TEMPERATURE CORROSION OF METALS: THE EROSION AFFECTED OXIDATION REGIME

BY

S.L. CHANG, F.S. PErTIT AND N. BIRKS

Materials Science and Engineering Department

University of Pittsburgh

INTRODUCTION

Degradation of metals by combined erosion and corrosion occurs in many industrial applications such as gas turbine engines, coal gasification plant and fluidized bed combustors. Metallic materials designed for high temperature applications usually rely on the development of a protective oxide scale for corrosion resistance and the addition of erosion to a high temperature, corrosive environment greatly intensifies the degradation rate. Furthermore, it has been shown[1-7] that there is a strong interaction between the erosion and corrosion processes when they occur together. The net degradation rate with combined erosion and corrosion is higher than either of the individual processes acting independently and can be higher than the sum of the rates of both processes under certain circumstances[1]. This situation presents a challenge to the design and development of materials for these applications and indicates a need for understanding of the degradation mechanisms and the various interactions that occur under combined erosion and corrosion.

One of the significant results from a previous study by Kang, Pettit and Birks[3] is the characterization of several regimes of interaction between erosion

1

and oxidation of pure metals using erosive streams incident at 90° in air at high temperature. The interaction regimes that were characterized were (1) pure erosion, (2) erosion enhanced oxidation and (3) oxidation affected erosion regimes, as shown in Figure 1. Under pure erosion by 20 micrometer angular alumina particles at temperatures between 25 and 800°C, nickel oxide was found to exhibit ductile behavior, being deformed primarily by cutting and ploughing. Pure erosion of the nickel metal under similar conditions, but in a nonoxidizing environment to exclude oxidation, also resulted in ductile behavior but the erosion rate was significantly lower than in the case of the oxide. In the erosion enhanced oxidation regime it was proposed that a steady state is established in which the oxide scale thickness remains constant when the rate of scale formation by the oxidation process is equal to the rate of scale removal by erosion. The interaction shifts to the oxidation affected erosion regime when the erosion rate is very high compared with the scaling rate. In this regime there is no continuous oxide scale formed but a composite layer of oxide, embedded particles and metal extrusion is formed on the surface of the specimen which also undergoes substantial plastic deformation. This results in the appearance of a series of surface undulations, also referred to as 'moguls', on the eroded surface as the plastic deformation accumulates in the substrate. The degradation rate in this regime is higher than either the pure erosion of the oxide or pure erosion of the metal or in the erosion enhanced oxidation regime.

The concept of a steady state situation has also been proposed by Wright, Nagarajan and Stringer[8] for alloy systems eroded in an oxidizing environment, assuming that the erosive particles have relatively low impact energy such that the resulting damage is contained within the oxide scale. However, such a steady state

2

situation has never been demonstrated under conditions of simultaneous erosion and oxidation.

It is the aim of this study to demonstrate that such a steady state situation, also called the erosion enhanced oxidation regime, can exist and to clarify the mechanism by which it arises for the growth of both single and multiple layer oxide. The parameters affecting the interaction and the degradation mechanisms will also be described and discussed.

EXPERIMENTAL

In order to study the erosion enhanced oxidation phenomenon, it was necessary to measure the degradation rate of both oxide and metal exposed to erosive airstreams at the same temperature, 780°C. Oxide specimens were prepared by the oxidation of pure metal at 1100° C in air for times such that a NiO scale, 80 to 100 micrometers thick, formed over the nickel substrate and cobalt oxide specimens had a Co_3O_4 layer of 120 to 150 micrometers thick over the bulk CoO substrate. In order to derive the mechanisms by which degradation occurred, of the eroded surfaces and cross sections were examined in detail and the degradation rates were established by measurement of both the weight change and scale thickness. In order to obtain meaningful results from weight change measurements, disk specimens with a diameter of 9 mm in the case of cobalt and coupon specimens 8.5 mm X 8.5 mm in the case of nickel were chosen such that most of the eroded surface was exposed to the erosive stream, emitted from a nozzle of 9.3 mm I.D. Furthermore aluminide coatings were applied to all the specimens in order to minimize the oxidation rate of surfaces not directly subjected to the erosive stream. The effect of oxidation of these coated

3

surfaces was found to be negligible, much less than 1% of the weight change measurement, hence the measured weight change data will reflect information relating to the interaction of erosion and oxidation on the active surface, from which the coating was removed by grinding. Several specimens were exposed to the same erosion-oxidation conditions such that both the weight change and scale thickness could be measured as a function of exposure time.

The erosion-oxidation experiments were performed using the apparatus previously described by Kang, Pettit and Birks[3] and shown in Fig. 2 in a slightly modified form. The modifications made to the apparatus include: (1) increasing the heating efficiency of the fluid heaters by connecting them in parallel; (2) installation of an exhaust system to contain the used erosive particles in a particle collector followed by a particle filter and a blower, the latter helps the movement of the gas through the exhaust system; and (3) installation of a sample holder which allows specimens to be moved in X, Y and Z directions independently.

Specimens were loaded in a sample exchange chamber such that the exposed surface would be normal to the gas, the specimen was then pushed into the reaction chamber to a preset position within the erosive stream, which was established previously using a dummy specimen. Specimens were heated directly by the preheated particle-laden gas up to 800°C within 1 minute, without using the infrared heater previously described[3]. A stream of compressed air was used to accelerate the erosive particles to velocities between 50 and 170 m/s at a constant loading rate of about 500 mg/min. Angular alumina particles of average dimension 20 micrometers were used as erosive particles in this study.

Specimen surfaces were finished with 600 grit SiC paper, cleaned in methanol, dried thoroughly and weighed prior to exposure. Metallographic

4

observation of the eroded surfaces after exposure was made using the optical microscope and SEM/EDS techniques. X-Ray diffraction analysis of the surface allowed the reaction products and phases present on the eroded surface to be identified. Nickel plating was applied to specimens with a thin oxide scale. Subsequently the specimens were mounted and polished following the standard procedures for cross section examination. Disk specimens were polished right across a diameter of 9 mm and the scale thickness was measured from the center of the specimen using SEM. Measurements were taken from a variety of positions and averaged to provide a value for the scale thickness. The phenomenon was studied by using samples of Ni, Co, NiO and Co_3O_4 as outlined below.

RESULTS

Erosion of Oxide

Since erosion enhanced oxidation is thought to involve the growth of a compact oxide scale with simultaneous erosive removal of the scale at the scale/gas interface, the erosion characteristics of the oxide were investigated at 780°C, the temperature at which all these experiments were carried out. The oxide was found to erode at a constant rate which increased with increasing velocity.

Examination of the eroded oxide specimens revealed signs of spallation of the cobalt oxide during the early stages of exposure. Spallation had occurred along the oxide ridges which were formed during the preoxidation of CoO to Co_3O_4 as shown in Fig. 3. Since specimens were heated quickly to temperature by the gas, sharp temperature gradients developed through the thickness of the specimens, moreover due to the presence of an uneven surface morphology in areas such as oxide ridges, thermal expansion of the surface material is constrained and, hence, tensile stresses develop on the ridges where spallation is observed.

5

Together with spallation, cobalt oxide is also deformed in a ductile manner so that the material is plastically deformed at impact sites with shearing at the edges of the impact crater. This resembles the ductile degradation mechanisms referred to as ploughing or Type I cutting by Hutchings and Winter[9,10]. Cutting and ploughing become the primary degradation mechanisms for cobalt oxide specimens after a longer exposure to the erosive stream, whereas nickel oxide specimens, which do not develop ridges on the outer surface, are deformed by cutting and ploughing from the beginning of the erosion process.

After prolonged erosion at high velocity, 140 m/s, intergranular cleavage was observed on both cobalt oxide and nickel oxide specimens when the erosion front approached an interface, i.e. the CoO/Co_3O_4 interface for cobalt oxide or the Ni/NiO interface for nickel oxide which is shown in Fig. 4. Spallation was observed to occur preferentially over the triple point of the grains in areas where the oxide scale was at a certain, apparently critical, thickness. The oxide scale was removed rapidly from the center of the gas stream where the erosive condition was most severe, and mogul formation due to plastic deformation of the metal substrate was observed on the nickel specimen at areas corresponding to the center of the gas stream as shown in Figure 4. The scale formed over the mogul surface is thin, nonuniform with a significant amount of embedded particles and is quite different from the scale formed by preoxidation.

The observation of spallation particularly as the thickness of the preoxidized scale was reduced, opens up the possibility that for certain combinations of scale, substrate and erodent properties and conditions, a further regime of interaction may exist which consists of spalling on impact at critical scale thicknesses.

6

Combined Erosion and Oxidation of Pure Metals

Most of the experimental work was carried out on the study of the degradation of cobalt under an erosive airstream at 780°C. The degradation was measured in terms of weight loss of the specimen as a function of time. Figures 5 and 6 give the results for nickel and cobalt respectively. The degradation proceeds at a constant rate which increases with increasing particle velocity in all cases.

The morphology of the eroded surface was examined using the SEM as shown in Figure 7 for cobalt. The eroded surface is relatively flat when eroded at low velocities such as 50 m/s. An undulated surface morphology, which is also referred to as moguls, develops at 100 m/s and becomes significant at higher velocities. Also shown on the eroded surface are impact craters with material displaced to the edges of the crater, indicating that material is deformed plastically at the impact site with cutting and ploughing as the dominant degradation mechanisms. The eroded surface morphology of nickel specimens is shown in Figure 8 in which mogul formation can be observed at all of the velocities studied.

The cross section of cobalt specimens that were eroded at between 50 and 100 m/s is shown in Figure 9. The oxide scale is continuous and uniform in thickness, consisting of an inner layer of CoO and an outer layer of Co_3O_4. The oxide thickness was measured at the center of the specimen as a function of exposure time at various velocities. The results are shown in Figure 10. Cobalt specimens that were eroded at velocities above 140 m/s and nickel specimens that were eroded above 50 m/s were found to have a nonuniform scale with a significant amount of plastic deformation in the substrate, measurements were not made on thesespecimens which were apparently being which degraded within the oxidation affected erosion regime[3].

7

DISCUSSION

Single Layer Scale

Kang, Pettit and Birks[3] proposed that a steady state condition could be reached such that the scale thickness remains constant in the erosion enhanced oxidation regime. This situation is interpreted as follows.

The rate of scale growth under combined erosion and oxidation can be expressed as the difference between the rate of formation of the scale by oxidation and the rate of its removal by erosion:

$$dX/dt = K_p/X - K_{eo} \tag{1}$$

Here X is the scale thickness, t is the exposure time, K_p is the parabolic rate constant defined as $X^2 = 2K_p t$ under pure oxidation, and K_{eo} is the rate at which the oxide surface is removed by the erosion process. The oxide scale is assumed to be continuous and protective such that the parabolic rate law is obeyed. In the early stages of the process the oxide scale is so thin that the growth rate exceeds the erosion rate. Consequently the scale thickens til a situation is achieved such that the growth rate equals the erosion rate. Under such conditions the oxide scale will reach a limiting thickness as expressed by

$$X^* = K_p/K_{eo} \quad \text{when } dX/dt = 0 \tag{2}$$

This situation represents the steady state in the erosion enhanced oxidation regime where the limiting scale thickness, X^*, varies with the values of the parabolic rate constant, K_p, and the erosion rate constant, K_{eo}. The existence of this regime has not been substantiated previously although it was predicted[3].

In order for the enhanced oxidation regime to be observed it is necessary, as seen from Figure 1, for the rate of oxide growth or scale thickening to be comparable with the rate of scale removal by erosion. Due to the slow rate of growth of nickel oxide or nickel, it is not possible, with the current apparatus, to enter the erosion enhanced oxidation regime with nickel specimens. Consequently it is necessary to study the behavior of cobalt which oxidizes sufficiently rapidly, however, in this case the scale is multi-layered having both an inner layer of CoO and an outer layer of Co_3O_4. This must be taken into account in a treatment of the erosion enhanced oxidation behavior for the case of cobalt.

Multi-Layered Scale

Figure 11 represents the section of a cobalt specimen under combined erosion and oxidation. Since a continuous and protective oxide scale develops under combined erosion and oxidation of cobalt as shown in Figure 7, chemical equilibrium can be assumed to be established at all the interfaces. Furthermore, oxidation proceeds by the transport of cobalt cations across the scale, similar to pure oxidation. The growth of CoO and Co_3O_4 layers, hence, follow behavior similar to that described by Yurek, Hirth and Rapp[11] for the oxidation of pure metals that develop scales consisting of layers of different oxides. However, the instantaneous scale thickness is modified by erosion because the oxide, Co_3O_4 in this case, is being removed at a constant rate from the outer surface by erosion.

Referring to Figure 11, consider that J_0 is the total flux of cobalt cations entering the oxide scale at the Co/CoO interface, part of the incoming flux, J_1, reacts with Co_3O_4 at the CoO/Co_3O_4 interface to form CoO as expressed by

$$Co + Co_3O_4 = 4 CoO \qquad (3)$$

9

The remaining flux of cobalt cations, J_2, diffuses across the Co_3O_4 layer to form Co_3O_4 at the scale/gas interface where erosion takes place at a constant rate. J_3 represents the rate of cobalt lost in the erosion process.

The rate of formation of the CoO layer, dX_1/dt, is proportional to J_1, the flux of cobalt, taking part in the interfacial reaction where 4 moles of CoO are formed for every mole of cobalt ions from J_1 entering the reation. Hence,

$$dX_1/dt = 4V_1J_1 = 4V_1(J_o - J_2) \tag{4}$$

also $J_o = K_{p,1}(CoO)/X_1V_1$

$$J_2 = 3K_{p,2}(Co_3O_4)/X_2V_2$$

Here X_1 is the scale thickness of the CoO layer, V_1 is the molar volume of CoO, X_2 is the scale thickness of the Co_3O_4 layer and V_2 is the molar volume of Co_3O_4, K_p1 and K_p2 are the parabolic rate constants for growth of CoO and Co_3O_4 respectively. The rate of formation of the CoO layer can be expressed therefore as

$$\frac{dX_1}{dt^a} = \frac{4K_{p,1}}{X_1} \frac{12V_1K_{p,2}}{V_2X_2} \tag{5}$$

Eqn. (5) shows that the growth rate of the CoO layer is also affected by the growth of the Co_3O_4 layer.

The rate of formation of the Co_3O_4 layer is determined by the following three factors: the instantaneous growth rate of Co_3O_4 at the scale/gas interface, the rate of oxide removal by erosion, and the growth rate of CoO because Co_3O_4 is consumed during this interfacial reaction. The instantaneous growth rate of Co_3O_4 at the scale/gas interface is directly controlled by the flux, J_2, of cobalt ions arriving at the interface. The rate of oxide removal by erosion is proportional to J_3 while the rate of Co_3O_4 consumption by the interfacial reaction is J_1V_2.

10

Therefore, the rate of formation of the Co_3O_4 layer can be expressed by

$$dX_2/dt = (J_2 - J_3 - 3J_1)(V_2/3)$$

$$= (4J_2 - 3J_0 - J_3)(V_2/3) \qquad (6)$$

This leads to

$$\frac{dX_2}{dt} = \frac{4K_{p,2}}{X_2} - \frac{V_2 K_{p,1}}{V_1 X_1} - \frac{V_2}{3} J_3 \qquad (7)$$

The last term of eqn. (7) varies only with the erosive flux and can be substituted by the erosion rate constant, K_{eo}^{ox}. This represents the rate of Co_3O_4 removal by erosion and has units of cm/sec.

Equation (5) and (7) show how the thicknesses of the CoO and Co_3O_4 layers will vary with time of exposure to an erosive, oxidizing environment. This variation was calculated using a finite difference method based on these two equations. The growth rate of both cobalt oxide layers under pure oxidation were measured in this study in the absence of any erosive influence. Values of the erosion rate constant of the oxide, K_{eo}^{ox}, were taken from experimental data which were also measured in this study. The calculated results are plotted in Figure 12 as solid lines for the growth of CoO and Co_3O_4 layers at 780°C under various conditions: (A) pure oxidation, (B) erosion and oxidation at 50 m/s, and (C) erosion and oxidation at 70 m/s. Figure 12 shows that the instantaneous oxide scale is much thinner under combined erosion and oxidation than under pure oxidation due to the simultaneous removal of oxide scale by erosion. Furthermore the oxide scale and both CoO and Co_3O_4 layers grow into limiting thicknesses under combined erosion and oxidation where the limiting scale thickness, independent of exposure time in the steady state, varies with the erosion rate as expressed by

11

$$X_1{}^* = (V_2/3V_1)(K_{p,1}/K_{eo}{}^{ox}) \qquad \text{for CoO (8)}$$

$$X_2{}^* = (K_{p,2} / K_{eo}{}^{ox}) \qquad \text{for Co}_3\text{O}_4$$

The presence of a steady state scale thickness can be viewed in mathematical terms when:

$$J_o = J_2 = J_3 \qquad \text{and} \quad J_1 = 0$$

This means that all cobalt cations entering the oxide scale are eventually removed at the scale/gas interface by erosion when the steady state is established. There is no net accumulation of cobalt ions or oxygen ions in either layer. The scale thicknesses, hence, remains constant and the weight change data will represent the amount of cobalt ions removed by erosion.

Since, in the erosion enhanced oxidation regime, the rate of degradation is primarily controlled by the rate at which the oxide is removed from the scale/gas interface, it should be possible to match the rate of degradation of the specimens with the rate of erosion previously measured for cobalt oxide. In order to demonstrate this it must be remembered that the degradation rates of the metal specimens derived from Figure 5 in the steady state are expressed in terms of the rate of metal loss per unit surface area per unit time. These values must be converted to weight of oxide loss per unit surface per unit time. This conversion and comparison were made in Figure 13 and it can be seen that the data for degradation of the metal in the erosion enhanced oxidation regime correspond well with the erosion data obtained from the oxide. It can also be seen from Figure 13 that the slope changes for velocities above 123 m/s, being below 123 m/s and above 123 m/s. This departure can also be seen in Figure 5 where there is a very large difference when the velocity is increased from 123 m/s to 140 m/s.

12

Examination of the surface of the specimens exposed to an erosive stream flowing at greater than 140 m/s, as shown in Figure 7, shows significant mogul formation indicating that substantial plastic deformation of the cobalt substrate has occurred. This behavior indicates that the specimen is entering the oxidation affected erosion regime. The data in Figures 5 and 13 both show clearly the enhancement in metal degradation rate when this regime is entered.

From the data given in Figure 13, it is possible to obtain values of the erosion rate constant of Co_3O_4 in units of cm/sec. These values can then be used to evaluate Equation 8 by plotting X_1^* and X_2^* against $1/K_{eo}$. If Equation 8 represents the correct situation, then this plot should give a straight line whose slope yields the value of the parabolic rate constant. These plots are shown in Figure 14 to be straight lines and the slopes yield values of 1.0×10^{-10} cm^2/sec and 2.9×10^{-11} cm^2/sec for the parabolic rate constants for CoO and Co_3O_4 oxidation respectively. These values compare well with the values of 1.7×10^{-10} cm^2/sec and 4.9×10^{-11} cm^2/sec respectively obtained directly from oxidation experiments. The agreement between the values derived from erosion-oxidation data and from oxidation data is regarded as very encouraging and confirms that the analysis of the erosion enhanced oxidation regime is basically correct.

The results for nickel are plotted in a similar manner in Figure 15 where the degradation rate of nickel is expressed in terms of the rate of NiO removed and compared to the rate at which NiO was found to be eroded. Figure 15 indicates that nickel is in the oxidation affected erosion regime for all the velocities studied, but the two lines converge at erosive velocities of about 50 m/s, below which it is anticipated that nickel will enter the erosion enhanced oxidation regime. Unfortunately it is not possible to study these conditions in the present apparatus.

13

The clear evidence of deformation of the substrate and the formation of a composite layer on the surface instead of a compact layer of oxide, substantiates that the nickel specimen is in the oxidation affected erosion regime for all the conditions studied, although the tendency for mogul formation decreases and the time required to achieve mogul formation increases as the velocity is decreased.

The deformation associated with particle impact is mainly confined within the oxide scale in the erosion enhanced oxidation regime. Hence, the type of degradation mechanisms and the extent of deformation are similar in both a metal specimen under combined erosion and oxidation and an oxide specimen under erosion. This results in the observation of similar degradation rates for the metal specimens and oxide specimens as shown in Figure 13. Observation of scales formed under the combined erosion and oxidation of cobalt specimens show that the oxide scale is deformed plastically at the impact site with material inside the crater displaced to the edges of the crater. This extruded material can gradually be removed by subsequent impacts. This is similar to a ploughing or Type I cutting mechanism as proposed by Hutching and Winter[9,10]. Such degradation mechanisms were observed during erosion of oxide specimens.

Since the steady state oxide thickness is reduced when the erosion rate is increased, it is possible to enter the oxidation affected erosion regime when the deformation, due to the particle impacts, starts to affect the underlying substrate and moguls form as a result of substantial plastic deformation of the substrate. The presence of an oxide scale can impose a constraint to the soft substrate while the substrate, which has a much higher ductility, is able to deformed to a greater strain level than the oxide and put the oxide layer in high tension, parallel to the

14

target surface. This can result in (1) a high strain level in the oxide without an immediate fracture or failure of the oxide; (2) tearing of the oxide around the impact site; or (3) ejection of liquid metal droplets as a result of quick release of hydrostatic pressure in the substrate when the erodent penetrates the scale as shown in Figure 16. Furthermore a significant number of erodent particles was found embedded in the scale, such embedded particles can act as stress concentrators and enhance the degradation of the scale. Nonetheless, all these factors can increase the deformation in the oxide scale and result in the observation of a higher degradation rate in the oxidation affected erosion regime than in the erosion of the oxide or in the erosion enhanced oxidation regime.

In addition to the above two regimes of degradation some signs of oxide spallation on impact have also been observed as shown in Figure 5. As mentioned earlier, such spallation is observed when the erosion front approaches an interface and when the oxide scale becomes thin. Thus the existence of a further regime of degradation of metal exposed simultaneously to erosive and oxidizing environments must be considered. Whether or not this spallation is observed, will depend on whether or not the conditions for spalling are exceeded before the conditions for ploughing, cutting and plastic deformation are exceeded. The system is expected to respond and degrade by whichever mechanism exceeds a critical criterion first.

15

REFERENCES

1. R. H. Barkalow, J. A. Goebel, and F. S. Pettit, Materials Problems in Fludized-Bed Combustion Systems, Final Report ERPI project 979-4, May 1980.

2. A. Levy, E. Slamovich and N. Jee, "Elevated Temperature Combined Erosion-Corrosion of Steel, LBL Report, LBL 19156, April (1985).

3. C. T. Kang, F. S. Pettit and N. Birks, Met. Trans., 18A, 1785-1803 X (1987).

4. S. M. Benford, G. R. Zellars and G. E. Lowell, "Synergistic Erosion/Corrosion of Superalloys in PFB Coal Combustion Effluent", NASA Technical Memorandum No. 81715, 1980.

5. I. G. Wright, V. Nagarajan and R. B. Herchoeder, "Some Factors Affecting Solid Particle Erosion/Corrosion of Metals and Alloys" Corrosion-Erosion Behavior of Materials edited by K. Natesan, Proceedings of a symnosium of the Metallurgical Society of AIME, St. Louis, MO, Oct. 1978.

6. V. Nagarajan, I. G. Wright, W. E. Merz and J. Stringer, "The Morphology of High-Temperature Erosion-Corrosion of Oxidation Resistant Alloys", The International Corrosion Forum sponsored by the National Association of Corrosion Engineers, Toronto, Ontario, April 1981.

7. Bahattacharys, S.C. Hales and V. Hill, "Erosion/Corrosion of Materials in Coal Gasifier Environments", Tech. Report, Corrosion-Erosion Behavior of Materials Edited by K. Natesan, Conf. Proceedings of AIME, St. Louis, MO, pp. 244-267, Oct. 1978.

8. I. G. Wright, V. Nagarajan and J. Stringer, Oxidation of Metals, 25, 175-199, (1986).

9. I. M. Hutchings and R. E. Winter, Wear, 27, 121-128, (1974).

10. I. M. Hutchings, "Erosion: Prevention and Useful Applications",pp. 59-75, 1979.

11. G. J. Yurek, J. P. Hirth and R. A. Rapp, Oxidation of Metals, 8, 265-281, (1974).

ACKNOWLEDGEMENT
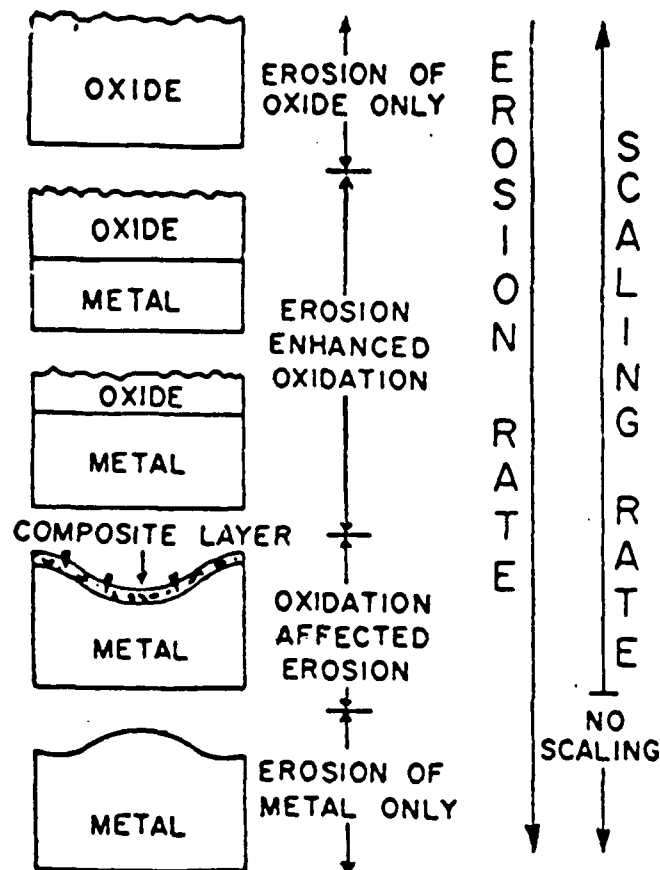
FIGURE 1. Regimes of interaction between erosion and corrosion indicating the effects of the relative severity of the erosion and oxidation components.
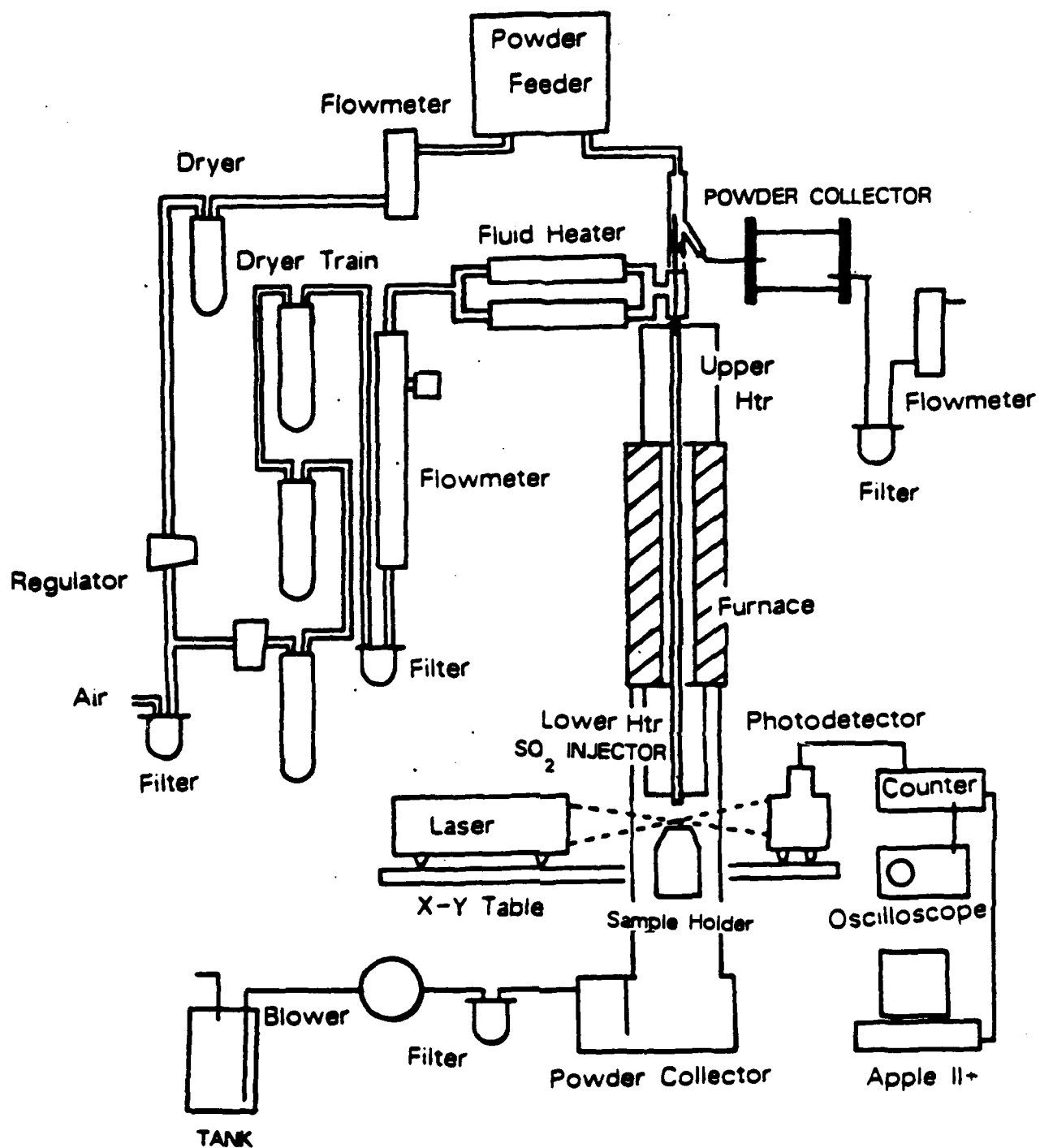
FIGURE 2. Diagrammatic representation of apparatus developed and used in the study of erosion-corrosion attack of metals.

(a) before erosion
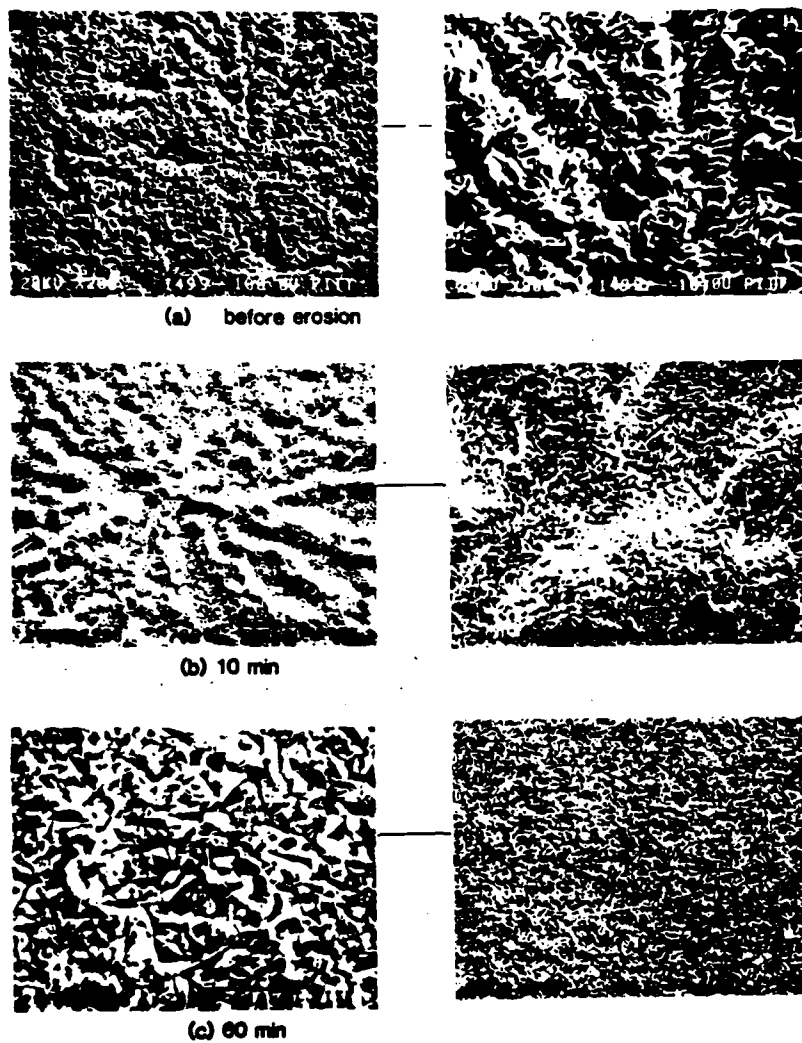
(b) 10 min

(c) 60 min

FIGURE 3.   SURFACE MORPHOLOGY OF COBALT OXIDE (a) PRIOR TO EROSION, (b) AFTER 10 MINUTES AND (c) AFTER 60 MINUTES OF EROSION AT 780°C TO AN AIRSTREAM FLOWING AT 70 M/S AND AT 90° INCIDENT ANGLE.
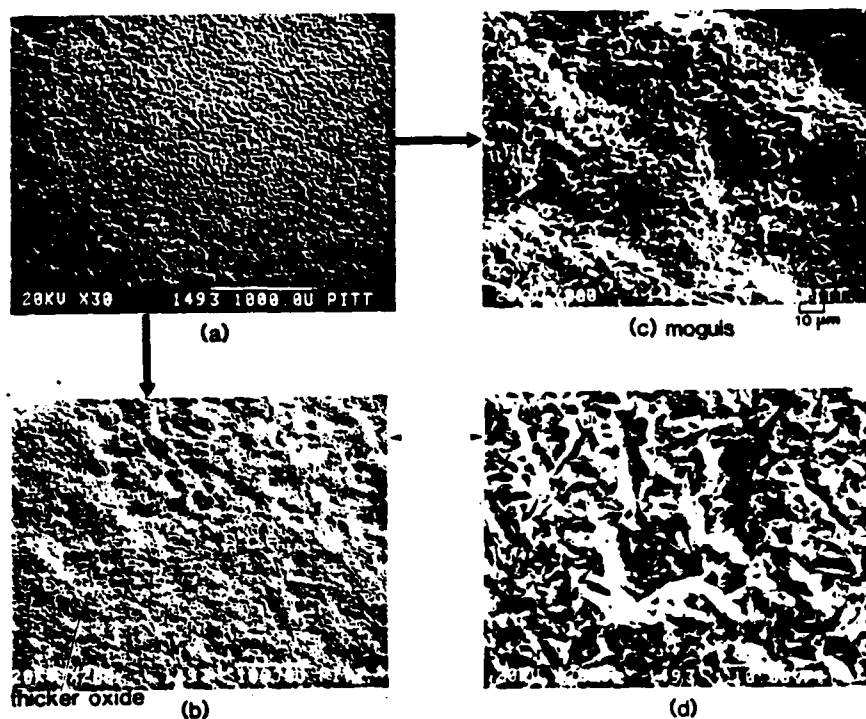
FIGURE 4.   EROSION OF NiO AT 780°C AND 140 M/S FOR 45 MINUTES TO SHOW
MOGUL FORMATION AT THE INTENSIVELY ERODED AREA (a), (c) AND
SPALLATION AT THE NEARBY AREA, (b), (d).

Erosion of Nickel
at 780°C and 90°
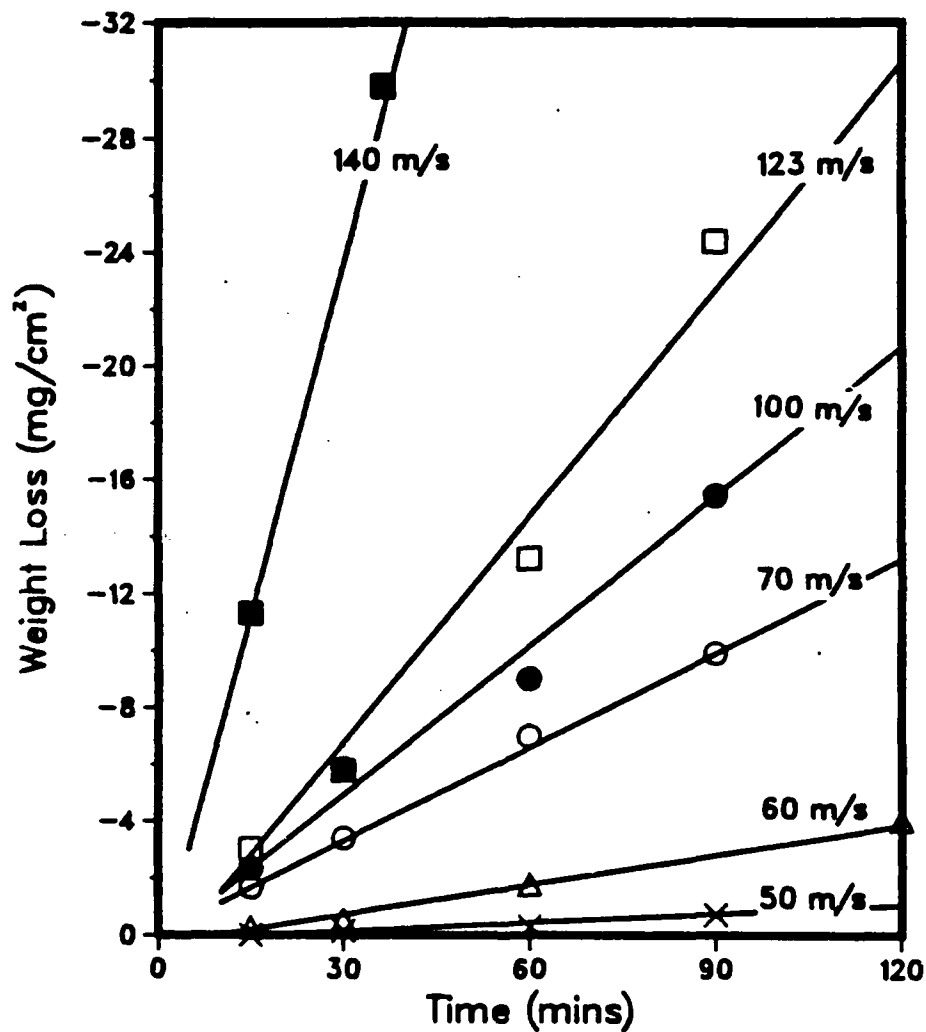
FIGURE 5. Degradation of nickel specimens expressed as mass loss vs. time exposed at 90° to the erosive airstream at 780°C.

Cobalt
Eroded at 780°C and 90°
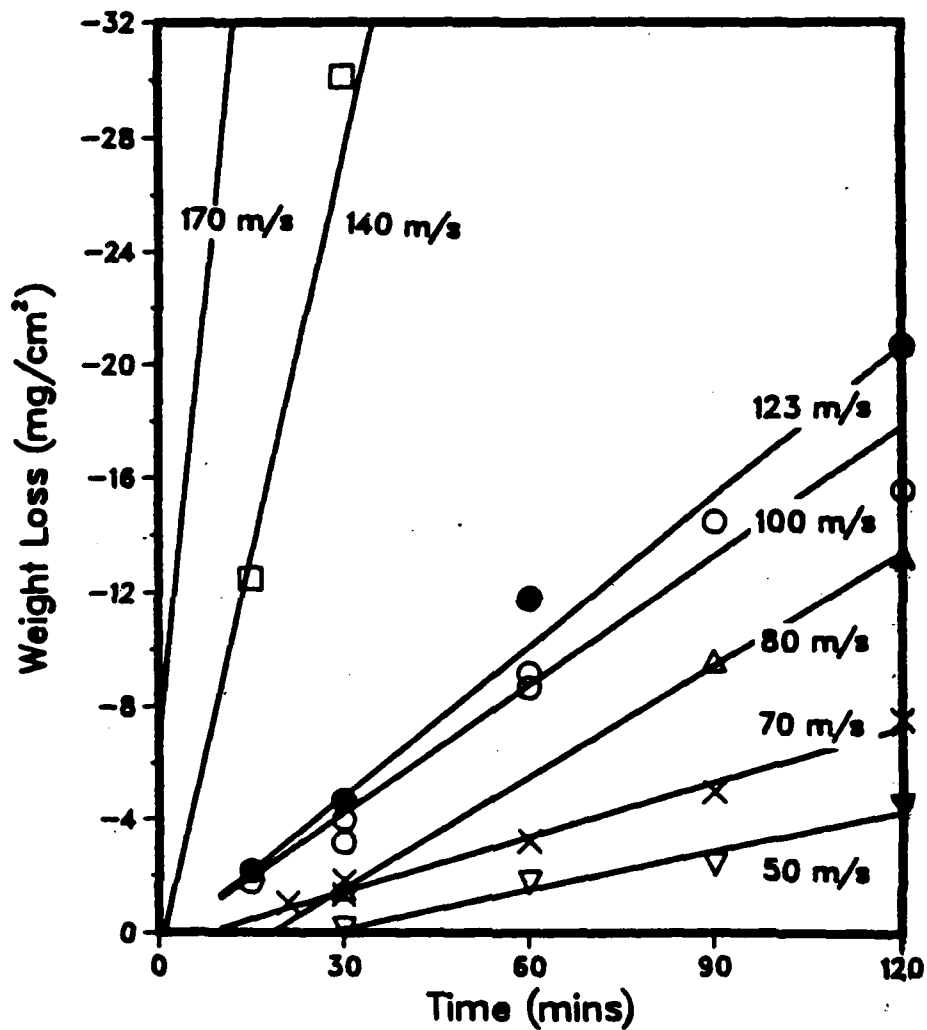
FIGURE 6. Degradation of cobalt specimens expressed as mass loss vs. time exposed at 90° to the erosive airstream at 780°C.

(a) 50 m/s

(b) 70 m/s

(c) 80 m/s

120 MINUTES

(a) 100 m/s

(b) 140 m/s
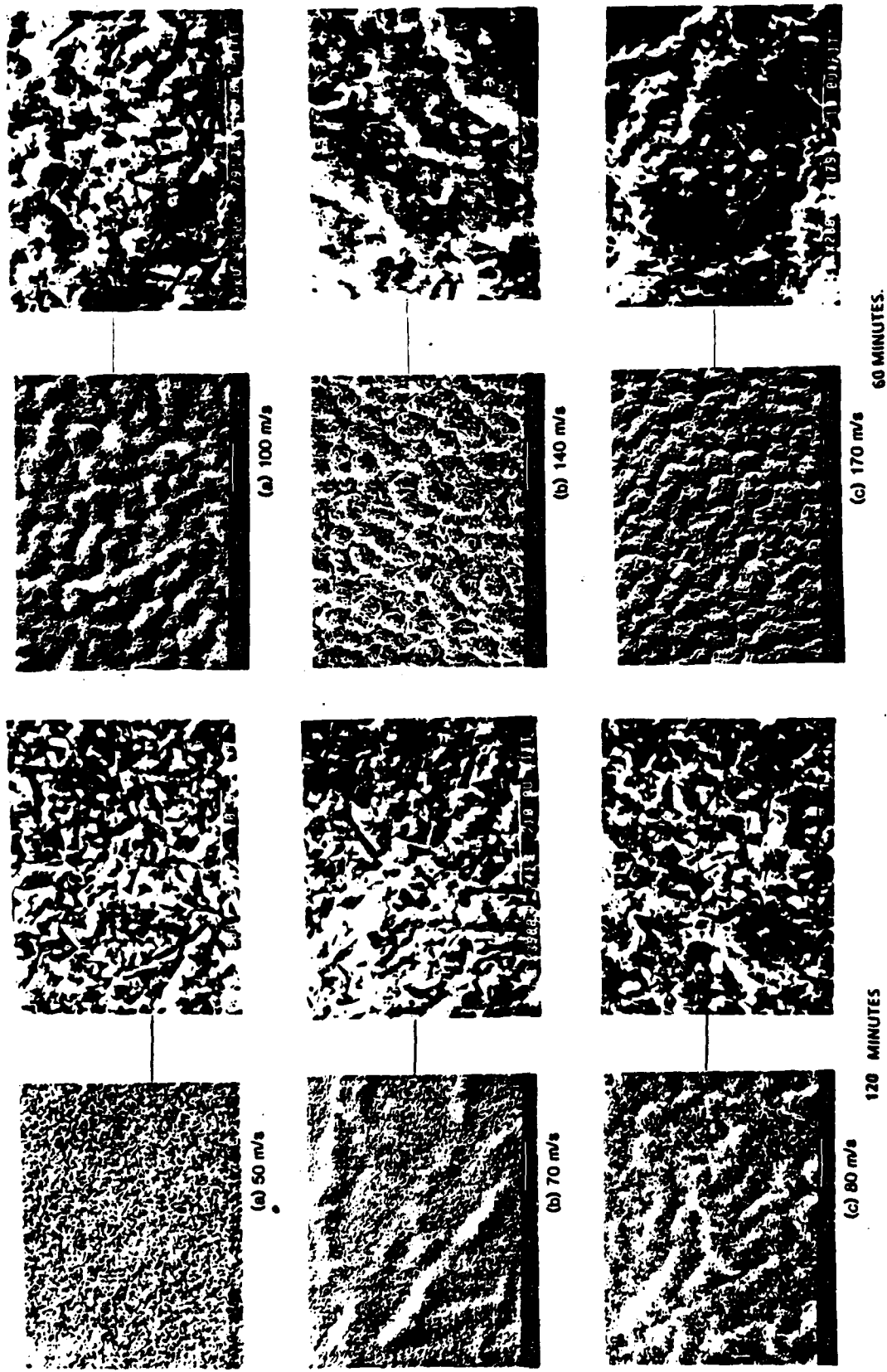
(c) 170 m/s

60 MINUTES.

FIGURE 7. Surface morphologies of cobalt eroded at 780°C and 90° incidence at velocities between 50 and 170 m/s.
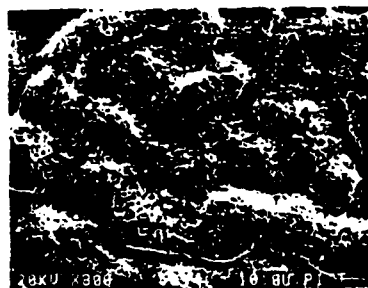
(a) 50 m/s
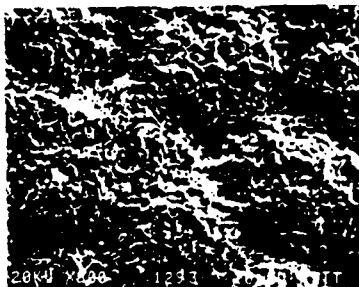
(c) 123 m/s
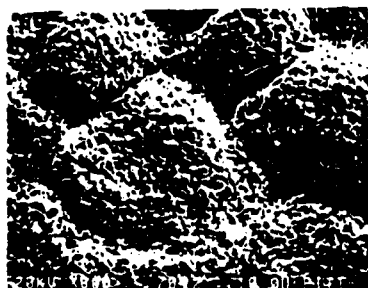
(b) 70 m/s

(d) 140 m/s

60 MINUTES.

FIGURE 8.   Surface morphologies of nickel eroded at 780°C and 90° incidence at velocities between 50 and 140 m/s.
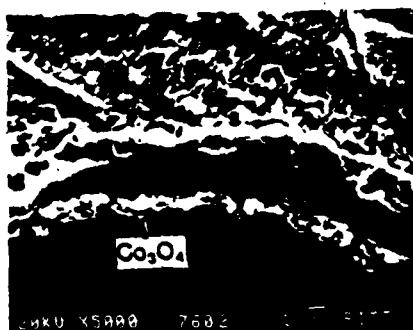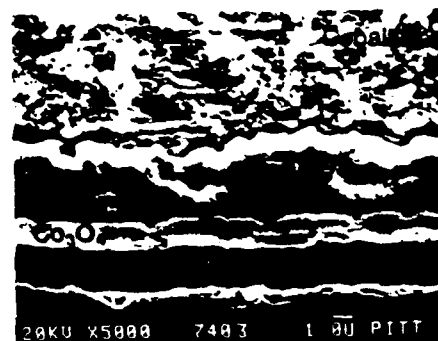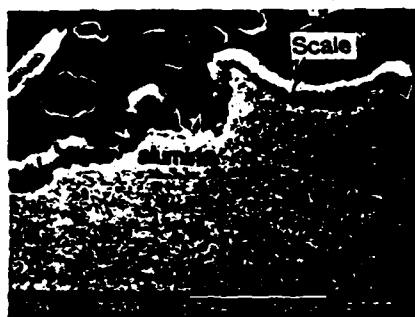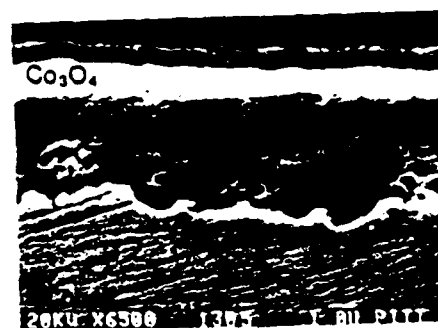
FIGURE 9. Cross section of cobalt specimens subjected to erosion-oxidation in air flowing at various velocities at 780°C and 90° incidence to airstream.

Erosion of Cobalt
at 780°C and 90°
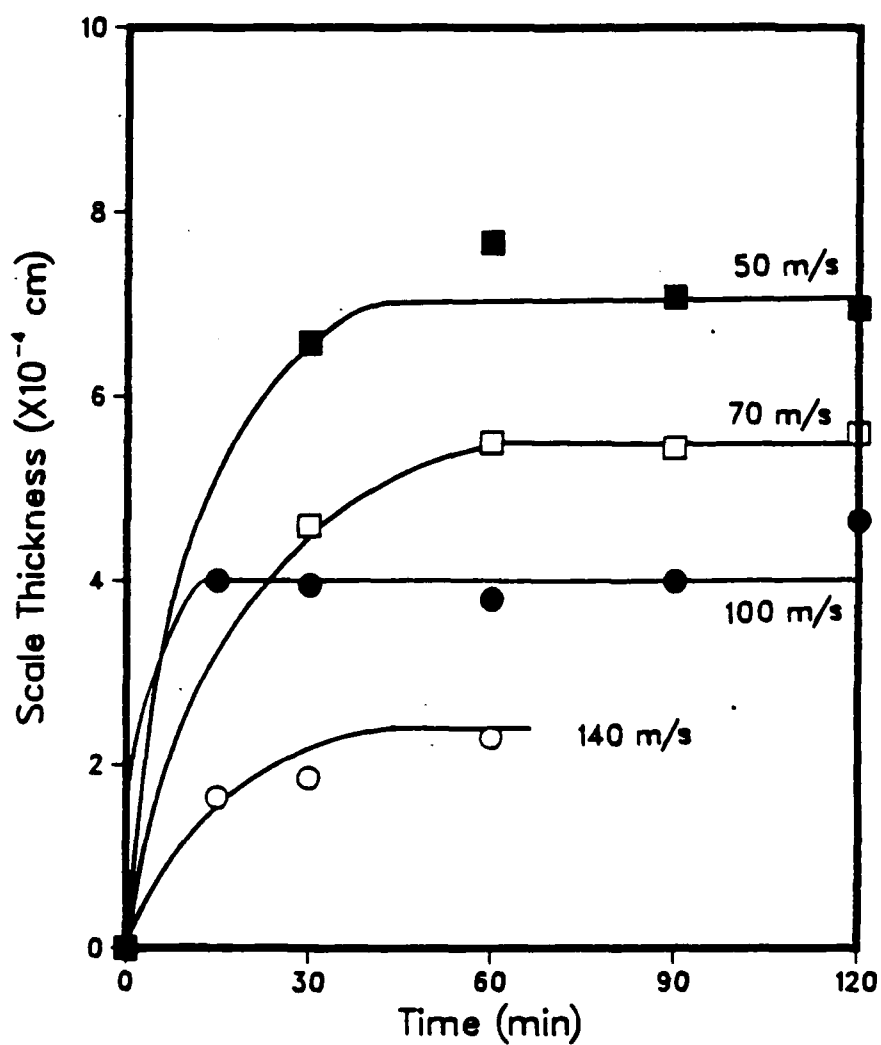
FIGURE 10. Variation of oxide scale thickness with time for cobalt exposed to erosion-oxidation at 780°C and 90° incidence to airstream.
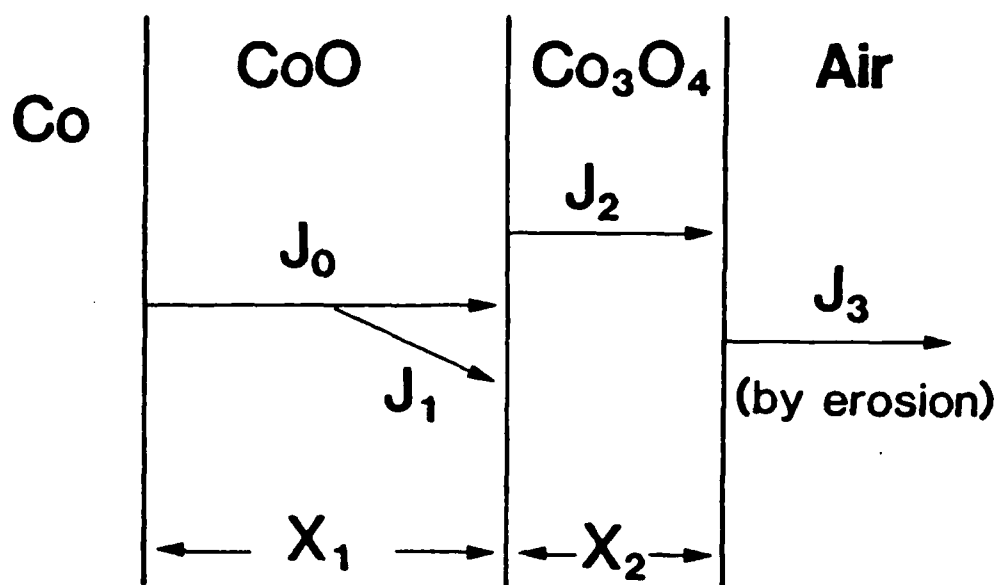
FIGURE 11. Schematic diagram of scale formation on cobalt during exposure to erosion-oxidation conditions.

EROSION AND OXIDATION OF COBALT
AT 780°C and 90°
CoO

Co_3O_4
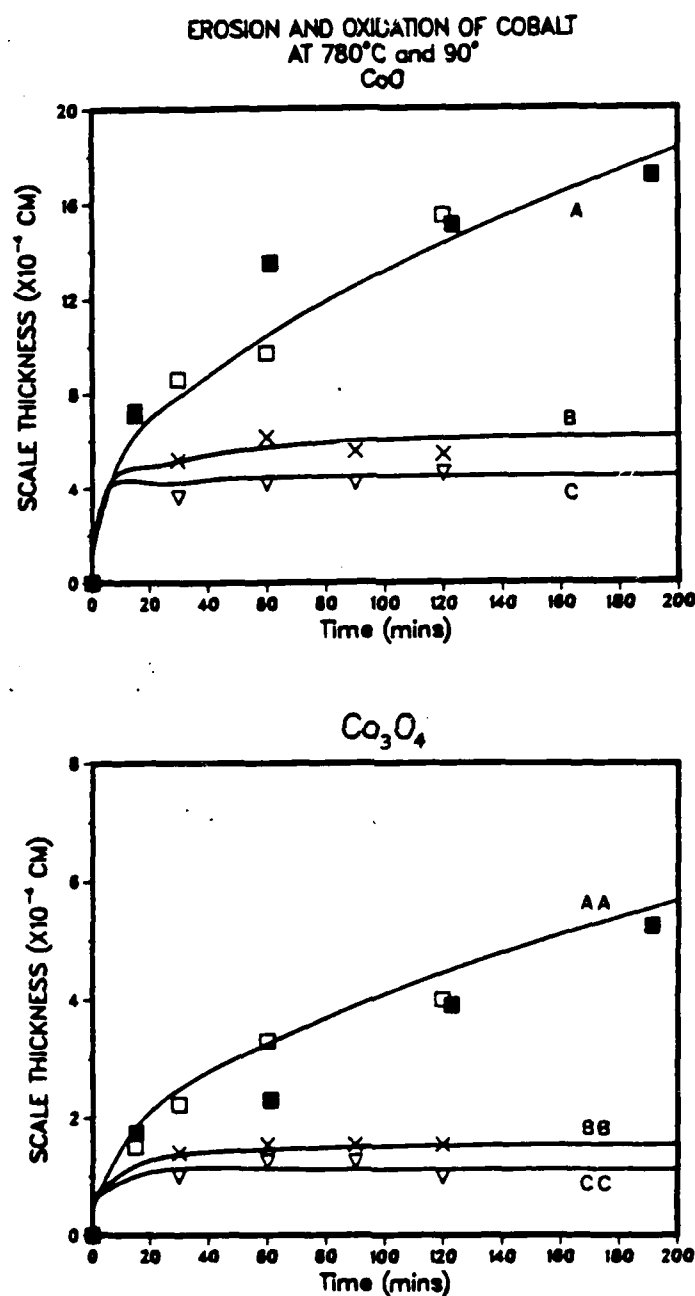
FIGURE 12. Dependence of scale thickness with time for pure oxidation (A), oxidation and erosion at 50 m/s and (C) oxidation and erosion at 70 m/s. Experimental measurements are shown superimposed on calculated lines.

Erosion at 780°C and 90°
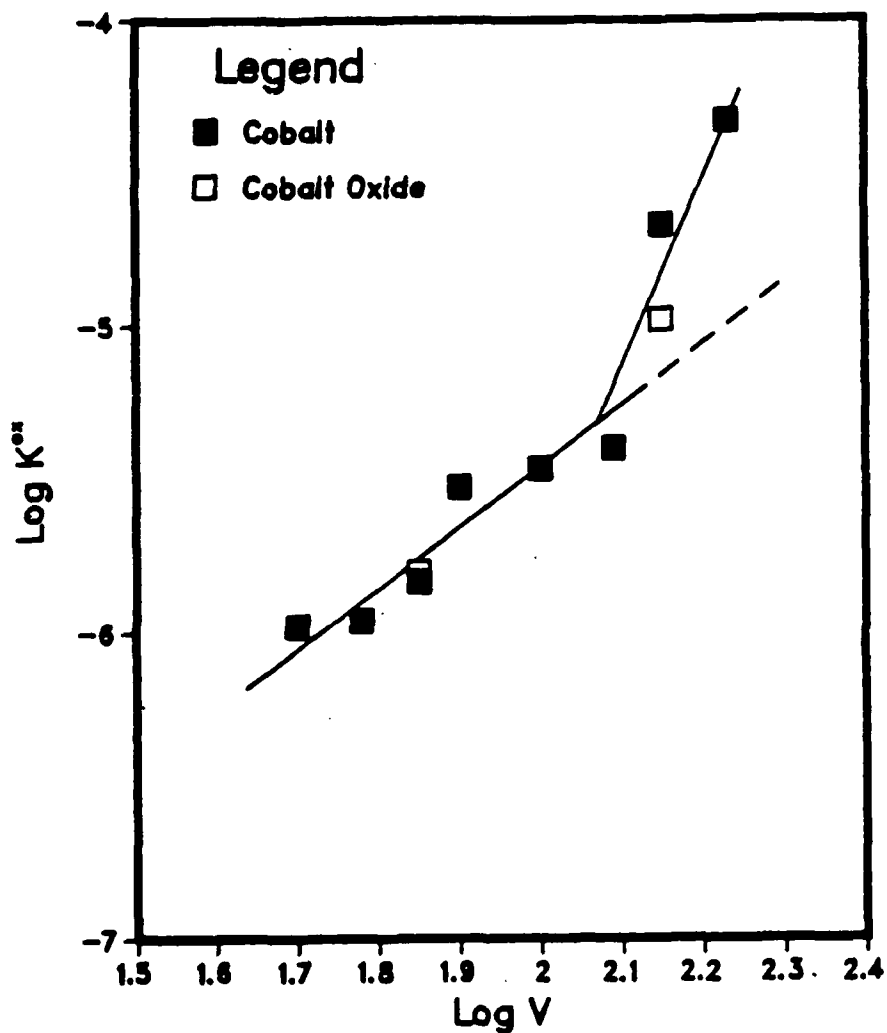
FIGURE 13. Variation of cobalt oxide erosion rate constant with velocity of erosive airstream. Results are calculated from cobalt exposure to erosion-oxidation and also measured directly from erosion of cobalt oxide.

Erosion of Cobalt at 780°C and 90°
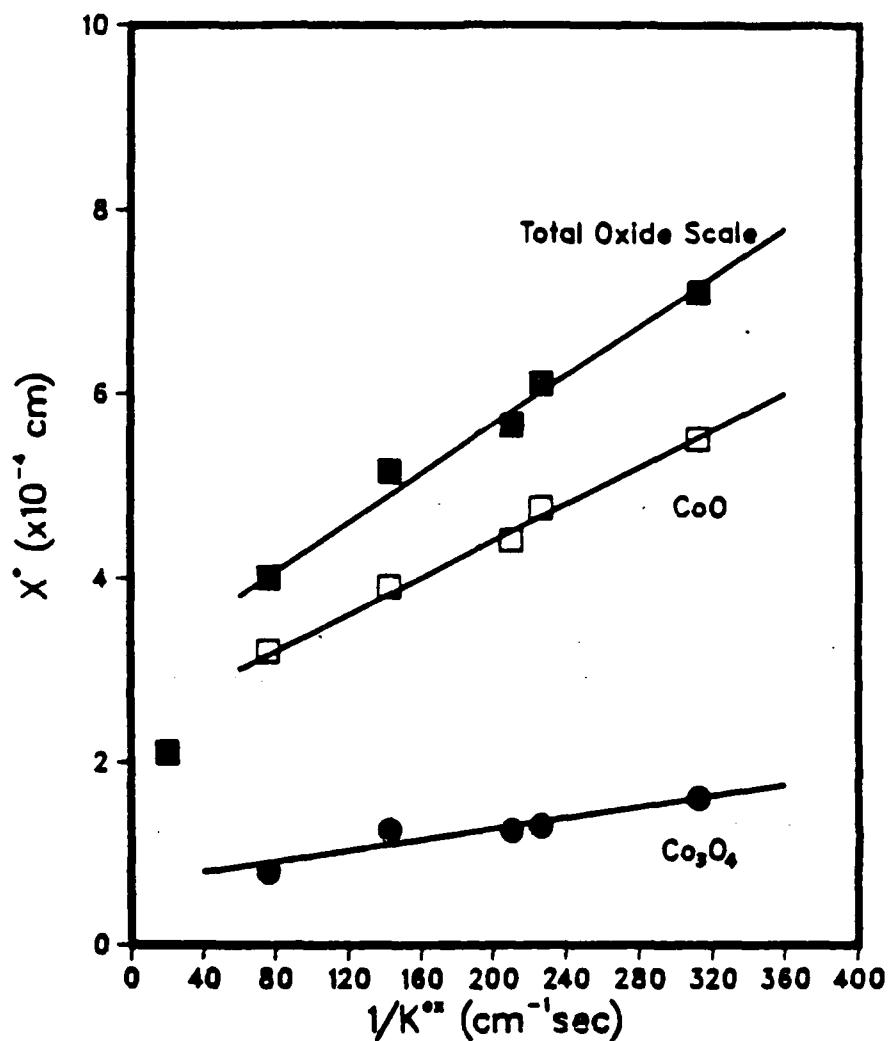
FIGURE 14. Dependence of steady state oxide thickness on the erosion rate constant of cobalt at 780°C and 90° incidence. The parabolic rate constant for oxidation of cobalt is proportional to the slope of the curves.

Erosion at 780°C and 90°
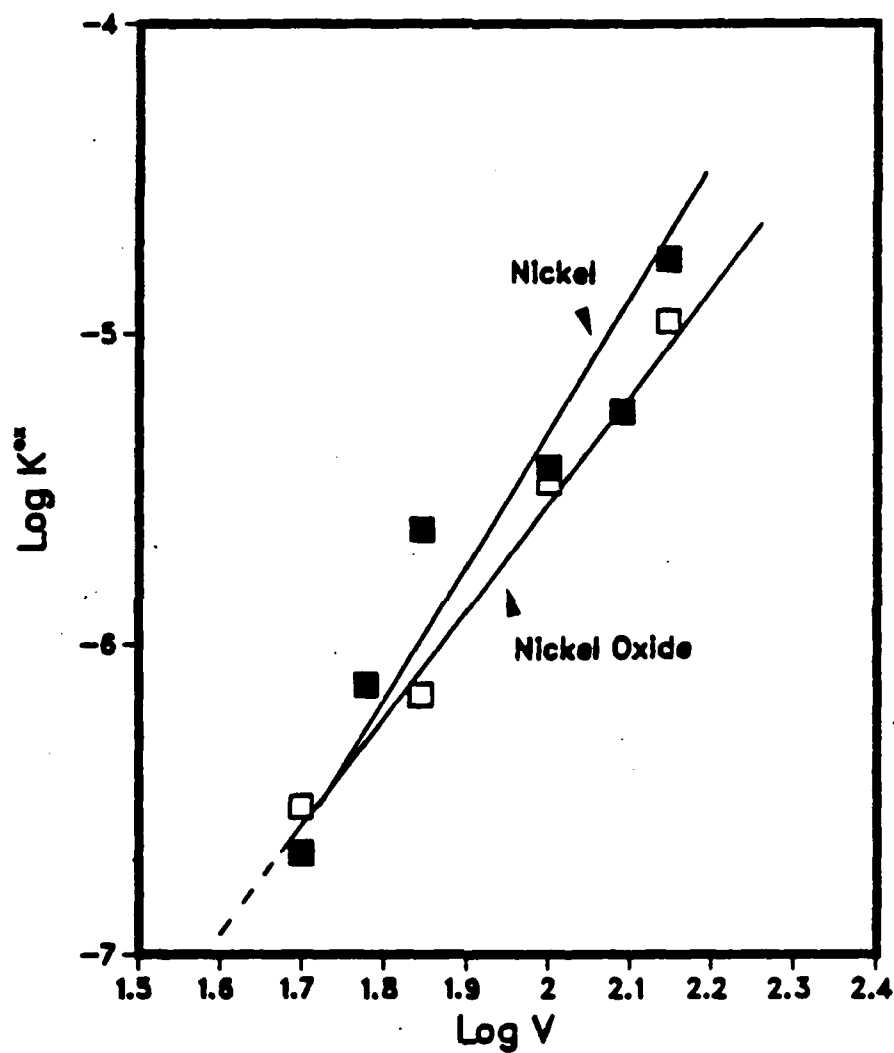
FIGURE 15. Variation of nickel oxide erosion rate constant with velocity of erosive airstream.
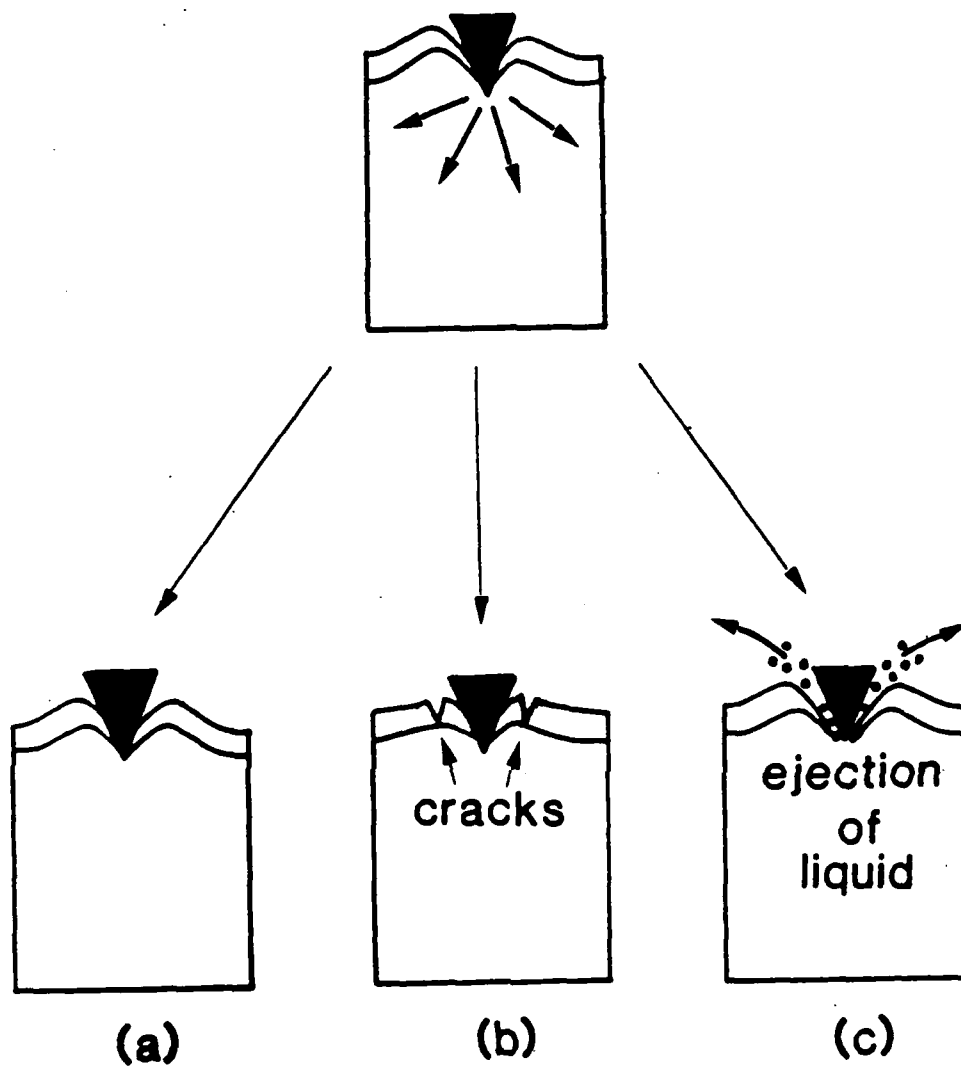
FIGURE 16. Possible events subsequent to impact of erosive particles during the exposure of a metal to erosion oxidation in the oxidation affected erosion regime.

EFFECT OF ANGLE OF INCIDENCE ON THE COMBINED EROSION-OXIDATION ATTACK OF NICKEL AND COBALT

BY
S. L. CHANG, F. S. PETTIT AND N. BIRKS

Department of Materials Science and Engineering
University of Pittsburgh

INTRODUCTION

Combined corrosion and erosion of metals by solid particles is a major degradation process that limits the lifetime of various machinery. Progress in improving the corrosion-erosion resistance of engineering materials requires good understanding of the interaction of erosion and corrosion and the processes by which material is removed. Previous studies[1,2] of the combined erosion and oxidation of pure metals at high temperatures and 90° incidence impact found strong interactions to occur between the individual erosion and oxidation processes and successfully characterized the individual interactions into the following four regimes: pure erosion of the oxide, erosion enhanced oxidation, oxidation affected erosion and pure erosion of the metal. Since the erosion-oxidation degradation of metals at high temperature is also likely to occur at various angles of incidence of the erosive particles, it is pertinent to study the effect of the incident angle on the degradation of material under combined erosion and oxidation at high temperatures.

As a result of erosion and oxidation at high temperature using a normal (90° incidence) erosive beam, many mounds and valleys, also referred to as moguls, were observed on the eroded surfaces[1,2]. The amplitude of the moguls decreased with particle velocity. When impact angles less than 90° were used, waves were formed and found to line up into ripples on the eroded surface[1]. Waves also form on water and sand as a result of wind action, the development of water waves has

1

been investigated in some detail and has been reported in the literature[3,4]. The parameters such as wavelength, speed and amplitude of water waves can be correlated with wind speed, depth of water and the slope of the bed. However the waves observed on eroded specimens are not produced by a simple high velocity airstream. Oxidation of pure metals at high temperature in a fast flowing airstream does not produce the wave pattern observed on the eroded specimens. This indicates that wave formation during combined erosion and oxidation is a result of particle impacts, although the basic concepts of such wave formation are not yet well characterized.

Finnie[5,6] predicted the effect of impact angle on the erosion rate of ductile materials on the basis of a cutting mechanism such that the degradation rate should be proportional to the volume of material removed by each impact. The theory gives a good correlation with experimental results at low impact angles, where a maximum erosion rate is often observed between 15° and 30° for ductile materials as shown in Figure 1. Large deviations arise between the theory and experimental results at higher impact angles however. The theory predicts a zero degradation rate at 90° incidence whereas a small degradation rate is usually observed experimentally. Since the erosive particle is treated as a single point with finite width in Finnie's treatment, the volume occupied by the erosive particle at the impact site is neglected in the treatment although, in reality, this volume is large. Hence the deviations observed at high impact angles can be due to the fact that the volume occupied by the erosive particle during impact has been neglected.

Bitter[7,8] proposed an additional mechanism deformation wear, for the degradation of ductile materials by erosion called deformation wear in which material can be removed by cutting and also by repeated deformation leading to work hardening. This can result in cracking and spallation of the deformed surface

2

layer and is more pronounced at higher impact angles. The angular dependence of erosion rate, when both mechanisms are considered, matches better with the experimental results as shown by curve C of Figure 1. Brittle materials, when deformed by cracking and spallation, show an angular dependence as shown in Figure 2 where the maximum erosion rate is observed at 90°. This indicates that the angular dependence of the erosion rate is related to the type of degradation mechanism operating during erosion.

Since nickel and cobalt were studied very carefully at 90° incidence of the erosive stream[1,2], and it is believed that a good representation of the mechanisms of degradation has been provided in which erosion played a major role, in this paper the study is extended to the effects of angle of incidence of the erosive stream on the mechanisms and kinetics of the degradation process.

EXPERIMENTAL

The apparatus used to carry out the erosion-oxidation experiments, shown in Figure 3, has been described previously[1,2]. An airstream is used to carry the erosive, 20 micrometer, angular, alumina particles at velocities up to 170 m/s. Both the gas and erodents are preheated to the required temperature and specimens can be heated to the desired temperature by the gas. The specimen temperature is measured by a thermocouple inserted to the center of the specimen and can be varied from room temperature up to 800°C for any incident angle between 15 and 90°. The particle velocity was measured by laser doppler velocimetry and could be varied between 50 and 170 m/s.

The reaction kinetics resulting from exposure to combined erosion and oxidation were obtained from measurements of the weight change of the specimen as a function of exposure time. In order to obtain meaningful weight change data, the shape and size of the specimens were carefully designed as shown in Figure 4.

3

For 15° and 30° incidence, both the front and back surfaces of specimens were subjected to the erosive stream at the same impact angle. Furthermore, aluminide coatings were applied to those surfaces that were not subjected to the erosive stream to minimize the effect of oxidation from these areas. The measured weight change data was then rationalized to compensate for impact angle and in the density of particle impact over the exposed area, represented by equation (1):

$$\Delta M = \frac{\text{weight change}}{WL \sin(O) F} \quad (1)$$

where

$$F = \frac{0.1772 + [WL \sin(O) - 0.1772]*0.5}{0.443}$$

where W and L are the width and length of the specimen respectively, PO is the angle of incidence and F is a factor to correct for the uneven distribution of particles across the gas. The concentration of erosive particles is found, during velocity measurement, to be significantly higher in the central area than near the edge of the gas flow. Accurate values of particle concentration can not be obtained at various positions across the gas. It is, therefore, assumed that the concentration of the erodent particles in the central area is twice that near the edge of the gas stream while the boundary between the two regimes is determined from the observations made during velocity measurement. The factor F is established from these assumptions and the dimension of the nozzle.

The specimen surfaces to be exposed to the erosive stream were finished with 600 grit SiC paper, cleaned ultrasonically in water and methanol and then dried thoroughly. After the erosion-oxidation experiments, dust chaser was used to blow away loose particles accumulated on the surface and in the thermocouple hole, followed by weight measurement and examination of the eroded surface using the

4

optical microscope and SEM coupled with EDS. X-ray diffraction analysis was applied to selected specimens for identification of the reaction products. Specimens were then plated with a layer of nickel to protect the thin oxide scale and mounted for cross section examination using standard metallographic procedures.

RESULTS & DISCUSSION

Erosion and Oxidation of Cobalt

Cobalt specimens were eroded at 780°C at various angles of incidence to an erosive airstream flowing at two different velocities, 70 and 140 m/s, with the particle loading rate maintained at around 500 mg/min and independent of the gas flow. The corrected or rationalized weight change results given in Figure 5, show that the degradation rates, vary with impact angle for both velocities. Both curves are very flat with a peak at 60°.

The eroded surface morphology was examined using SEM/EDS. Specimens eroded at 70 m/s were found to have a flat eroded surface with many impact craters as shown in Figure 6. Previous work[2] showed that erosion and oxidation of cobalt under this condition is in the erosion enhanced oxidation regime where a relative thick and protective oxide scale forms over the surface. The deformation introduced by particle impact is confined to the oxide scale with negligible disturbance of the substrate metal. Hence, the eroded surface is relatively flat but the shapes of impact craters as shown in Figure 6 are found to vary with impact angle. Triangular craters are observed at high impact angles while shallow, elongated scratches are pronounced at low angles such as at 15°. It is believed that cutting and ploughing, as proposed by Hutchings and Winter[9,10], are the important degradation mechanisms under these conditions.

5

The eroded surface morphology developed at 140 m/s is shown in Figure 7. It can be seen that ripples are formed on the eroded surface aligned parallel to the front of the incident beam. The shape of the ripples vary with impact angle. Ripples with a sharp slope at the lee side of the crest are observed at lower impact angles such as 30°, whereas ripples formed at 60° incidence show less continuity but have a smooth and rounded shape at the edges of the wave, which is similar to the shape of moguls formed at 90° incidence. This indicates that moguls are a degenerated form of ripples because the impact energy under normal, 90° incidence is dissipated in all the directions, whereas, at oblique angles, the energy tends to dissipate preferentially along the direction in which the erosive particles impact. This directionality is more pronounced at lower impact angles because the erosive component parallel to the target surface is large. Ripples formed under these conditions extend over a long distance while those generated at high angles extend over a shorter distance and finally degenerate into individual mounds and valleys at 90°.

Cross sections of the specimens are shown in Figure 8. It can be seen that wave formation is associated with plastic deformation of both the substrate metal and the oxide scale. It is also clear that the lee face of the wave is strongly supported by a substantial growth of oxide, apparently without interference from erosive particles. It is believed that the cobalt at the crest of the wave is deformed by the erosive stream against this oxide buttress to form a thin flake over the ripple front. However, due to the fast oxidation rate of cobalt at elevated temperatures, the ripple surface is covered by a continuous oxide scale which can absorb a large fraction of the energy associated with particle impact and act as a barrier to suppress the deformation of the metal substrate. Therefore the thin flake formation is not pronounced in the case of cobalt at high temperatures due to

6

the presence of a thick oxide layer around the wave crest and the small amount of impact energy available to be absorbed by the substrate. However, should the oxide scale lose continuity at the ripple front, thin flake formation can become extensive due to the release of hydrostatic pressure and spiral features as shown in Figure 8(c) can develop.

The amplitude of the ripples formed at various angles of incidence is summarized in Table 1. Since ripple formation is a result of plastic deformation of the substrate, the amplitude of the waves is expected to be proportional to the depth of the plastic deformation zone in the substrate, which is, in turn, related to the incident erosive energy component perpendicular to the target surface and decreases with the angle of incidence. Ripple formation, hence, becomes less significant at low angles and is not observed at very low angles because insufficient energy is available normal to the surface to deform the substrate plastically.

Figure 8 also shows the impact craters at the wave crests facing the erosive beam. Since the particle velocity is sufficiently high and the oxide scale is thin, the deformation can now extend to both the scale and the substrate. Small pieces of material are seen to become detached from the ripple front at 140 m/s due to extensive shearing, however, this mechanism is estimated to contribute only approximately 5% to the degradation rate based on an estimation made in previous research[11]. It is believed that cutting and ploughing are the predominant degradation mechanisms under these conditions, similar to the situation at 70 m/s. It should be noted that ductile behavior, with material plastically deformed around the impact site, was observed under all the conditions used in this study. During the combined erosion and oxidation of cobalt at 70 m/s only the oxide scale is deformed and removed by erosion whereas, at 140 m/s, both the scale and substrate are deformed and the degradation rate is greater than that of pure oxide due to

7

increased damage to the scale that is introduced by the back extrusion of the substrate. Although the natures of the targets are different at 70 and 140 m/s, combined erosion and oxidation under both conditions show dependence of the erosion rate on the incident angle with a peak rate being observed at 60°. This type of behavior is also observed[12] during erosion and oxidation of alloy MA754 where cutting and ploughing are also the predominant degradation mechanisms. A similar angular dependence was also observed by Pettit et. al[13] during combined erosion and oxidation of various alloys at high temperatures. It is worth mentioning that the degradation rate in Pettit's study was determined by measuring the rate of metal recession from the cross section of a cylindrical specimen where the impact angle varies across the diameter and should be an accurate method of determining the 'true' degradation rate. These results indicate that the angular dependence of the erosion rate is itself highly dependent on the type of degradation mechanism operating during the process. The behavior shown in Figure 5 is expected when cutting and ploughing are the predominant degradation mechanisms.

Since the shape of the crest of the wave is believed to be important in terms of degradation mechanisms, combined erosion and oxidation of cobalt specimens was carried out at 600°C with an airstream flowing at 140 m/s such that the oxidation rate of cobalt can be reduced, the oxide layer will be thinner and the flake formation at the wave crest is expected to be more pronounced than at 780°C.

The corrected weight change results are shown in Figure 5 where the shape of the curve is different from those observed at 780°C, and the maximum degradation rate is observed at a lower angle, 30°. The eroded surface morphology is shown in Figure 9. Thin flakes can be seen on the eroded surface and such features are more pronounced at 30° than at a higher angle of 60°. The cross section is shown

8
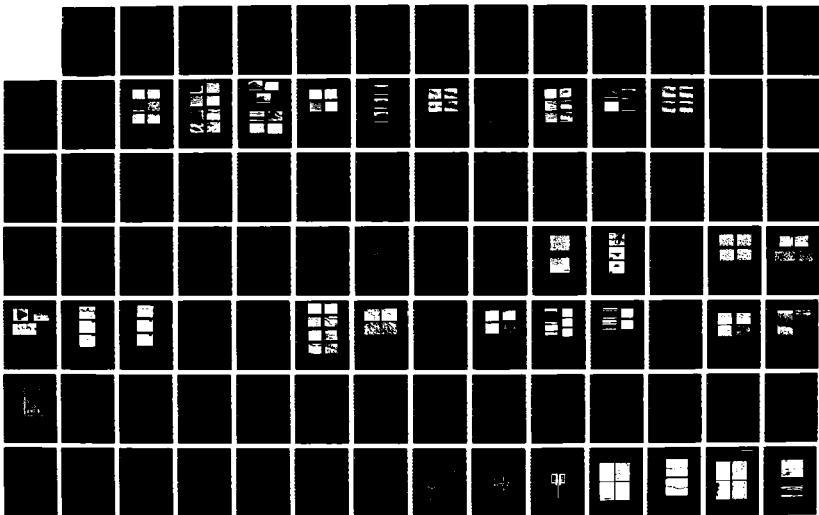
MICROCOPY RESOLUTION TEST CHART

in Figure 10. It can be seen that thin flakes will be detached from the ripple front after extensive shearing and extrusion, resulting in an additional degradation mechanism of material removal. This mechanism is enhanced by the erosive component parallel to the target surface and it becomes more pronounced and effective at low angles such as 30°. Combined erosion and oxidation of cobalt at 600°C therefore occurs by both cutting/ploughing and detachment of thin flakes over the ripple front. While cutting and ploughing give an almost constant degradation rate within the angular range between 30° and 90°, detachment of thin flakes has a strong dependence on impact angle being very effective at low angles such as 30°. As a result of both mechanisms, the angular dependence on the erosion rate as shown in Figure 5 shows a peak at 30° indicating the presence of an additional degradation mechanism in these conditions and confirming the strong dependence of the angular characteristics on the degradation mechanisms.

It was found that special marks applied to the eroded surface remained on the surface after several short exposures, it was therefore possible to use the SEM to follow the plastic deformaton of the wave front at different times of exposure to the erosive airstream as shown in Figure 11. Using the embedded particles which are not removed immediately as reference points, it was observed that the ripple front moves with the incident beam at about 10^{-4} cm/hr at 780°C with an airstream flowing at 140 m/s and at 30° incidence. This result confirms the dynamic nature of the ripples.

Erosion and Oxidation of Nickel

Nickel has a much lower oxidation rate than cobalt at elevated temperatures in air. Erosion and oxidation of nickel at 780°C in an airstream flowing at 140 m/s forms a thin complex surface scale on the surface. This implies that a large fraction of the impact energy will be dissipated in the substrate as plastic

9

deformation and, hence, flake formation should be significant. The rationalized rate of weight change results for the erosion-corrosion of nickel at 780°C and 140 m/s and various angles are shown in Figure 12 where the degradation rate is seen to vary with the incident angle and a sharp peak is observed at 30°. The eroded surface morphology is shown in Figure 13. Ripple formation can be observed even at very low angles such as 15° although the ripple amplitude is small. It can also be seen that the development of thin flakes is very pronounced in the case of nickel especially at 30°. The flakes are frequently split, possibly due to extensive shearing or very high deformation rates which might enhance detachment of the flakes. From the cross section, as shown in Figure 14, it evident that the flakes are composed of, mainly, substrate metal surrounded by a thin surface layer due to oxidation. The flakes are thinned further after extended extrusion and finally are separated from the ripple front resulting in loss of material.

Figure 15 compares the eroded surface morphology at the same location on a nickel specimen after several successive one minute exposures and emphasises that the formation and removal of thin flakes at the wave crest is an important component of the degradation mechanism. From these results it is estimated that the rate of material removal by detachment of thin flakes accounts for at least .25% of the measured degradation at 30° incidence, this calculation probably underestimates the significance of this mechanism due to the fact that some smaller flakes can be formed and removed within one minute of exposure and are neglected in the calculation. It is believed that material is also removed from the crest surface facing the erosive stream by cutting and ploughing. Since the dependence of the erosion rate of cobalt on impact angle as shown in Figure 5 is relatively flat between 30° and 90° incidence when cutting and ploughing are the predominant degradation mechanisms, it is considered that this type of relationship

10

can be applied to nickel specimens for the estimation of the effect of cutting/ploughing on the degradation rate of material. The degradation rate of nickel at 90° where the flake formation is not significant was therefore used as the degradation rate of nickel at 30° due to the cutting/ploughing mechanism alone. This gives an estimation that about 40% of the material is removed by cutting/ploughing at 30° incidence. And thus, from this estimation about 60% of the material removal is by flake formation and detachment.

Due to the presence of both cutting/ploughing and detachment of thin flakes as degradation mechanisms, the degradation rates of nickel specimens show a strong dependence on impact angle with a sharp peak at 30° indicating the significance of the second mechanism. For the same reason nickel specimens have higher degradation rates than those of cobalt at 30°, however, the opposite result was observed at 90° where cutting and ploughing are predominant. This demonstrates that the degradation rate of a material under combined erosion and oxidation is affected by many parameters including the nature of the oxide, substrate and the degradation mechanisms.

Mechanisms of Degradation

Various mechanisms have been proposed for the degradation of materials during erosion, including cutting and ploughing[9,10], flake formation[14], platelet formation[15], melting[16,17], and repeated deformation such as fatigue[18,19]. Cutting and ploughing mechanisms were proposed based on the observation of the geometry of impact craters during single impact exteriments[9,10]. It was found that material inside the crater was displaced to the edges of the crater as rims or to the leading edge of the crater as lips. The rim and lip can be removed during subsequent impacts leading to loss of material. This is referred to as a ploughing mechanism when spherical erodents are used and as a Type I cutting mechanism

11

when angular erodents are used. When the particles travel at high velocities or low rake angles, the extruded material can be removed by single impact and this situation is considered as Finnie's cutting model or Hutching and Winter's Type II cutting. In real situations the target material is subjected to multiple impacts where the impact craters as well as extruded materials overlap and interact with each other. When the material is very ductile, the deformed surface material can be extruded into thin platelets or thin flakes whose detachment can contribute to a greater degradation rate than deformation simply by cutting and ploughing. Since the kinetic energy of the erosive particles is high, local temperature rise in the surface area might even exceed the melting point of many materials if the deformation is converted into heat within the deformed region. Melting or adiabatic shearing were proposed as alternative degradation mechanisms. In the case of erosion at very low velocities and at normal impacts, where surface shearing is not pronounced, a fatigue model was proposed to account for the degradation of the material.

The formation of ripples has been observed during room temperature erosion of ductile materials and even on plate glass when eroded at low angles by small erosive particles[20]. This indicates that ripple formation is strongly connected with shear deformation of the target. Formation of thin flakes was observed at the ripple front or in the troughs at 90°, where extensive shearing occurs, during room temperature erosion[14]. Thin flakes were also observed in the present study under combined erosion and oxidation when the oxide scale was relatively thin. The results indicate that formation of ripples can enhance the degradation rate of material by formation and detachment of thin flakes over the ripple front due to extensive shearing and this is another form of interaction between erosion and high temperature oxidation.

12

The mechanisms of ripple formation during erosion are not well characterized, however, from the above discussion it is clear that ripple formation is associated with solid particle impact and shear deformation of the target. Wave formation is also observed during explosive cladding[21, 22, 23], when a wavy interface, similar in section to the ripples generated by erosion, can be formed between cladded materials to enhance the adherence at the interface. Although various mechanisms have been proposed to explain the wave-like morphology, the mechanism of formation is still in doubt. Of particular interest in the case of explosive cladding is the high strain rate of deformation associated with the processs during which shock waves are generated. Since the pressure at the shock front is much higher than the yield strength of the material, the material can be considered as a viscous fluid and its flow treated using models of fluid mechanics. Another feature associated with explosive cladding is that a large amount of heat is released rapidly and adiabatically leading to temperature rises of up to thousands of degrees centepade. Erosion also involves high strain rate deformation with strain rates of the order of 10^5 to 10^7 per second as estimated by Hutchings[24], which is either of the same order or several orders less than the strain rate associated with explosive cladding. Shock wave generation can be expected during erosion, and adiabatic heating or melting has been widely discussed and observed in several systems. It would be pertinent to consider the eroded target material as a semi-infinite viscous fluid during particle impact assuming that the erosive particles are considerably smaller than the thickness of the target. The deformation from each impact can be viewed as a pulse of shock wave which propagates to a finite region, after which the shock wave is quickly attenuated. As a result of repeated impacts there is a wide spectrum of wavelengths at which shock waves propagate and interact with one another. The propagation and

13

interaction of nearby waves is the most efficient at a certain wave length and wave morphology will develop at this wavelength on the eroded surface. A computer model has been developed[25] to simulate mogul formation at 90° incidence by choosing random numbers as the coordinates of impact was defined of individual incident particles. In this model the size of the deformed region from each impact and the condition that material was not removed but simply deformed or displaced plastically was assumed. It was found that the dimension of the deformed region was proportional to the wavelength of moguls generated by the computer simulation. This indicates that the favored wavelength at which a wave develops can be affected by parameters such as the mechanical properties of the target as well as the properties of the erosive beam such as incident energy, particle size, impact angle and perhaps the spacing between the particles in the gas. From the experience of water waves in the sea the wavelength of water waves tends to increase over a period of time because less energy is required to propagate waves with longer wavelength. Similarly the wavelength of waves formed on eroded surfaces tends to increase with exposure time, possibly for the same reason as the water waves.

Figure 16(a) shows the mechanisms by which moguls are thought to be developed and stabilized. Figure 16(b) shows the development of ripples and the mechanisms by which the shape of the crest is stabilized. The incident beam is considered to have two components: one parallel to the original target surface, v_x, and the other perpendicular to the target surface, v_y. The parallel component leads to shear deformation of the target and promotes the formation of thin flakes over the ripple front. The vertical component controls the depth of the plastic deformation zone and affects the amplitude of the waves. Since crests of the waves actually proceed at a certain velocity, both vertical and parallel components

14

lead to a forward displacement of material towards the ripple front as shown in Figure 16(b), which can further stabilize the shape of the crest. In order to characterize the wave formation further, future study should address the relationships between wavelength, amplitude and propagation speed of the crest in terms of the mechanical properties of the target and properties of the erosive beam such as velocity, impact angle, size of the erosive particles, dimension of the impact crater and temperature.

The shape of the crests of the waves developed under combined erosion and oxidation is an important factor in terms of the degradation mechanisms and it is affected not only by the properties of the target material or erosive beam but also by the corrosion process. As demonstrated in this study the presence of a relatively thick oxide scale over a cobalt surface can suppress flake formation, such that cutting and ploughing are the primary degradation mechanisms operating in cobalt at 780°C leading to an angular dependence on the erosion rate as shown in Figure 5. However when the oxide scale is thin, the detachment of thin flakes becomes more effective. The angular dependence of the erosion rate can be characterized by Figure 13 where the maximum degradation rate, at 30°, is greater than that introduced simply by cutting and ploughing. This shows the synergistic nature of combined erosion and oxidation in which the type of degradation mechanisms are also influenced by the interaction of erosion and oxidation.

References

1. C. T. Kang, F.S. Pettit and N. Birks, "Mechanisms in the Simultaneous Erosion-Oxidation Attck of Nickel and Cobalt at High Temperature", <u>Met. Trans.</u>, (1987), to be published.

2. S. L. Chang, N. Birks and F. S. Pettit, Interaction Between Erosoin and Corrosion of Metals The Erosion Enhanced Oxidation Regime, Appendix 4A to be published.

3. B. L. Mechante; <u>Introduction to Hydrodynamics and Waterwaves</u> Published by Springer-Verlag (1976).

4. B. Kinsman; "Wind Waves," Pentice Hall, NJ (1965).

5. <u>Proceedings of the Third Conf. of Applied Mechanics</u>, "The Mechanism of Erosion of Ductile Metals, I. Finnie", (1958), 527-533.

6. I. Finie, A. Levy and D. H. McFadden, "Fundamental Mechanisms of the Erosive Wear of Ductile Metals by Solid Particles", in <u>Erosion: Prevention and Useful Applications</u>, W. F. Adler, ed., (1979), pp. 36-58.

7. J. G. A. Bitter, "A Study of Erosion Phenomena, Part I", <u>Wear</u>, Vol. 6, (1963), pp. 5-21.

8. J. G. A. Bitter, A Study of Erosion Phenomena, Part II", <u>Wear</u>, Vol. 6, (1963), pp. 169-190.

9. I. M. Hutchings and R. E. Winter, "Particle Erosion of Ductile Metals: A Mechanism of Material Removal", <u>Wear</u>, Vol. 27, (1974), pp. 121-128.

10. I. M. Hutchings, "Mechanisms of the Erosion of Metals by Solid Particles", in <u>Erosion: Prevention and Useful Applications</u>, W.F.Adler, ed., (1979), pp. 59-75.

11. S. L. Chang; Interaction of High Temperature Erosion and Oxidaton of Selected Metals and Alloys, Ph.D. Thesis, Materials Science and Engineering Department, University of Pittsburgh, 1987.

12. S. L. Chang, N. Birks and F. S. Pettit, Some Interactions in the Erosion Oxidation of Alloys, Appendix 4C, to be published.

13. R. H. Barkalow, J. A. Goebel and F.S. Pettit, <u>Materials Problems in Fludized-Bed Combustion Systems: High-Temperature Erosion-Corrosion by High-Velocity (200 m/s) Particles</u>, Pratt & Whitney Aircraft Group, May, 1980, Final Report, CS-1448 Res. proj. 979-4.

14. R. Brown, E. J. Jun and J. W. Edington, "Erosion of α-Fe by Spherical Glass Particles", <u>Wear</u>, Vol 70, (1981), pp. 347-363.

15. A. V. Levy, "The Platelet Mechanism of Erosion of Ductile Metals", <u>Wear</u>, (1984).

16. T.Christman and P.G.Shewmon, "Adiabatic Shear Localization and Erosion of Strong Aluminum Alloys", Wear, Vol. 54, (1979), pp. 145-155.

17. R. Brown and J. E. Edington, "Occurrence of Melting during the Solid Particle Erosion of Copper", Wear, Vol 73, (1981), pp. 193-200.

18. Proc. of Intern. Conf. on Metallurgical Applications of Shock-Wave and High Strain-Rate Phenomena, "High-Strain-Rate Deformation in FCC Metals and Alloys, P. S. Fallansbee", (1985), Oregon.

19. M. M. Mamoun, "Analytical Models for the Erosive-Corrosive Wear Process", (1975), pp. 38-81, Arganne National Lab. Material Science Div. Coal Technology Second Quarterly report. Tech. Report ANL-75-XX-2.

20. G. L. Sheldon and I. Finnie, "On the Ductile Behavior of Nominally Brittle Materials during Erosive Cutting", J. Eng. for Industry, ASME, Vol. 88B, (1966), pp. 387-392.

21. Book: Shock Waves and the Mechanical Properties of Solid, ed. by J. J. Burke and V. Weiss. Published by Syracuse University Press (1971).

22. Book: Shock Waves and High-Strain-Rate Phenomena in Metals, ed. by M. A. Meyers and L. E. Murr, published by Plenum Prss (1981).

23. Book: Metallurgical Applications of Shock-Wave and High-Strain-Rate Phenomena, ed. by L. E. Murr, K. P. Staudhammer and M.A. Meyers. Published by Marcel Dekker, Inc. (1986).

24. I. M. Hutchings, "Strain Rate Effects in Microparticle Impact", J. Phys. D: Appl. Phys, Vol. 10, (1977), pp. L179-L184.

25. Chih-Tsung Kang, The Interactrions between Erosion and Oxidation of Metals at Elevated Temperatures, PhD Dissertation, University of Pittsbugh, (1985).

Acknowledgement
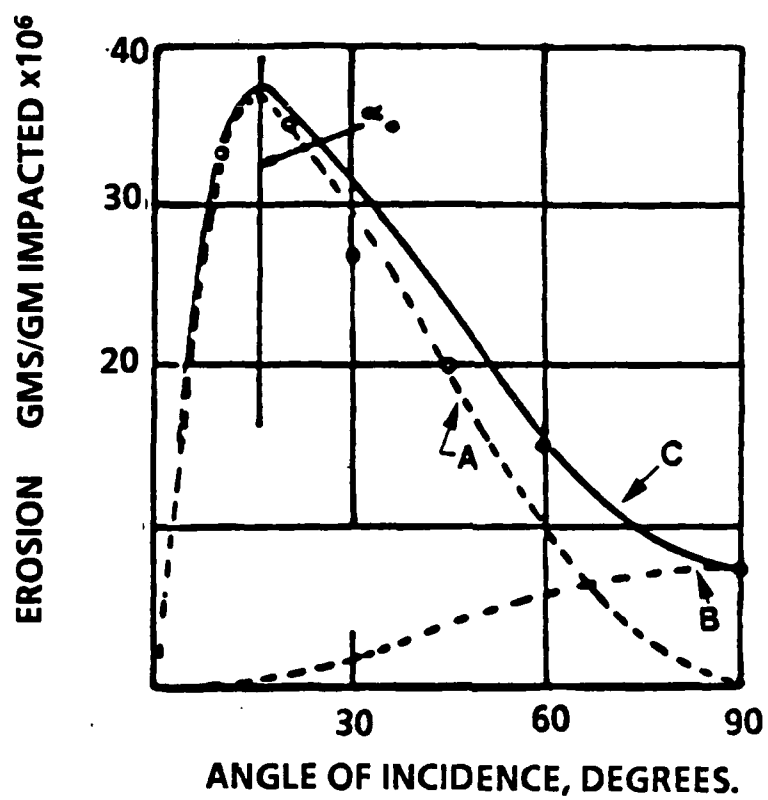
FIGURE 1.   Angular dependence of erosion rate for ductile materials.
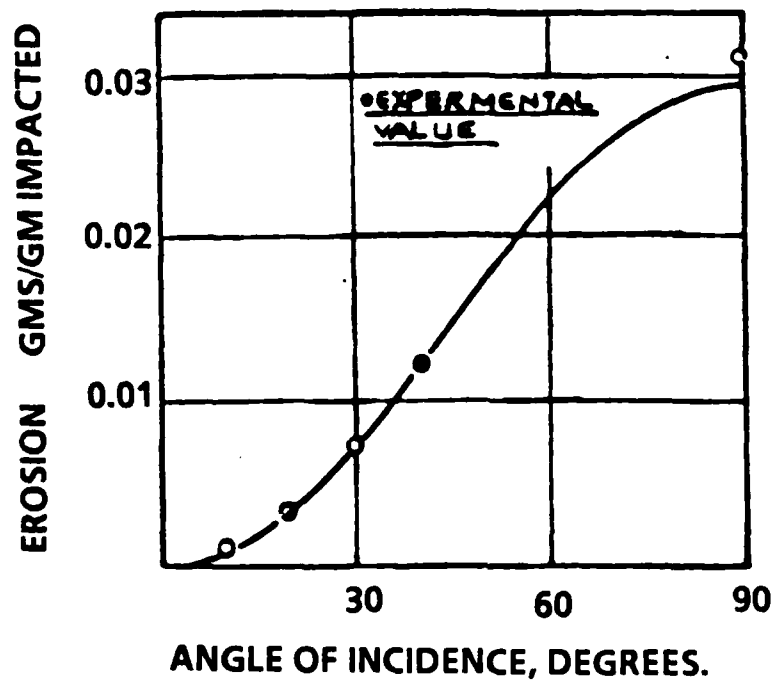
FIGURE 2. Angular dependence of erosion rate for brittle materials
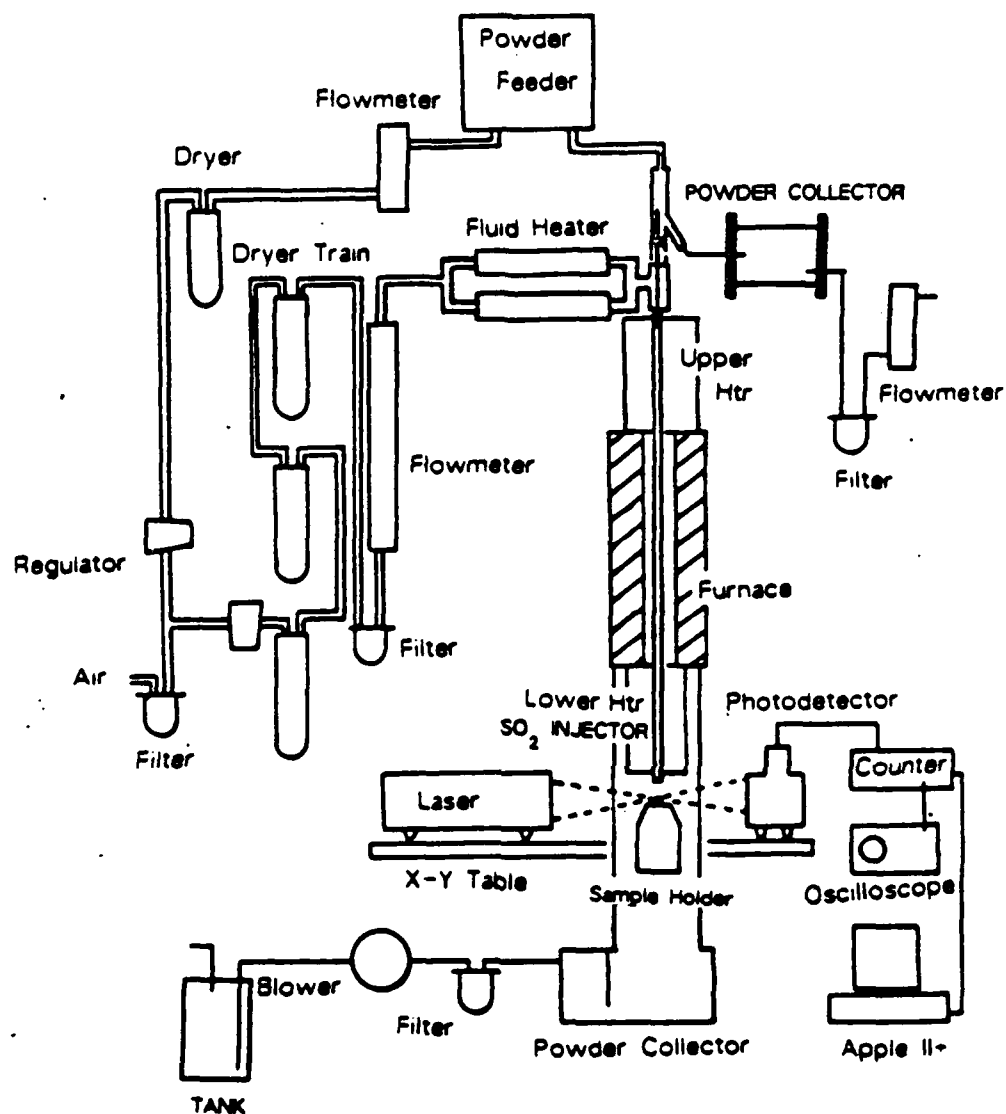
FIGURE 3. Diagram of apparatus used in studies of the erosion-oxidation of metals.
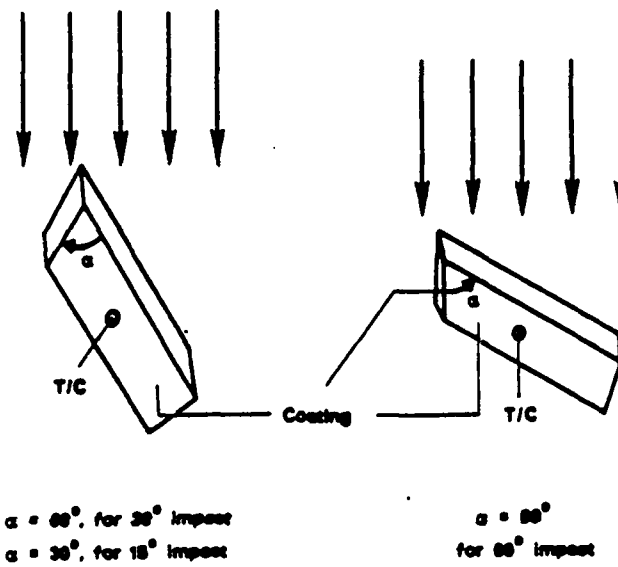
FIGURE 4.   Specimen configuration for oblique impact experiments.

Erosion and Oxidation of Cobalt
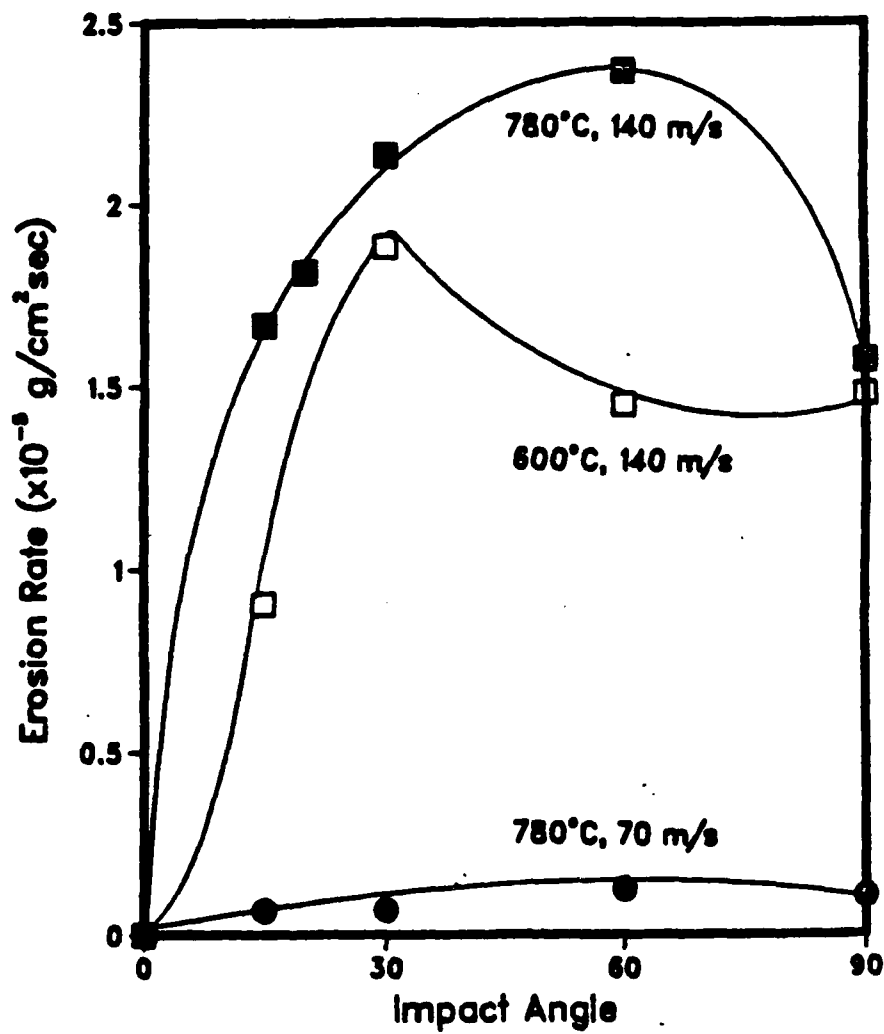
FIGURE 5. Angular dependence of degradation rate for erosion-oxidation of cobalt.
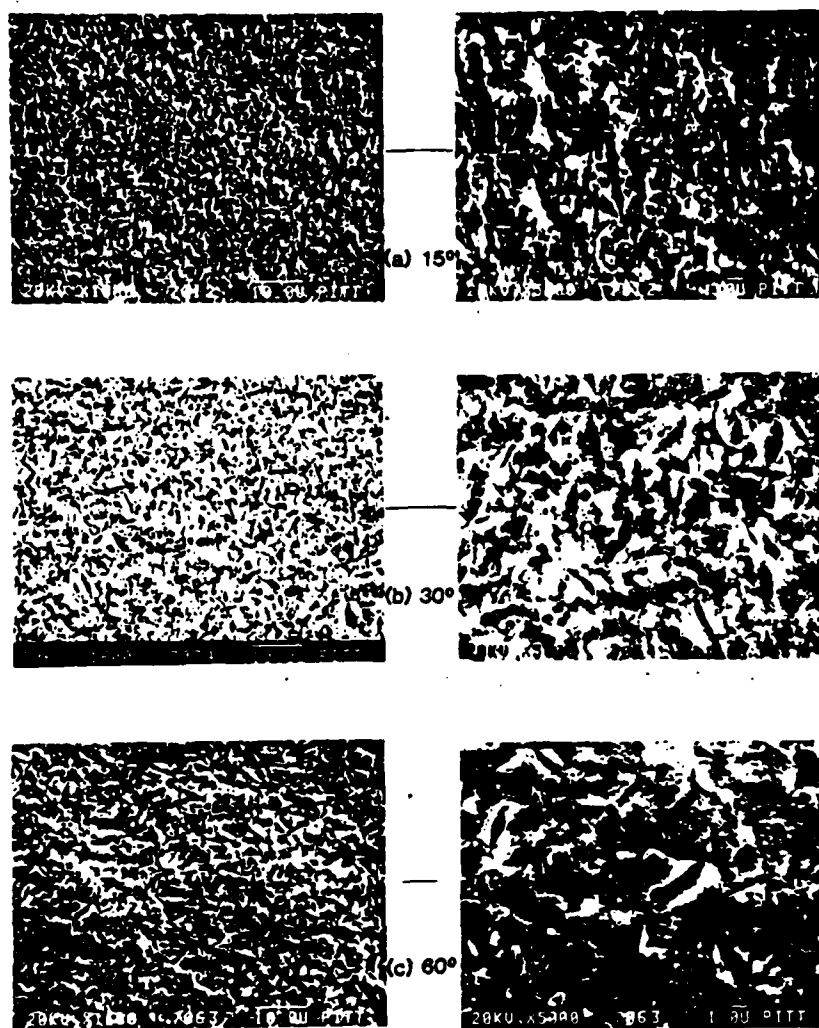
FIGURE 6. Surface morphology of cobalt exposed at 780°C to an airstream flowing at 70 m/s for 90 minutes at (a) 15°, (b) 30° and (c) 60° incidence.
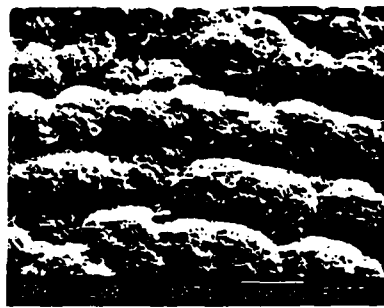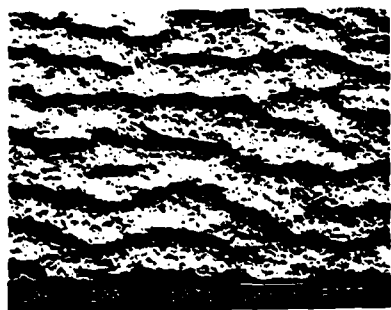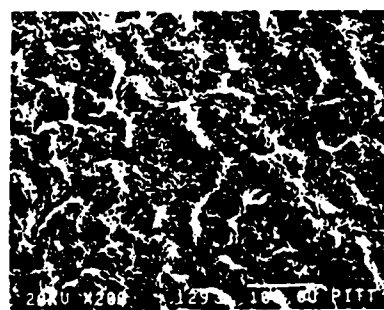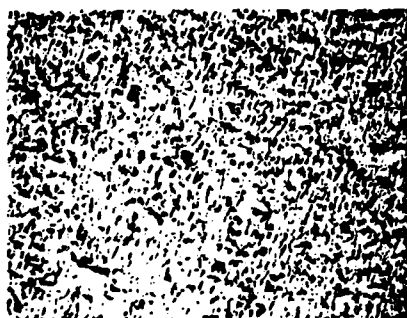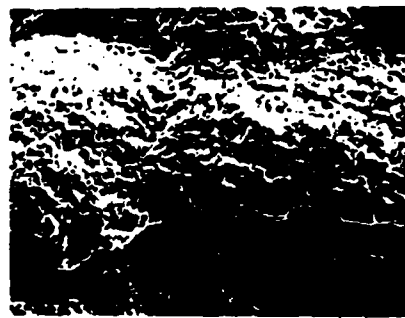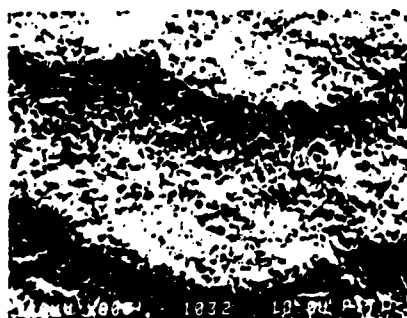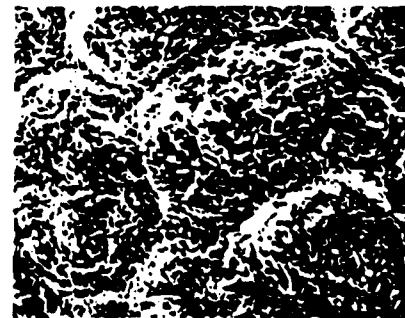
FIGURE 7. Surface morphology of cobalt exposed at 780°C to an airstream flowing at 140 m/s for 90 minutes at (a) 10°, (b) 30°, (c) 60° and (d) 90° at 123 m/s for 60 minutes.
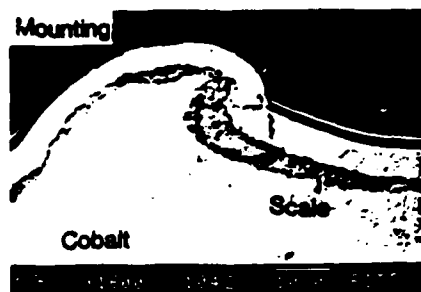
(a)

(b) Oxygen Map of (a)
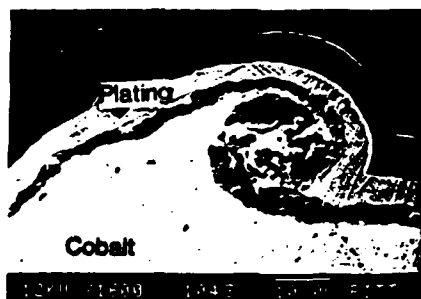
(c)

Cross section of cobalt specimen exposed at 780°C to an airstream flowing at 140 m/s at 60° incidence.

(a) 10°
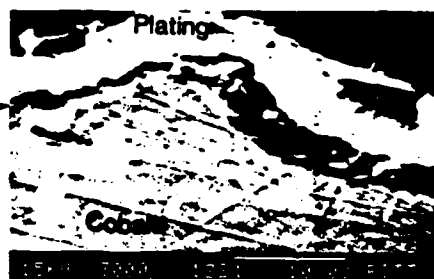
(b) 30°
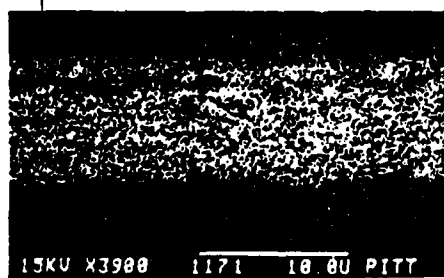
Oxygen Map
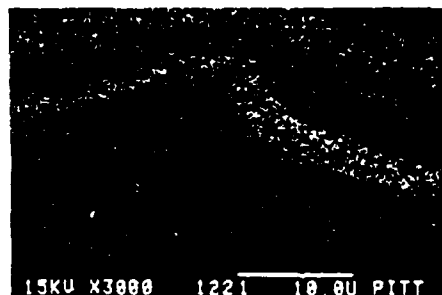
Oxygen Map

Cross section of cobalt specimen exposed at 780°C to an airstream flowing at 140 m/s at (a) 10° for 30 minutes and (b) 30° for 61 minutes.

FIGURE 8.
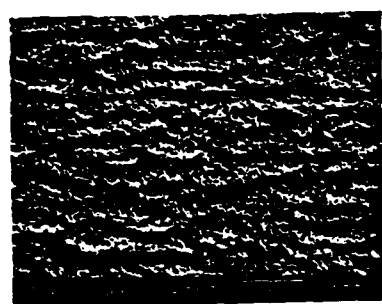
(a) 15°
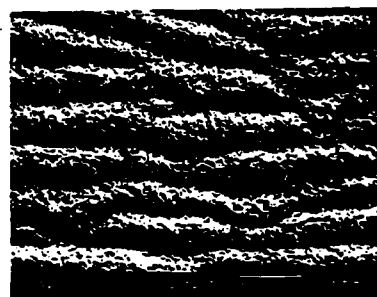
(c) 60°
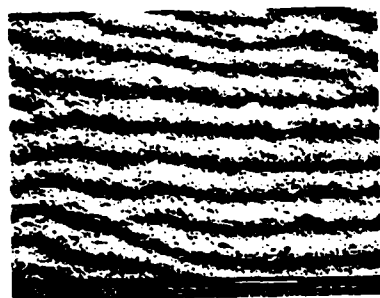
(b) 30°
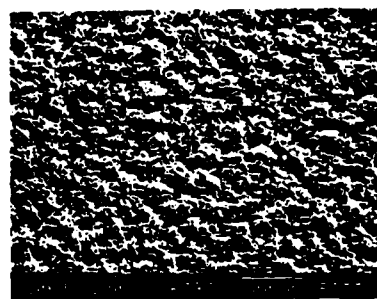
(d) 90°

FIGURE 9.   Surface morphology of cobalt specimen exposed at 600°C to an airstream flowing at 140 m/s for 60 minutes at (a) 15°, (b) 30°, (c) 60° and (d) 90° incidence.

Cobalt

(a)   600°C

Cobalt

(b)   600°C

Cobalt

(c)   780°C
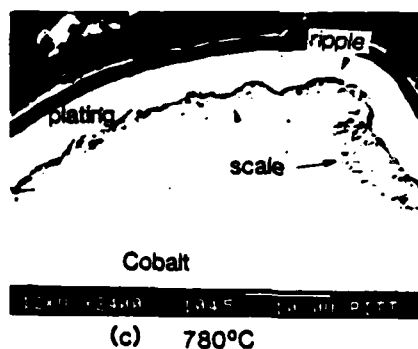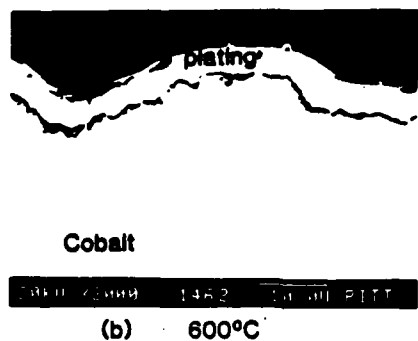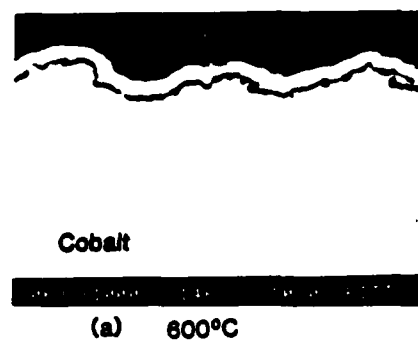
FIGURE 10.   Cross sections of cobalt specimens exposed at 600°C to an airstream flowing at 140 m/s for 60 minutes at (a) 15°, (b) 30°, (c) 60° and (d) 90° incidence.
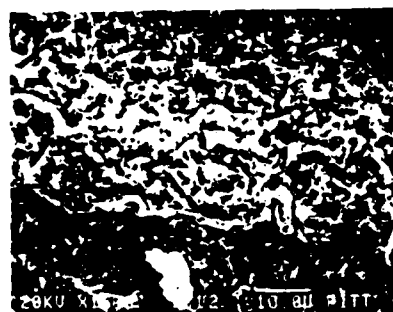
(a) 30 min   (c) 32 min
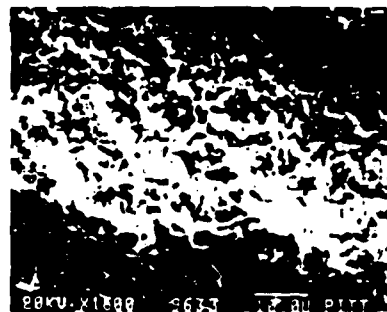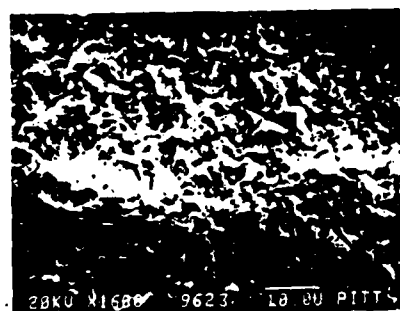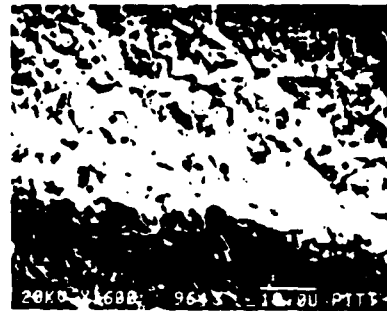
(b) 31min   (d) 33 min

FIGURE 11. Surface morphology variation at the same location of a cobalt specimen exposed at 780°C to an airstream flowing at 140 m/s and 30° incidence for increasing times.

Erosion of Nickel
at 780°C and 140 m/s
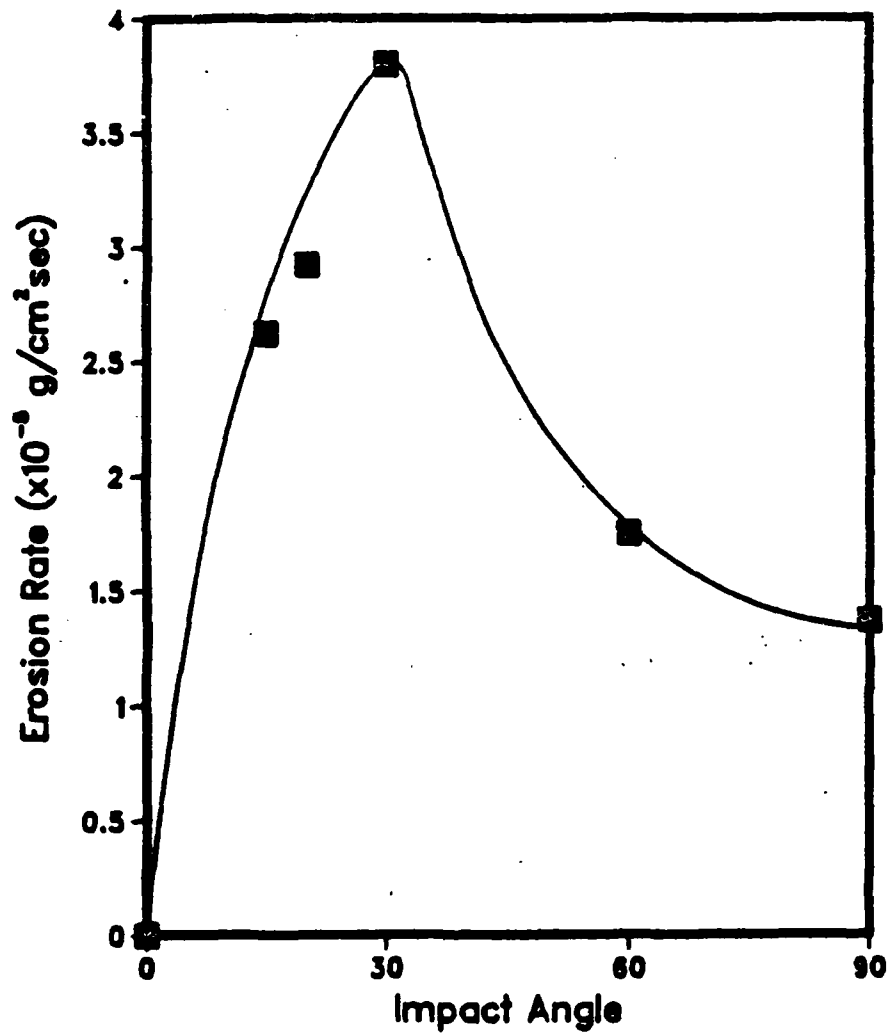
FIGURE 12. Angular dependence of degradation rate of nickel after erosion-oxidation at 780°C exposed to an airstream flowing at 140 m/s.
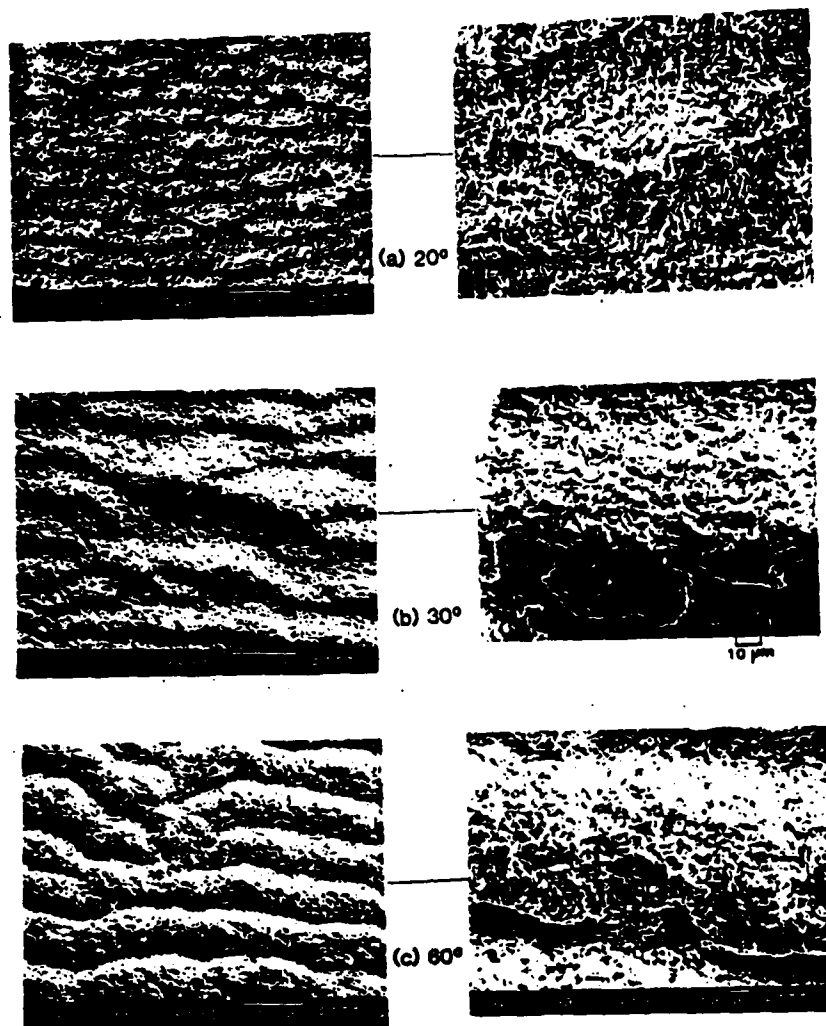
FIGURE 13. Surface morphologies of a nickel specimen exposed at 780°C to an erosive airstream flowing at 140 m/s for 90 minutes at (a) 20°, (b) 30° and (c) 60° incidence.
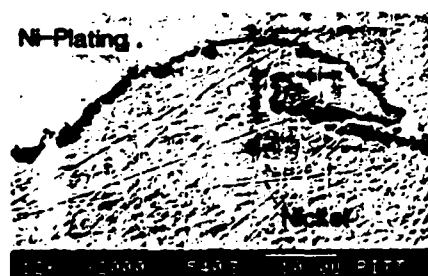
(a) 60°
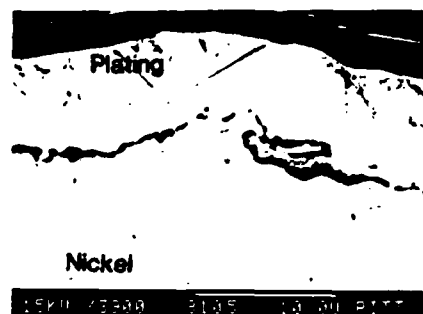
(c) 30°
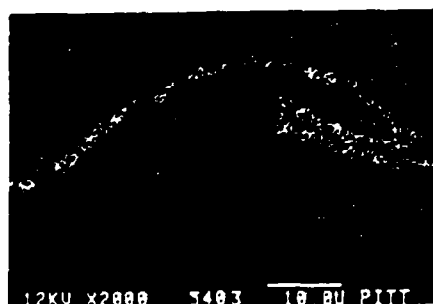
(b) Oxygen Map of (a)
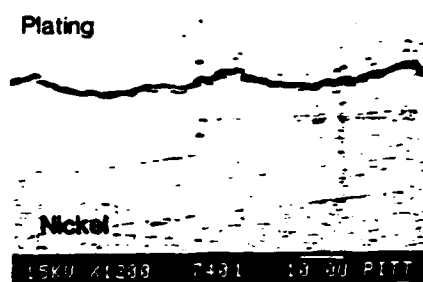
(d) 20°

FIGURE 14. Cross section of nickel specimen exposed at 780°C and 140 m/s at (a) 60° for 60 minutes, (b) 30° for 61 minutes and (d) 20° for 90 minutes.
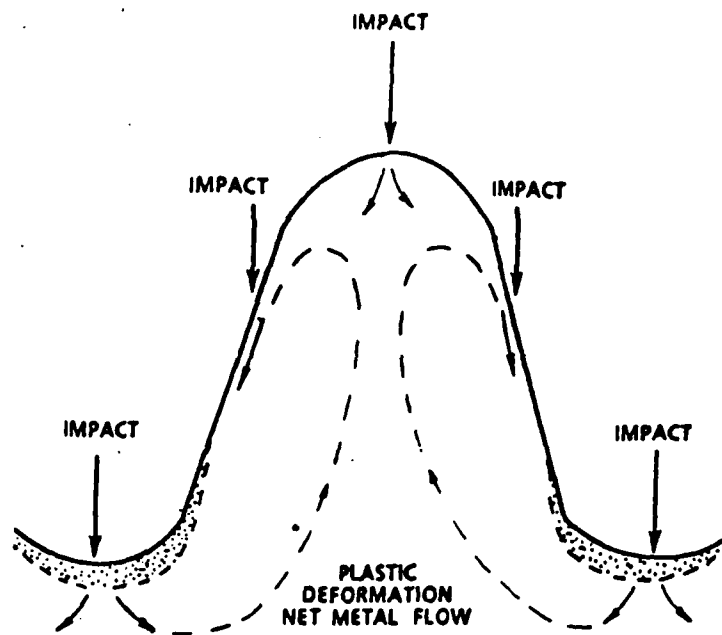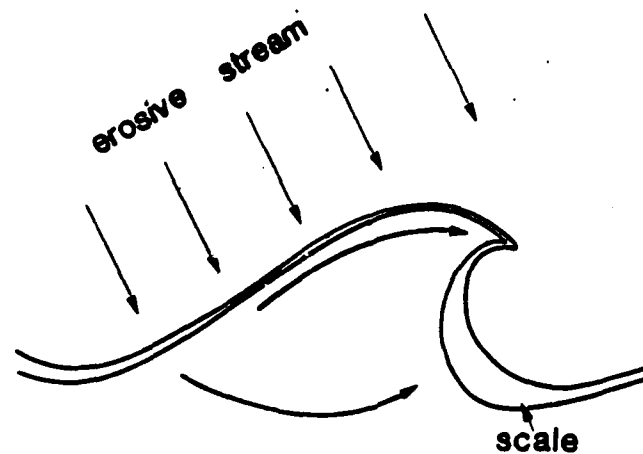
(A) 30 MIN   (C) 32 MIN
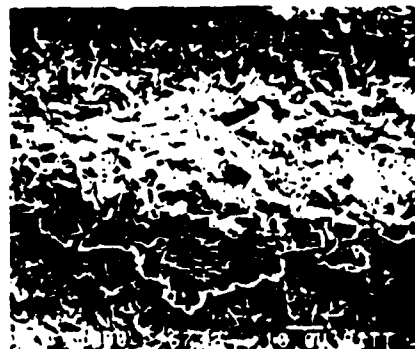
(B) 31 MIN   (D) 33 MIN

FIGURE 15. Surface morphology variation at the same location of a nickel specimen exposed at 780°C to an erosive airstream flowing at 140 m/s and 30° incidence for increasing times.

(a) Mechanism of mogul formation showing transport of surface material from the peak to the valleys.

(b) Mechanism of ripple formation at oblique angle of incidence of the erosive airflow.

FIGURE 16.

SOME INTERACTIONS IN THE EROSION-OXIDATION OF ALLOYS

by

S. L. CHANG F. S. PETTIT AND N. BIRKS

Department of Materials Science and Engineering
University of Pittsburgh

INTRODUCTION

Recent papers[1-5] concerning the combined erosion and oxidation of pure metals at high temperatures have examined a range of erosive conditions in which metals were eroded by 20 micrometer alumina particles at velocities from 50 to 170 m/s and at 780°C with impact angles ranging from 15° to 90°. It has been shown that several regimes of interaction exist. At the present time a fairly clear understanding has been obtained for such regimes as (1) erosion enhanced oxidation and (2) oxidation affected erosion. Oxide spallation has also been observed under certain conditions tht involve a critical scale thickness, this is currently regarded as belongng to the erosion enhanced oxidation regime but the incorporation of spallation into the sequence of regimes has not yet been completed. These have been summarized in recent publications[1,3,4]. Basically the regimes that were observed were found to depend on the relative intensities of the erosion and oxidation components. This is shown in Fig. 1 from which it can be seen that the erosion enhanced oxidation regime occurs under conditions where the rate of scale removal by erosion is similar to the rate at which the scale grows by oxidation. This regime is therefore normally expected to be observed in systems with rapidly growing scales. The oxidation affected erosion regime is found to exist when the erosive component is rapid compared to the oxidation component. The oxide scale is thin, discontinuous and the erosion impacts cause substantial plastic deformation to the underlying metal. This regime can be observed in systems that form a

1

rapidly growing scale if the erosion intensity can be increased sufficiently, i.e. as in the case of cobalt[3]. It has also been observed in the case of nickel[1] which has much lower rates of scale formation over a very wide range of erosion conditions.

Both nickel and cobalt form scales which are generally regarded as having 'rapid' scale growth characteristics. In order to extend experiments to systems which have very slow scale growth characteristics, it is necessary to study alloys that form chromia or alumina scales. The use of alloys introduces several other complications such as transient oxidation and changes in composition at the scale/alloy interface due to selective oxidation. This paper reports on the initial work undertaken on combined erosion and oxidation of alloys to study these effects and also to extend the understanding of interactions between erosion and oxidation to alloy systems.

The effect of a high velocity gas stream on the oxidation characteristics of chromia forming alloys was also investigated because chromium is known to form volatile oxides under oxidizing conditions at elevated temperatures[6-10]. Volatilization is significant at temperatures above 1100°C in still air and can result in an appreciable weight loss. Since the erosive stream flows at high temperature and at high velocities, it is pertinent to determine the extent to which the evaporation of CrO_3, due to high velocity airflow, can modify the normally observed oxidation phenomenon in the absence of erosive particles.

EXPERIMENTAL

(1) Dynamic Oxidation

Figure 2 is a schematic drawing of an apparatus for the investigation of the effect of high velocity gas flow on the oxidation behavior of metals. The apparatus is capable of delivering a compressed airstream at velocities up to 85 m/s and at

2

temperatures up to 1100°C. The gas was preheated by direct contact with a heating coil while the specimen, loaded at the top of a sample holder with a thermocouple attached, was heated by the gas. The gas velocity was calculated using the flow rate, gas temperature, and dimension of the nozzle. This type of calculation was also used in a parallel program for combined erosion and oxidation in which the gas velocity can be measured using a Laser Doppler Velocimeter and it has been shown[1,11] that the results from the measurement match well with the calculation. An alloy, MA754, whose composition is given in Table 1 and which develops an adherent chromia scale in still air at high temperatures, was used in this study.

(2) Combined Erosion and Oxidation

The apparatus for combined erosion and oxidation is shown in Fig. 3 and has been described in detail previously[1,3,4]. A compressed air stream is used to deliver the erosive, 20 micrometer, angular alumina particles, at a constant loading rate about 500 mg/min. Specimens were heated directly by the gas up to 800°C. The particle velocity, measured by the Laser Doppler Velocimeter, can be varied between 50 and 170 m/s with the impact angle varied between 15° and 90°.

Both chromia and alumina forming alloys, of compositions given in Table I, were chosen for the study of combined erosion and oxidation. Both MA754 and Ni-30Cr are chromia formers. MA754 is mechanically alloyed and contains dispersed yttria particles in the alloy matrix. The chromia scale formed over MA754 is expected to exhibit better adherence than that formed on Ni-30Cr due to the development of a thinner chromia scale at elevated temperatures on the former. The Ni-20Al and CoCrAlY alloys are both alumina formers which are commonly used in systems operating at high temperatures because of their good oxidation resistence.

3

The reaction kinetics were measured by weight change[3,4] and the degradation rates of these alloys were, compared after exposure to determine the important parameters for combined erosion and oxidation. The eroded surface morphologies were examined by the optical microscope and the scanning electron microscope coupled with an energy dispersive spectrometer. X-ray diffraction was applied to selected specimens for the analysis of the microstructure of alloy and the identification of the reaction products.

RESULTS AND DISCUSSION

(1) Dynamic Oxidation

Oxidation of MA754 in still air at elevated temperatures forms a thin and continuous chromia scale with a lot of chromia nodules on the oxide surface as shown in Figs. 4 and 5. The period of transient oxidation is very short. It appears that at, 800°C the formation of chromia becomes dominant within a few minutes of exposure to the oxidizing environment and the evaporation of CrO_3 is not significant at 800°C in still air.

Specimens used for the dynamic test at 800°C were preoxidized at 1100°C for two hours. This caused a relatively thick chromia scale to form such that the oxidation rate was greatly reduced. The weight change results obtained from subsequent dynamic oxidation tests will, therefore be related primarily to the effect of vaporization. The effect of vaporization was found to be too small to be detected at 800°C even under an airstream flowing at 85 m/s, furthermore the surface morphology developed is the same as that developed under static conditions.

4

The vaporization process was detectable at 1000°C under dynamic conditions and was very significant at 1100°C. Figure 6 compares the weight change results obtained at 1100°C under both static and dynamic conditions. It can be seen that a small weight gain is associated with dynamic oxidation at 65 m/s during the early stage of the process, followed by a significant weight loss at longer exposure time whereas only weight gain was observed under static conditions, indicating that the vaporization process is greatly enhanced in the presence of a high velocity air stream. This was also observed in other studies[12,13,14] which were designed to select alloys for the simulated shuttle re-entry conditions in which both the gas velocity and temperature were much higher than those used in this study.

The oxide morphology was modified by the vaporization process as shown in Fig. 7 in which the chromia scale was examined at the same location after different exposure times. It can be seen that the chromia scale, especially with respect to the oxide nodules, is gradually lost due to the formation of volatile oxides. After a longer exposure time, about 25 hours at 65 m/s, NiO was found to develop along the leading edge of the specimen as shown in Figure 8. When the exposure time was increased further, e.g. to 40 hours, the development of NiO became more extensive such that NiO could be observed not only at the leading edge but also over the specimen surface at further downstream areas. It can also be seen from Figure 8 that NiO grows initially as spheres from various positions on the oxide surface, very often from the chromia nodules. Since the growth rate of NiO is much greater than that of chromia, the NiO spheres soon cover the original chromia scale and become connected with each other by lateral growth. This NiO scale can spread to a large area, but it is prone to spallation during thermal cycling.

5

A cross section of a specimen after 89 hours of exposure at 65 m/s at 1100°C is shown in Figure 9 in which a thick scale can be observed over the leading edge of the specimen. The thicker scale is composed of a porous outer layer of NiO, a central zone of mixed NiO and spinel, and an inner layer of chromia. Another chromia layer can be seen between the outer NiO layer and the central zone. This chromia layer, though not continuous, is believed to be the chromia scale developed earlier in the process. Fig. 10(a) shows the sections of the specimen near the leading edge. It can be seen that there is a continuous layer of chromia on the specimen surface. Internal chromia islands can be observed at isolated spots within the metal located immediately beneath the scale as indicated by an arrow. Also shown in Figure 10(a) is that the large oxide nodules contain appreciable amounts of nickel and chromium whereas the small nodules in Figure 10(b) are primarily metal peninsulas with a surface layer of Cr_2O_3. It should be noted that although the metal peninsulas observed in Figure 10(b) were commonly observed in the specimens dynamically oxidized at 1100°C, such features were either not significant or very small in the specimens oxidized in still air for up to one week. Such features are developed as a result of loss of chromium in the vaporization process. A chromium depletion zone was observed in the alloy beneath the oxide scale and the depth of the Cr-depletion zone was measured to be about 60 micrometers thick at an area near the leading edge of the specimen.

The experimental results described above have shown that: (1) the evaporation process is greatly enhanced in the presence of a high velocity gas flow at 1100°C; (2) the protective chromia scale developed during the early stage of the process broke down after extended exposure and was replaced by a faster growing, less protective, porous outer scale of NiO with a mixture of NiO and spinel in the

6

central zone, followed by an internal chromia scale; and (3) the development of the NiO scale starts at the leading edge of the specimen and gradually extends to the down stream area.

The high Reynolds number of the stream used in this study, 3.5×10^3, is characteristic of turbulent flow. The gas flows parallel to the specimen surface and hence gas boundary layers develop as shown in Fig. 11 from which can be seen that the boundary layer is thin at the leading edge and increases in thickness at downstream positions, indicating that the rate of CrO_3 removal is much greater at the leading edge than at the downstream area. Furthermore, since the thickness of the boundary layer decreases as the gas velocity increases, the vaporization rate should be enhanced by high gas velocity.

The treatment of reaction kinetics for the combined oxidation and vaporization were initially developed by Tedmon[15] and have been modified in this study[16] such that the reaction kinetics can be described in terms of weight change. The behavior of a chromia forming alloy under dynamic oxidation conditions can be divided into three stages as shown in Fig. 12. The oxidation of chromium into chromia is the rate controlling step in the first stage and a thin and continuous chromia scale with nodules of chromia forms on the specimen surface. As the chromia scale gets thicker, the scaling rate is reduced and a competing process from which Cr_2O_3 is lost by further oxidation to form volatile CrO_3 becomes relatively important.

The second stage begins as the chromia scale reaches a limiting thickness such that the scaling rate equals to the vaporization rate, the scale thickness temporarily remains relatively constant. The behavior in this second stage parallels that in the erosion enhanced oxidation regime in which outer layers of the

7

scale are removed by erosion. Since the vaporization process proceeds at a constant rate, a weight loss can be detected in the second stage whose rate is equal to the rate of Cr lost in the vaporization process. In the case of pure metals where the activity of Cr at the scale/metal interface does not vary with time, the second stage could last for very long times during which the scale thickness should remain constant. But in the case of alloys, such as MA754, continuous removal of chromium from the oxide surface leads to a severe depletion of Cr and enrichment of Ni in the alloy near the scale/alloy interface. Initially this reduces the parabolic rate constant and the limiting scale thickness should decrease accordingly. The oxide morphology is gradually modified at this stage such that metal peninsulas develop inside the nodules as shown in Figure 10(b). This can reduce the diffusion distance of Cr in the alloy and can also balance the scaling rate and the vaporization rate by maintaining a thin scale over the nodules.

After a long exposure, the scale thickness is progressively reduced and NiO begins to form as the activity of chromium at the scale/alloy interface is reduced down to a level where the formation of NiO is thermodynamically stable. Since NiO was observed to grow as individual spheres from the center of chromia nodules, it is felt that the formation of NiO at stage III is due to both high activity of nickel at the scale/alloy interface and to the formation of physical defects in the scale, possibly generated by the vaporization process, that allows oxygen to reach the nickel-rich metal surface.

Once the formation of NiO is initiated, a period of extensive growth of NiO is observed. Since the growth rate of NiO is higher than that of chromia, the NiO layer will eventually cover the original chromia scale. The formation of CrO_3 gas could remain significant so long as the partial pressure of oxygen over the chromia

8

scale is relatively high. This can lead to a porous NiO scale when CrO_3 manages to escape or result in spallation of the NiO layer during thermal cycling because of poor adherence between the NiO and chromia layer.

Since the depletion of Cr is more severe at the leading edge of the specimen where the removal of volatile oxides is more effective under dynamic conditions, the NiO formation is observed to occur initially at the leading edge. Since the scaling rate of nickel is high, a reduction in the weight loss rate can be detected at stage III as shown in Fig. 12. The oxide morphology in the area where NiO is formed is similar to that of transient oxidation except that the Cr-content at the scale/alloy interface is now lower than in the bulk alloy or in a fresh specimen. Hence the oxide morphology developed here, as shown in Fig. 9, is similar to the transient oxidation of alloys with lower Cr-content. Consequently the Cr-depletion will become less severe when the scale/alloy interface advances into the alloy, also the presence of an external NiO layer will slow down the loss of Cr by vaporization.

The development of internal chromia islands as shown in Figure 10(a) is an important feature that develops in the second stage. These internal chromia islands form in the alloy at the positions where the activity of Cr is high enough to react with oxygen dissolved in the alloy to form Cr_2O_3. It would be a great benefit if, when the internal oxidation point reaches the high Cr content beyond the surface denudation zone, a continuous chromia layer could be developed internally underneath the nodules such that the NiO formation observed at stage III can be greatly minimized and the time required to develop a new external chromia scale be reduced. The results of the dynamic oxidation of MA754 suggest that chromia forming alloys should not be used at temperatures above 1000°C especially under

9

dynamic conditions because the degradation from the vaporization process is significant and can not be reduced effectively except by switching to an alumina forming system. The results obtained in this study can be applied to the combined erosion and oxidation of the same alloy in which the depletion of chromium at the scale/alloy interface can result in similar problems, such as the breakdown of the chromia scale and formation of NiO scale, if a continuous chromia scale can develop initially under combined erosion and oxidation.

(2) Combined Erosion and Oxidation

(A) Chromia Forming Alloys

Combined erosion and oxidation of alloys was studied at 780°C with an erosive airstream flowing at both 50 and 140 m/s. Ripple formation was observed when these alloys were eroded at 140 m/s due to the accumulated plastic deformation of the substrate alloy. The eroded surface morphology of MA754 is shown in Figure 13 in which the wave pattern varies with impact angle. A series of ripples aligned parallel to the front of the erosive beam can be observed at both 30° and 60° incidence being more pronounced at 30°. At 90° incidence, the incident energy is dissipated radially around the impact site, hence, a degenerated ripple pattern, or moguls, can be observed on the eroded surface. These features show that the alloy was deformed in a ductile manner during erosion. The oxide scale developed under these conditions was too thin to be examined either the X-ray diffraction analysis or cross section examination using the SEM.

The eroded surface morphology developed on Ni-30Cr is similar to that on MA754. Figure 14 compares the surface morphology of both alloys eroded at 140 m/s and at 30° incidence. It can be seen that a significant amount of material was displaced to the edge of the impact crater. These extruded edges can be removed

10

gradually after repeated impacts, hence, cutting and ploughing mechanisms as proposed by Hutchings and Winter[17,18] are probably the most important degradation mechanisms in the combined erosion and oxidation of these alloys under these conditions. Figure 15 shows the degradation rate of MA754 as a function of impact angle. It can be seen that the maximum erosion rate occurs at 60° incidence. This type of angular dependence was also observed[4] in the case of cobalt at 780^oC where both cutting and ploughing were the primary degradation mechanisms. Hence the results on MA754 substantiates that the angular dependence of the degradation rate is dependent on the type of degradation mechanisms operating under combined erosion and oxidation. It also shows that the behavior of alloys in terms of degradation mechanisms and wave formation is generally similar to that of pure metals.

Figure 16 shows the surface morphology developed on the chromia forming alloys eroded at 780^oC and at 30° to an airstream flowing at 50 m/s. Wave formation was not observed under these conditions due to insufficient energy being available to deform the alloy substrate. The circular or elongated features shown in Figure 16 are related to the grain structure of the alloy. The lighter areas being over the alloy grain boundaries and covered with deeper craters with significant extrusion of materials to the edges of the crater, whereas the darker area over the alloy grains is covered with shallow craters with less extrusion. The uneven deformation observed on the eroded surface is related to the development of an uneven oxide scale as shown in Figure 17 in which the scale is thicker over the alloy grains and thinner over the grain boundaries. Hence, the deeper craters observed over the boundaries is associated with a thinner oxide scale. Both NiO and Cr_2O_3 were identified in the X-ray diffraction analysis from the eroded

11

surface. The thicker scale in Figure 17 is composed of a very thin outer layer of NiO and an inner zone mixed with NiO and chromia while the thinner scale is basically a mixture of NiO and chromia. This type of oxide morphology is similar, but not identical, to that developed during the early stages of the transient oxidation period in static oxidation where a thick NiO scale with spinel and an inner layer of chromia develops over the alloy grains and a thin chromia layer forms over the alloy grain boundaries due to an enhanced transport of chromium through the short circuit paths.

A separate experiment was carried out in which a Ni-30Cr specimen was eroded and oxidized under the above condition for 100 minutes, followed by dynamic oxidation under the same conditions but in the absence of erosive particles for 20 minutes. Significant amounts of NiO and chromia were detected from the X-ray diffraction analysis on this specimen. From the cross section as shown in Figure 18, the oxide scale is composed of an outer layer of NiO and a central zone mixed with NiO, chromia, and possibly some spinel. It can also be seen that a chromia layer develops at the scale/alloy interface and over the alloy grain boundaries where the scale is thinner. This indicates that the oxide morphology, as well as the period of transient oxidation developed under combined erosion and oxidation, is dependent on the relative magnitude of the erosive beam and the oxidation component.

Figure 19 illustrates various types of oxide morphology developed under combined erosion and oxidation of Ni-Cr alloys. These oxide morphologies can also be developed under the same experimental condition but at different exposures under a very low erosive rate. When the erosion rate or the scaling rate varies, the

oxide morphology would change accordingly, hence, Figure 19 also represents the various oxide morphologies expected to develop under different experimental conditions. Figure 19(a) represents the situations when the erosive component is very rapid compared to the oxidation component, such as at 140 m/s. The oxide formed on the specimen surface is quickly removed by particle impact, hence, the composition of the new oxide film is directly related to the distribution of the alloy constituents on the surface.

When the erosive component is reduced, e.g. down to 50 m/s, the oxide morphology as shown in Fig. 19(b) develops. NiO is formed by the outward diffusion of nickel cations across the oxide scale while Cr_2O_3 is formed by the internal oxidation of chromium in the alloy near the scale/alloy interface. Since material is removed from the outer surface by erosion and the oxidation rate is greatly enhanced in the presence of erosion, the scale/alloy interface advances quickly into the alloy. The internal chromia islands which were formed in the alloy matrix are not mobile and would be engulfed into the NiO scale when the scale/alloy interface passes these internal islands. Both NiO and chromia islands will then be removed from the oxide surface by erosion. Figure 19(b) represents the situation when the internal chromia islands are quickly engulfed and taken into the NiO scale before they are coarsened enough to form a continuous chromia layer. Alloys developing this type of oxide morphology will experience a much longer transient oxidation period under combined erosion and oxidation than under pure oxidation. It is also possible that an internal chromia scale may never develop.

If the erosive component can be reduced further or the selective oxidation of chromium can be enhanced, it is possible that an internal chromia layer, as shown

13

in Figure 19(c), can develop by the lateral growth of the internal islands. Once an internal chromia layer is completed, further growth of NiO layer is prohibited because the transport of nickel cations across the chromia layer is slow. The external NiO layer can be removed quickly by erosion. This will enhance the development of a second external chromia scale as shown in Figure 19(d).

It is possible that the external chromia scale developed under combined erosion and oxidation is neither continuous nor protective or is so thin such that erosive particles can penetrate the scale during impact. NiO can grow from the area where the chromia scale loses continuity and the alloy will undergo transient oxidation locally with the oxide morphology similar to those shown in Figure 19(b) and (c). If the chromia scale is continuous and protective, the erosion enhanced oxidation regime observed on cobalt is expected to occur to chromia forming alloys. However the composition of chromium at the scale/alloy interface will decrease rapidly with exposure time due to erosion. This is similar to the situation of dynamic oxidation of chromia forming alloys where the depletion of chromium is caused by the vaporization process. Hence the results obtained from the dynamic oxidation tests can be applied to predict the behavior of similar alloys under combined erosion and oxidation.

(B) Alumina Forming Alloys

Alumina forming alloys under combined erosion and oxidation behave in a manner similar to chromia forming alloys. Figure 20 shows the surface morphology of two alumina forming alloys eroded at 780°C by an erosive stream flowing at both 50 and 140 m/s at 30° incidence. Ripple formation is significant for both alloys eroded at 140 m/s. The features observed on the eroded surface, deep craters with significant extrusion of material to the edge of the crater, are similar

14

to those observed in Figure 14 for chromia forming alloys. When eroded at 50 m/s, the eroded surface is relatively flat without any wave formation. The impact craters are much smaller in size at 50 m/s than at 140 m/s but both alloys are still deformed in a ductile manner by cutting and ploughing.

Cross sections of the specimens are shown in Fig. 21 in which an aluminum depletion zone can be observed underneath the eroded surface for the specimens eroded at 50 m/s. The Al-depletion zone can be seen as a continuous white band of alpha-cobalt(FCC) and epsilon-cobalt(HCP) in CoCrAlY, and as a lighter band with much lower Al-content than the alloy matrix in Ni-20Al. Such features are not observed on the specimens eroded at 140 m/s, however. Since erosion is a mechanical process, the particle impact should deform the target material over an area several micrometers wide and will not remove the aluminum atoms preferrentially. The presence of the aluminum depletion zone is, hence, developed by a chemical process from which aluminum is selectively oxidized into alumina. Although this alumina scale is too thin to be measured using SEM, its presence on the target surface can modify the behavior and the degradation rate of the material under combined erosion and oxidation. The results also show that the oxide morphology is dependent on the erosion and oxidation components.

Selective oxidation of aluminum can only be detected when the erosion rate is relatively low, 50 m/s in this case. The alloy may be in a situation as described by Figure 19(d) in which an Al-depletion zone develops due to the selective oxidation of aluminium into alumina with the removal of the alumina scale by erosion. Combined erosion and oxidation of these alloys at higher velocities such as at 140 m/s follows a behavior similar to that described in Fig. 19(a) except that the target surface now is covered with a thin film of NiO, Cr_2O_3 and Al_2O_3.

15

(3) Comparisons

Figure 22 summarizes the degradation rate of all the materials used in this study. The results were obtained at both 600° and 780°C with an airstream flowing at 140 m/s and at 30° incidence so that the degradation rate of these materials can be compared under the same conditions. The results show that materials with a high scaling rate such as nickel and cobalt exhibit a high degradation rate under combined erosion and oxidation. Chromia forming alloys have an intermediate scaling rate and show an intermediate degradation rate whereas the alumina forming alloys, with the best resistence to oxidation, show the best resistence to the combined erosion and oxidation. This indicates the importance of the scaling rate of a material on the overall degradation rate under combined erosion and oxidation. Considering that most of the degradation introduced during erosion results from the removal of oxide scale, systems with high scaling rate can develop new oxide soon after the scale is removed, which leads to a rapid cycling of removal and regrowth of oxide and gives a high degradation rate. In the systems with low scaling rates, the oxide scale is removed and regrown at a lower rate. A large fraction of incident energy is absorbed in the substrate but it has been shown[1,19,20] that the degradation rate of the substrate is much lower than that of the scale. The overall degradation rate is, therefore, low.

Since the deformation induced by particle impact at 140 m/s extends to both the oxide scale and the substrate, both the degradation rate and the scaling rate, will be affected by the properties of the substrate and oxide scale as well as the degradation mechanisms. The data in Figure 22 also show that the degradation rate of the materials studied is higher at a higher temperature, 780°C, than at 600°C. Although the mechanical properties of the target such as its hardness and

16

ductility are important parameters in terms of the degradation rate of material, the degradation rates of an oxide or of a pure metal in the absence of oxidation have been found to decrease in magnitude when the temperature increases[1,21,22], which is opposite to the behavior observed in this study. Hence the results shown here must be influenced by the effect of oxidation, the rate of which increases with temperature. The dependence of erosion rate with temperature has been studied by Levy et al[23]. Using an undried nitrogen stream, it was found that the erosion rates of various steels decrease when the temperature increases from room temperature to an intermediate temperature between 400 and 500°C. The erosion rates of these steels then increase significantly when the temperature is increased from the intermediate temperatures to 900°C. The initial fall in erosion rate is thought to occur because the ductility of the target increases with temperature and it absorbs more energy due to plastic deformation. At higher temperatures, even in an undried nitrogen stream, the oxidation process becomes effective leading to the dramatic increase in the erosion rate at higher temperatures. These results indicate that oxidation can interact with erosion and result in a higher degradation rate than pure erosion of metal in the absence of oxidation. This has been shown in earlier publications[1,3]. The results also show that the erosion rate obtained from the oxidation affected erosion regime, in which the oxide scale is thin and may not be continuous, is higher than the erosion rate of metals in the absence of oxidation or the erosion rate of oxide under the same conditions. The results shown in Figure 22 are obtained in the oxidation affected erosion regime and it is clear that the degradation rate in this regime will increase with temperature due to the strong interaction between the erosion and oxidation processes.

17

CONCLUSIONS

1. The rate of removal of a volatile species is enhanced in fast flowing oxidizing gas streams and can lead to the formation of greatly modified and less protective scales.

2. Although the erosion and oxidation of alloys follows generally similar behavior to pure metals, additional factors such as the extension of the transient oxidation period and the modification of concentration profiles in the alloy at the alloy-scale interface also have a strong influence on the pattern and extent of degradation.

3. The type of oxide formed is controlled, to some extent, by the relative intensities of the erosion and oxidation components. In particular, a higher erosion erosion intensity tends to prevent the formation of a protective scale.

4. In all cases the interaction between erosion and oxidation of alloys leads to increased degradation rates.

REFERENCES

1. C. T. Kang, F. S. Pettit and N. Birks, "Mechanisms in the Simultaneous Erosion-Corrosion Attack of Nickel and Cobalt at High Temperatures", Met. Trans., (1987), Met. Trans. 18A, 1785-1803, (1987).

2. C. T. Kang, S. L. Chang, F. S. Pettit and N. Birks, "Synergism in The Degradation of Metals Exposed to Erosive High Temperature Oxidizing Atmospheres" in Proceedings, Third Berkeley Conf. on Corrosion-Erosion-Wear of Materials at Elevated Temperatures, Ed. by Levy, A. V., Berkeley, CA, Jan. 1986.

3. S. L. Chang, N. Birks and F. S. Pettit, Interaction Between Erosion and High Temperature Corrosion of Metals: The Erosion Enhanced Oxidation Regime, Appendix 4A, to be published.

4. S. L. Chang, N. Birks and F. S. Pettit, Effect of Angle of Incidence on the Combined Erosion-Oxidation Attack of Nickel and Cobalt, Appendix 4B, to be published.

5. C. T. Kang, F. S. Pettit and N. Birks., "Simultaneous Erosion and Oxidation of Nickel at High Temperature", Proc. Third Int. Conf. on Non-Stoichiometic Compounds, Penn State Univ., p. 411 (1985) Plenum Press, NY.

6. D. Caplan and M. Cohen, "The Volatilization of Chromium Oxide", Journal of the Electrochemical Society, Vol. 108, (1961), pp. 583-599.

7. W. C. Hagel, "Factors Controlling the High-Temperature Oxidation of Chromium", Transactions of the ASM, Vol. 56, (1963), pp. 583-599.

8. J. Stringer, B. A. Wilcox and R. I. Jaffee, "The High-Temperature Oxidation of Ni-20 wt.% Chromium Alloys Contining Dispersed Oxide Phases", Oxidation of Metals, Vol. 5, (1972), pp. 11-47.

9. R. T. Grimley, R. P. Burns and M. G. Inghram, "Thermodynamics of the Vaporization of Cr_2O_3: Dissociation Energies of CrO, CrO_2, and CrO_3", Journal of Chemical Physics, Vol. 34 (1961), pp. 664-667.

10. J. Stringer, "The Functional Form of Rate Curves for the High-Temperature Oxidation of Dispersio-Containing Alloys Forming Cr_2O_3 Scales", Oxidation of Metals, Vol. 5, (1972), pp. 49-58.

11. S. L. Chang, "The Interaction of High Temperature Erosion and Oxidation of Selected Metals and Alloys", Ph.D. dissertation, University of Pittsburgh (1987).

12. C. E. Lowell and W. A. Sanders, "Mach 1 Oxidation of Thoriaed Nickel Chromium at 1204°C (2200°F)", TN-D-6562, NASA, (1971).

13. M. J. Graham and M. Cohen, "On the Mechanism of Low-Temperature Oxidation (23°-450°C) of Polycrystalline Nickel", Journal of the Electrochemical Society, Vol. 119, (1972), pp. 879-882.

14. G. H. Geiger and D. R. Poirier, Transport Phenomena in Metallurgy, Addison-Wesley Publishing Co., (1980).

15. E. A. Gulbransen and G. H. Meier, "Thermochemical Stability Diagrams for Condensed Phases and Volatility Diagrams for Volatile Species Over Condensed Phases in Twenty Metal-Sulfur-Oxygen Systems Between 1150 and 1450°K", Under Contract No. DE-AC01-79-ET-13547, (May 1980).

16. S. L. Chang, "The Effects of Gas Velocity on the High Temperature Oxidation Characteriistics of Some Metals and Alloys", Master's thesis, University of Pittsburgh, (1984).

17. I. M. Hutchings and R. E. Winter, "Particle Erosion of Ductile Metals: A Mechanism of Material Removal", Wear, Vol. 27, (1974), pp. 121-128.

18. I. M. Hutchings, "Mechanisms of the Erosion of Metals by Solid Particles" in Erosion: Prevention and Useful Applications, W. F. Adler, ed., (1979), pp. 59-75.

19. I. G. Wright and V. Nagarajan and J. Stringer, "Observations on the Role of Oxide Scales in High-Temperature Erosion-Corrosion of Alloys", Oxidation of Metals, Vol. 25, (1986), pp. 175-199.

20. I. G. Wright and V. Nagarajan, Erosion Characteristics of High-Temperature Alloys at 760°C", Proc. UK Corrosion 1984, pp. 55-62, pub. Inst. of Corros. Sci. & Tech. (1984).

21. C. E. Smeltzer, M. E. Gulden and W. A. Compton, "Mechanisms of Metal Removal by Impacting Dust Particles", J. of Basic Engineering, Vol. 92 (1970), pp. 639-654.

22. N. Gat and W. Tabakoff, "Some Effects of Temperature on the Erosion of Metals", Wear, Vol. 50, (1978), pp. 85-94.

23. Intern. Conf. on Wear of Materials, "Elevated Temperature Erosion of Steels, A. Levy, J. Yan and J. Patterson", ASME, (1985) Vancouver, Canada.

Acknowledgement

Table 1: Chemical Compositions of the Alloys

	Co/Ni	Cr	Al	Y
Ni-30Cr	Base	28.76%	——	——
Ni-20Al	Base	——	21.82%	——
CoCrAlY	Base	22.18%	11.50%	0.17%
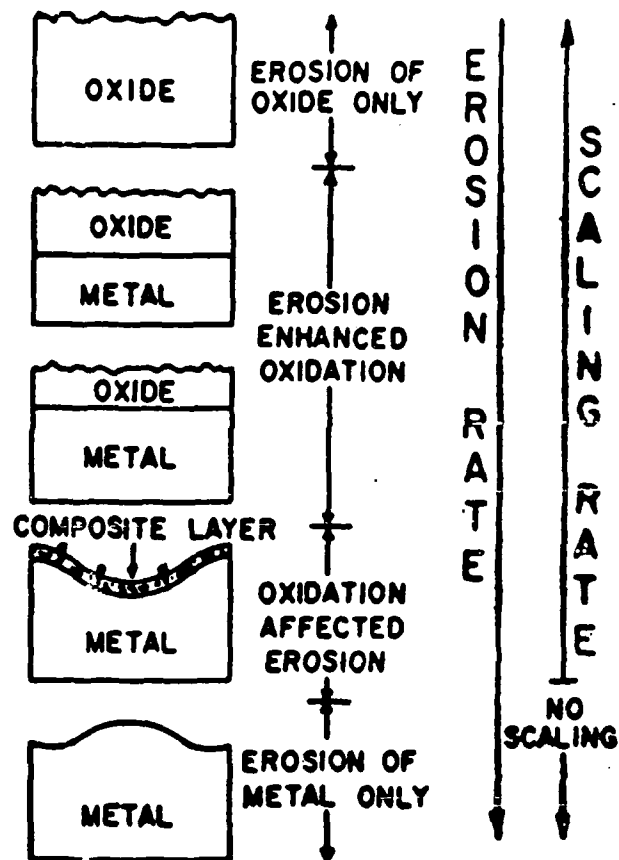
FIGURE 1.   Proposed regimes of interaction in the erosion-corrosion attack of metals.
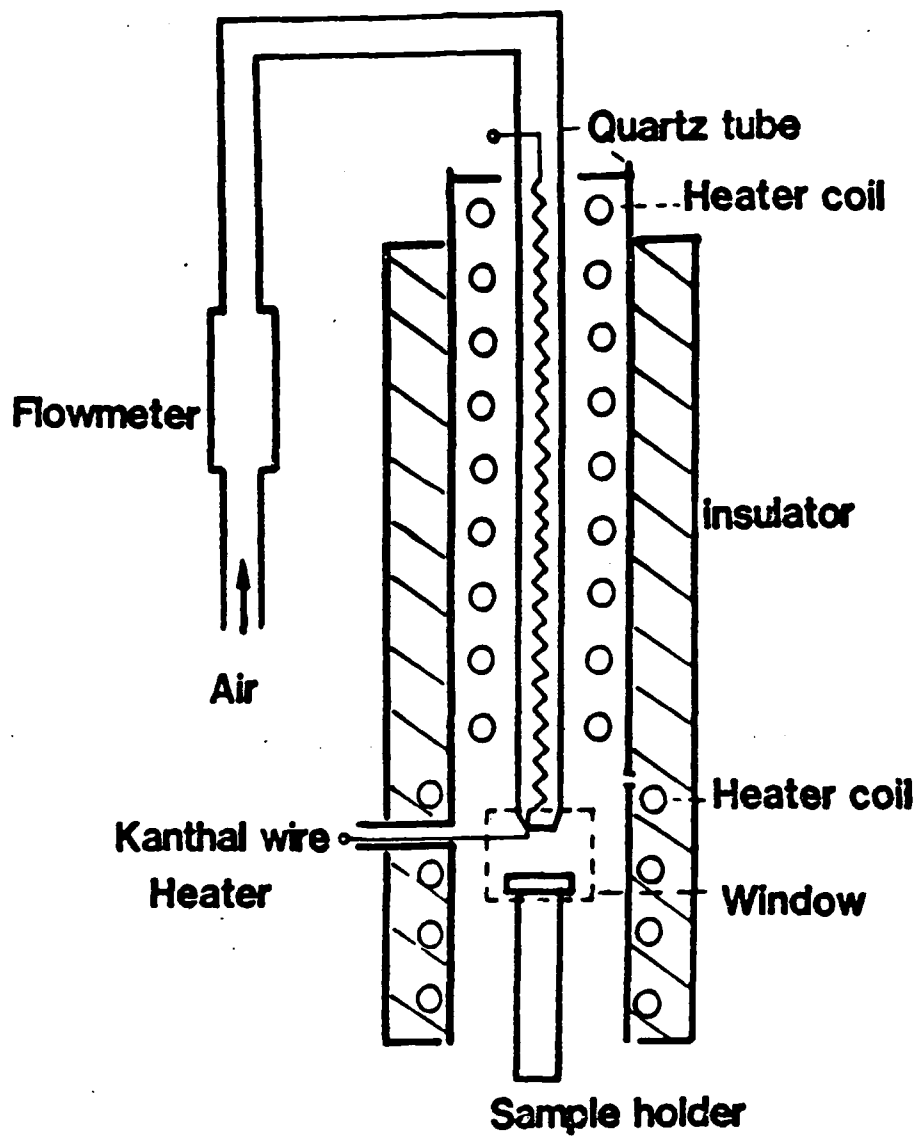
FIGURE 2. Diagram of apparatus used for dynamic oxidation experiments.
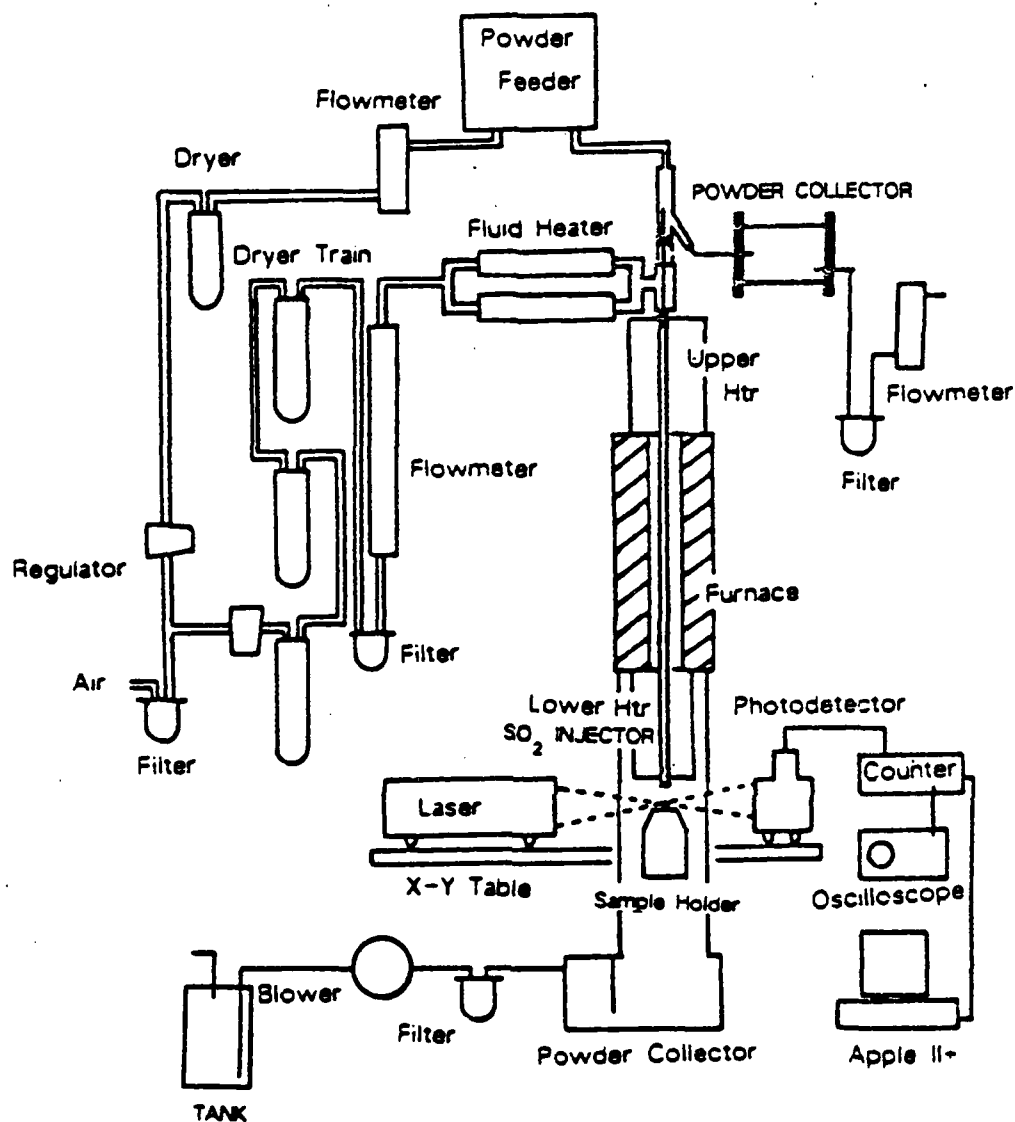
FIGURE 3. Diagram of apparatus used in studies of the erosion-oxidation of metals.

For Two Hrs.

25 µm
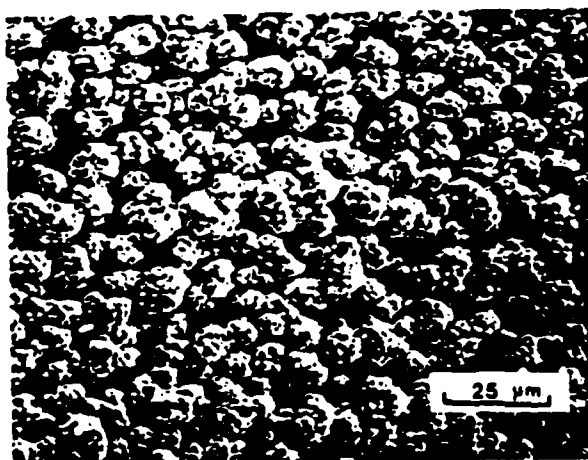
For One Week

FIGURE 4. Surface of MA754 specimen oxidized at 1100°C in still air.
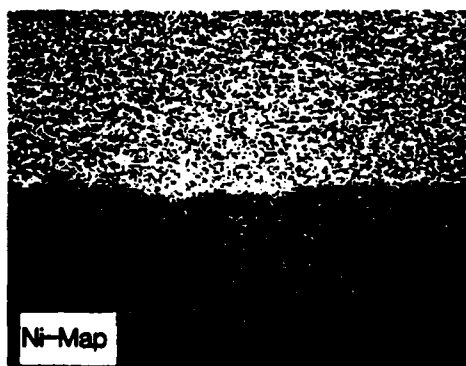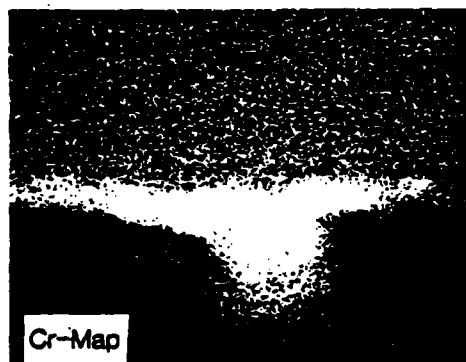
FIGURE 5. Cross section of MA754 specimen oxidized in still air for 168 hrs.
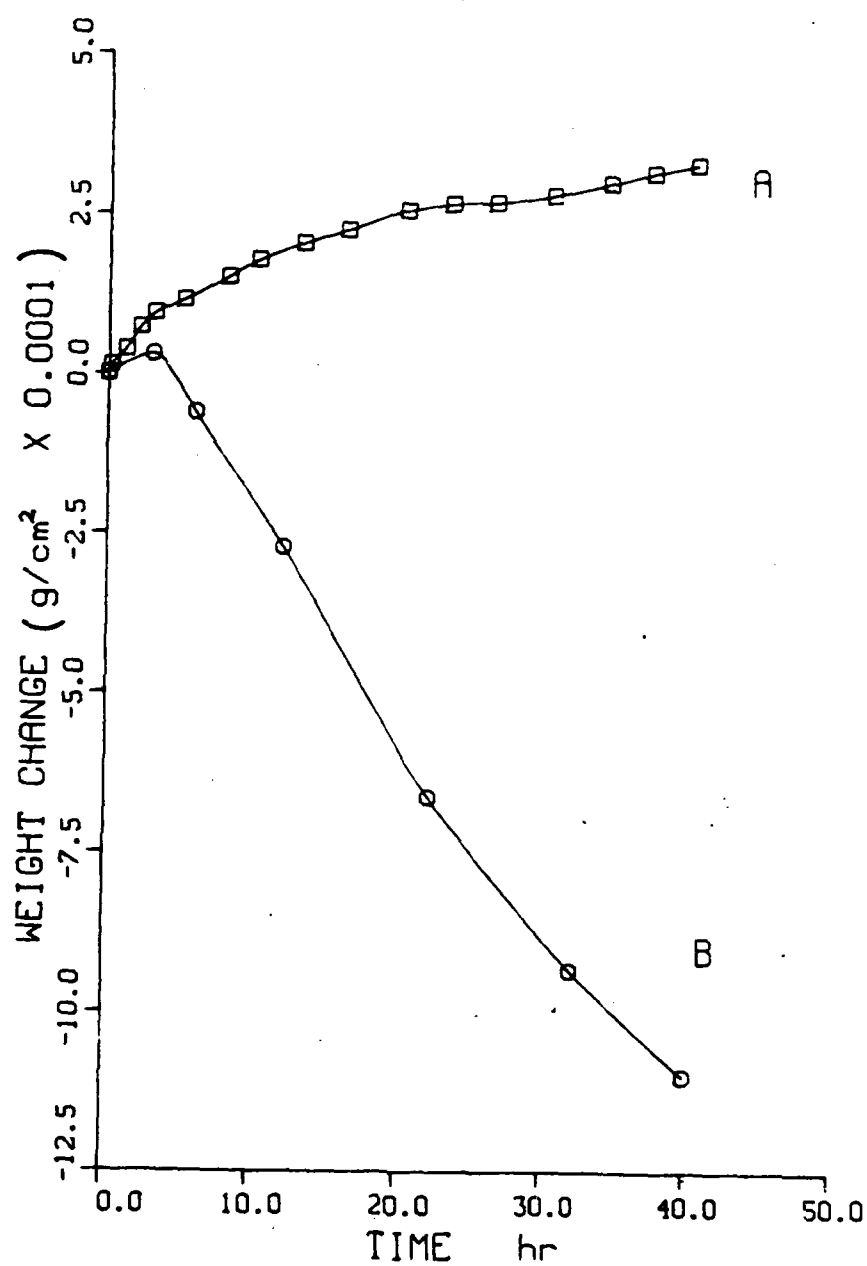
FIGURE 6. Weight change characteristics for MA754 specimen oxidized at 1100°C in (A) still air and (B) air flowing at 65 m/s.
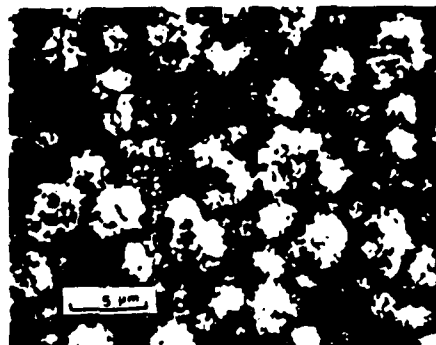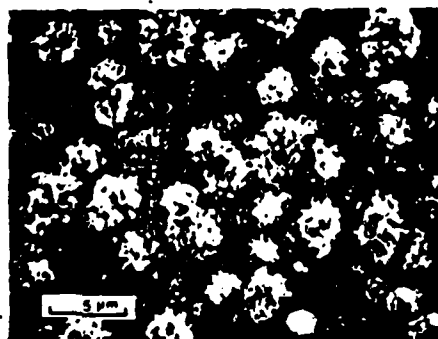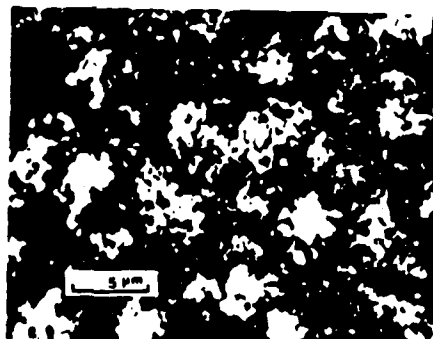
FIGURE 7. Surface of MA754 specimen exposed at 1100°C to an airstream flowing at 65 m/s.
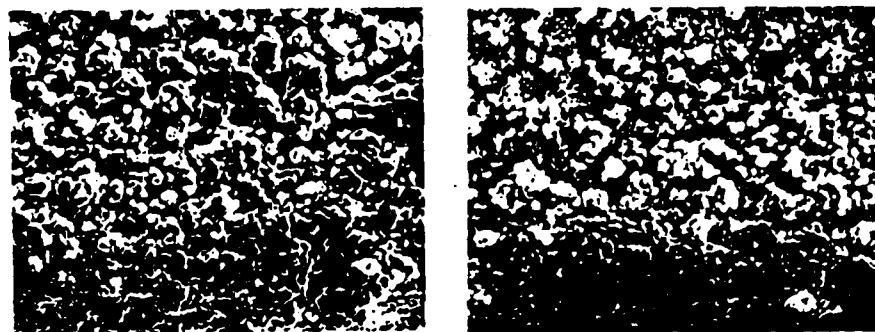
23 Hours LEADING EDGE
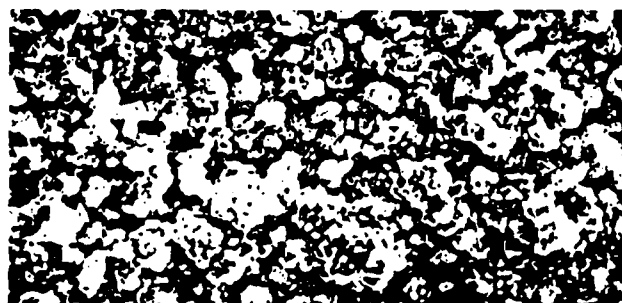
39.5 Hours

43 Hours 10 μm

FIGURE 8. Surface of MA754 specimen exposed at 1100°C to an airstream flowing at 65 m/s.
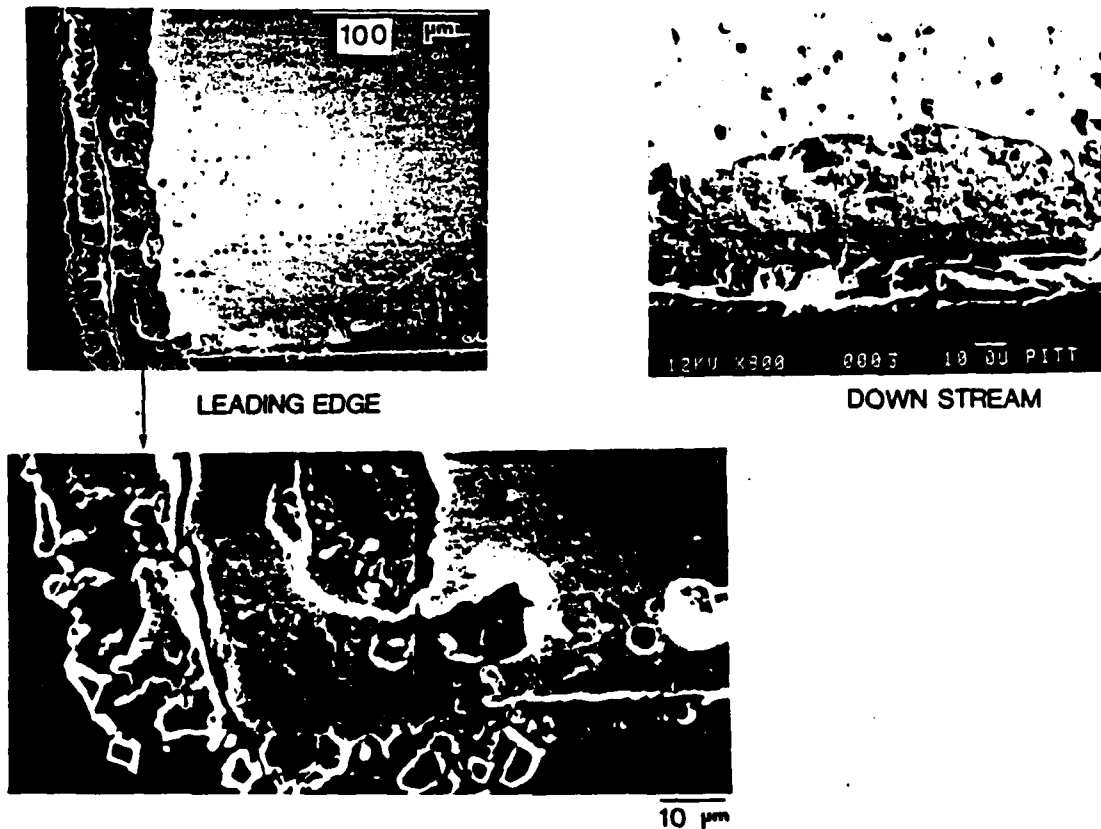
FIGURE 9. Cross section of MA754 specimen exposed at 1100°C for 88.5 hours to an airstream flowing at 65 m/s.

5 μm

Ni–Map

Cr–Map
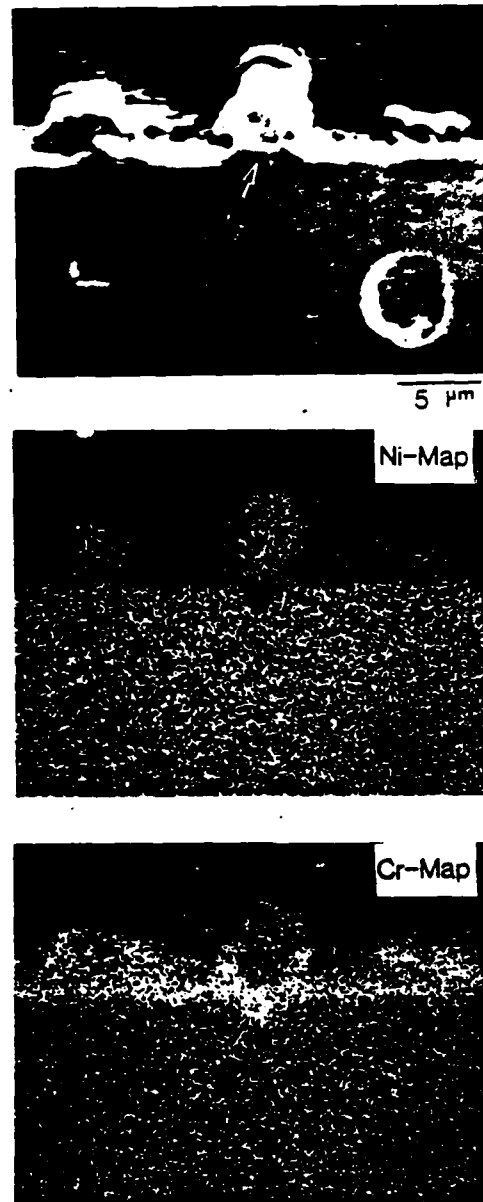
FIGURE 10. (a) Cross section taken close to the leading edge of an MA754 specimen exposed for 88.5 hours at 1100°C to an airstream flowing at 65 m/s.

$\overline{10 \ \mu m}$

Gr-Map

Ni-Map
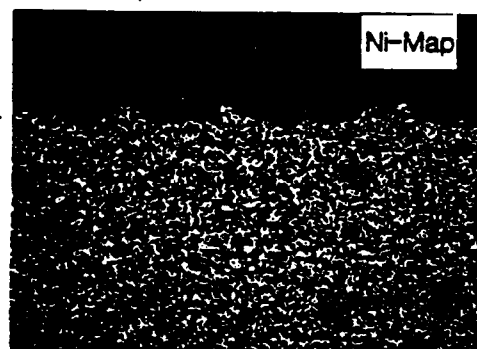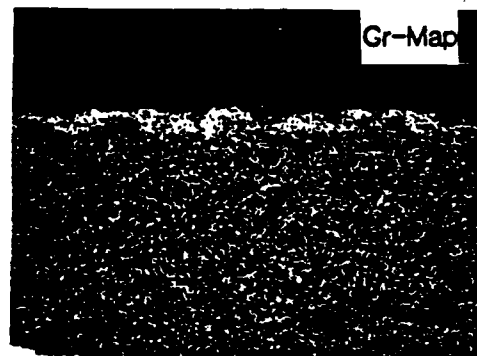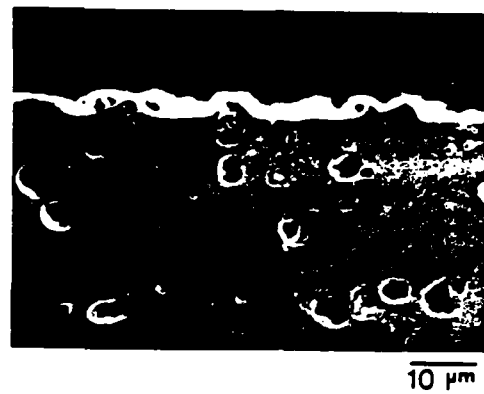
FIGURE 10 (b) Cross section taken down stream of the leading edge of an MA754 specimen exposed at 1100°C for 88.5 hours to an airstream flowing at 65 m/s.

(a)

V_0

laminar
boundary layer

turbulent boundary layer

laminar sublayer

1

(b)

INTENSITY

A

thickness of
the boundary layer

B

flux of Cr evaporated
from the scale surface

LENGTH OF THE SPECIMEN
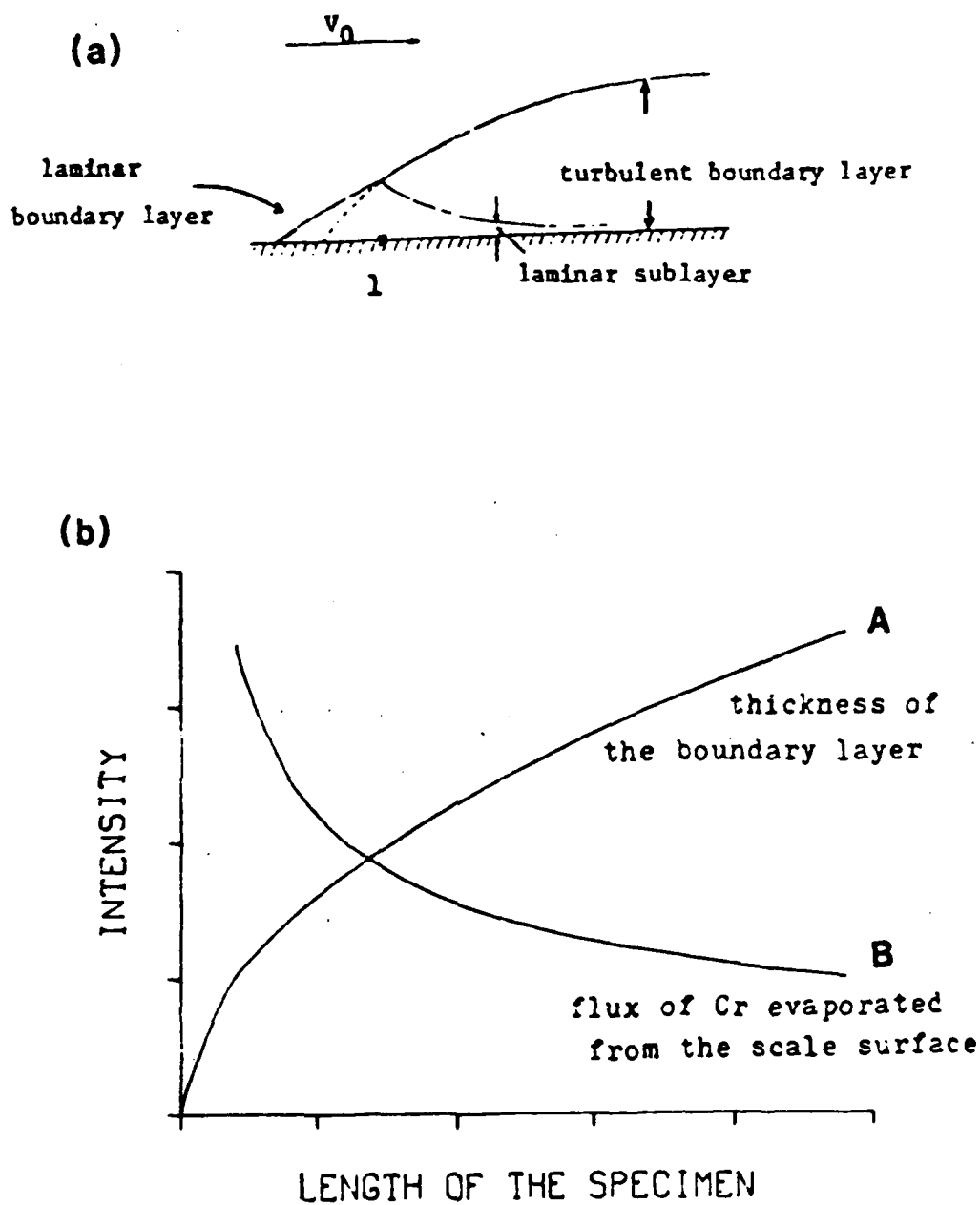
FIGURE 11.   (a) Variation in boundary layer thickness over a flat slab.

(b) Boundary layer thickness and CrO_3 flux variations
along the specimen length.
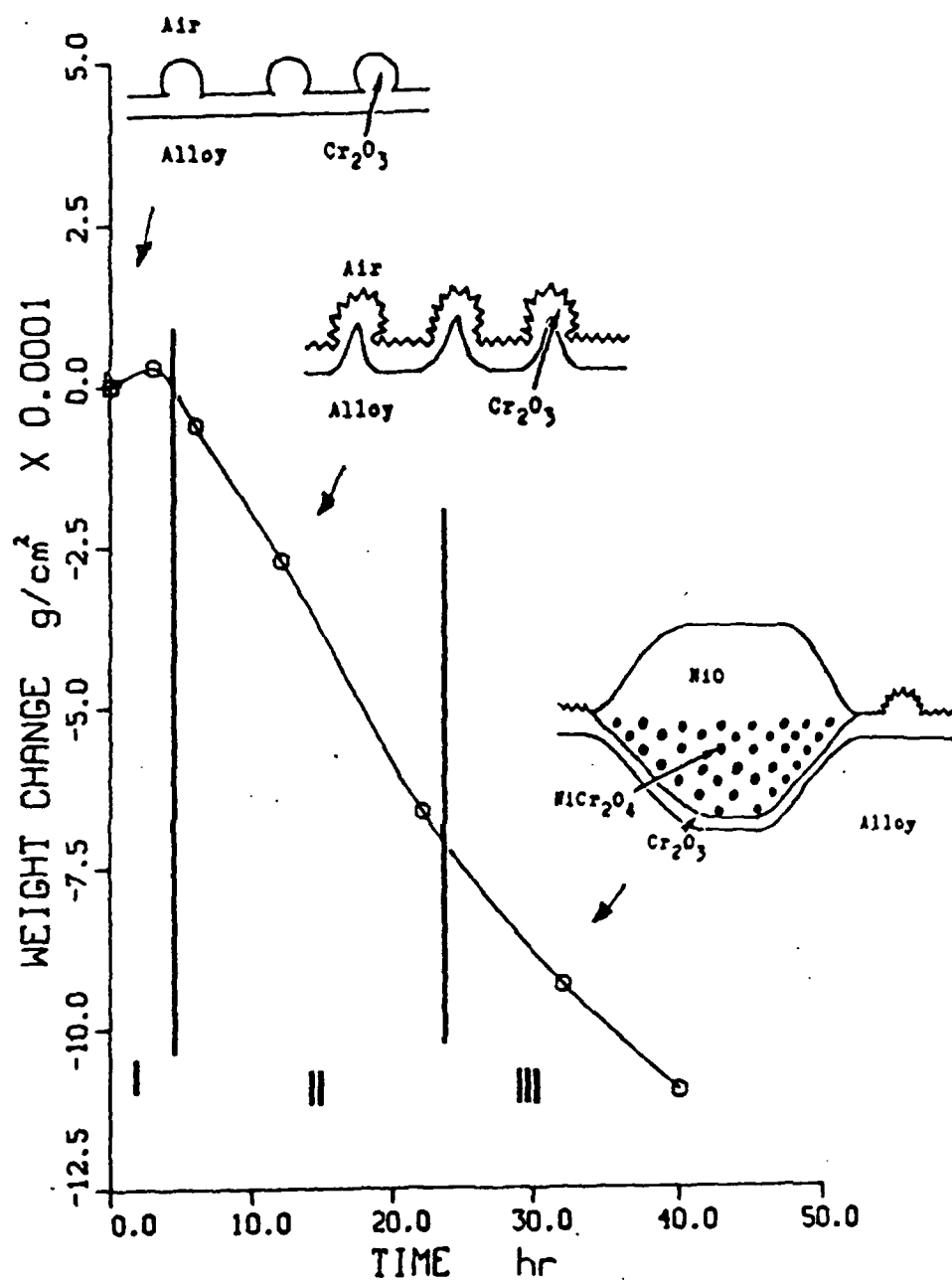
FIGURE 12. Weight change characteristics and associated microstructures in the progressive oxidation of chromia forming alloys under dynamic oxidation at high temperature.
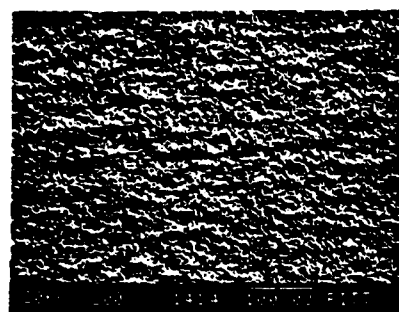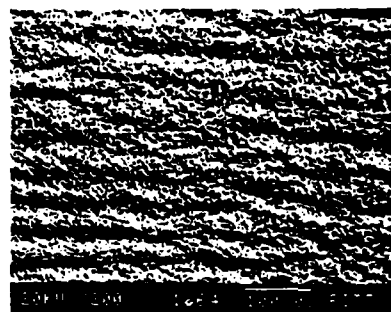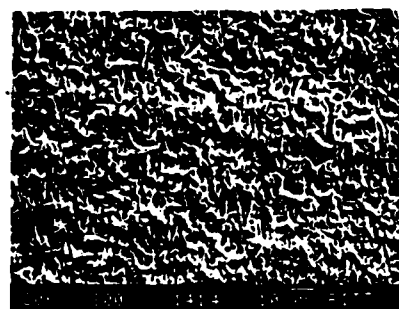
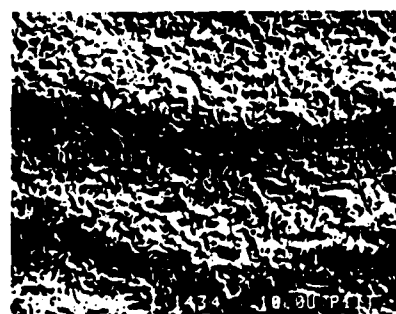**FIGURE 13.** Surface morphology of an MA754 specimen exposed at 780°C to erosion-oxidation in an airstream flowing at 140 m/s for 120 minutes at (a) 15°, (b) 30°, (c) 60° and (d) 90° incidence.
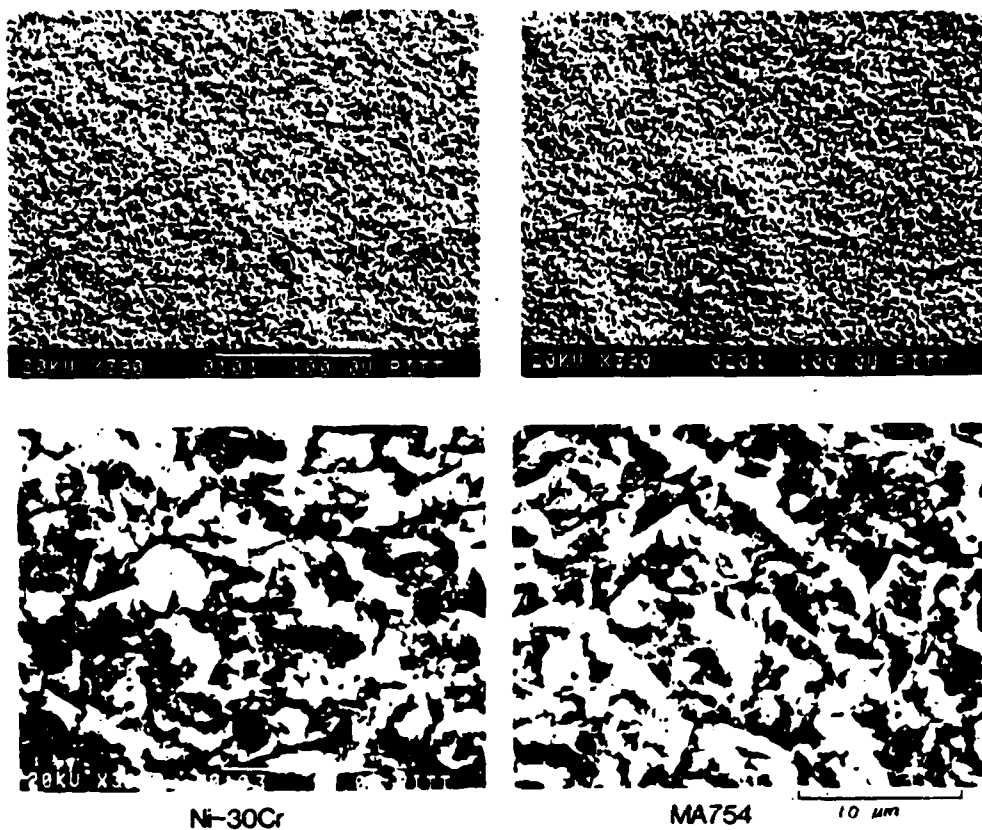
FIGURE 14. Surface morphologies of MA754 and Ni30Cr specimens exposed at 800°C to erosion-oxidation in an airstream flowing at 120 m/s and 90° incidence.

Erosion of MA754
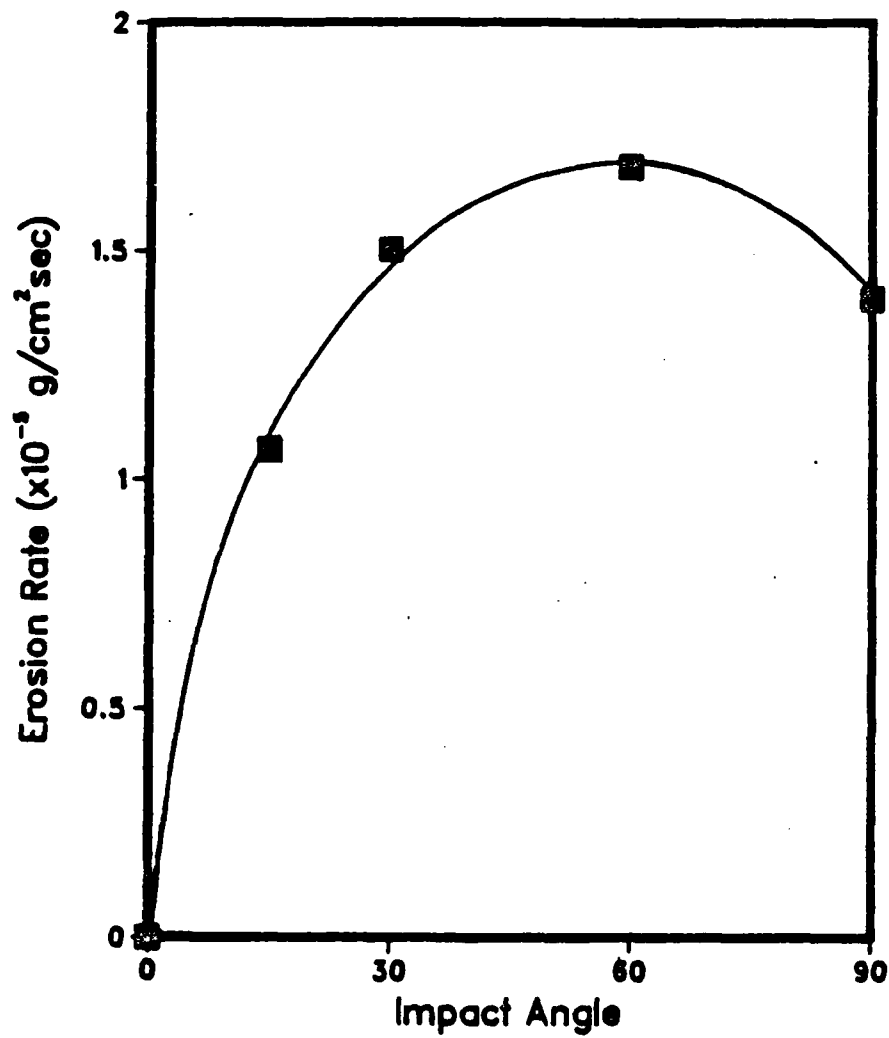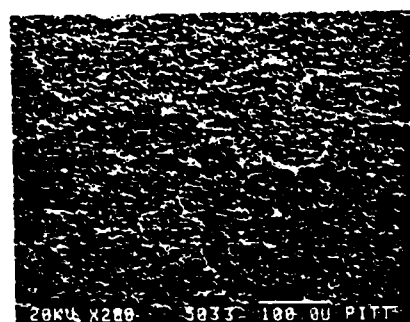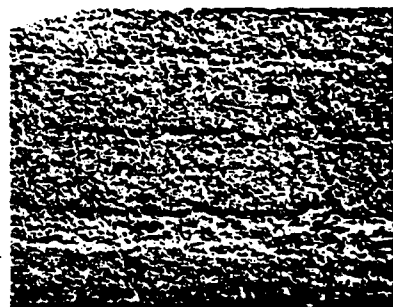## at 780°C and 140 m/s

FIGURE 15. Angular dependence of the degradation rate of MA754 exposed at 780°C to erosion-oxidation in an airstream flowing at 140 m/s.

(a) 60min   (b) 120min

FIGURE 16. Surface morphology of an MA754 specimen exposed at 780°C to erosion-oxidation in an airstream flowing at 50 m/s and 30° incidence for (a) 60 minutes and (b) 120 minutes.
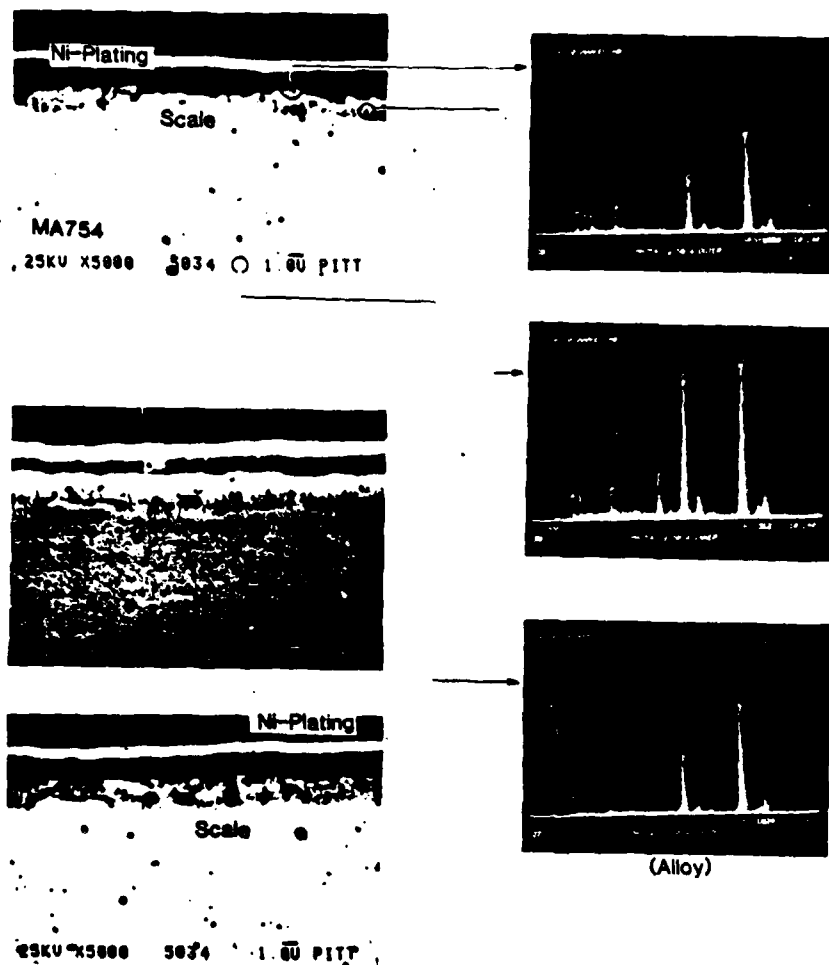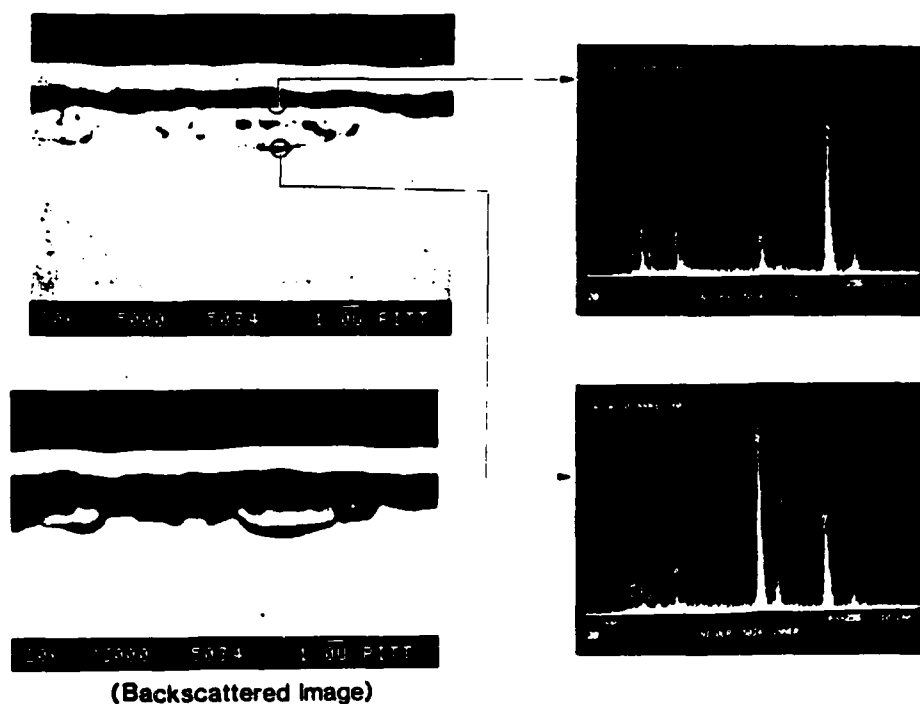
FIGURE 17. Cross section of an MA754 specimen exposed at 780°C to erosion-oxidation in an airstream flowing at 50 m/s for 120 minutes.

(Backscattered Image)

FIGURE 18. Cross section of a Ni30Cr specimen exposed at 780°C to erosion-oxidation for 100 minutes followed by oxidation for 20 minutes in an airstream flowing at 50 m/s.
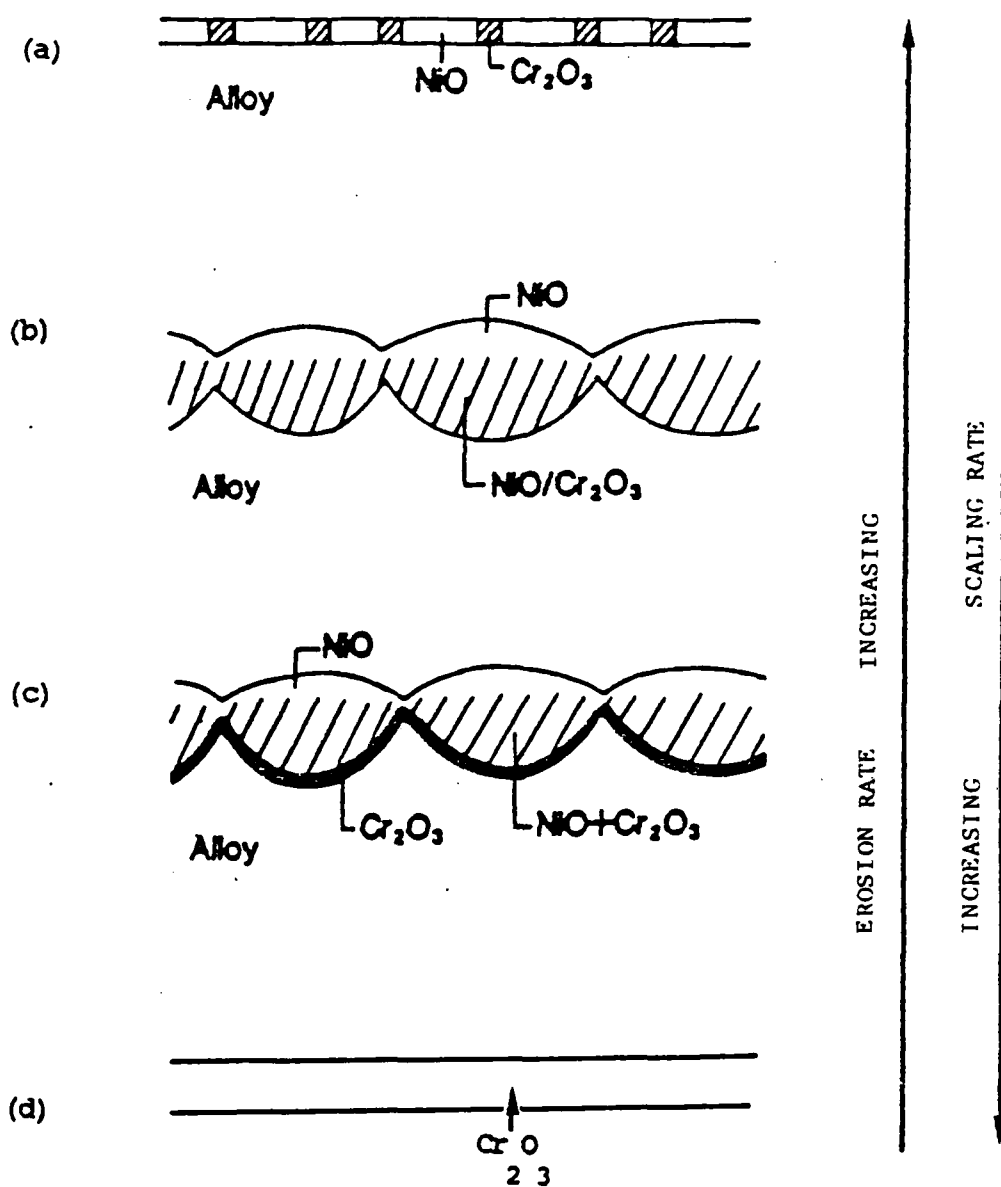
FIGURE 19. Diagram illustrating stages in scale development during the erosion-oxidation of Ni-Cr alloys.

Co22Cr 10Al0.2Y — Ni20Al
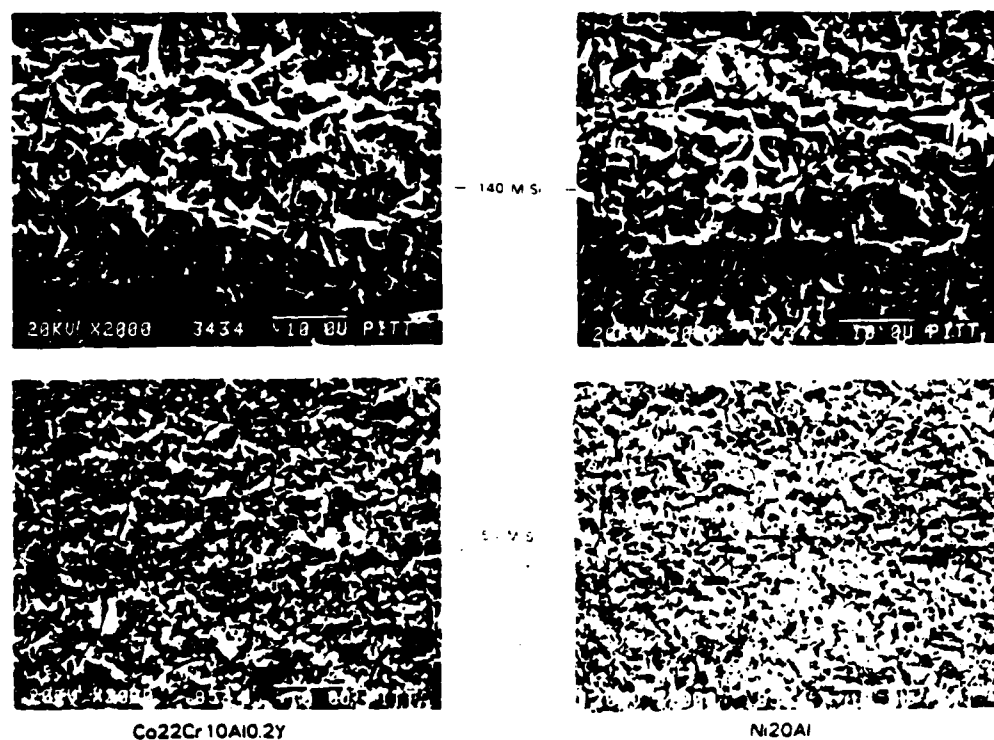
FIGURE 20. Surface morphologies of CoCrAlY and Ni20Al after exposure at 780°C for 120 minutes to erosion-oxidation in an airstream flowing at 50 m/s and 140 m/s at 30° incidence.
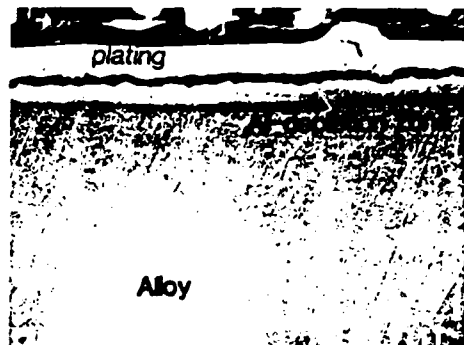
FIGURE 21. Cross sections of CoCrAlY and Ni20Al exposed at 780°C to erosion-oxidation in an airstream flowing at 30° incidence, showing the Al-depletion zone near the alloy-scale interface.

Erosion and Oxidation
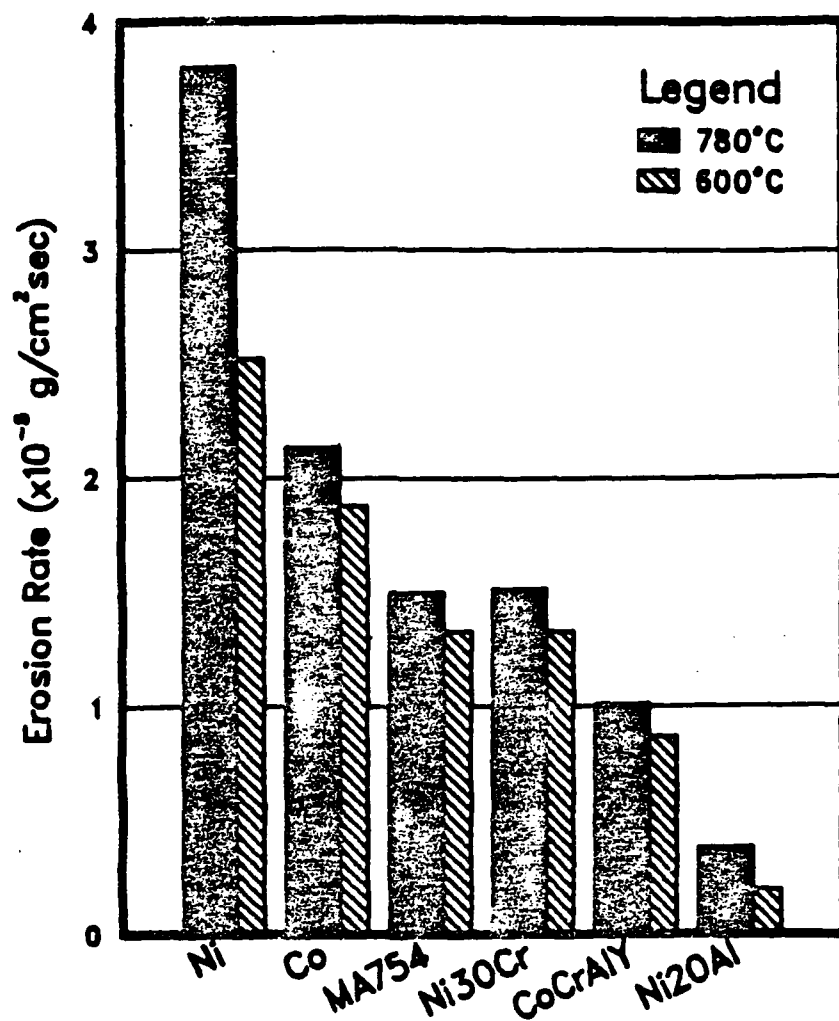## at 140 m/s and 30°

FIGURE 22. Summary showing the relative rates of degradation of different metals and alloys under combined erosion-oxidation attack.

THE EROSION-CORROSION BEHAVIOR OF
NICKEL IN MIXED OXIDANT ATMOSPHERES

D. M. Rishel, F. S. Pettit and N. Birks

Department of Materials Science and Engineering

848 Benedum Hall

University of Pittsburgh

Pittsburgh, Pa. 15261

ABSTRACT

Nickel-270 (Ni-99.98, C-0.01, Mn-0.003, balance < 0.007) specimens were exposed to erosion-corrosion conditions in an alumina particle ($20\mu m$ in size) laden gas stream at 70 m/s, normal incident angle, 600°C and to differing degrees of erosion and corrosion severity. The level of erosive severity was adjusted by setting the alumina particle loading rates to three different levels subsequently referred to as low, medium and high; whereas the degree of corrosivity was controlled by the atmosphere to which specimens were subjected. The atmospheres used included air, air + 1730 ppm SO_2, and air + 1730 ppm SO_2/42 ppm SO_3.

It was found that definite interaction regimes existed between erosion and corrosion, depending upon the specific atmosphere and particle loading rate. For instance, compared to that of atmospheres containing air and air + SO_2, atmospheres of air + SO_2/SO_3 were found to significantly increase the corrosion rate of Ni-270, and thus influence its erosion-corrosion response. Examination of the effect of particle loading rates, revealed that relative to atmospheres of air and air + SO_2, erosion-corrosion of nickel in air + SO_2/SO_3 under high particle loading rates exhibited a large weight loss, whereas for low and medium particle loading rates, relatively large weight gains were noted.

Key Words; erosion-corrosion, nickel, sufidation/oxidation, mixed oxidants.

INTRODUCTION

In the operation of gas turbines and energy conversion processes such as coal gasification and fluidized bed combustors, the degradation of construction and component materials due to combined erosion and corrosion (henceforth referred to as erosion-corrosion) is a real and considerable problem.[1-4] This is primarily due to the fact, that the protective oxide scale developed in non-erosive high temperature conditions is severely damaged when impacted by erodent particles. The degradation which occurs however, as shown by a number of investigations[5-10], is more complicated than simple scale removal. Instead a complex interaction exists between the erosion and corrosion processes.

Kang, Pettit and Birks[8] found that the high temperature erosion-corrosion process for pure metals involves several interaction regimes. Depending upon the relative severity of erosion and corrosion, these interaction regimes are, (1) pure erosion, (2) erosion enhanced oxidation and (3) oxidation affected erosion, as shown in Figure 1.

The pure erosion of oxide regime encompasses the situation where the oxidation rate is rapid and scale damage or removal occurs along lines similar to that found for the erosion of ductile and brittle materials at room temperature.[11] As shown in Figure 1 the pure erosion of oxide regime may dominate for erosion-corrosion of an oxide at high temperatures whereas pure erosion of metal represents erosion-corrosion of a pure metal when exposed to low temperatures and/or non-oxidizing environments.

The erosion enhanced oxidation regime dominates under conditions where a metal sample is subjected to a high temperature, erodent laden, oxidizing environment. In this situation, the oxide scale develops under two opposing processes; one is growth due to corrosion and the other is removal due to erosion. Under certain circumstances and at the start of the erosion-corrosion process, if the corrosion rate exceeds the erosion rate the scale will grow to a certain thickness. As the scale thickens however, its rate of growth decreases (due to the reduced transport through a thick scale), and a point is reached whereby the growth and erosion rates are equal. When this occurs, the scale has achieved a "steady state" thickness.

When a metal is subjected to a high temperature erodent laden oxidizing environment, but where either the corrosion rate is relatively low (i.e. the parabolic rate constant is small) or the erosion rate is high, the oxidation affected erosion regime dominates. The existence of this regime, as shown by Kang et. al.[8], occurred when a slowly oxidizing metal such as pure Ni is exposed to an erodent laden airstream at 800°C and 140 m/s. In this situation, the erosive stream thinned or removed the slowly growing oxide scale to the point where deformation of the substrate resulted. When this occurred, the formation of a series of undulations or moguls was noted. An additional feature of this regime is that erodent particles can penetrate the thin oxide and embed into the metal substrate. Although only a relatively small amount of oxide is observed to form, the presence of an oxidizing atmosphere, has an important effect on the measured weight loss. For instance it was found[8] that for nickel exposed to erosion at 140 m/s in a high temperature, (800°C), non-oxidizing environment such as nitrogen, the measured weight loss is over an order of magnitude lower than in oxidizing atmospheres such as air.

The work of Hogmark et. al.[10] proposes degradation regimes which are in many ways similar to those proposed by Kang et. al.[8] These workers looked upon the erosion-corrosion of a metal, parameterized in terms of corrosive aggressiveness versus erosive aggressiveness, as a process which can be divided into six regimes. Unlike Kang[8] however, where spallation was not observed for the experimental conditions used, Hogmark[10], considered flaking or spallation of the oxide scale to play an important role. For instance, in their first regime, pure corrosion, material removal is considered to be in the form of flaking and is a result of either a combination of poor adhesion between the oxide layer and the substrate or internal stresses. In the second regime, erosion affected corrosion, material removal by flaking is influenced or enhanced by a relatively mild erosion component. In regime number three, erosion of the corrosive film without flaking occurs either by brittle or ductile mechanisms. Regime number four is entered when local flaking of the oxide scale at individual impact sites is observed. The dimensions of the individual craters is of the same order of magnitude as the instantaneous layer thickness. In the fifth regime, simultaneous erosion of the oxide layer and metallic substrate occur. This is due to the fact that, when erosion dominates over

corrosion, impinging particles penetrate into the substrate and detach oxide as well as metallic fragments. The last regime, pure erosion, is restricted to conditions of no corrosion or in situations where the oxide thickness is much less than the average depth of particle penetration, and where the mechanisms of material removal occur, depending upon the material, in a ductile or brittle manner.

Of the six regimes discussed, a dramatic increase in the wear rate is expected in the erosive-corrosive conditions of regimes four and five. This is particularly true if the adhesion of the oxide layer is poor.

In the present work the major emphasis was to examine the effects of SO_2/SO_3 on the erosion behavior of nickel and it will be shown that, depending upon the experimental conditions, the observed behavior generally falls into one of the regimes proposed by either Kang et. al.[8] or Hogmark et. al.[10]

EXPERIMENTAL

Ni-270 (Ni-99.98, C-0.01, Mn-0.003, balance < 0.007)[*] plate was fabricated into coupons nominally 8 x 8 x 2.5 mm in size. A 1 mm diameter hole (≈5 mm in depth) was drilled into one edge of the specimen providing a means of monitoring temperature with a K-type thermocouple. To measure the kinetics of the erosion-corrosion process, any weight change due to corrosion was minimized on the five sides of the specimen not directly exposed to the erosive stream by an applied aluminide coating. The specimen surface exposed to the erosive stream was ground down to a 600 grit finish with SiC paper and cleansed in methanol.

Samples were exposed in a modified version of the apparatus previously described by Kang et. al.[8] Major changes included the addition of a sample holder to provide 4 degrees of motion (x,y and z + rotation) and a means by which the sulfurous gases used in this research are introduced, contained and removed. An integral part of the containment/removal system is a regenerative blower manufactured by EG & G Rotron. This device not only conveys the carrier gas which is used to accelerate the erodent particles, but also places a

---

[*]   Metal composition is given is weight percent.

slight negative pressure on the containment system thus preventing the leakage of sulfurous gases into the laboratory environment. After impinging the exposed specimen, the exhausted sulfur bearing carrier gas is discharged into a water filled, pH adjusted, 55 gallon barrel where complete removal of the SO_2 and SO_3 is accomplished. A schematic of the apparatus is shown in Figure 2.

In order to prevent its contamination and degradation, sulfur dioxide is introduced into the main carrier gas stream at the end of the acceleration tube by means of a device referred to as the SO_2 injector, shown in Figure 3. Although filled with platinum foil and wire in order to catalyze the reaction $SO_2 + 1/2O_2 = SO_3$, it has been found, through measurement, that full equilibrium is not achieved. The gas analysis technique used to measure the SO_2 and SO_3 concentrations is described in Appendix A of reference 12 and involves the condensation/absorption of the SO_3/SO_2 gases and the titration of the resulting SO_4^- ions.

The research program followed was divided into two phases. In the first phase, erosion-corrosion experiments were conducted at 600°C, 70 m/s, and at normal incidence with 20µm alumina particles in atmospheres containing air/SO_2/SO_3. The particle loading rate employed, was about 1100 mg/min., whereas the SO_2/SO_3 concentrations were 1730 and 42 ppm respectively. Additional erosion-corrosion tests in air and corrosion tests in air + SO_2/SO_3(using the above mentioned concentrations) were conducted in order to provide a baseline with which to gauge the erosion-corrosion degradation behavior of air + SO_2/SO_3 environments. Specimen exposure intervals of 15, 30, 45, 60, 75, 90 and 120 minutes were selected in order to determine the weight change and scale growth kinetics.

The purpose to the second phase of this study was to supplement the results of phase I by providing a comparison of the erosion-corrosion behavior of nickel under conditions of varying erosivity and corrosivity. Erosivity was varied was through adjustment of the particle loading rates, while the corrosivity or corrosion rates were adjusted by changing the atmospheres to which samples were subjected. The three particle loading rates employed (as measured) were approximately 280, 700, and 1140 mg/min. For the sake of brevity these loading rates were designated as low, medium and high, respectively. The three atmospheres to which specimens were exposed

included, (a) air, (b) air + SO_2(1730 ppm)(no SO_3) and (c) air + SO_2/SO_3(1730 ppm/42 ppm). Since it was desired in Phase II to only compare the effects due to variations in erosive and corrosive conditions, specimen exposures were held constant at 30 minute intervals.

Exposed specimens were weighed using an analytical balance with an accuracy of 0.1 mg and were examined by a variety of techniques. Examination of the surface morphologies and cross-sectional features was conducted by both SEM/EDAX and optical microscopy. Phases within the bulk of the corrosion product were determined by X-Ray diffraction, while the phases or layers on the specimen surface were examined by ESCA.

RESULTS AND DISCUSSION

Erosion-corrosion in air

The surface morphologies for a nickel sample exposed to erosion-corrosion in air at 600°C, 70 m/s, 90° incidence angles and high particle loading rates, for 30 minutes is shown in Figure 4. As seen in this figure moguls have developed. With the exception that mogul development is less pronounced, a similar observation was noted for specimens exposed to the same conditions above, but at low and medium loading rates. As explained by Kang[13], the advent of mogul formation is related to the total number of impact events. Since at the low and medium particle loading rates less impacts per unit time have occurred, it is reasoned that the necessary number of impacts for mogul formation have not yet been attained after 30 minutes exposure:

Cross-sections taken near the center of a specimen exposed for 30 minutes, to the above mentioned conditions, as shown in Figure 5, illustrate that the surface layer is comprised of a combination of oxide, extruded nickel and embedded alumina fragments. This layer is referred to as a composite layer[8]. A similar feature, was also noted for both low and medium particle loading rates.

From the definition described earlier, these observations indicate that the erosion-corrosion process for nickel in air, was in the oxidation affected erosion regime for all the particle loading rates studied.

Erosion-corrosion in air + SO₂

The surface morphological features for nickel specimens exposed to erosion-corrosion in air + SO_2(1730 ppm) atmospheres at 600°C, 70 m/s, normal incidence angles and at low, medium and high particle loading rates, for 30 minutes all exhibit a mogul like appearance. At high magnification as in Figure 6, the surface is seen to be highly jagged, deformed and, in many regards similar to that observed for specimens subjected to erosion-corrosion in air, indicating that the erosion-corrosion behavior of nickel in air + SO_2, is similar to that which occurs in the oxidation affected erosion regime.

However, when the specimens are viewed in section a different picture emerges. For erosion-corrosion in air + SO_2 at low and medium particle loading rates, rather than exhibiting a thin composite layer as seen for erosion-corrosion in air, a relatively thick($\approx 3\mu m$) continuous scale was noted. This is illustrated in Figure 7, for the case of erosion-corrosion in air + SO_2 at medium particle.

On the other hand, for exposures using high particle loading rates as shown in Figure 8 a composite layer was developed.

It is important to note, that as compared to erosion-corrosion in air, the presence of SO_2 was found to promote the corrosion of nickel, as evidenced by the thick scales found for low and medium particle loading rate conditions. In addition, X-Ray diffraction results showed stronger NiO and weaker Ni peaks as compared to samples exposed to erosion-corrosion in air. In addition, one Ni_3S_2 weak (205) peak was observed.

These observations indicate that, for erosion-corrosion in air + SO_2, the material response may fall into two regimes. In the case of low and medium particle loading rates, since a relatively thick scale developed, the material response may be described as belonging in the erosion enhanced oxidation regime.

On the other hand, since both a composite layer and a heavily deformed substrate was observed for exposures in air + SO_2 under high particle loading rates, the erosion-corrosion response of nickel is typical of that described by the oxidation affected erosion regime.

Erosion-corrosion in air + SO₂/SO₃

Of the gaseous atmospheres studied, the erosion-corrosion response of nickel in air + SO_2/SO_3(1730 ppm/42 ppm) at 600°C, 70 m/s, normal incidence angles and at low, medium and high particle loading rates is perhaps the most interesting. For instance, when exposed to these atmospheres, the resulting scale morphologies and measured weight changes have been found to be very sensitive to the particle loading rate. Figures 9 and 10 illustrate the surface morphological features for specimens exposed to low and medium particle loading rate conditions, respectively. These micrographs differ from those observed for erosion-corrosion in air and air + SO_2, in that the surface is almost flat. This implies that, due to the existence of a relatively thick scale, the substrate is not severely deformed. In addition, Figures 9 and 10 show that for both low and medium particle loading rate conditions, numerous and relatively large craters are observed.

The resulting scale thickness for specimens exposed to atmospheres containing air + SO_2/SO_3 for low and medium particle loading rates can be seen in the cross-sectional views illustrated in Figures 11 and 12 respectively. The scale thickness of the low particle loading rate condition is about 40μm whereas for medium particle loading rates the measured thickness is about 30μm. These scale thicknesses are between 1.5 to 2 times greater than that developed for specimens (not shown) when exposed to a particle free, flowing air + SO_2/SO_3 atmosphere at 600°C, 70 m/s for 30 minutes. Figures 11 and 12 also show that a Ni_3S_2 layer (as determined by X-Ray diffraction and EDAX), approximately 3-4μm thick was formed at the metal scale interface.

For erosion-corrosion with high particle loading rates, the specimen surface morphology of a specimen exposed for 30 minutes as shown in Figure 13 is radically different. As can be seen, the center of the specimen appears to be very heavily deformed or degraded. This deformation or degradation "signature" however is not in the same as that observed for erosion-corrosion in air, where moguls developed. Close inspection reveals that in and around the specimen center, numerous craters or spallation sites exist. Under this particle loading rate condition, the occurrence of spallation was noted to be an important feature regardless of the exposure interval. For example Figure 14, illustrates the occurrence of spallation on a specimen

exposed for 120 minutes. Spall sizes are generally similar to that of the erodent particles, (i.e. 10-30µm). Examination of the specimen periphery however, (see Figure 13) reveals that the surface is covered with an apparently thick scale, pockmarked with craters, about 100µm in diameter. This feature is in many regards similar to that observed for erosion-corrosion in air + SO_2/SO_3 atmospheres with low and medium particle loading rate conditions. This set of features: a heavily degraded specimen center with a thick scale covering the periphery (labeled with arrows in Figure 13), is termed the "rim effect".

Initially it was thought that the rim effect was an artifact due to the similarity in size of the specimen and the projected cross-sectional area of the SO_2 injector nozzle. It was reasoned that, since the velocity of the erodent particles exiting near the nozzle wall, (as determined by Laser Doppler Velocimetry), was lower than that of the particles exiting near the nozzle center-line, not as much energy was available to damage the specimen near its periphery as in the center. Experiments using specimens (5.5mm square), smaller than the projected cross-sectional area of the SO_2 injector nozzle, were carried out but gave the same results as large specimens in that a rim was formed. This rim effect may in part be explained by aerodynamic influences. First it has been shown by Laitone[14], that for a high velocity two phase fluid impinging a flat object at normal angles, a significant deflection of the particles, (more pronounced at the specimen edge), from the initial straight-line trajectory may occur as the particles near the specimen surface. Some of the factors influencing this deflection are velocity, temperature and particle size. It is not known however, that for the conditions used in these experiments whether 20µm Al_2O_3 particles will experience a significant deflection. A second aerodynamic factor may arise if it is considered that the incoming partricles are be deflected by rebounding particles and/or target debris. This is suggested by the experimental observation that the rim effect is only noted when large weight losses were recorded, (i.e. conditions for which a large amount of target debris is ejected). Assuming that spallation is more likely to occur under normal incidence impacts (as observed near the specimen center.), it is reasoned that, due to the significant deflection near the specimen periphery, particles are more likely to cause cutting or plowing of the oxide there than to cause spallation.

A cross-sectional view of a specimen exposed, for 90 minutes, to a high particle loading rate condition is shown in Figure 15. This figure illustrates that, in the central, more heavily deformed region of the sample the scale has a thickness of about 2-3μm, (Figure 15(a)), becoming thicker towards the specimen periphery, (Figure 15(b-c)). The white areas within the scale seen in the optical micrographs have been determined to be Ni_3S_2. It was observed that, for all exposure times, the scale near the specimen center maintained a constant thickness of ≈2-3μm whereas around the specimen periphery, the scale thickness increased with time. The scale formed under high particle loading rate conditions was also found to be relatively plastic, (at least in the outer portions of the specimen), as shown in Figure 16. Here the scale was observed to have flowed approximately 40-50μm over the specimen edge.

Erosion-corrosion in air + SO_2/SO_3 atmospheres under high particle loading rates show that a net weight loss was recorded, despite the significant uptake of oxygen and sulfur as evidenced by the thick scale buildup described above. On the other hand despite the loss of scale as evidenced by crater formation under low and medium particle loading rates, a net weight gain was found. For instance, comparing 30 minute exposures, the weight change for samples exposed to high particle loading rates was approximately -12.8 mg/cm², whereas for medium loading rates it was +2.7 mg/cm².

Figure 17 shows weight change data at 600°C and 70 m/s velocities, for (1) erosion-corrosion in air at high particle loading rates, (2) corrosion in air + SO_2/SO_3 atmospheres and (3) erosion-corrosion in air + SO_2/SO_3 atmospheres at high particle loading rates. For erosion-corrosion in air, the rate of weight loss is 0.11 mg/cm²/min., whereas for corrosion only in air + SO_2/SO_3 environments, the rate of weight gain is 0.05 mg/cm²/min. Under conditions of erosion-corrosion in air + SO_2/SO_3 environments, the rate of weight loss is more significant, 0.32 mg/cm²/min. As can be seen, this rate of weight loss is about 3 times that for erosion-corrosion in air, despite the significant uptake of oxygen and sulfur to form the thick scales shown. A more accurate picture of the total degradation can be obtained by considering, the amount of nickel consumed, to form a corrosion product or lost due to erosion. The data shown in Figure 17, is used to calculate the nickel consumed versus time and plotted in Figure 18. In this graph it can be seen that the sum of the nickel consumption

for <u>erosion-corrosion in air</u> and <u>corrosion in air + SO$_2$/SO$_3$</u> is less than that consumed for <u>erosion-corrosion in air + SO$_2$/SO$_3$</u>.

The results thus far have indicated that (a) the atmosphere and (b) the particle loading have a significant influence on the erosion-corrosion response of nickel. For instance, in this study, the extent of degradation measured, in terms of atmospheres used, in the order, air < air + SO$_2$ < air + SO$_2$/SO$_3$. The strong effect of the presence of SO$_3$ is believed to be connected with the tendency towards NiSO$_4$ formation. It should be recognized that, although the average SO$_2$ pressures (when catalyzed SO$_3$ was <u>not</u> present) employed was high enough to favor the reaction,

$$NiO + SO_2 + \frac{1}{2}O_2 = NiSO_4 \tag{1}$$
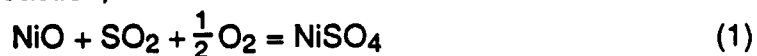
a significant increase in the corrosion rate was not observed until the average SO$_3$ pressure (4.2x10^{-5} atm.) as produced by unequilibrated catalysis via,

$$SO_2 + \frac{1}{2}O_2 = SO_3 \tag{2}$$

was slightly higher than the equilibrium SO$_3$ pressure (3.6x10^{-5} atm.) according to,

$$NiO + SO_3 = NiSO_4 \tag{3}$$

The increase in the corrosion rate of Ni in O$_2$/SO$_2$/SO$_3$ atmospheres, has been related to NiSO$_4$ formation and described in detail elsewhere,[15-17]. Referring to Figure 19, a Ni-O$_2$-S phase stability diagram constructed for 600°C, it is observed that the formation of NiSO$_4$ at the scale-gas surface represented by the reaction path labeled 1→2 (pt. "1" being the bulk gas composition) would lead to an increase in sulfur activity. Beneath this sulfate layer, at pt. "2", conversion of NiSO$_4$ to NiO and Ni$_3$S$_2$(into a 3D network) would be expected to according to the following reactions;

$$4Ni + NiSO_4 = NiS + 4NiO \tag{4}$$
$$Ni + 2NiS = Ni_3S_2 \tag{5}$$

or

$$9Ni + 2NiSO_4 = 8NiO + Ni_3S_2 \tag{6}$$

As the NiSO$_4$ "layer" grows, at the inner face of this layer, away from the gas phase, conversion of the sulfate locally to NiO and Ni$_3$S$_2$ occurs. The presence of Ni$_3$S$_2$ has been found to greatly enhance the outward migration of Ni cations[18] and the inward diffusion of sulfur anions[19]. Progressing inward from

pt. "2" it is assumed that the sulfur activity decreases through the scale until pt. "3" is reached at the metal-scale interface. In sum, the presence of $NiSO_4$ on the surface, may provide the conditions conducive for Ni_3S_2 formation and hence the subsequent increase in the corrosion rates.

It has been shown[17,19], that if the corrosion of nickel involves sulfate formation in the mechanism, only a very thin layer (on the order of 100Å) of $NiSO_4$ typically forms on the scale surface, and that a dedicated surface analytical technique must be employed to determine its presence. In this research, ESCA analysis indicates that, for samples exposed to atmospheres containing air + SO_2/SO_3, the surface consists of Ni configured in a oxidic and sulfate binding state, whereas sulfur is in a sulfate binding state. This strongly suggests that the surface of the specimen consists of both NiO and $NiSO_4$. It is also important to note that in accordance with equilibrium thermodynamics, the absence of Ni_3S_2 on the specimen surface is inferred by the fact that sulfur was not detected in a Ni_3S_2 binding state.

An alternative scheme by which corrosion in non-$NiSO_4$ forming air + SO_2 mixtures (also applicable in $NiSO_4$ forming air+SO_2/SO_3 conditions) may occur is, given by the following mass balance equation,

$$7Ni + 2SO_2 = 4NiO + Ni_3S_2 \qquad (7)$$

As explained by Hocking and Sidky[19], although Ni_3S_2 is unstable in such a gas phase, it is possible for it to form beneath the outer NiO layer. Unlike the case previously discussed, where the inward diffusion of sulfur resulted from the sulfur chemical potential gradient within the scale, established due to the formation of $NiSO_4$, the inward transport of sulfur may occur as described by Pope and Birks[20]. It was postulated that the inward transport of sulfur (from the scale-gas to the scale-metal interface) may occur by either the bulk diffusion of sulfur or the transport of SO_2 molecules down microcracks, grain boundaries and/or dislocation pipes. It was also shown that when the SO_2 partial pressure in the bulk gas was greater than that corresponding to the SO_2 isobar defined by the Ni-NiO-Ni_3S_2 triple point, the formation of a second phase beneath the external oxide by dissociation of SO_2 is feasible. It is shown in Figure 19 that the SO_2 partial pressure used in these experiments, (1.7×10^{-3} atm.) is greater than that required, (7.5×10^{-8} atm.), as shown by the dashed lines and thus such a mechanism is theoretically feasible.

The influence of particle loading rates in air + SO_2/SO_3 atmospheres will now be discussed. Evaluation of the microstructural features and the measured weight change data, suggests that two distinct regimes of erosion-corrosion may exist. Specifically, the erosion-corrosion behavior for low and medium particle loading rates fall into one regime, while that of high particle loading rates fall into another. For instance, for low and medium particle loading rates, a thick scale developed whose surface was pock-marked by a few large craters, about 100-300μm is size, whereas, for high particle loading rates, the scale is thinner (particularly in the specimen center) and covered with numerous smaller craters, about 10-30μm in size.

From these observations, it was concluded that, at high particle loading rates, the dominant degradation mechanism is weight loss due to spallation. In many regards, the observations made under these conditions in this study match closely those described by Hogmark et. al.[10] where local flaking of the oxide scale at individual impact sites is observed in their regime number four. The influence of spallation on the erosion-corrosion process and how it is related in all three particle loading rates situations will be discussed at the end of this paper.

The erosion-corrosion behavior of nickel under low and medium particle loading rates will now be considered. Although not precisely fitting the definition described by Kang et. al.,[8] the erosion-corrosion response observed under low and medium particle loading rates in air + SO_2/SO_3 atmospheres may be considered to fall into the erosion enhanced oxidation regime. As defined before, the erosion enhanced oxidation regime was described to occur when, due to erosion, the oxide scale is thinned to a point where the oxidation rate is increased sufficiently to balance the erosion rate and a constant, steady-state, thickness results. Implicit in this definition is that erosion is a continuous process, (i.e. no spallation occurs) and that the oxidation process is diffusion controlled.

In order to differentiate between these two cases, and by using the scale thickness resulting from pure corrosion as a reference point, additional descriptors are hereby defined. When the steady state thickness resulting from combined erosion-corrosion is less than that resulting from pure corrosion, the degradation mechanism is defined as Type I erosion enhanced oxidation. On

the other hand, when the steady state thickness, resulting from combined erosion-corrosion is greater than that resulting from pure corrosion, the degradation mechanism is defined as Type II erosion enhanced oxidation. The observation of Type II erosion enhanced oxidation in this research is very similar (although different scales and conditions were involved) to that made by Levy et. al.[21] for the erosion-corrosion behavior of chromium steels. The thicker scale found in Type II erosion enhanced oxidation indicates that 1) the corrosion component dominates the erosion component and 2) the erosion component in some manner *modifies* and *enhances* the corrosion process or mechanism. One explanation of this enhancement is related to $NiSO_4$ formation in atmospheres containing SO_3. In pure corrosion, $NiSO_4$ forms on the surface of the specimen at the oxide gas interface. When a growing oxide is exposed to a low or "mild" erosion component, cracks (micron in nature) are developed (within the scale) which allow the inward permeation of gaseous SO_2/SO_3. Once inside these cracks, the SO_3 reacts with NiO to form $NiSO_4$. In a manner described above, the resulting $NiSO_4$ which is believed to form rapidly reacts with Ni and form NiO and Ni_3S_2. The scale which results is thus believed to be in the form of a fine, highly intertwined continuous three dimensional Ni_3S_2 network within the NiO matrix. The formation of this Ni_3S_2 network promotes the rapid outward diffusion of Ni cations resulting in a corrosion rate higher than would be the case in pure corrosion. It is considered that this mechanism is initiated at the commencement of specimen exposure and that this 3-D network is incorporated within the oxide as it grows.

It was mentioned previously that the predominant degradation mechanism for erosion-corrosion under high particle loading rates is due to spallation. Although more important under high particle loading rate conditions, spallation may in fact occur under all particle loading rate conditions. In essence, spallation may be described or envisioned as a pseudo-nucleation and growth process. A high spallation rate, (with the spalls considered as nuclei) in turn keeps the oxide scale, as a whole thin, and this in turn enhances *the corrosion rate. Because the corrosion rate is so high, the oxide/sulfide scale* rapidly redevelops. However, due to the high particle loading rate, onc the scale has obtained a certain thickness (subsequently referred to as the critical scale thickness) spallation occurs and the process repeats itself.

As the particle loading rate was reduced, the relative occurrence of spallation events decreases, (i.e. the pseudo nucleation rate decreases). Due to the large corrosion component (i.e. high corrosion rate), scale growth is enhanced, and the scale thickness grows beyond the critical thickness required for spallation and a thick "stable" scale develops. The large craters observed for samples exposed to medium and low particle loading rates are thought to be the remains or results of earlier spallation events, when the scale was at the critical thickness for spallation. Once the oxide-gas front passed this thickness, craters which formed earlier now continue to grow in size, (thus the origin of the pseudo growth analogy). The concept of crater growth as illustrated in Figure 9(d), and discussed by Wert and McKechnie[22], is related to the fact that, for a given material such as a brittle oxide, on a unit volume basis, less energy is required to remove the edge of a crater wall than is the case for a flat surface.

The approach to the discussion on spallation, has purposely been phenomenological and concerned mainly with the effect spallation has on the erosion-corrosion process. The issue as to how and under what circumstances spallation occurs, is a topic in itself and will be addressed in a future publication.

CONCLUSIONS

1. The presence of sulfurous gases was found to influence the erosion-corrosion behavior of nickel. Particularly when SO_3 was present.
2. The erosivity, as controlled by the particle loading rate did influence the regime in which the erosion-corrosion process occurs for atmospheres containing air + SO_2 and air + SO_2/SO_3.
3. The erosion enhanced oxidation regime may be divided into two sub-categories, termed Type I and Type II.
4. The spallation process for erosion-corrosion in air + SO_2/SO_3 for low, medium, and high particle loading rates may be looked upon as a pseudo-nucleation and growth process. For high particle loading rates, the numerous small spallation sites (considered as nuclei) which result due to the relative large number of impacts, may be envisioned along the lines of a high nucleation process. On the otherhand, the low and

medium paticle loading rates result in a "low" nucleation rate, and the large craters observed are the result of spalls which subsequently grew.

5. Depending upon the experimental conditions, a number of erosion-corrosion interaction regimes exist. For the experimental conditions employed in this study the interaction regimes are summarized as follows:

(a) Erosion-corrosion in air for low, medium and high particle loading rates is in the oxidation affected regime.

(b) Erosion-corrosion in air + SO_2 atmospheres for low and medium particle loading rates is believed to be in the Type I erosion enhanced oxidation regime; whereas, erosion-corrosion in air + SO_2 at high particle loading rates is in the oxidation affected regime.

(c) Erosion-corrosion in air + SO_2/SO_3 atmospheres for low and medium particle loading rates is in the Type II erosion enhanced oxidation regime; whereas, erosion-corrosion in air + SO_2/SO_3 atmospheres for high particle loading rates is in a regime characterized by spallation. This latter condition however, may also in turn be a special of limiting case for erosion enhanced oxidation. Further research is required to clarify this point.

Bibliography

1. Smock, R., "Pressurized Fluid Bed Combustion Aims for Utility Acceptance," Power Engineering, (September, 1986), pp. 31-34.

2. Brunetaud, R., Coutsouradis, D., Gibbons, T. B., Lindbloom, Y., Meadowcroft, D. B. and R. Strickler, ed., High Temperature Alloys for Gas Turbines 1982, "High Temperature Erosion and Erosion-Hot Corrosion of Superalloys and Coatings, by J. C. Galsworthy, J. E. Restall and G. C. Booth" (Dordrecht, Holland, D. Reidel Publishing Co., 1982), pp. 207-235.

3. Wright, I. G., "High Temperature Erosion in Coal Combustion and Conversion Processes: A Review," Materials Science and Engineering, Vol. 88 (1987), pp. 261-271.

4. Stephenson, D. J., Nicholls, J. R. and P. Hancock, "The Erosion of Gas Turbne Blade Materials by Solid Sea Salt," Corrosion Science, Vol. 25, No. 12 (1985), pp. 1181-1192.

5. R. H. Barkalow, J. A. Goebel and F. S. Pettit, Materials Problems in Fluidized-Bed Combustion Systems: High-Temperature Erosion-Corrosion by High-Velocity (200 m/s) Particles, Pratt and Whitney Aircraft Group, May 1980, EPRI CS-1448, Project 979-4, Final Report.

6. Wire, G. L., Vesely, E. J. and S. Agarwal, "Erosion-Corrosion of Metals in Coal Gasification Atmospheres," Journal of Materials for Energy Systems, Vol. 8, No. 2, (Sept. 1986), pp. 150-167.

7. Wright, I. G., Nagarajan, V. and W. E. Merz, Erosion-Control of Metals and Alloys at High Temperatures, Battelle, Columbus Laboratories, June 1984, EPRI CS-3504, Project 979-8, Interim Report.

8. Kang, C. T., F. S. Pettit and N. Birks, "Mechanisms in the Simultaneous Erosion-Oxidation Attack of Nickel and Cobalt at High Temperatures," Met. Trans. A., Vol. 18, (1987), pp. 1785.

9. Wright, I. G. Nagarajan, V. and J. Stinger, "Observations of the Role of Oxide Scales in High-Temperature Erosion-Corrosion of Alloys," Oxidation of Metals, Vol. 25, Nos. 3/4. (1986), pp. 175-199.

10. Proceedings of the 6th International Conference on Erosion by Liquid and Solid Impact, "On the Combined Effects of Corrosion and Erosion, by S. Hogmark, Å. Hammersten and S. Söderberg," (University of Cambridge, 1983, pp. 37-1 through 37-8).

11.   <u>Proceedings of the 6th International Conference on Erosion by Liquid and Solid Impact</u>, "Erosion Mechanisms in Ductile and Brittle Materials, by Alan V. Levy," (University of Cambridge, 1983, pp. 39-1 through 39-7).

12.   Rishel, D. M., "The Erosion-Corrosion Behavior of Ni at 600°C in Mixed Oxidant Atmospheres," (unpublished M. S. Thesis, Department of Materials Science and Engineering, University of Pittsburgh, 1987).

13.   Kang, Chih-Tsung, "The Interactions Between Erosion and Oxidation of Metals at Elevated Temperatures," (unpublished Ph.D. Dissertation, School of Engineering, University of Pittsburgh, 1985).

14.   Laitone, J. A., "Aerodynamic Effects in the Erosion Process," <u>Wear</u>, Vol. 56, (1979), pp. 239-246.

15.   Haflan B. and P. Kofstad, "The Reaction of Nickel with $SO_2 + O_2/SO_3$ at 500-900°C," <u>Corrosion Science</u>, Vol. 23, No. 12, (1981), pp. 1333-1352.

16.   Alcock, C. B., M. G. Hocking and S. Zador, "The Corrosion of Ni in O_2+SO_2 Atmospheres in the Temperature Range 500-700°C," <u>Corrosion Science</u>, Vol. 9, (1969), pp. 111-122.

17.   Lillerud, K. P., B. Haflan and P. Kostad, "On the Reaction Mechanism of Nickel with $SO_2 + O_2/SO_3$," <u>Oxidation of Metals</u>, Vol. 21, Nos. 3/4, (1984), pp. 119-134.

18.   Mrowec, S. and K. Przybylski, "Transport Properties of Sulfide Scales and Sulfidation of Metals and Alloys," <u>Oxidation of Metals</u>, Vol. 23, Nos. 3/4, (1985), pp. 107-139.

19.   Hocking, M. G. and P. S. Sidky, "The Hot Corrosion of Nickel-Based Ternary Alloys and Superalloys for Gas Turbine Applications-II. The Mechanism of Corrosion in SO_2/O_2 Atmospheres," <u>Corrosion Science</u>, Vol. 27, No. 2, (1985), pp. 205-214.

20.   Pope, M. C. and N. Birks, "The Penetration by Sulfur of NiO Scales Growing on Nickel," <u>Oxidation of Metals</u>, Vol. 12, No. 2, (1978), pp. 173-181.

21.   Levy, A. Slamovich, E. and N. Jee, <u>Elevated Temperature Combined Erosion-Corrosion of Steels</u>, LBL-19159 Preprint, (Berkeley, California: Lawrence Berkeley Laboratory, University of California, April, 1985).

22.   Wert, J. J. and T. N. McKechnie, "The Effect of Composition and Process Parameters on the Erosion Resistance of Sputtered Ni-TiB$_2$ Coatings," <u>Wear</u>, Vol. 116, (1987), pp. 181-200.

THIS PAGE LEFT INTENTIONALLY BLANK
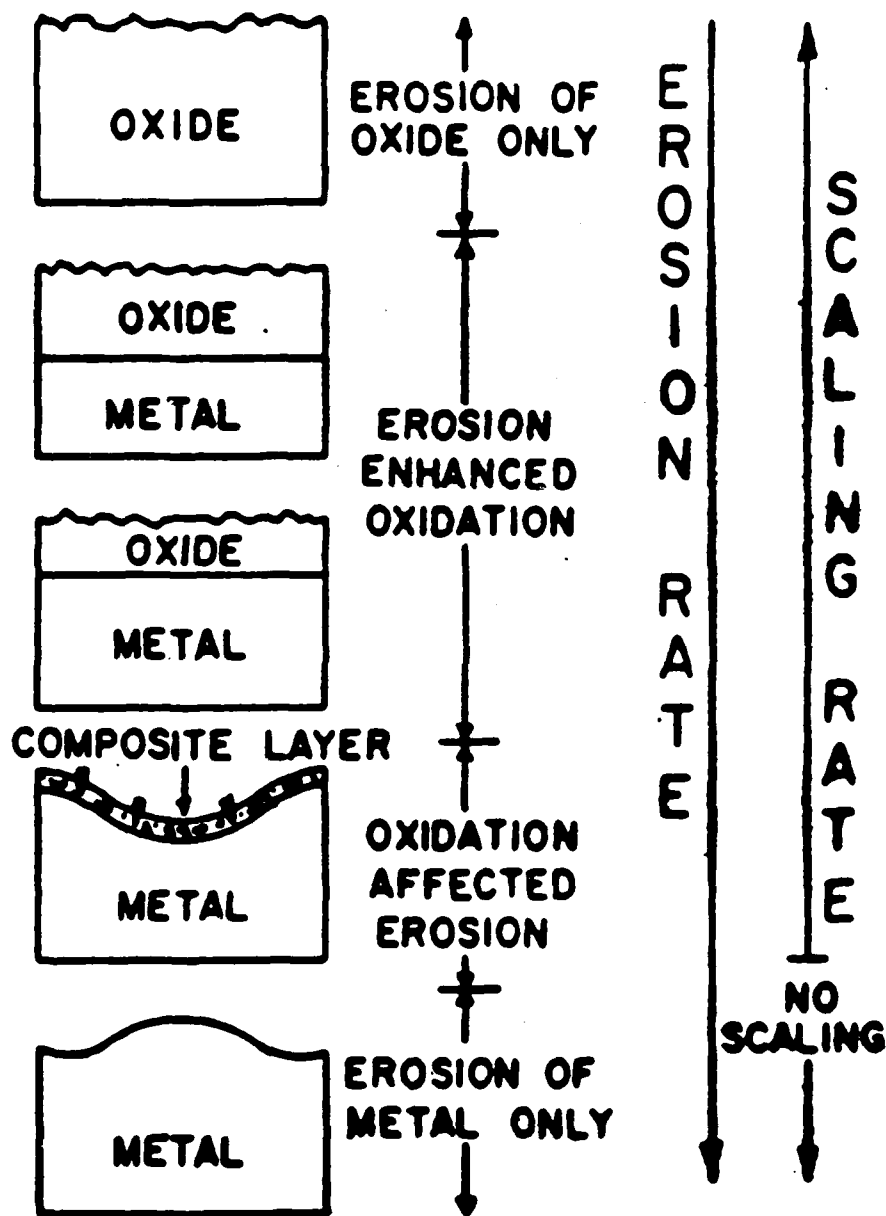
Figure 1: Suggested interaction regimes for combined erosion and oxidation[13].
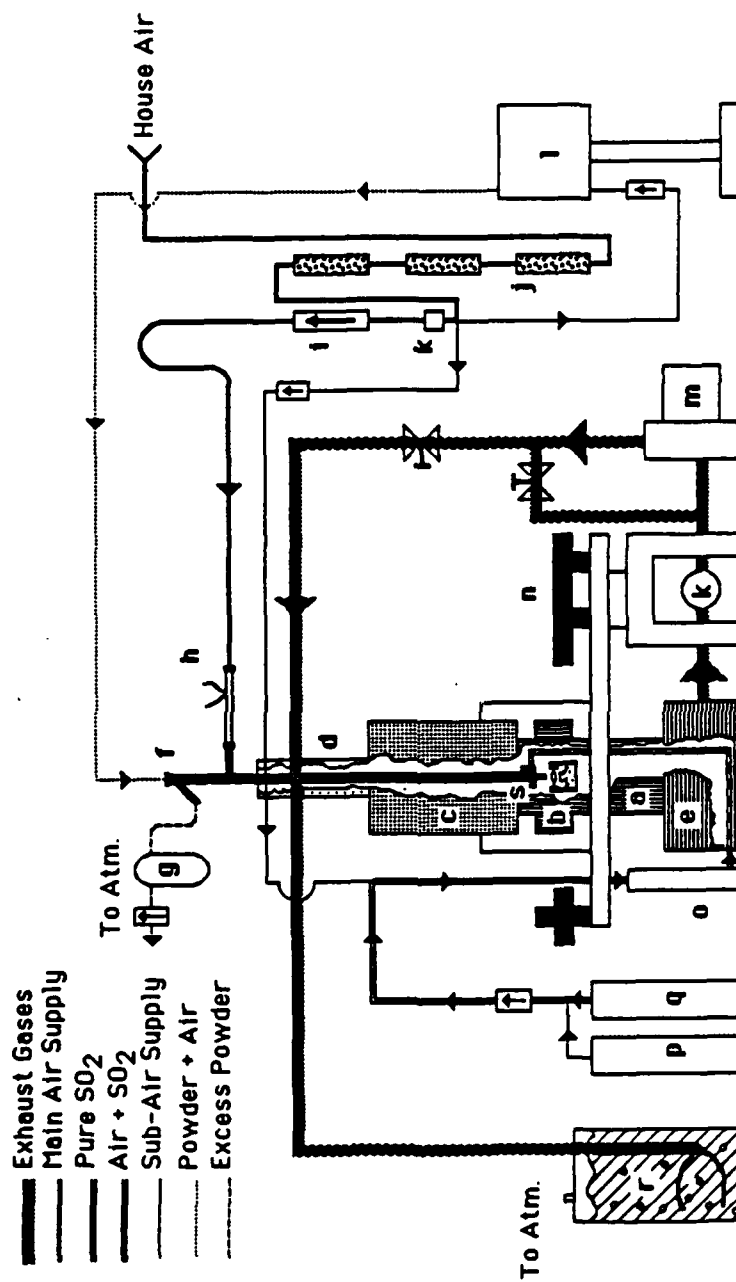
Figure 2: Erosion Apparatus Schematic Cutaway with Sample In Position: (a) reaction chamber; (b) sample holder; (c) Lindberg furnace; (d) upper heater; (e) powder collection sump; (f) powder injector/divider; (g) excess powder collector; (h) fluid heater; (i) flow meter; (j) oil/moisture separators; (k) filter; (l) powder feeder; (m) blower; (n) LDV equipment; (o) SO₂ heater; (p) nitrogen; (q) liquid SO₂; (r) 55 gallon drum; (s) SO₂ injector.

22
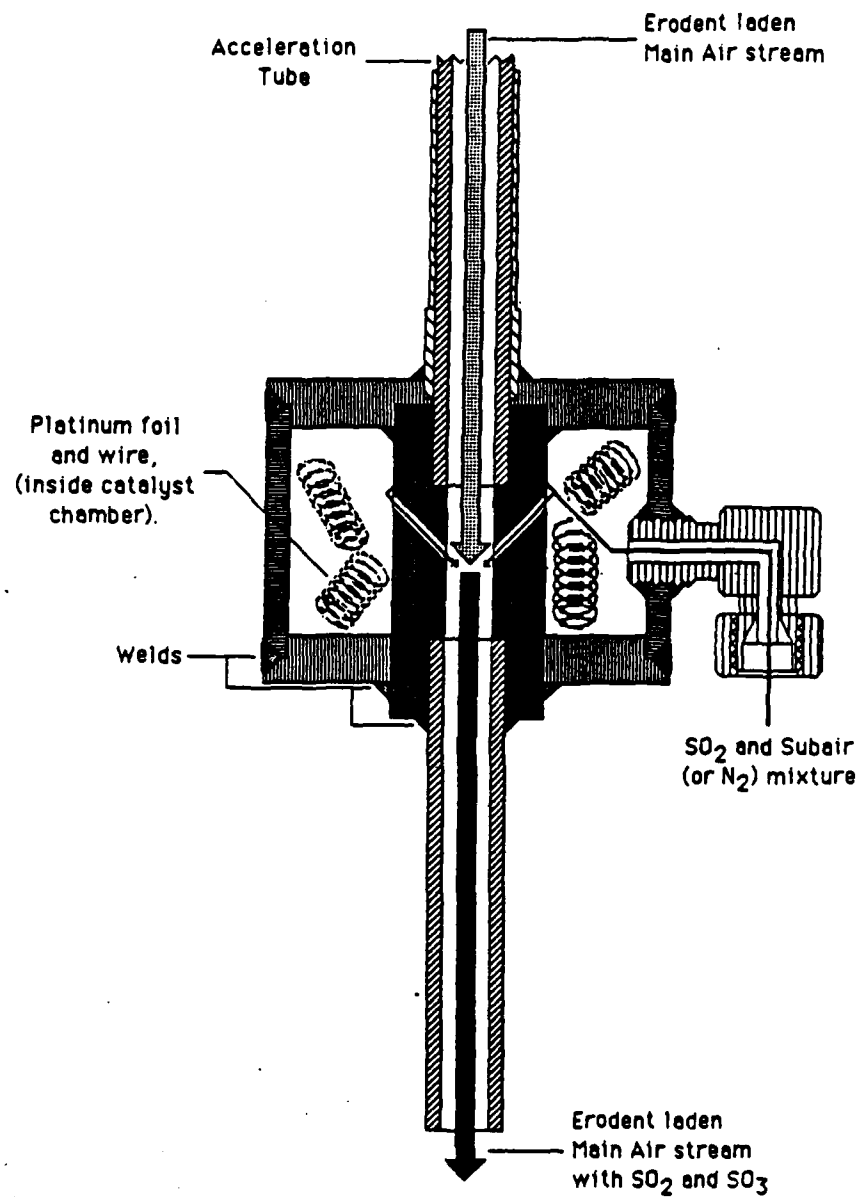
Figure 3: Cutaway of SO₂ Injector.

24
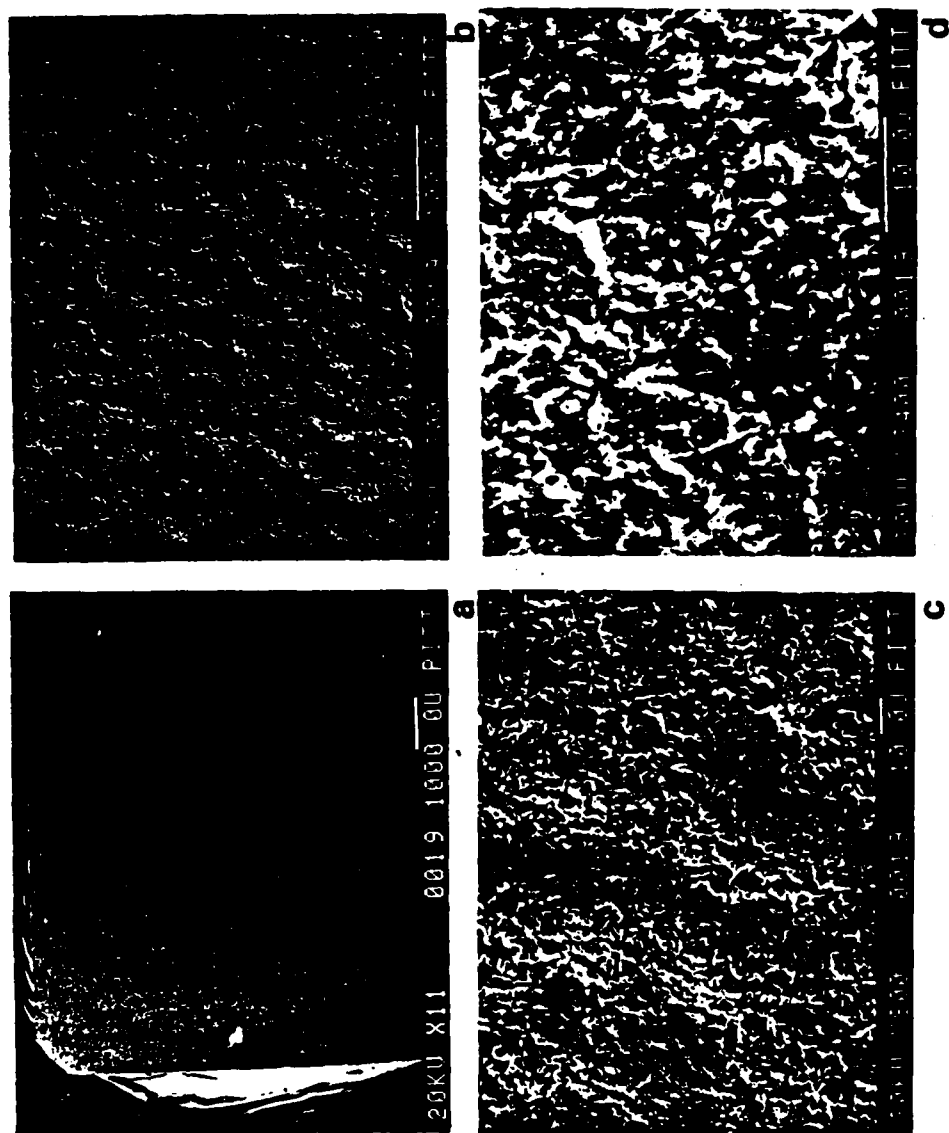
Figure 4: (a) Nickel exposed to erosion-corrosion in air at 600°C, 70 m/s, under high particle loading rates, for 30 minutes; (b), (c) and (d) High magnification of (a) near Region A.
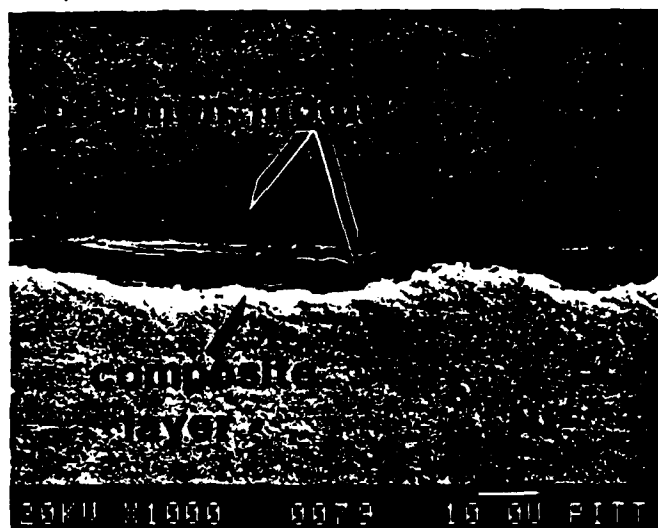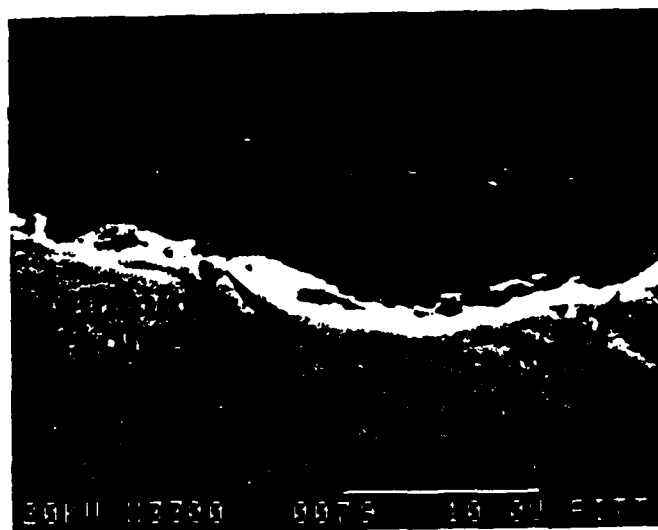
Figure 5: (a) Sections of a nickel specimen exposed to erosion-corrosion in <u>air</u> at 600°C, 70 m/s, under <u>high particle loading rates</u>, for 30 minutes; (b) High magnification of (a).
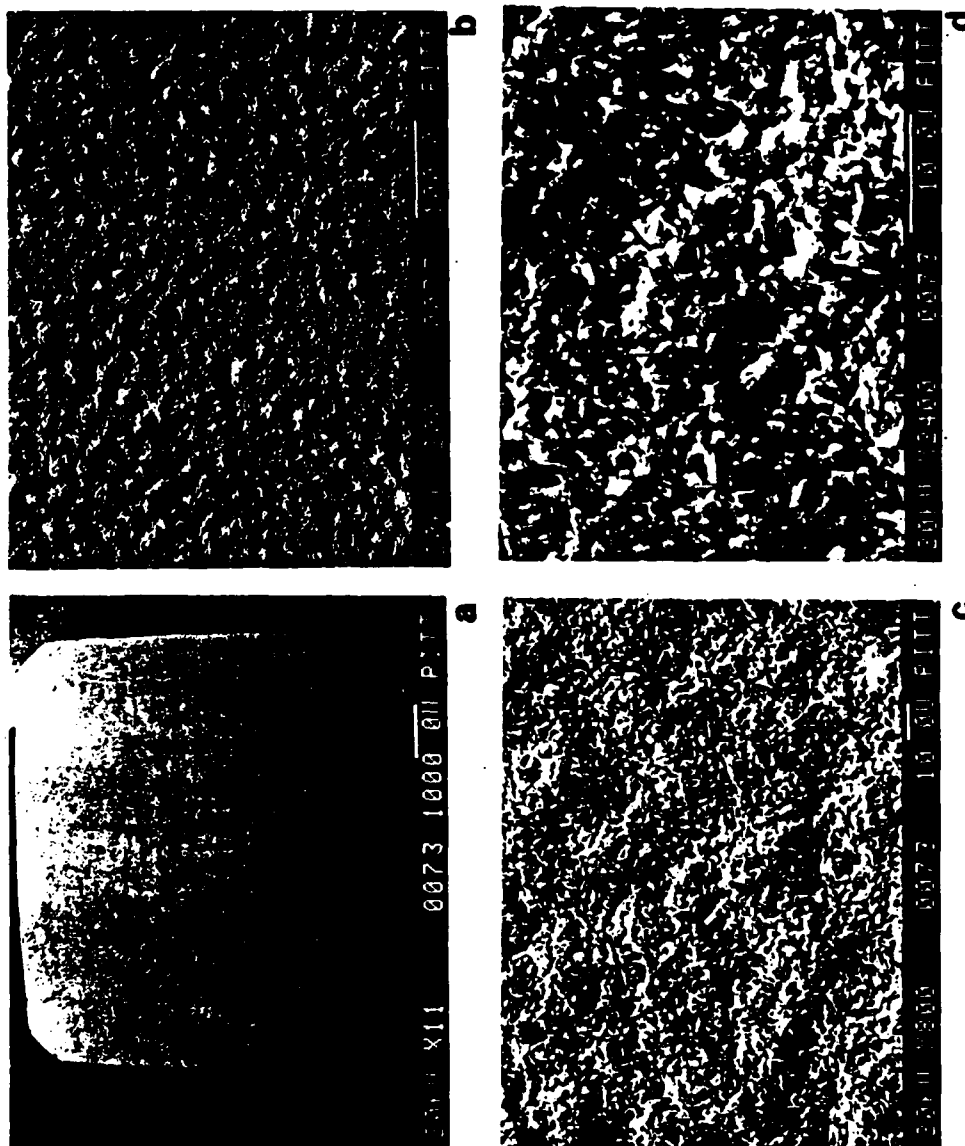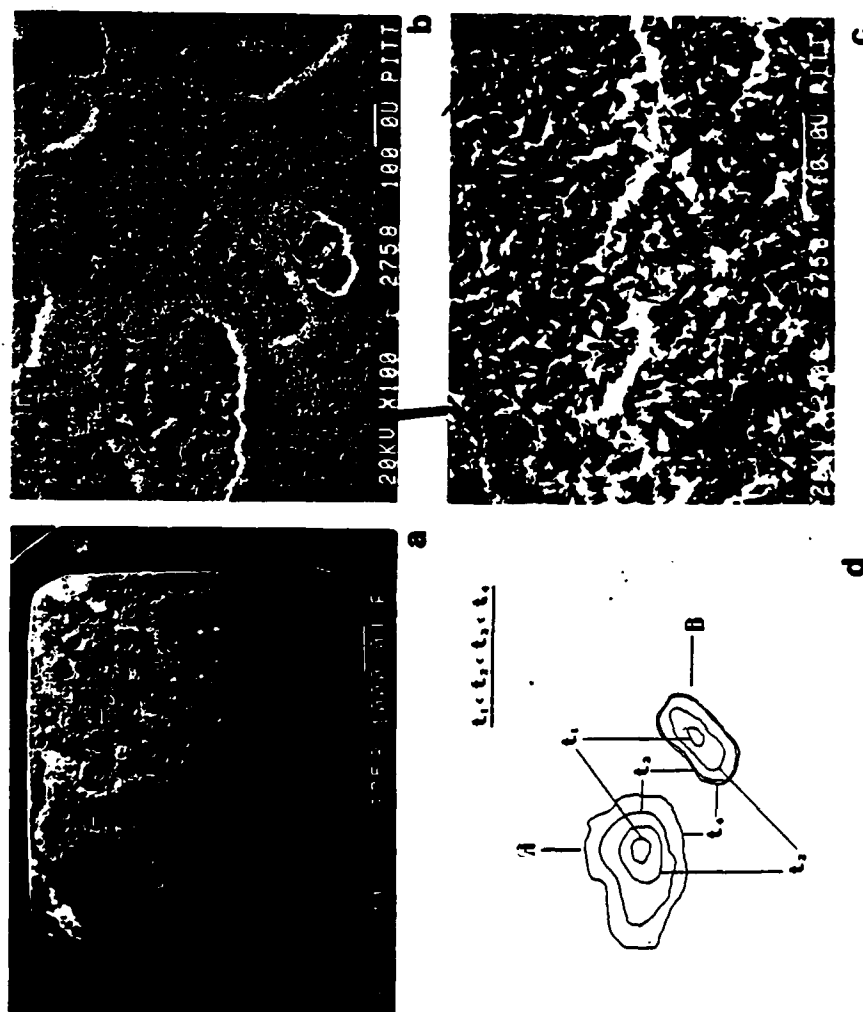
Figure 6: (a) Nickel exposed to erosion-corrosion in air at 600°C, 70 m/s, under low particle loading rates, for 30 minutes; (b), (c) and (d) High magnification of (a) near Region A.
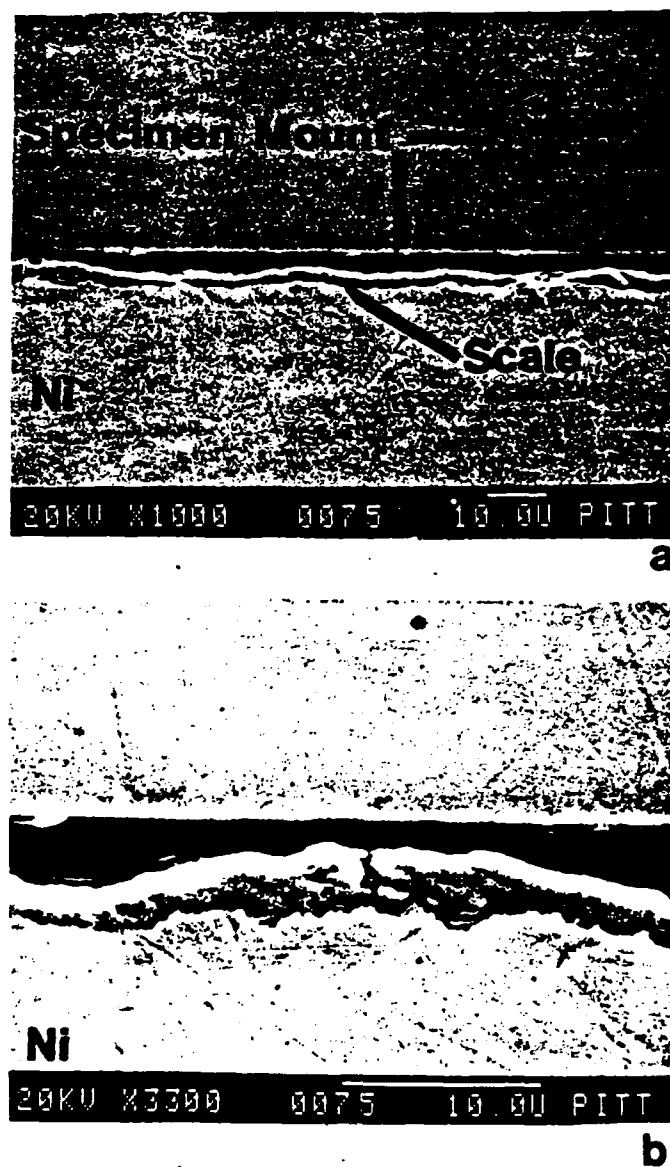
Figure 7:　(a) Sections of a nickel specimen (near center), exposed to erosion-corrosion in <u>air + 1730 ppm SO₂</u> at 600°C, 70 m/s and under <u>medium particle loading rates</u>, for 30 minutes; (b) High magnification of (a).

MICROCOPY RESOLUTION TEST CHART
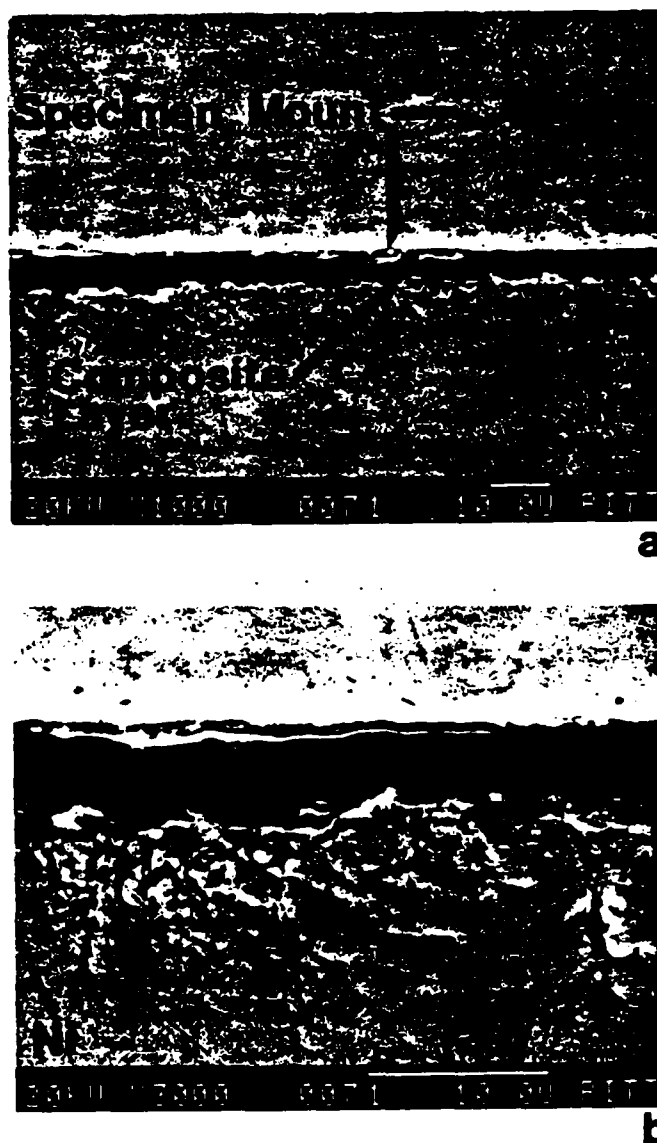
Figure 8: (a) Sections of a nickel specimen (near center), exposed to erosion-corrosion in <u>air + 1730 ppm SO₂</u> at 600°C, 70 m/s and under <u>high particle loading rates</u>, for 30 minutes; (b) High magnification of (a).

Figure 9: (a) Nickel exposed to erosion-corrosion in air + 1730 ppm SO₂/42 ppm SO₃ at 600°c, 70 m/s, under low particle loading rates, for 30 minutes; (b) High magnification of Region A in (a), illustrating growing (1 & 3) and stable (2 & 4) craters; (c) High magnification of (b) illustrating a crater wall; (d) Schematic of craters 1 & 2 (from (b)), showing growth vs. time. Note: The absence of small spalls or craters (≈ 10-30μm in size).
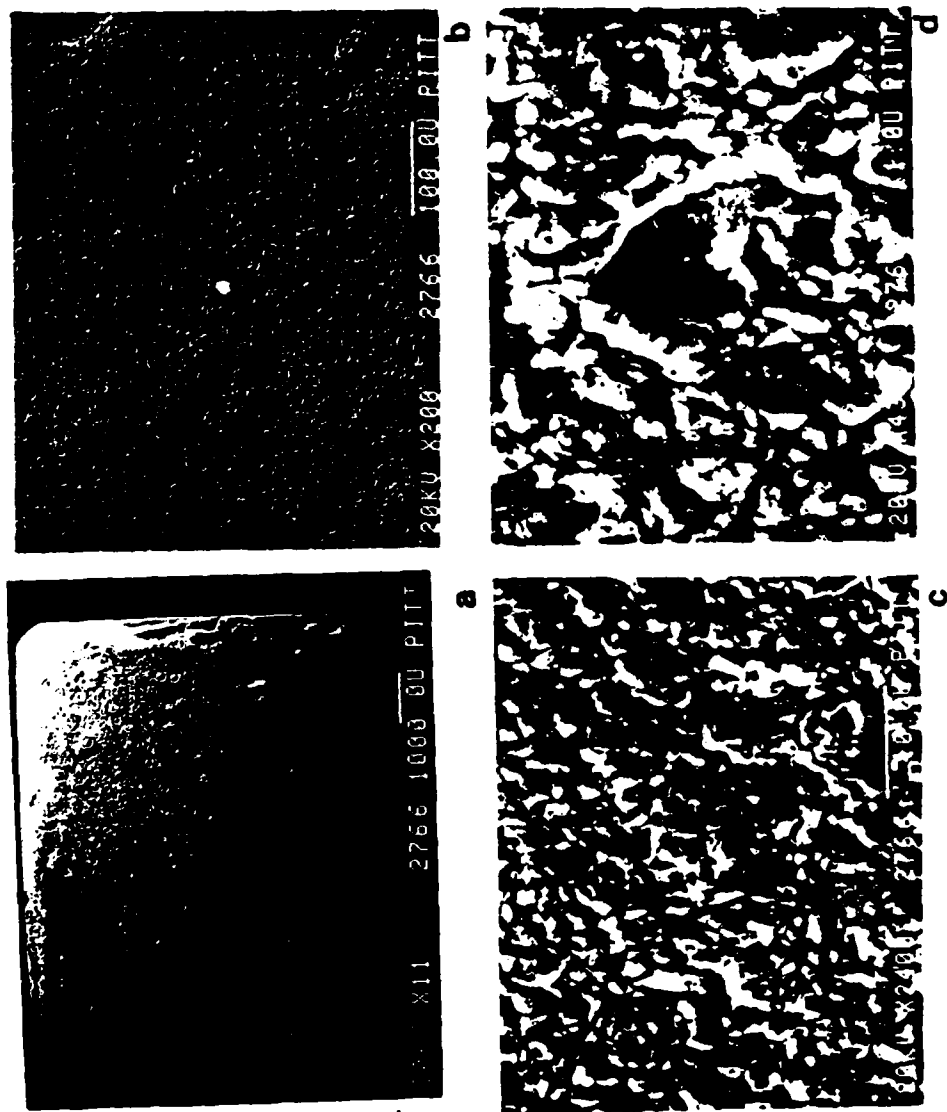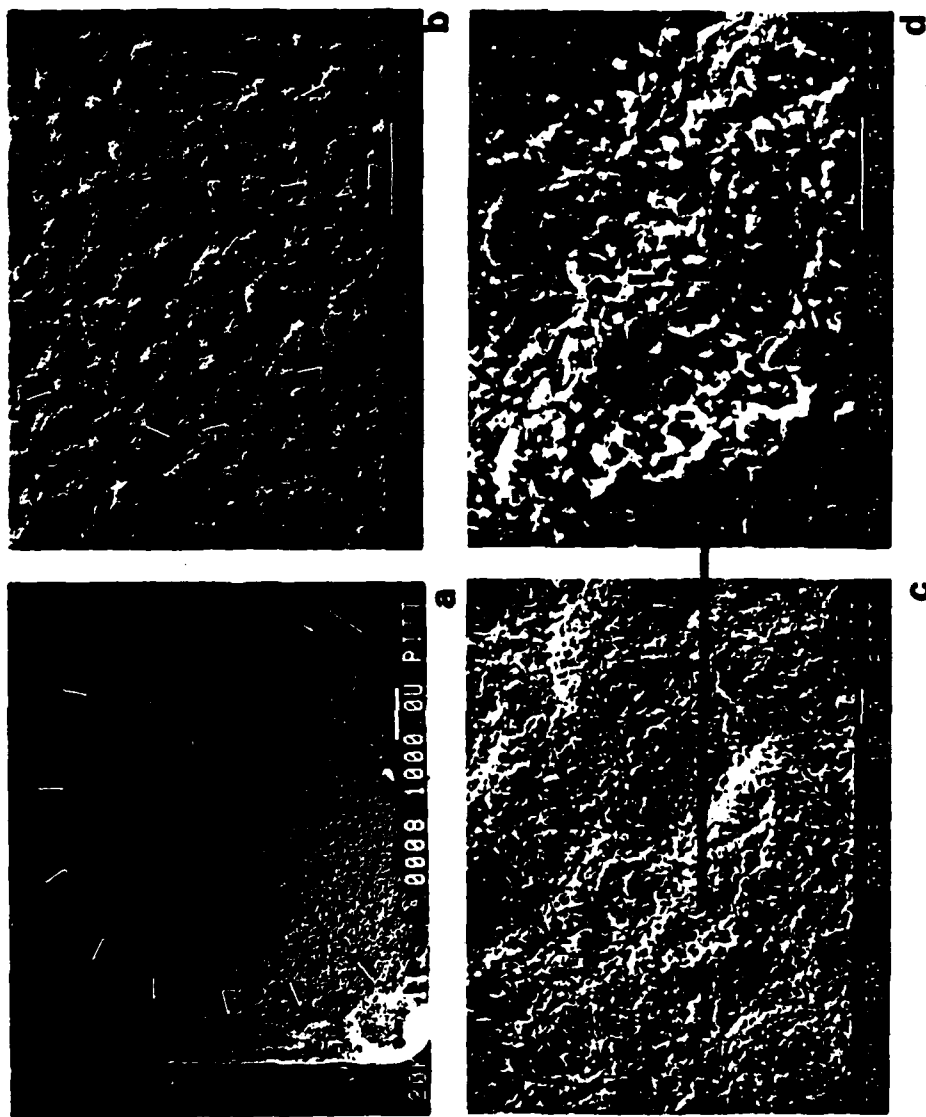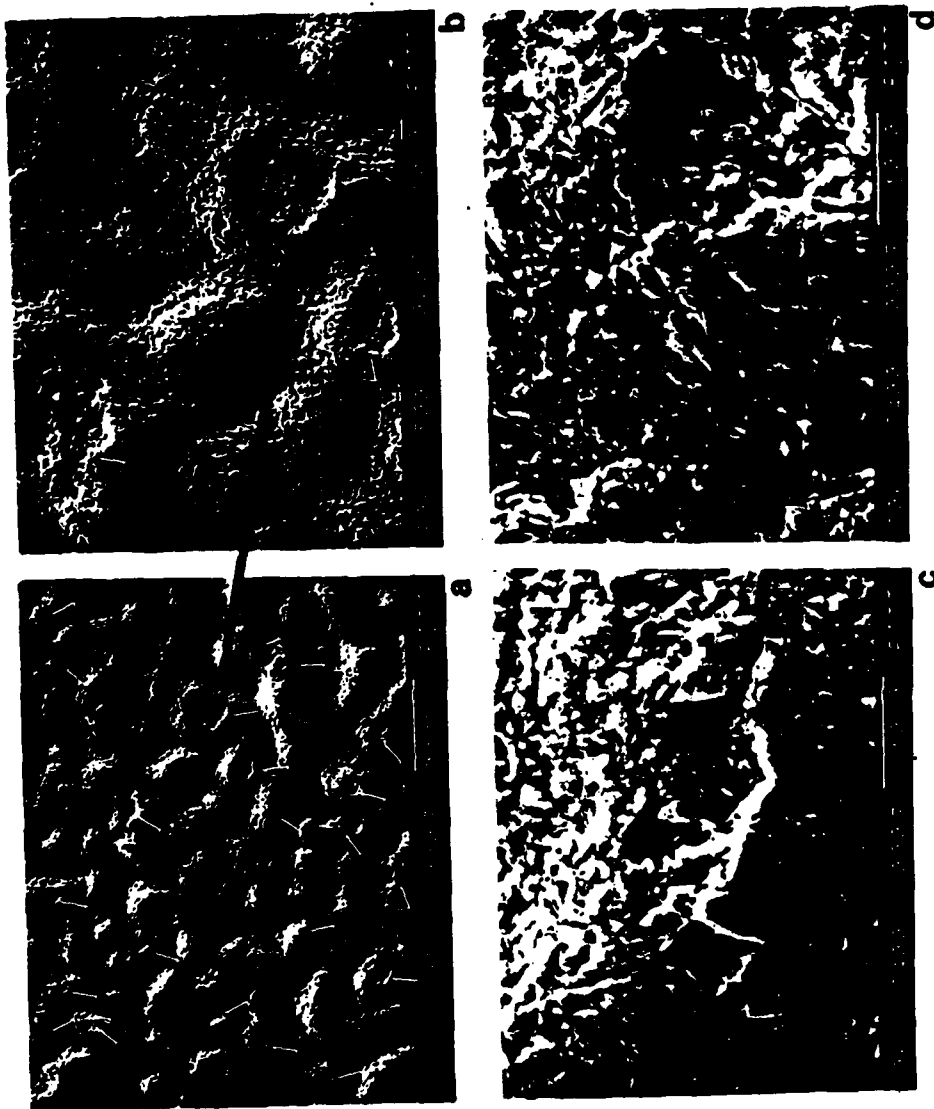
Figure 10: (a) Nickel exposed to erosion-corrosion in air + 1730 ppm SO_2/42 ppm SO_3 at 600°C, 70 m/s, under medium particle loading rates, for 30 minutes; (b), (c) and (d) High magnification of Region A in (a).
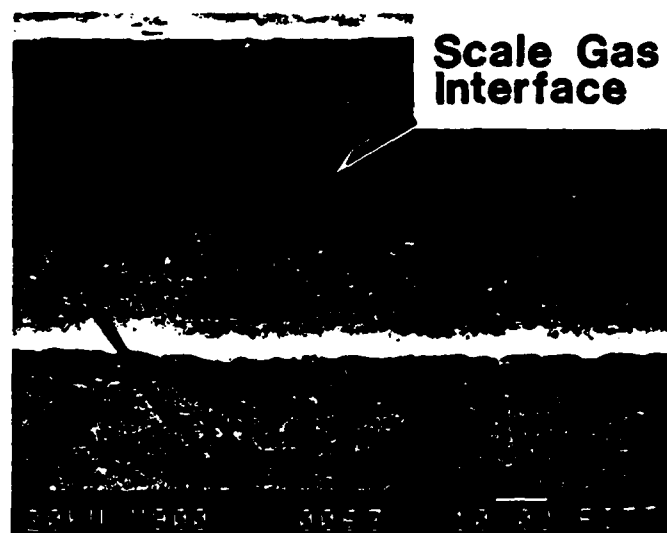
Figure 11: Section of a nickel specimen exposed to erosion-corrosion in air + 1730 ppm SO_2/42 ppm SO_3 at 600°C, 70 m/s, and under low particle loading rates for 30 minutes.
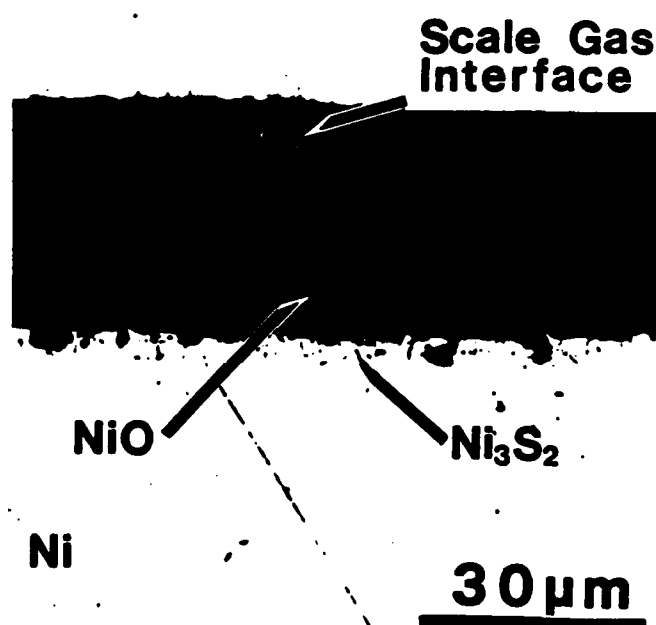
Figure 12: Section of a nickel specimen exposed to erosion-corrosion in <u>air + 1730 ppm SO$_2$/42 ppm SO$_3$</u> at 600°C, 70 m/s, and under <u>medium particle loading rates</u> for 30 minutes.

Figure 13: (a) Nickel exposed to erosion-corrosion in air + 1730 ppm SO₂/42 ppm SO₃ at 600°C, 70 m/s, under high particle loading rates for 30 minutes, (arrows indicate "rim effect"); (b) High magnification of region A as shown in (a), (arrows indicate spalls); (c) and (d) High magnification of spall labled B in (b).

Figure 14: (a) Nickel exposed to erosion-corrosion in air + 1730 ppm SO_2/42 ppm SO_3 at 600°C, 70 m/s, under high particle loading rates for 120 minutes. (arrows indicate spalls); (b) detail of (a); (c) and (d) detailed micrographs of spalled regions.
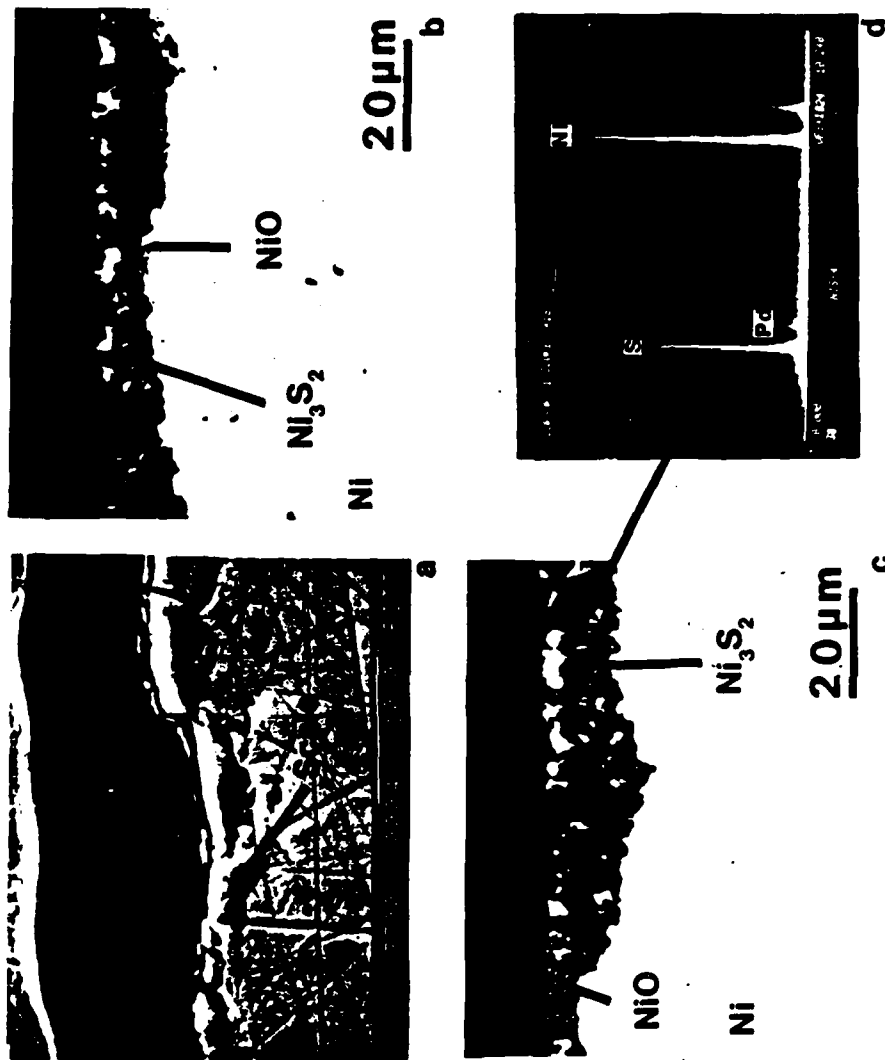
Figure 15: Illustration of the variation in scale thickness, for a nickel specimen exposed to erosion-corrosion in air + 1730 ppm SO_2/42 ppm SO_3 at 600°C, 70 m/s, under high particle loading rates, for 90 minutes; (a) SEM micrograph taken near center of specimen; (b) and (c) Optical micrographs taken near specimen edge; (d) EDS of the white area shown in (c).
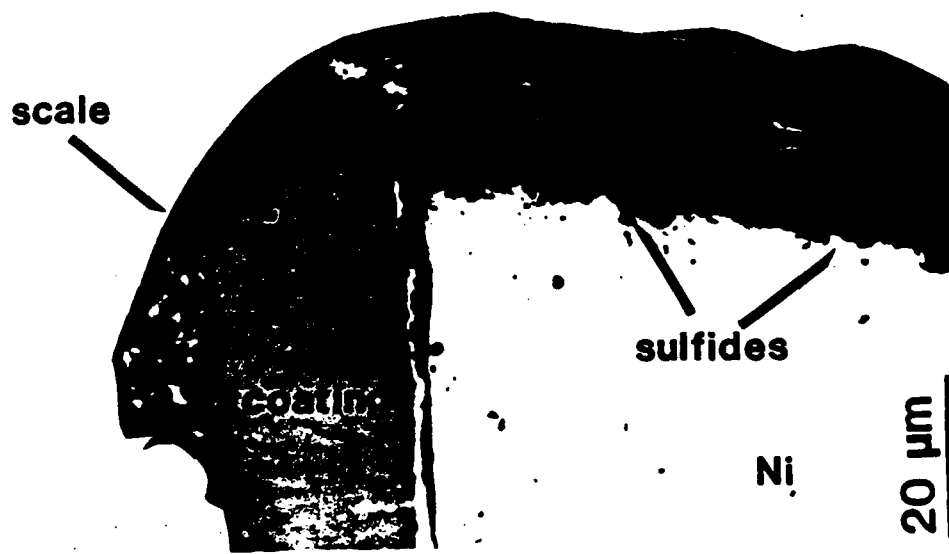
Figure 16: (a) Cross-sectional optical micrograph, illustrating scale overflow on a nickel specimen exposed to erosion-corrosion in air + 1730 ppm SO₂/42 ppm SO₃ at 600°C, 70 m/s, under high particle loading rates for 60 minutes; (b) SEM micrograph of (a); (c) Sulfur X-Ray map of (b).
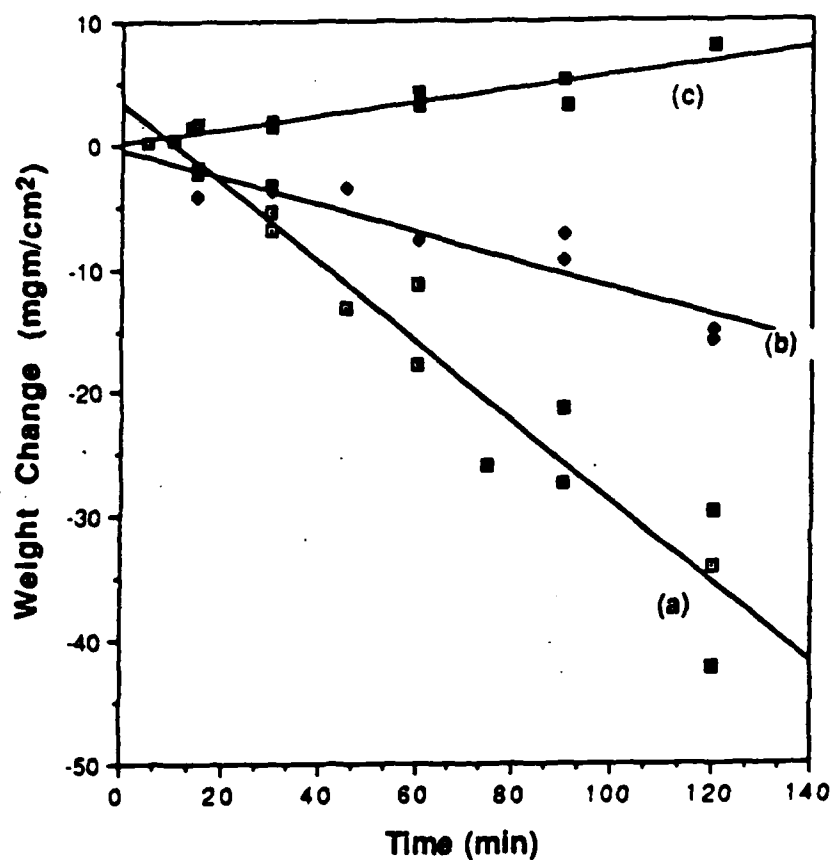
Figure 17: Plot of degradation defined in terms of weight change
vs. time data, for Ni exposed at 600°C, 70 m/s in; (a) Air
+ 1733 ppm SO_2/42 ppm SO_3 with 20μm Al_2O_3 erodent
particles, (weight loss rate = 0.32 mgm/cm²/min); (b) Air
with 20μm Al_2O_3 erodent particles, (weight loss rate =
0.11 mgm/cm²/min); (c) Air + 1733 ppm SO_2/42 ppm
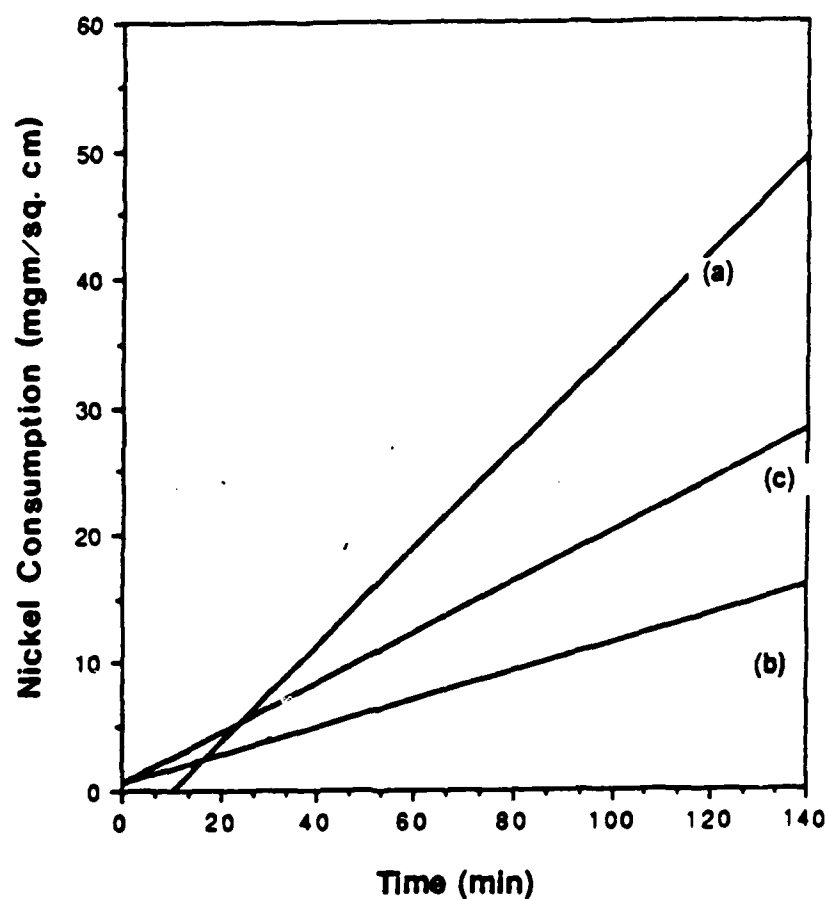SO_3, (weight gain rate = 0.05 mgm/cm²/min.).

Figure 18: Plot of degradation defined in terms of nickel
consumption (calculated) vs. time data, for Ni exposed at
600°C, 70 m/s in; (a) Air + 1733 ppm SO_2/42 ppm SO_3
with 20μm Al_2O_3 erodent particles, (Ni consumption rate
= 0.38 mgm/cm^2/min); (b) Air with 20μm Al_2O_3 erodent
particles, (Ni consumption rate = 0.11 mgm/cm^2/min); (c)
Air + 1733 ppm SO_2/42 ppm SO_3, (Ni consumption rate =
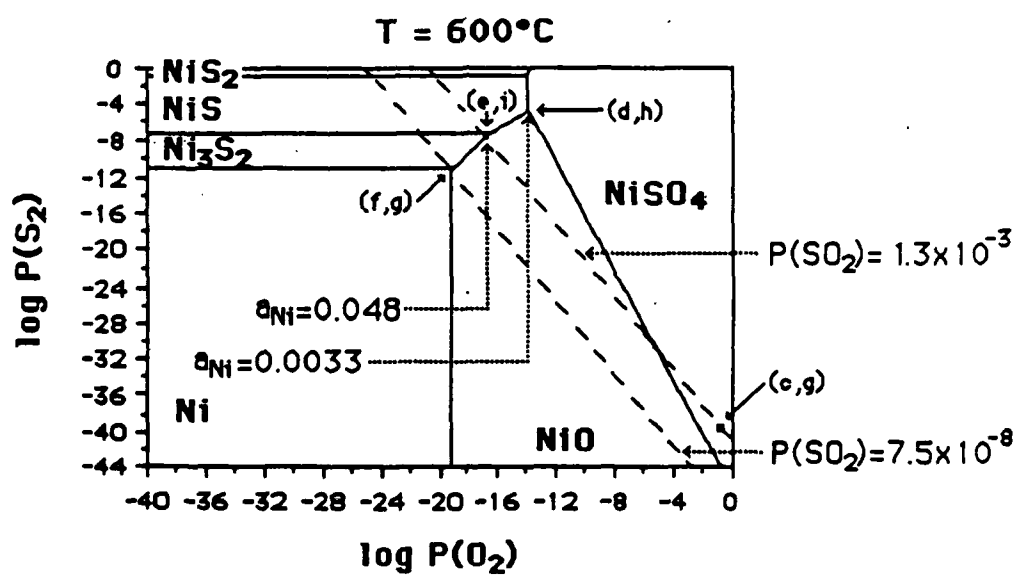0.19 mgm/cm^2/min.).

Figure 19: Ni-S-O Phase Stability Diagram for 600°C.

END

DATE

FILMED

8-88

DTIC